Aus dem Physiologischen Institut der Ludwig-Maximilians-Universität München,

Lehrstuhl zelluläre Physiologie

Vorstand: Frau Prof. Dr. Claudia Veigel

Identification of lipid binding sites in myosin VI and XXI and regulation by the cargo-binding domain

Dissertation

zur Erlangung des Doktorgrades der Naturwissenschaften

an der Medizinischen Fakultät

der Ludwig-Maximilians-Universität München

eingereicht von

Heike Ellrich

aus Mainz

2014

Gedruckt mit Genehmigung der Medizinischen Fakultät der Ludwig-Maximilians-Universität München

Betreuerin: Priv.-Doz. Dr. rer. nat. Beate Averbeck

Zweitgutachter: Prof. Dr. Axel Imhof

Dekan: Prof. Dr. med. Dr. h. c. Maximilian Reiser, FACR, FRCR

Tag der mündlichen Prüfung: 17.03.2015

Abstract

The cytoskeleton along with its motor proteins plays a central role in the realization of essential biological processes such as cell motility, muscle contraction, chromosome segregation, intracellular transport of organelles, and endo- and exocytosis. A vast array of motor proteins are utilised to achieve these highly specific tasks.

Myosin VI, the subject of this study, is unique amongst myosins. Being ubiquitously expressed it is the only known minus-end directed myosin which is involved in a variety of tasks including autophagy, endo- and exocytosis and has the capability to directly interact with lipids, or bind cargo via binding partners. Its depletion results in hearing loss and secretory diarrhoea. It is overexpressed in certain human prostate and ovarian cancer types. Although containing the requirements for dimerisation, a coiled-coil region in the C-terminal tail, it is unable to dimerise, at least under all concentrations and conditions tested in this study. Under certain circumstances myosin VI is able to adopt a 'folded back' conformation which we hypothesise inactivates the motor and makes it incapable of binding to cargo.

Myosin XXI is a newly described myosin from the parasite *Leishmania sp.*. Being the sole known expressed myosin motor in this organism it is possibly a very versatile motor, like myosin VI, since it has to reclusively perform all tasks in the cell that normally are performed by an array of myosins. Depletion of myosin XXI expression in *Leishmania* results in impairment of flagellar assembly and intracellular trafficking.

The objective of this study is to increase our understanding of how myosins bind to lipids and lipid cargo. It is important to understand how and where different lipids bind to the tail region. The ability of myosins to selectively bind different cargoes is poorly understood but is integral to their specific function within cells. Myosins must bind cargo specifically to transport it to its cellular destination, navigating a complex and densely packed environment and thus relocate the cargo in a specific and timely fashion. Furthermore, cargo binding and mechanical regulations of the motor protein are linked to avoid futile and unnecessary ATP hydrolysis. Understanding how these two processes are connected is critical to understand how the protein is regulated.

To investigate this, a variety of biochemical and biophysical techniques are employed including bulk protein experiments such as co-sedimentations, western-, far-western and

dot-blots. Motility assays, affinity titrations and ATPase assays explore the activity, lipid binding abilities and regulatory mechanisms of myosin VI.

The back-folding of the tail of myosin VI is an interaction of the first 65 N-terminal amino acids of the cargo-binding domain with the calmodulin bound to the IQ-motifs, and not to the motor domain as previously thought. Calcium disrupts this interaction and provides a simple mechanism by which myosin can be activated by calcium fluctuations within the cell. Another remarkable new finding is that myosin VI not only binds to a particular phosphatidylinositolphosphate (PIP) with a formerly described special binding motif in the cargo-binding domain, but that it is capable of binding to a range of lipids along the entire tail. This interaction also seems to be regulated or rather co-regulated by calcium, which changes the affinity of the motor to certain lipids. Furthermore it was discovered that myosin VI and XXI are able to translocate actin filaments faster and with a higher affinity for binding to the surface when bound to lipid surfaces. Similar to myosin VI lipid binding in myosin XXI is shown to occur along the length of the entire tail, although with different affinities for different tested lipids. A PX domain, which specifically binds $PI(3,5)P_2$, was found in the converter region of this myosin. This myosin is capable of dimerisation and here it is shown that lipid binding and dimerisation are mutually exclusive.

Myosin VI has the ability to bind to various lipids along its entire tail and calcium seems to co-regulate this interaction by enhancing or disrupting the interaction. This gives the motor flexibility in cargo-transport through the cell and might enable it to quickly exchange and deposit different cargoes. Differences in PIP affinities revealed regulatory options for cargo-transport in cells as well. Since calcium disrupts the interaction of the back-folded C-terminal tail to the N-terminal calmodulin, it as well seems to play a role in activation and inactivation of myosin VI. The PX domain in the converter region of myosin XXI and its ability to switch between a dimeric motor that does not bind lipids and a monomeric motor which can bind lipids might give further insights towards the yet unknown set of tasks myosin XXI fulfils in *Leishmania sp.*.

Zusammenfassung

Die Filamente des Zytoskeletts eukaryotischer Zellen erfüllen vielseitige Aufgaben. Sie sind wichtig für die Formgebung und die Stabilität der Zellen, sowie für die Fortbewegung. Darüber hinaus dienen die Filamente als Transportwege für Motorproteine für den intrazellulären Transport. An der Ausführung zentraler biologischer Prozesse von der Muskelkontraktion über die Bewegung ganzer Zellen, Chromosomensegregation bis hin zum intrazellulären Transport ganzer Organellen oder Vesikel ist eine Vielzahl von Motorproteinen beteiligt.

Die Motorproteine Myosin VI und XXI sind in vielerlei Hinsicht besondere Motoren. Myosin VI ist das einzige bislang bekannte Myosin, welches sich rückwärts in Richtung des Minus-Endes der Aktinfilamente bewegt. Ubiquitär exprimiert ist es an einer Vielzahl von Aufgaben in der Zelle beteiligt wie z.B. der Exo- und Endozytose sowie der Autophagozytose. Ein Mangel oder eine Fehlfunktion von Myosin VI können unter anderem zu Hörverlust und sekretorischer Diarrhoe führen, wohingegen bei bestimmten Prostata- und Ovarialkarzinomen eine Überexpression dieses Motors in betroffenen Zellen gemessen wurde. Myosin XXI ist ein in der Literatur neu beschriebenes Myosin, das soweit bekannt, das einzige exprimierte Myosin im Parasiten *Leishmania sp*. ist. Es erfüllt im Parasiten alle Aufgaben, die in anderen Zellen meist verschiedene Myosinklassen übernehmen. Folglich stellt es wahrscheinlich einen ebenso vielseitigen Motor wie Myosin VI dar. Wird die Expression von Myosin XXI unterdrückt, folgen daraus Schädigungen der Struktur des Flagellums und Beeinträchtigungen des intrazellulären Transports. Beide Myosine, VI und XXI, interagieren direkt mit Lipiden. Myosin VI bleibt, obwohl strukturell mittels einer coiled-coil (Doppelwendel) Region im C-terminalen Schwanz zur Dimerisierung befähigt, unter den bislang bekannten Bedingungen monomerisch. Unter bestimmten Voraussetzungen faltet sich der C-terminale Schwanz auf den N-terminalen Schwanzanteil zurück und nimmt ihm die Möglichkeit an Lipide zu binden.

Ziel dieser Arbeit ist es, ein tieferes Verständnis der Bindung von Myosinen an Lipide und Lipid-Vesikel (lipid cargo) zu erlangen. Es ist wichtig zu verstehen, wo und wie die verschiedenen Lipide in der Schwanzregion des Myosinmotors binden. Die Fähigkeit der Myosine selbst verschiedene Transportgüter zu binden, ist bislang kaum verstanden, sie stellt jedoch einen wesentlichen Bestandteil der spezifischen Funktion der Myosine in

Zellen dar. Die Myosinmotoren müssen, um ihre Aufgaben in der Zelle erfüllen zu können, spezifisch mit ihrem jeweiligen Transportgut interagieren, um es durch das dichte und komplexe Netzwerk der Zelle zum Bestimmungsort transportieren zu können. Die Bindung an Cargo ist mit den mechanischen Eigenschaften des Motors verknüpft, um einer sonst möglicherweise resultierenden Energieverschwendung (ATP-Hydrolyse) vorzubeugen. Das Erfassen, wie die beiden Prozesse Bindung und Motilität miteinander verknüpft sind, ist entscheidend für das Verständnis der Regulation der Motoren.

Als Methoden zur Untersuchung der Bindung an Lipide und der Analyse der regulatorischen Mechanismen für die Lipidbindung werden Western-, Far-Western und Dot-Western-Blots sowie Gleitfilament-Versuche (motility assays), Ko-Sedimentationen und Affinitätstitrationen angewendet. ATPase-Versuche geben Aufschluss über die Aktivität der Motorproteine.

Ein wesentliches Ergebnis dieser Arbeit ist, dass Myosin VI nicht ausschließlich über ein schon bekanntes Sequenzmotiv im C-terminalen Schwanz an ein bestimmtes Phosphatidylinositolphosphat (PIP) bindet, sondern das es, wie Myosin XXI auch, mit einer Reihe von Lipiden auf der gesamten Länge des Schwanzes interagieren kann. Die Lipidbindung ist nicht stereospezifisch, sondern beruht auf unspezifischen elektrostatischen Protein-Lipid-Wechselwirkungen. Calcium spielt dabei eine regulatorische bzw. co-regulatorische Rolle, indem es die Interaktion unterbricht oder verbessert. Die *in vitro* Gleitfilament-Versuche auf Lipidoberflächen zeigen für beide Myosine, VI und XXI, dass die Translokation von Aktinfilamenten schneller und mit einer höheren Bindungsaffinität zum Untergrund stattfindet als ohne Lipide. Ferner wird für Myosin VI gezeigt, dass die Rückfaltung des C-terminalen Teils des Schwanzes in Richtung Motor eine Interaktion der ersten 65 N-terminalen Aminosäuren mit der Cargo-bindenden Domäne darstellt. Da Calcium diese Interaktion verändert, ist eine Beteiligung der in der Halsregion des Proteins gebundenen Calmoduline wahrscheinlich. Für Myosin XXI wurde eine phox homology (PX) Domäne in der Converter Region gefunden, die spezifisch an $PI(3,5)P_2$ bindet. Myosin XXI kann entweder dimerisieren oder Lipide binden.

Die Fähigkeit von Myosin VI verschiedene Lipide auf der gesamten Länge seines Schwanzes zu binden, erlaubt dem Motor die Aufgabe des Transports innerhalb der Zelle flexibel auszuführen und das Transportgut schnell austauschen oder abladen zu können.

Die Unterschiede in den Affinitäten und Bindungen von Myosin VI an PIP zeigen die Vielfältigkeit dieses Transporters auf. Da Calcium die Wechselwirkung zwischen dem N-terminalen Calmodulin und dem darauf zurückgefalteten C-terminalen Schwanz unterbricht, spielt es eine Rolle bei der Aktivierung und Inaktivierung von Myosin VI. Die gefundene PX Domäne im Nackenbereich von Myosin XXI und dessen Fähigkeit zwischen der dimeren nicht lipid-bindenden Form und der monomeren lipid-bindenden Form umschalten zu können, verdeutlicht die Wandlungsfähigkeit dieses Motors und gibt einen Einblick in seine zahlreichen noch weitgehend unbekannten zellulären Aufgaben in Leishmanien.

Contents

Figures

Introduction

Material and Methods

Tables

Abbreviations

AB	assay buffer
AB+	assay buffer including ATP
ACEX	actin extraction buffer
ADP	adenosine diphosphate
APS	ammonium persulphate
ATP	adenosine triphosphate
BSA	bovine serum albumin
CK	creatine kinase
CP	creatine phosphate
DAG	diacylglycerol
H_20dd	double deionised water
DTT	dithiothreitol
E64	trans-epoxysuccinyl-L-leucylamido(4-guanidino)butane
EDTA	ethylenediaminetetraacetic acid
EGTA	ethylene glycol tetraacetic acid
ELC	essential light chain
F-actin	filamentous-actin
FL	full-length protein
FPLC	fast performance liquid chromatography
g	grams or gravity
G-actin	globular (monomeric) actin
HMM	heavy meromyosin
HPLC	high performance liquid chromatography
IPTG	isopropyl-β-D-thiogalactopyranoside
IQ	light chain binding motif
kb	kilobases
kd	dissociation constant
kDa	kilo-Daltons
k rpm	thousands of rotations per minute
LMM	light meromyosin
M	molar
µg	micrograms
mg	milligrams
min	min
µl	microlitre
ml	milliliter
mM	millimolar
mm	millimetres
µm	micrometre
µs	microseconds
ms	milliseconds
N	number of filaments
NEM	N-ethylmaleimide
ng	nanograms
nm	nanometres
OD	optical density
PBS	phosphate buffered saline
PC	phosphatidylcholine

PE	phosphatidylethanolamine
PH	pleckstrin homology domain
P_i	inorganic phosphate
PIP	phosphatidylinositol
PIP_2/ $PI(4,5)P_2$	4,5-Phosphatidylinositol-bisphosphate
PI(4)P	phosphatidylinositol-4-phosphate
$PI(3,5)P_2$	3,5-Phosphatidylinositol-bisphosphate
RhPh	rhodamine phalloidin
RLC	regulatory light chains
Papain S1	myosin subfragment 1 (produced by papain digestion)
SD	standard deviation
SDS	sodium dodecyl sulphate
SDS-PAGE	sodium dodecyl sulphate polyacrylamide gel electrophoresis
TBST	tris buffered saline with Tween 20
TEMED	tetramethylethylenediamine
v	velocity
v/v	volume per volume
w/v	weight per volume

Introduction

1.1 The cytoskeleton and its motor proteins

With progression past the single-cell state cellular motility becomes essential and is required for almost all the cellular processes that accomplish life itself. Wherever exact positioning is necessary, active motility is needed and outperforms diffusion. Accumulation of immune cells at sites of infection, active movements within a cell that provide nourishment of distal parts in nerve or plant cells or muscle contraction are only a few examples were active motility is indispensable. Intracellular cargoes are moved over short distances along actin filaments and over long distances along microtubules to reach their destinations. Most of these intracellular movements are accomplished by motor proteins, small nano-scale machines. These motor proteins convert chemical energy (ATP) into mechanical energy and take nanometre steps along their tracks to transport cargo from one location inside the cell to another. The motor proteins that move along actin filaments are known as myosins and transport along microtubules is mediated by kinesins and dyneins (Langford 1995). In addition, these molecular motors are specialized regarding their directional movement along their appropriate track. While the majority of kinesin motors move towards the plus end of microtubules, all dyneins exhibit minus end directed movements on the microtubule. With the exception of myosin VI, which moves toward the minus end, all myosins described to date perform plus end directed movement on actin filaments (Buss and Kendrick-Jones 2007).

1.1.1 Actin

The cytoskeleton is an interconnected network that resists deformation and is capable of transmitting mechanical forces and therefore provides support and organisation to cells. The three polymer classes are referred to as actin filaments, microtubules and intermediate filaments and are composed of specific protein subunits. In this thesis, actin filaments and associated transport proteins stand in focus and are therefore described here in more detail. Globular actin (G-actin) is the most abundant protein in eukaryotic cells (1-10% of all cellular protein) it has a size of 42 kDa and a diameter of approximately 5 nm (Kabsch *et al.* 1990). In muscle cells about 10% of all protein is actin. The actin concentration in non-muscle cells is approximately 0.5 mM. Filamentous actin (F-actin; approx. 8 nm in diameter) consists of G-actin subunits polymerised to form polar, helical filaments in which subunits are connected by a 167° rotation and 2.7 nm axial rise (Holmes *et al* 1990). The pitch of the helical turn is approximately 36 nm long and

consists of 13 monomers. The G-Actin subunit consists of two lobes with an adenosine triphosphate (ATP) and Mg^{2+}-binding cleft (see figure 1A) where the former is hydrolysed to ADP and phosphate. G-Actin is only functional with ATP or ADP bound, in cells the ATP-bound form is predominant. Ions (Mg^{2+}, K^+ or Na^+) induce polymerisation. This process is reversible and F-actin is depolymerised as soon as the ion concentration in solution is reduced to a critical concentration. Filaments grow in both a minus- and a plus-direction but polymerisation in the plus direction happens faster due to the asymmetry of the monomers. The attachment and detachment rates of actin monomers to F-actin polymers are different at either end, giving rise to a process known as treadmilling (figure 1C) (Small 1995). The rate of treadmilling is $r = k_+^B(C_{SS} - C_C^B) = k_+^P(C_C^P - C_{SS})$ where k_+^B and k_+^P forward rate constants for association of G-actin to the barbed (+) and pointed (-) end, and C_C^B and C_C^P the corresponding critical concentrations. For pure actin C_{SS} = 0.1 mM, C_C^P= 0.6 μM, k_+^B= 10 μM $^{-1}$ s^{-1}, k_+^P= 0.6 μM $^{-1}$ s^{-1} and r= 0.3 s^{-1}. Within the cell F-actin does not exist in isolation, two kinds of proteins regulate treadmilling: actin depolymerising factor or cofilin and capping proteins such as gelsolin (Pantaloni *et al.* 2001, Schmoller *et al.* 2011).

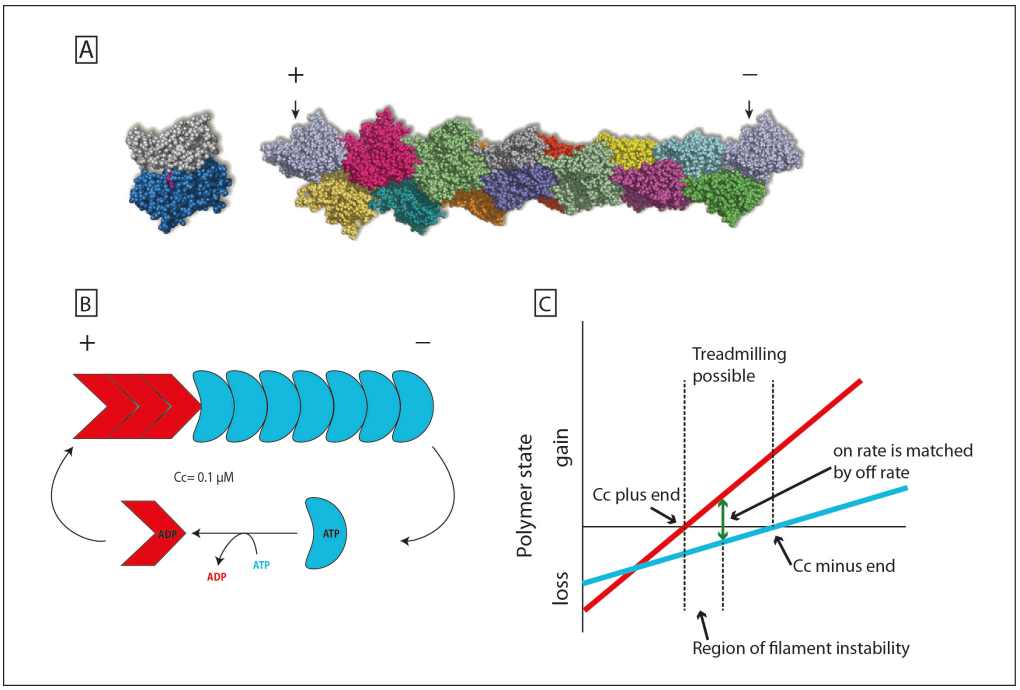

Figure 1: **Actin structure and treadmilling. (A):** Structure of the actin monomer (G-actin) (Holmes *et al.* 1990) with its two similar domains (grey and blue). And F-actin helix; each repeat contains 13 molecules so that the first molecule of each repeat is in identical orientation (arrows) (Holmes 2009). **(B):** Intrinsic treadmilling of actin filaments represents the energetic imbalance between the plus and the minus end. **(C)** shows the polymer state as a function of the concentration of protein present. In polymerising conditions no polymer is observed until the monomer concentration exceeds that of the critical concentration (C_c) of the plus end. However the filament formed would not be stable until after the point indicated above, where the off rate at the minus end equals that of the plus end (adapted from Pantaloni *et al.* (2001)).

F-actin is both flexible and strong with a persistence length of approximately 15 μm; it builds up a cytoskeletal transport as well as a motility system, which is present in all eukaryotes. A further function of actin was discovered in *Listeria* bacteria where plus ends of the actin are inserted in the leading edge of the lamellipodia where they are growing whilst the minus ends of the filaments are depolymerised at the rear in a treadmilling process (see figure 1C) (Loisel *et al.* 1999). During further studies it was revealed that the process of actin assembly and disassembly is the driving force for *Listeria* movements (Pantaloni *et al.* 2001). Studies support the thesis that in eukaryotes the plus ends of actin are inserted in or near the plasma membrane and at intracellular organelles such as the Golgi or the phagosome and that the minus ends reach into the cytosol (Geeves *et al.* 1980, Yengo and Sweeney 2004). The actin cytoskeleton complements and interacts physically with cytoskeletal structures composed of microtubules and intermediate filaments (Hartman and Spudich 2012).

1.1.2 Myosin

In this study the focus will be myosins which are a large superfamily of structurally diverse yet conserved actin based molecular motors. Myosins are actin-activated Mg^{2+}-ATPases that use the chemical energy derived from ATP hydrolysis to move along actin tracks (Lymn and Taylor 1971). There are known to be 47 myosin classes (Foth *et al.* 2006, Odronitz and Kollmar 2007, CyMoBase 2013) (see figure 2), whose classification is based on the amino-acid sequence of the globular motor domain. This motor domain remains highly conserved across the whole family with variations in velocity, direction of movement and processivity. Through the different kingdoms myosins perform a large variety of functions and are involved in a number of cellular pathways. They play fundamental roles in the cell, such as cell crawling, cytokinesis, maintenance of cell shape, phagocytosis, vesicle trafficking, growth cone extension, signal transduction and possibly even actin polymerization (Berg *et al.* 2001). The myosin superfamily is highly conserved and its members are defined by a collective structural design: a heavy chain with a conserved catalytic domain (~80 kDa) which is normally followed by an α-helical light-chain binding neck region which is capable of binding up to 6 calmodulins or calmodulin-like proteins; a C-terminal tail and/or N-terminal extension with class-specific properties such as binding-partner interactions, lipid binding or kinase-activity. The functions of the three conserved regions motor, neck and tail can be summarized as follows. The motor binds to F-actin filaments and is capable of

hydrolysing ATP to produce force and movement, the neck domain which acts as a lever arm that amplifies the movement generated by the motor domain. The lever arm is stabilised by different myosin light chains (or calmodulin) that also have regulatory functions and form part of the macromolecular complex. This neck domain typically consists of one or more IQ-motifs (consensus sequence IQxxxRGxxxR, ~24 amino acids (Cheney and Mooseker 1992)) that serve as binding sites for calmodulins. The tail is thought to have regulatory functions, and often binds different cargoes either directly or via binding partners. All myosins known to date move from the minus end of the actin filament towards the plus end. Myosin VI, on which this study focuses, is the only known minus end directed myosin and therefore serves in a different range of tasks in cells than plus end directed myosins (see section 1.4) (Buss and Kendrick-Jones 2007).

Since muscle-myosin II was the first myosin to be described, it is known as 'conventional', the subsequent discovery and description of different non-muscle myosins are therefore termed 'unconventional'.

The importance of unconventional myosins can be seen when looking at the genome of *Drosophila melanogaster* where 11 out of 13 myosin encoding genes are unconventional. Approximately two thirds of the myosin genes in humans encode for unconventional myosins (Berg *et al.* 2001). Additionally it can be seen as a general rule that the more complicated the organism the greater the number of myosin isoforms it contains. For example *Saccharomyces cerevisiae* contain three myosin families (I, II and V), whereas *C. elegans* encodes seven (I, II, V, VI, VII, IX and XII). Analysis of the human genome revealed 39 different genes coding for representatives from 12 different families (I, II, III, V, VI, VII, IX, X, XV, XVI, XVIII and an unclassified novel short-tailed myosin) (Berg *et al.* 2001).

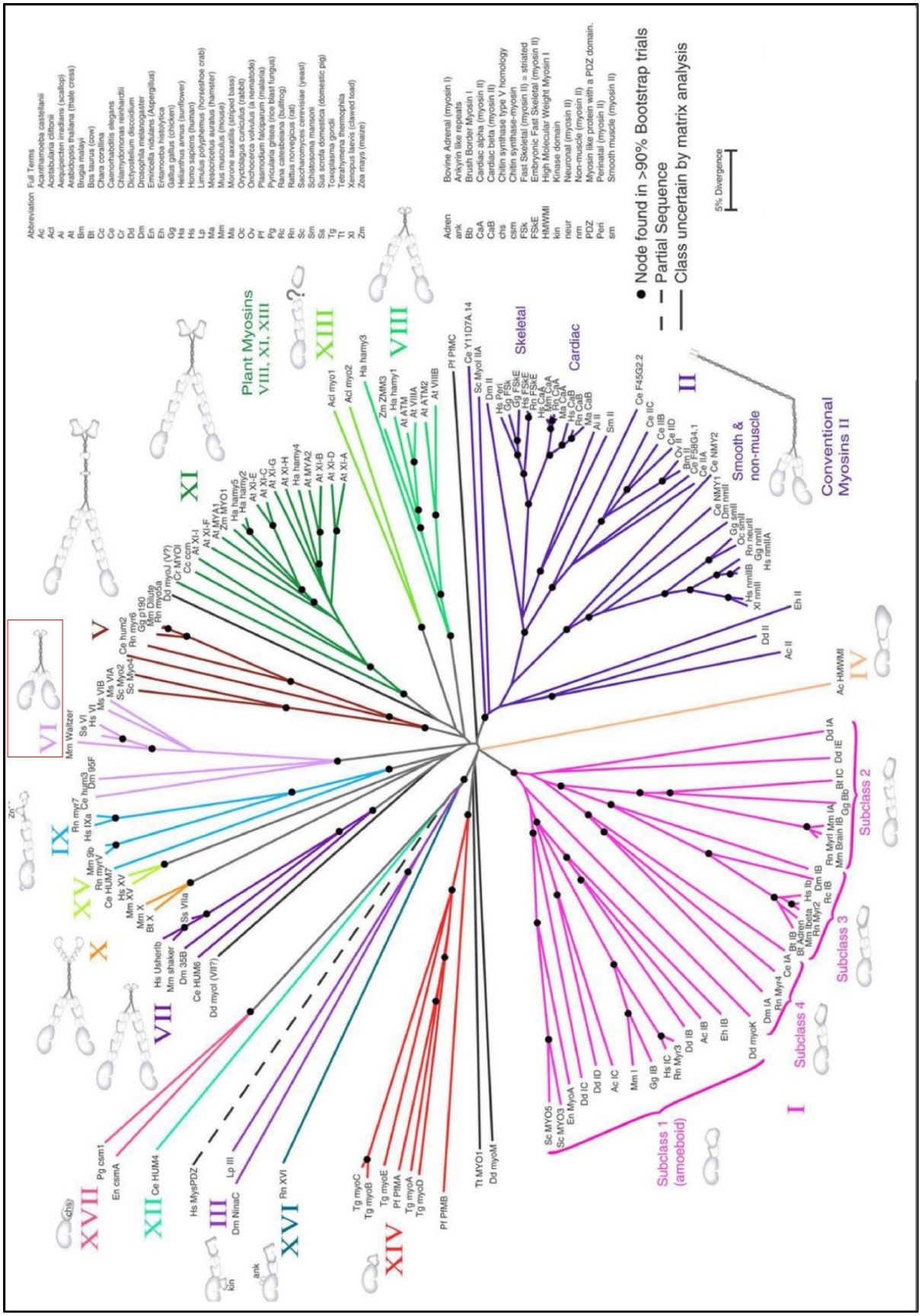

Figure 2: An unrooted phylogenetic tree of the myosin superfamily (Hodge and Cope 2000). Note that myosin VI is depicted as a dimer.

1.2 Skeletal muscle myosin II

Muscle cells have evolved to perform a highly specialised task, contraction. The contractile unit of skeletal muscle is the sarcomere. Myosin II is one of the two main proteins in the sarcomere. It was named by Wilhelm Kühne (1864) who described a muscle protein ("myo") he isolated by saline extraction. The second main type of protein in the sarcomere is actin (Straub 1943), which is described in more detail in chapter 1.1. Each sarcomere consists of interwoven myosin containing thick filaments and actin containing thin filaments. The plus ends of the actin filaments are anchored in the Z-disc's scaffold-like structure which forms the boundaries of the sarcomere in the middle of the sarcomere a zone of overlapping thick and thin filaments forms the AI zone (Hanson and Huxley 1953). Many other proteins are located in the sarcomere and are responsible for the structural integrity and the regulation of muscle contraction. Myosin II is a double-headed myosin with a molecular weight of 520 kDa which is susceptible to proteolysis that results in HMM and LMM fragments or a further HMM digestion to S1 and S2 (figure 3D). In skeletal muscle, myosin II tails form a thick filament from which the myosin heads project at regular angles (3 per crown, in vertebrate muscle every 145 Å, figure 3B and C). Therefore each thick filament can interact with the six thin filaments arranged around it. Figure 3A depicts how the thick filament is bipolar resulting in a bare zone in the middle of the filament devoid of myosin heads where the two bipolar filaments meet. This central zone is anchored to the centre of the sarcomere by proteins of the M-line. As described above, the thin actin filaments are fixed at both Z-discs and extend towards the middle of the sarcomere overlapping with the thick filaments as far as the central bare zone where the minus ("pointed") end of the actin filament is capped and regulated by tropomodulin (Bagshaw 1993).

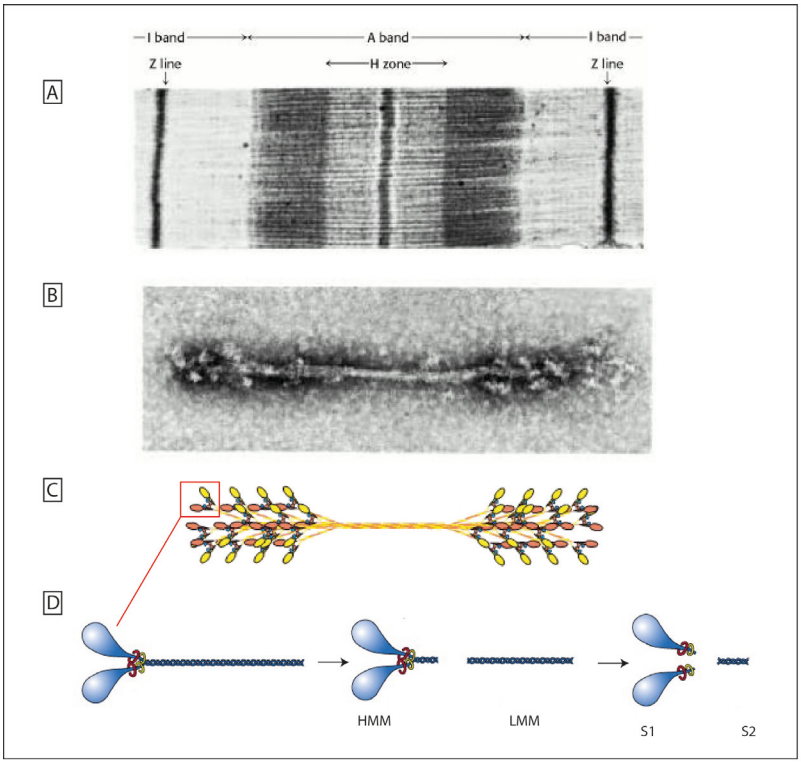

Figure 3: Striated muscle structure and myosin II thick filament. A: Electron micrograph of a longitudinal section of a skeletal muscle myofibril representing a single sarcomere. **B:** electron micrograph of a reconstituted thick filament showing the bare zone in the middle. **C:** schematic representation of (**B**).(modified after Berg *et al.* (2012)). D: representation of a single myosin II molecule and the different functional fragments it can be digested to.

1.2.1 Sliding filament model

The sliding filament model (figure 4) describes the process of muscle contraction in more detail. Activation of the interwoven thin and thick filaments produces muscle contraction. The thick filaments move towards the Z-disc which results in the thick filaments sliding past each other. While the length of the filaments remains the same the sarcomere shortens. This causes muscle contraction (Gordon *et al.* 1966). Muscles can only shorten actively, so that the relaxed muscle must be extended by the contraction of an antagonistic muscle.

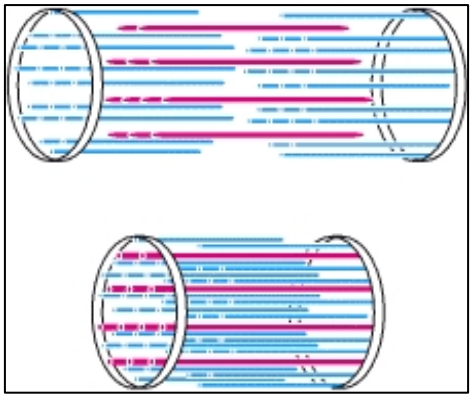

Figure 4: Sliding filament model. The thin filaments (blue) move relative to the thick filaments (red) and thus create muscle contraction. (Berg *et al.* 2012)

1.2.2 Swinging lever arm hypothesis

The interaction of individual myosin heads with actin units creates the sliding force that gives rise to muscle contraction.

The molecular mechanism of muscle contraction was for a long time seen as 'cross bridge hypothesis' (see figure 5A) in which the relative sliding of the thick and thin filaments in striated muscle is accomplished by the 'cross bridges', parts of the myosin molecules that protrude from the thick filaments and interact cyclically with the actin filaments, creating a rowing action that is powered by ATP-hydrolysis (Holmes 1997). This hypothesis gave a good insight into the whole muscle-contraction cycle but left out the molecular details of the actual movement of the cross bridge. This was largely based on electron microscopy (EM) studies by Hugh E. Huxley (1969). Today the swinging lever arm hypothesis has elucidated these missing aspects (figure 5B). It is a modification of the 'rocking cross bridge'-model which was put forward by Andrew F. Huxley and Robert Simmons (1971), and was based on mechanical experiments on muscle fibres. This again was a modification of the former model by Andrew F. Huxley (1957) which was entirely based on mechanical studies, still lacking the crystal structure of myosin.

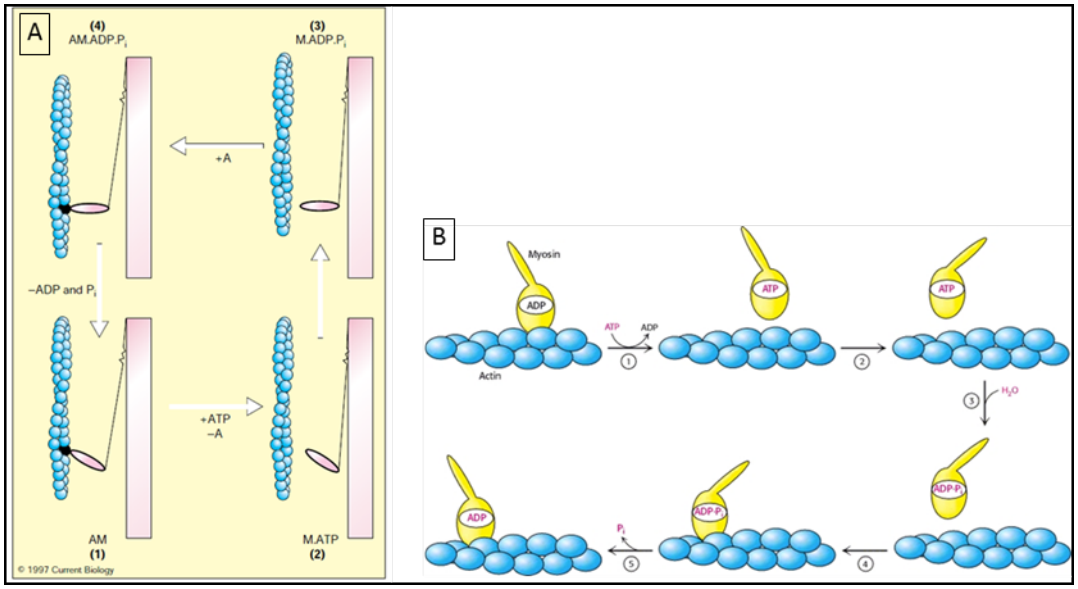

Figure 5: Swinging cross bridge model versus swinging lever arm model. (A): The myosin cross bridges are shown in their conventional conformations at 90° and 45° to the actin filament. Initially the nucleotide-free cross bridge is bound to the actin filament in the 45° conformation (state 1, rigor). The binding of ATP brings about rapid release from actin of the cross bridge (state 2), still in the 45° position. The subsequent hydrolysis of ATP puts the cross bridge into the 90° conformation (state 3), whereupon it rebinds to actin (state 4). The binding to actin brings about the release of products of hydrolysis and the cross bridge returns to its initial state, thereby 'rowing' the actin past the myosin. **(B):** A myosin head (yellow) in the ADP form is bound to an actin filament (blue). The exchange of ADP for ATP results in (1) the release of myosin from actin and (2) substantial reorientation of the lever arm of myosin. Hydrolysis of ATP (3) allows the myosin head to rebind at a site displaced along the actin filament (4). The release of P_i (5) accompanying this binding increases the strength of interaction between myosin and actin and resets the orientation of the lever arm (Uyeda *et al.* 1996, Berg *et al.* 2012).

The swinging lever arm model became more substantial with the obtained crystal structure of the myosin II molecule by Rayment *et al.* (1993). A key feature of myosin motors seems to be the lever arms ability to act as an amplifier of movement. The lever arm amplifies small structural changes at the nucleotide-binding site to accomplish the 110-Å movement along the actin filament that takes place in each ATP hydrolysis cycle (for the detailed ATPase cycle see section 1.3). A prediction of the mechanism proposed for the movement of myosin along actin is that the length travelled per cycle should depend on the length of this lever arm. Therefore the length of the lever arm should have an influence on the overall rate at which actin moves relative to the myosin heads. To test this prediction mutations of S1 fragments with different lever arm lengths were used (Uyeda *et al.* 1996). The lever arm was lengthened or shortened by adding or subtracting the light-chain-binding regions. *In vitro* motility assays then revealed that the speed of actin transport was linearly related to the number of light-chain binding-sites in the neck region of the S1 molecules (Uyeda *et al.* 1996, Holmes 1997) (figure 6). These *in vitro* studies of isolated myosin motors interacting with actin filaments were developed in the 1980s by Japanese and American laboratories (Yanagida *et al.* 1985, Umemoto and

Sellers 1990, Winkelmann *et al.* 1995), and revolutionised the studies of muscle mechanics and cell motility and paved the way for single molecule experiments.

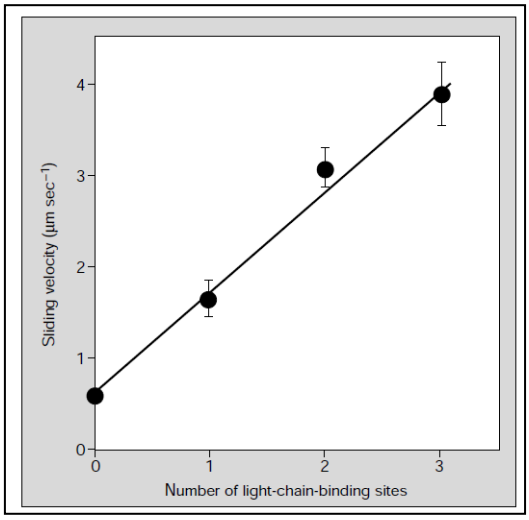

Figure 6: The speed of actin along a lawn of myosin heads as a function of the length of the S1 neck region. The observed speed is linearly related to the number of light-chain binding sites in the lever arm (Uyeda *et al.* 1996, Holmes 1997)

1.3 The myosin ATPase cycle

1.3.1 Chemomechanical transduction

There were 3 lines of evidence for the relation between biochemical, structural and mechanical states of the chemomechanical cross bridge cycle: (1) biochemical studies using solution kinetics, (2) structural studies using EM and crystallography and (3) mechanical studies using fibres and single molecule experiments. In landmark experiments these lines of evidence were pursued and helped complete the view of the chemomechanical coupling in myosins (Holmes 2005). Rayment *et al.* (1993) were able to investigate crystal structures of myosin in different nucleotide states albeit only in the absence of actin. With high-resolution cryo-electron microscopy it was possible to investigate myosin bound to actin (Milligan and Flicker 1986, Jontes *et al.* 1995, Whittaker *et al.* 1995) although only in rigor and ADP bound state. Finally fibre studies and single-molecule experiments allowed further insight into the mechanics of single molecules. Experiments with optical tweezers revealed a two-step working-stroke where two mechanical steps of the working stroke were linked to the transition between three biochemical states (Veigel *et al.* 1999, Veigel *et al.* 2002, Sellers and Veigel 2010) These

studies and the formerly mentioned EM studies proved and further developed the swinging lever arm hypothesis.

Myosin converts the chemical energy stored in ATP into directional movement on the actin filament by hydrolysation. In order to understand how this chemomechanical transduction works the following features need to be highlighted: (1) binding of different ligands (ATP or the products of ATP hydrolysis) induces different conformations in the nucleotide binding pocket of the myosin head, (2) a small conformational transition in the nucleotide pocket is amplified through rigid structural elements and appears as a large swinging movement of the head relative to the tail and (3) myosin exhibits different affinities for actin in different nucleotide states because the actin and nucleotide binding sites communicate with each other. Based on these principles, figure 7 represents a simplified flowchart of the motor cycle (Fischer *et al.* 2005). This model is an updated version of the chemomechanical model proposed by Lymn and Taylor (Lymn and Taylor 1971) and based on structural studies, i.e. EM, biochemical and mechanical studies (Huxley 1957, Huxley 1969, Huxley and Simmons 1971). The present diagram shows only the main flux pathway of the intricate mechanism.

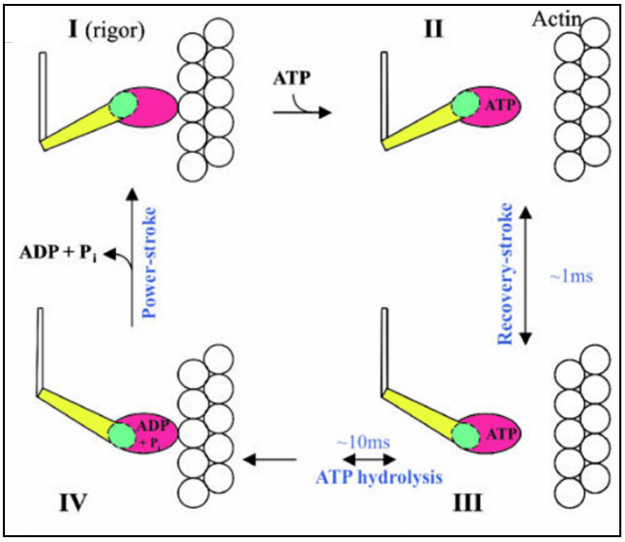

Figure 7: The actomyosin contraction cycle (Fischer *et al.* 2005) The myosin head fragment is represented in colors. Red: motor domain, Green: hinge, Yellow: lever arm or neck.

The upper left corner of figure 7 shows a "rigor" (nucleotide-free) actomyosin complex. Upon ATP binding the actin affinity of the myosin head decreases dramatically and the myosin rapidly releases actin (I-II). A reversible conformational transition follows (II-III). This is the "cocking" of the myosin. The resulting conformation (III) hydrolyses the bound ATP. After hydrolysis, the residual myosin-ADP+ P_i complex rebinds to actin (III-

IV). Finally, the products (P_i and then ADP) sequentially dissociate from the nucleotide binding site. Product dissociation is linked to the power-stroke, the directional pull on the actin filament. Although detailed biochemical data on the ATPase cycle and crystal structures of several conformational states are available the assignment of biochemical steps to the structural changes is ambiguous (Trentham *et al.* 1976, Murphy *et al.* 2001, Kovács *et al.* 2004, Paavilainen *et al.* 2008). For instance, one of the important points under debate is the relationship between the re-formation of the strong actin binding interaction, product release and the power stroke (Llinas *et al.* 2012).

Depending on the configuration of the motor (myosin) and the track (actin), the above demonstrated motor cycle leads to either contraction or transport. If the myosin is anchored by its tail it is the actin filament which is translocated upon movement of the myosin head. This is what happens in the muscle where thousands of anchored myosin molecules pull on each actin filament generating muscle contraction (see section 1.2.1). In another scenario actin is anchored (to the cytoskeleton) and the myosin power-stroke will displace the centre of mass of the myosin itself. This is the basis of intra-cellular transport.

1.3.2 Kinetics-processivity-duty ratio

A more detailed view on the biochemical scheme of myosin working reveals that every step is thermodynamically reversible. However, ATP-binding to the myosin head and P_i release afterwards, in the absence of external forces, keeps the cycle going predominantly in one direction. Although actin is an enzyme itself, it is traditionally considered as an activator or track throughout the actomyosin cycle since myosins can only interact with filamentous actin. Therefore, when characterizing a myosin actin is treated as a ligand. Binding of ATP to myosin is observed as a two-step process whereby a diffusion limited collision step is followed by a rapid isomerisation of the myosin head. ATP hydrolysis occurs mainly in the detached state and is reversible as measured with isotope labelled ATP or H_2O (Geeves *et al.* 1980). ATP binding to actomyosin at physiological ATP concentrations (2-5 mM) and the following, actin-detached hydrolysis step are both faster than the steady-state ATPase in all known myosins. Therefore the rate limiting step in the enzymatic cycle must be one of the product release steps. Whether this is the dissociation of P_i or ADP will determine the stepping behaviour of the motor. If the release of P_i is slow, the myosin head will spend most of its cycle time with the hydrolysis products bound ($AM.ADP.P_i$) in which state the myosin has a low affinity for actin (a so-called

"weak actin binding state"). This happens in low duty ratio myosins (duty ratio = strong actin attachment / lifetime of total cycle time). Fast P_i and slow ADP dissociation, however, will result in a relatively long-lived actomyosin-ADP state (a strong actin binding state). Myosins that have their kinetic bottle neck at the ADP release step are high duty ratio myosins that spend most of their cycle time strongly bound to actin (figure 8) (De La Cruz and Ostap 2004). Several examples of these myosins have been discovered (myosins V, VI, VII) and it became clear that their cellular role requires the kinetic feature of slow ADP release (Mehta *et al.* 1999, Rock *et al.* 2001, Yang *et al.* 2005). With two high duty ratio heads a myosin can "walk" a large number of steps on actin, without dissociating from the track. This property is called processivity. In the light of the kinetic features of duty ratio and processivity we can identify two major types of functional adaptation in myosins. The low duty ratio enables a large complex of motors to work together because the short actin attachment of each head imposes little drag on the others. Most conventional type II myosins belong to this category. Low duty ratio is a property of ensemble contractile systems such as muscles or the cytokinetic contractile ring.

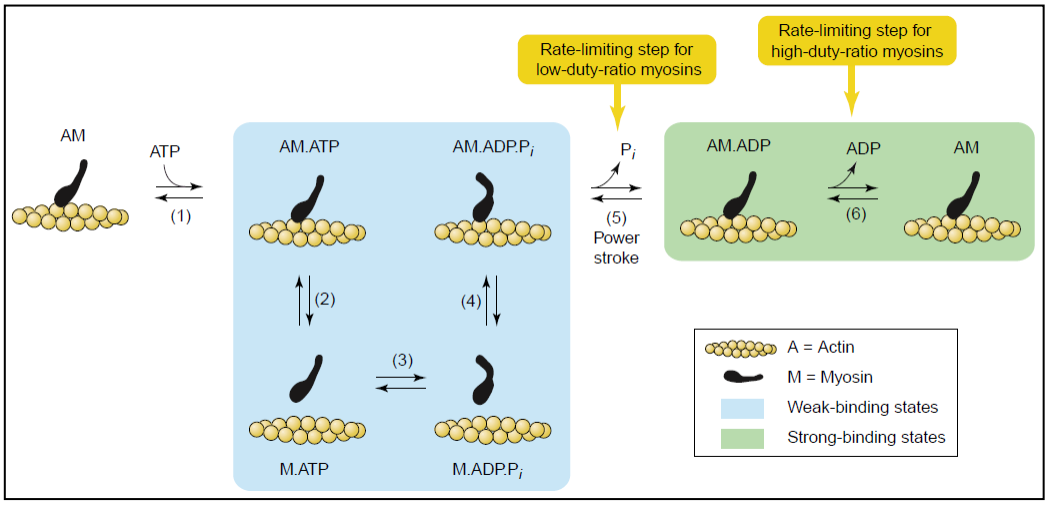

Figure 8: The actomyosin enzymatic cycle with focus on the rate-limiting step and its consequences (De La Cruz and Ostap 2004). Note the weak and strong actin binding states. Low duty ratio results from the fact that myosin dwells in the weak actin binding states whereas in high duty ratio myosins the cycle time is spent mostly in a strongly bound AM.ADP state.

High duty ratio, processive myosins on the other hand can typically perform intracellular transport with high efficiency as a double-headed molecule. They are able to carry their cargo long distances upon one diffusional encounter with an actin filament. Another cellular task often performed by high duty ratio myosins is tension bearing. Non-muscle myosin IIB performs this task within stress fibers by having a high duty ratio and a very

slow ATPase rate that leads to long lifetimes of the actin-attached states and efficient tension maintenance instead of contractility (Wang, Kovacs *et al.* 2003). Long lifetimes of the force-bearing intermediates are not a direct consequence of the high duty ratio but that of slow ADP release from actomyosin. A low duty ratio myosin with a very long ATPase cycle (slow motor) may assume long attachment periods and therefore is also suitable for tension maintenance. Myosin Ib belongs to this category and is a membrane motor that may be responsible for maintaining the structure and/or shape of different organelles. Finally, it is important to point out that processivity is an inherent property of every functional unit of molecular motors. Whether the unit consists of one, two, or hundreds of motors it is defined by the above discussed structural and kinetic parameters.

A very important aspect of processivity is mechanical gating. In a double-headed molecule, the fraction of the time spent strongly bound to actin must be above 0.5 for a single head as a prerequisite for processivity. Vertebrate myosin V satisfies this condition (Rosenfeld and Sweeney 2004). Additionally to the inherent kinetics of one head, communication (‘gating’) between the two heads of myosin V can increase duty ratio and processivity (Veigel *et al.* 2002, Veigel *et al.* 2005, Sellers and Veigel 2010).

1.4 Myosin VI

Myosin VI is a ubiquitously expressed unconventional myosin that has the unique ability to translocate towards the minus end of the actin filament. Structurally, like all myosins it consists of an N-terminal motor domain, which binds and hydrolyses ATP and can bind filamentous actin. The conversion of chemical energy (ATP hydrolysis) into mechanical energy is accomplished by conformational changes in the motor domain and then transmission through the converter region into a large movement of the lever arm. The unique insert of myosin VI between the converter region and the lever arm is the 'reverse gear' that enables it to move backwards. Stabilised by a calmodulin this reverse gear swings in the opposite direction to all other known myosins. The reverse movement of myosin VI is made possible by the rotation of the converter which is attached to the lever arm (made up of variable numbers of IQ-motifs) (Hasson and Mooseker 1994) that then amplifies the movements of the converter (Geeves and Holmes 1999, Houdusse and Sweeney 2001, Bahloul *et al.* 2004). The unique insert (see figure 9), which is located between the conventional IQ-motif and the converter, seems to be involved in altering the converter to reposition the lever arm and allowing therefore a minus end directed movement (Wells *et al.* 1999). A second calmodulin is reversibly bound to a more canonical IQ-motif in the neck region adjacent to the first IQ (Bahloul *et al.* 2004). Additionally myosin VI exhibits an intriguingly large working stroke (18 nm) as monomer (Lister *et al.* 2004) and step size of 30-36 nm length (as enforced dimer) similar in size to those of myosin V (Rock *et al.* 2001, Veigel *et al.* 2002, Rock *et al.* 2005, Veigel *et al.* 2005) despite the lever arm was expected to be shorter than that of myosin V which binds six calmodulins to its neck region in contrast to two in myosin VI, as proposed by Bahloul *et al.* (2004). Therefore other structures might contribute to the effective lever (Lister *et al.* 2004). The region immediately following the IQ-motif (proximal tail) was proposed as candidate for being the flexible element responsible for the large step size (Rock *et al.* 2005). Recent findings suggest that in the C-terminal tail a central single α-helix (SAH) domain exists (Peckham 2011) which is followed by the globular cargo-binding domain that exhibits lipid binding as well as interactions with different binding and interaction partners. This single α-helix was suggested to give mechanical stability to extend the lever arm and thus helping to explain how the large working stroke is made possible. Another theory was that the myosin VI lever arm was

achieving the relatively large step size not by extending the lever arm but by changing the angular swing to 180° (Lister *et al.* 2004).

Despite there being many studies presenting data for description of an artificial myosin VI dimer (Rock *et al.* 2001, Sweeney and Houdusse 2007, Ali *et al.* 2011, Bond, Arden *et al.* 2012), so far it has not been shown whether myosin VI acts as a monomer or dimer in cells or if it possibly switches between both states depending on the cell's requirements. It seems likely, given myosin VI's diverse roles in cells, that it is a 'flexible' motor protein (Buss and Kendrick-Jones 2007) that could function either as non-processive monomer or processive dimer depending on its localisation or target. Non-processive monomers would be sufficient for tethering vesicles to actin filaments or maintaining membrane tension. Processive dimers on the other hand would be more suitable for vesicle transport to diverse cellular compartments. A predicted coiled-coil α-helical region in the myosin VI tail (see figure 9) was long seen as an indication of myosin VI being dimeric (Rock *et al.* 2005). Lister *et al.* (2004) showed that endogenous myosin VI is almost entirely monomeric (< 1% dimeric) upon purification. As said above it was then suggested that the formerly predicted coiled-coil region more likely forms a single α-helix domain (Peckham 2011), i.e. a single α-helical domain that is stable in solution on its own without the necessity of stabilising calmodulins as in the lever arm of myosin II or myosin V. Nevertheless myosin VI might have the ability to function either as a monomer or a dimer. Binding to cargo or other ligands may induce and regulate dimerization (Spudich *et al.* 2007). Indeed it has been shown that binding to optineurin and Dab2 can induce dimerization (Phichith *et al.* 2009, Yu *et al.* 2009). It was discussed whether there is a dynamic transition between the inactive, folded, monomer state and as active, unfolded dimeric state when bound to clathrin-coated vesicles via Dab2 (Buss *et al.* 2004, Lister *et al.* 2004, Spink *et al.* 2008).

As mentioned in chapter 1.1.1 the plus ends of actin filaments are inserted in or near the plasma membrane and at intracellular organelles such as the Golgi or the phagosome while the minus ends reach into the cytosol (Geeves *et al.* 1980, Yengo and Sweeney 2004). This and the fact that myosin VI is a minus end directed motor gives an indication for a completely different set of tasks in the cell. Myosin VI performs various roles in the cell: it clusters and transports transmembrane receptors in the area of a clathrin-coated pit, transports internalised vesicles away from the cell surface during endocytosis, stabilizes actin during spermatid individualisation (Tumbarello *et al.* 2013), facilitates movement of

vesicles through the peripheral actin cytoskeleton towards the early endosome and/or regulates a signalling platform for newly endocytosed receptors (Aschenbrenner *et al.* 2003). Additionally myosin VI functions in the exocytic pathway as well and helps to maintain Golgi morphology and facilitates the fusion of secretory vesicles at the plasma membrane (Sahlender *et al.* 2005, Bond *et al.* 2011). The role of myosin VI as a short-range transporter is supported by its relatively slow speed (ca. 30-60 nm/s) as measured in the *in vitro* motility assay.

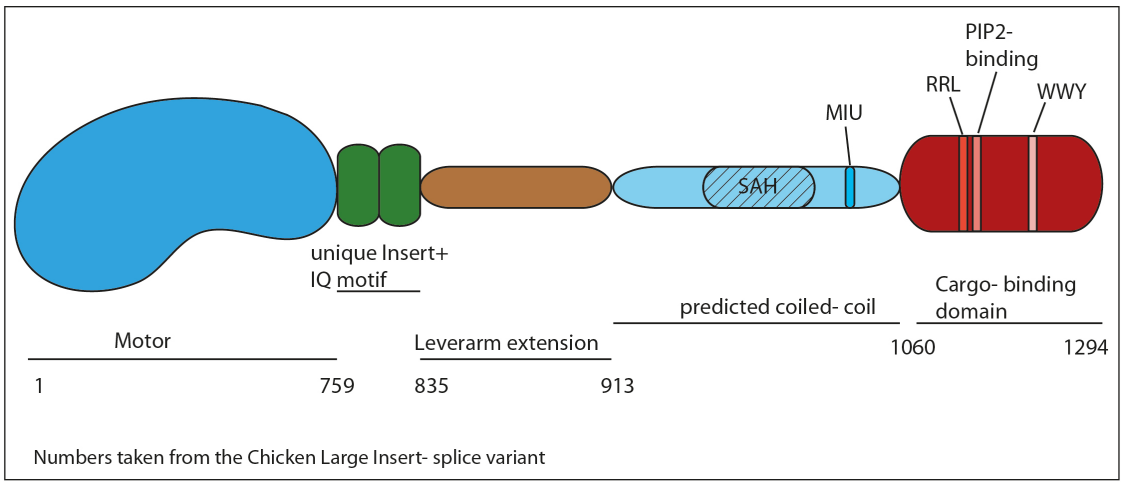

Figure 9: Myosin VI full-length protein. Myosin VI Chicken full-length protein with motor domain, Calmodulin binding unique insert, IQ-motif, lever arm extension, predicted coiled coil region with Single-α-helix (SAH) and the globular cargo-binding domain. Numbers denominate amino acids (taken from sequence of chicken full-length sequence, large-insert splice-variant). MIU: Motif Interacting with Ubiquitin, RRL: binding motif for binding partners such as NDP52, optineurin and GIPC; WWY: binding motif for binding partners as Dab2, Tom1 and LMTK1. PIP_2-binding: binding site for binding of $PI(4,5)P_2$ (Spudich *et al.* 2007).

1.4.1 Myosin VI and endocytosis

Myosin VI is expressed as a number of different splice variants, as first described in *Drosophila* (Millar and Geeves 1983). Cremo and Geeves (1998) identified myosin VI isoforms containing either a large 13 or 17 amino acid (aa) insert or a small 9 aa insert in the C-terminal tail in the striped bass (*Morone saxatilis*). In human and other mammalian tissues a tissue-specific expression of splice variants of myosin VI containing a large, a small or no insert in their tails can be found (Buss *et al.* 2001).

The isoforms containing the large insert (LI) and no insert (NI) provide the faculty for function in at least two different stages of the endocytic pathway because the isoforms target at different intracellular interfaces (Tumbarello *et al.* 2013). Myosin VI LI is linked to clathrin-mediated receptor endocytosis and degradation, whereas the NI splice variant is coupled with a subpopulation of early endosomes under the plasma membrane. This

process is mediated through binding to GIPC and Tom1. GIPC promotes backwards movement of endosomes through the peripheral actin cytoskeleton to the early endosome (Aschenbrenner *et al.* 2003). According to Arden *et al.* (2007), myosin VI and GIPC are recruited to the cleavage furrow in dividing cells and are required during cytokinesis.

1.4.2 Myosin VI and exocytosis

Exocytosis can be divided into two different pathways: constitutive secretion and regulated secretion. During constitutive secretion proteins synthesised on ribosomes of the ER are transported in carriers to the Golgi complex where they are processed and sorted for further transport to the plasma membrane for immediate release from the cell. The proteins on the regulated secretion pathway are transported on the same route from ER to Golgi to plasma membrane but are then stored in either neuronal synaptic vesicles or secretory granules. Instead of releasing their contents immediately, these carriers remain near the plasma membrane until the release is triggered by a specific intracellular signal or ligand (e.g. change in Ca^{2+} ion concentration) (Zucker 1996).

By targeting proteins to one pathway or the other, the cell can carefully control rates and levels of secretion into the extracellular environment.

The final steps of the secretory pathway can be divided into four stages: (1) approach of vesicles/granules to plasma membrane, (2) docking of these vesicles/granules to the plasma membrane, (3) priming for the fusion process and (4) fusion with the plasma membrane to release contents from the cell (Bond *et al.* 2011). Throughout these stages constant remodelling and reshaping of the cortical actin network plays a key role. To let secretory vesicles through this dense barrier during regulated secretion, a constant reorganisation and partial disassembly of the cross-linked actin network underneath the plasma membrane is important. In many cell types complete depolymerisation of actin filaments inhibits secretion (Bond *et al.* 2011). Therefore actin filaments seem to provide the tracks for transport of secretory carriers through the network.

Myosin VI interacts with its binding partner optineurin and seems to be a control point for regulation of the dynamics of the fusion pore formation at the plasma membrane (Bond *et al.* 2011). It has been suggested that myosin VI might provide the tension/force that is necessary to stabilize or open the fusion pore by moving towards the minus end of the actin filament (Bond *et al.* 2011) and the small-insert splice variant tethers secretory

granules to the cortical actin (Tomatis *et al.* 2013). Another recent discovery highlights a similar role for myosin VI in the regulated secretion where it interacts with otoferlin, an endocytic calcium sensor which directly regulates SNARE-mediated membrane fusion in auditory hair cells (Dulon *et al.* 2009, Roux *et al.* 2009).

1.4.3 Myosin VI and autophagy

Autophagy is the basic lysosomal degradation pathway that involves all deterioration of unnecessary or dysfunctional cellular components through fusion of double-membrane autophagosomes which deliver their contents to lysosomes for decomposition. The membranes needed for autophagosome expansion and maturation may be derived from the plasma membrane, ER, Golgi complex, mitochondria and endosomes (Razi *et al.* 2009, Ravikumar *et al.* 2010). Through binding to the autophagy related partners NDP52, optineurin, Tom1 and T6BP myosin VI is involved in targeting of ubiquitylated cargo and autophagy-related degradation (Morriswood *et al.* 2007, Tumbarello *et al.* 2012, Tumbarello *et al.* 2013).

1.4.4 Myosin VI pathogenies

Since myosin VI is involved in so many aspects of the endo- and exocytic pathways as well as autophagy, it is quite obvious that a loss of function or changes in expression patterns must result in more or less severe changes in cell health and maintenance.

Studies on the *Snell's waltzer* mice provided evidence for myosin VI's role in hearing. These mice have a mutation in the myo 6 gene and are deaf, other symptoms are hyperactivity, head-tossing and circling (Avraham *et al.* 1995). Histopathology of hair cells of the mutant mice showed a great dysmorphism: they do not contain stereocilia and degenerate about six weeks after birth (Avraham *et al.* 1995). The cuticular plate of the hair cells is an area with high membrane transporting activity, crucial for continuous stereocilia rebuilding, it is probable that a lack of functional myosin VI leads to the impairment of intracellular transport of vesicles and in consequence to the collapse of stereocilia and dysmorphology of hair cells (Redowicz 2002). In this mouse model it was revealed as well that myosin VI is essential for cystic fibrosis transmembrane conductance regulator endocytosis in enterocytes (Mehta *et al.* 1999). Defects of myosin VI in this pathway lead to secretory diarrhoea.

Myosin VI is an early marker of prostate and ovarian cancer development. It is required in border cell migration during *Drosophila* ovary development (Geisbrecht and Montell 2002). Yoshida *et al.* (2004) found that there is a functional link between myosin VI expression and aggressiveness of ovarian cancers. Myosin VI is abundantly expressed in high-grade ovarian carcinomas but not in indolently behaving ovary and ovarian carcinomas. Inhibiting myosin VI expression in high-grade ovarian carcinoma cells impedes cell spreading and migration *in vitro*. In prostate cancer similar overexpression levels have been reported but a correlation between aggressiveness of the cancer and myosin VI expression was not found (Dunn *et al.* 2006).

Myosin VI has also been linked to hypertrophic cardiomyopathy and neurodegeneration through reduction in endocytic uptake of AMPA receptors in hippocampal neurons (Osterweil *et al.* 2005, Yang *et al.* 2005)).

Little is known about the role of Myosin VI in the nervous system. It has already been established that the physiological loss-of-function of myosin VI is associated with astrogliosis in the brain, hypertrophic cardiomyopathy, defects in endocytosis in neuronal and epithelial tissues, disruption in the integrity of the intestinal brush border and various metabolic dysfunctions (Osterweil *et al.* 2005). Myosin VI is highly expressed throughout the brain, localized to synapses, and enriched at the postsynaptic density. Myosin VI deficient (*Snell's waltzer; sv/sv*) hippocampus exhibits a decrease in synapse number, abnormally short dendritic spines, and profound astrogliosis (Osterweil *et al.* 2005). Myosin VI contributes to synaptic transmission and development at the *Drosophila* neuromuscular junction (Kisiel *et al.* 2011). This study concludes that Myosin VI is important for proper synaptic function and morphology. Myosin VI may be functioning as an anchor to tether vesicles to the bouton periphery and, thereby, participating in the regulation of synaptic vesicle mobilization during synaptic transmission. It has recently been shown that myosin VI maintains exocytosis by tethering secretory granules (SG) to the cortical actin (Tomatis *et al.* 2013). The precise mechanism is unkown. Tomatis *et al.* (2013) have shown, using a secretory granule pull-down assay and mass spectrometry, that myosin VI is recruited to SGs in a Ca^{2+} dependent manner.

1.4.5 Myosin VI binding partners

Several binding partners are interacting with myosin VI, targeting it to different cellular destinations (figure 10).

1.4.5.1 NDP52 (Nuclear dot protein 52 kDa)

NDP52 (52 kDa) is a mainly cytosolic protein, which is highly similar to T6BP (see 1.4.6.3) in terms of structure and binding to myosin VI. Like T6BP it consists of an N-terminal SKICH domain, a coiled-coil region and a C-terminal zinc-finger arrangement (Morriswood *et al.* 2007). The zinc-finger domain interacts with ubiquitin and the SKICH domain with Nap1 (Ivanov and Roy 2009). The interaction with ubiquitin points at the involvement of NDP52 in the autophagy pathway. It binds to the RRL motif of myosin VI via its C-terminal zinc-finger like structure (Morriswood *et al.* 2007) and together they are localised on cytoplasmatic vesicles at the *trans* side of the Golgi. Interestingly NDP52 and T6BP can interact with each other and with myosin VI. These complexes may play a role in coordinating membrane transport pathways and cytokine signalling with actin filament organisation and cell adhesion (Morriswood *et al.* 2007).

1.4.5.2 Dab2 (Disabled homolog-2 / DOC-2)

Dab2 is a 96 kDa protein that contains various known signalling domains and motifs and is thought to be a specific adaptor for members of the Low Density Lipoprotein receptor (LDLR) family. With its N-terminal phosphotyrosine (PTB) domain it interacts not only with the LDLR receptor but as well with phosphoinositides such as PIP_2 (Mishra *et al.* 2002). Different interaction patterns are located in the central and C-terminal regions of Dab2. It binds to clathrin via the amino acid motif DPW, endocytic accessory proteins such as Eps15 (NPF) and myosin VI (SYF) (Morris and Cooper 2001, Morris *et al.* 2002). By acting as a cargo-specific adaptor protein Dab2 plays a key role in clathrin-mediated endocytosis, where it sorts and links membrane receptors to the endocytic machinery at the plasma membrane (Buss and Kendrick-Jones 2007). Spudich *et al.* (2007) revealed by alanine scanning mutagenesis that residues 1184 to 1186 (WWY) in the globular tail of myosin VI are the Dab2 binding site, whereas the amino acids SYF (682-684) in the C-terminal region of Dab2 are the myosin VI binding site (Morris *et al.* 2002). Since Dab2 and myosin VI colocalise in clathrin-coated pits and vesicles in the apical domain of polarised cells they seem potentially to be involved in the early stages of

clathrin-mediated endocytosis (Morris *et al.* 2002, Aschenbrenner *et al.* 2003, Spudich *et al.* 2007).

1.4.5.3 T6BP (Traf6-binding protein)

This 82 kDa protein is very similar to NDP52. It binds the RRL motif on the myosin VI cargo-binding tail via the two zinc-fingers (Morriswood *et al.* 2007).

1.4.5.4 GIPC (G-Alpha interacting protein C)

GIPC is a myosin VI interacting protein (Bunn *et al.* 1999) with a size of 36 kDa that binds to the RRL motif in the globular tail of myosin VI via its C-terminal domain (Reed *et al.* 2005, Spudich *et al.* 2007). Since GIPC interacts with a number of transmembrane receptors, it is possible that myosin VI and GIPC are involved in the endocytosis of these receptors (Gotthardt *et al.* 2000, Hu *et al.* 2003, Naccache *et al.* 2006). This theory is supported by the findings that myosin VI isoforms with no insert or small insert co-localise with GIPC in uncoated endocytic vesicles and seem to be involved in the movement through the actin filament network below the plasma membrane (Aschenbrenner *et al.* 2003, Dance *et al.* 2004).

1.4.5.5 SAP97 (synapse-associated protein 97)

SAP97 is a mammalian member of the MAGUK (membrane associated guanylate kinase) protein family that is expressed throughout the body in epithelial cells and in neurons. With its three PDZ domains, a SH3 domain and a region with a guanylate kinase like sequence (Fujita and Kurachi 2000), it interacts with diverse proteins. Interaction with myosin VI was shown as well by Wu *et al.* (2002), as it immunoprecipitates as a complex from neuronal cells with myosin VI and GluR1 (subunit of the α-amino-3-hydroxy-5-methyl-4-isoxazolepropionic acid receptor (AMPA)). In the Snell's waltzer mouse the number of synapses and dendritic spines is reduced as well as the internalisation of AMPA receptors (Osterweil *et al.* 2005, Nash *et al.* 2010). This led to the conclusion that myosin VI together with SAP97 appears to be involved in the clathrin-mediated recycling, endocytosis of AMPA receptors or in the exocytic transport of them to the cell surface. Furthermore myosin VI may link cell adhesion molecules such as E-cadherin and β-cadherin and SAP97 to the actin cytoskeleton at cell contact sites and may therefore have a role in membrane protrusion and cell adhesion (Buss and Kendrick-Jones 2007).

1.4.5.6 Optineurin

Optineurin is a 67 kDa protein with four predicted coiled-coil regions, two leucine zipper domains and a putative zinc-finger (Buss and Kendrick-Jones 2007). Optineurin binds to the myosin VI globular tail via the RRL motif (Sahlender *et al.* 2005). Interestingly phosphorylation of two threonine residues upstream of this site (T1089 and T1092) regulates the interaction between optineurin and myosin VI (Sahlender *et al.* 2005). In unpolarised cells optineurin and myosin VI co-localise at the *trans*-side of the Golgi complex and in vesicles right below the plasma membrane. In polarised cells on the other hand myosin VI and optineurin are both found on recycling endosomes where they are involved in cargo-sorting to the basolateral membrane (Au *et al.* 2007). Depletion of optineurin in unpolarised cells resulted in loss of myosin VI from the Golgi complex and the Golgi itself was fragmented and a reduction of secretion to the plasma membrane could be observed (Sahlender *et al.* 2005). Therefore optineurin and myosin VI, possibly together with Rab8 (Ras-related protein 8), are responsible for maintaining the Golgi structure and secretion from the Golgi to the plasma membrane.

1.4.5.7 LMTK2 (Lemur tyrosine kinase 2)

The transmembrane protein LMTK2 is a Ser/Thr specific protein kinase with a predicted N-terminal transmembrane sequence and a long C-terminal cytoplasmic tail domain. Several binding partners and potential substrates have been identified (Wang and Brautigan 2002) including myosin VI (Chibalina *et al.* 2007). LMTK2 is the first kinase and transmembrane protein known to bind directly to myosin VI. Chibalina *et al.* (2007) show not only that LMTK2 binds to myosin VI's WWY motif but also that both proteins are required for delivery of cargo such as transferrin from the early endosome to the endocytic recycling compartment. However, further roles of LMTK2 in the cell remain to be elucidated.

1.4.5.8 DOCK7 (dedicator of cytokinesis 7)

DOCK7, expressed mainly in neuronal cells, is a guanine nucleotide exchange factor (GEF) for small GTPases (Rac1 and Cdc42), which are major regulators of the actin cytoskeleton. Majewski *et al.* (2012) show that Myosin VI and DOCK7 co-localize in neuronal PC12 cells at different cellular locations and during the whole cell cycle. It was shown that depletion of Myosin VI in neuronal PC12 cells caused significant changes in actin cytoskeleton organisation (Majewski *et al.* 2011).

1.4.5.9 Phospholipase Cδ3

Phospholipase Cδ3 (PLCδ3) is a key enzyme in the phosphoinositide metabolism, but its physiological functions remain mostly unknown. PLCδ3 binds myosin VI via a PH and a C2 domain. Myosin VI and PLCδ3 are limitedly co-expressed in the inner and outer hair cells of the cochlea, but although a myosin VI knock-out will cause deafness, a PLCδ3 knockout did not prove to do so (Sakurai *et al.* 2011). But since Sakurai *et al.* (2011) found a massive decrease of expression of myosin VI in PLCδ3-KO mice in intestines, where microvilli structure is well developed show that PLCδ3 might play a role in stability of microvilli structure via regulation and anchoring of myosin VI to the plasma membrane.

1.4.5.10 Tom1

Tom1 binds to myosin VI via the WWY motif, which also binds to Dab2 and LMTK2. Myosin VI and Tom1 co-localise on vesicles along the cell periphery. With Tom1 absent in cells, myosin VI is lost from endosomes (Tumbarello *et al.* 2012). Myosin VI is targeted by Tom1 to endocytic structures in mammalian cells and they function together in the final stages of autophagy.

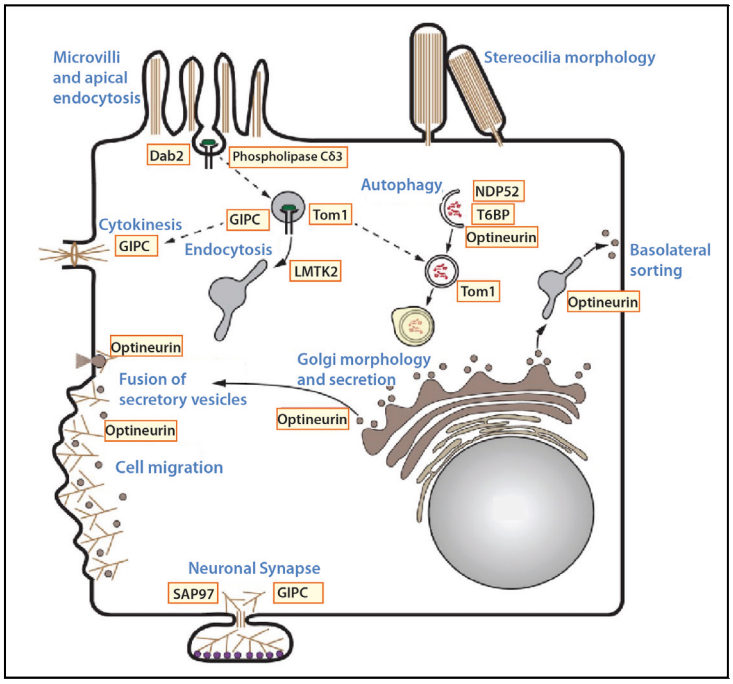

Figure 10: Cellular functions of myosin VI are directed by its distinct cargo adaptors. Myosin VI functions in various membrane trafficking pathways, such as clathrin-dependent endocytosis through interaction with Dab2, sorting at the early endosome, through interaction with Tom1, GIPC and LMTK2 and, in autophagy, through interactions with T6BP, NDP52, optineurin and Tom1. Myosin VI has multiple other functions in the secretory pathway as well as maintaining Golgi morphology, facilitation of vesicle fusion at the plasma membrane and regulation of basolateral sorting through interactions with optineurin. Modified after Tumbarello *et al.* (2013).

Binding Partner	Interaction motif	Function	Protein domains	Localization	References
NDP52	RRL	Exocytosis, Autophagy receptor, signalling	SKICH, coiled-coil, UBD, zinc-finger	Golgi	Morriswood *et al.* (2007)
Dab2	WWY	Endocytic adaptor, clathrin-mediated endocytosis	Phsophotyrosine-binding motif, AP-2 clathrin-binding	endocytic vesicles	Bond *et al.* (2012), Morris *et al.* (2002)
T6BP	RRL	Exocytosis, Autophagy receptor, signalling	SKICH, coiled-coil, UBD, zinc-finger	Golgi	Morriswood *et al.* (2007)
GIPC	RRL	Endocytosis, cargo sorting	PDZ	Vesicles	Aschenbrenner *et al.* (2003), Spudich *et al.* (2007)
SAP97		Endocytosis		endocytic vesicles	Osterweil *et al.* (2005)
Optineurin	RRL	Exocytosis, secretion, signalling, autophagy receptor	coiled-coil, UBD, zinc-finger	Golgi/ Endosomes	Buss and Kendrick-Jones (2011), Sahlender *et al.* (2005)
LMTK2	WWY	Endocytosis , cargo sorting	Transmembrane, serine/threonine kinase	Endosomes	Chibalina *et al.* (2007)
TLS		RNA-binding			Takarada *et al.* (2009)
DOCK7		intracellular signalling			Majewski *et al.* (2012)
phospholipase Cδ3		anchoring MVI to cell membrane	C2, PH, EF-hand	cell membrane	Sakurai *et al.* (2011)
Tom1	WWY	autophagy, endocytosis, cargo sorting	VHS; GAT		Tumbarello *et al.* (2012)

Table 1: Binding partners of myosin VI. Modified after: Tumbarello *et al.* (2013)

Optineurin, T6BP, NDP52 and GIPC share the RRL motif as interaction site on the myosin VI CBD whereas Tom1, LMTK2 and Dab2 interact with the WWY motif (table 1). For a number of interaction partners no interacting motif is defined yet.

1.5 Myosin XXI

Most eukaryotes express diverse isoforms of myosin, which perform manifold cellular tasks. The genome of *Leishmania* encodes for two different myosin isoforms: namely a myosin class IB and a class XXI. It has been reported that only myosin XXI is expressed (Foth *et al.* 2006, Katta *et al.* 2009). Being possibly the only myosin motor in these cells it must be a multifunctional motor that is capable of performing multiple tasks in the cell (Batters *et al.* 2012), similar to myosin VI with its scope of duties. Although the associated tasks in the cell are different between these myosins there are structural similarities. A basic-hydrophobic (BH) plot of myosin VI revealed a possible lipid-binding domain around the IQ-motif (see 3.3.1.1) which is potentially not functional since calmodulin binds to it and additionally it is able to bind to lipids along its tail (see 3.3.1.1). Myosin XXI shows a lipid binding domain at the converter domain and lipid binding propensity along the tail too (see 3.4.1). Therefore myosin XXI was used in this study as a second model system for a multifunctional cellular motor.

Myosin XXI is a plus end directed motor, which preferentially localizes at the proximal region of the flagellum (Katta *et al.* 2009). The depletion of the encoding gene *Myo21* results in impairment of flagellar assembly and intracellular trafficking (Katta *et al.* 2010). This shows that myosin XXI is essential for assembly of the *Leishmania* flagellum and that there must be other mechanisms than expression level control that allow myosin XXI to perform its tasks in the cell. Myosin XXI is expressed in both the pro- and amastigote stage of the parasite but expression is reduced ~20 fold in the non-motile amastigote stage (Katta *et al.* 2009). Two subpopulations of XXI can be found in the cells, one that is fixed to the flagellar proximal region and one that can be found in the cell with a low abundance (Katta *et al.* 2010). Under the conditions used, this myosin is a monomeric, mechanically functional molecular motor that binds a single calmodulin and moves actin filaments at a very low speed. It can therefore act as an anchor during endocytic processes within the flagellar pocket and possibly as well in the formation of the paraflagellar rod structure (Katta *et al.* 2009). One of the most intriguing facts about this myosin is that it contains two ubiquitin-associated domains (UBA) in the tail and has no structural or functional relationship with the myosin proteins in other ciliates or flagellates (Batters *et al.* 2012, Katta *et al.* 2010). Several coiled-coil regions in the tail (figure 11) could point towards the possibility that myosin XXI is capable of dimerisation or even oligomerisation (Batters *et al.* 2012). In a very recent study connected to this

thesis, we were able to show that myosin XXI is indeed able to dimerise under certain conditions (Batters *et al.* 2014). We were as well able to show that it has, besides the N-terminal extension SH3-like domain and its unique UBAs, the ability to bind lipids along its tail (Batters *et al.* 2012, Batters *et al.* 2014).

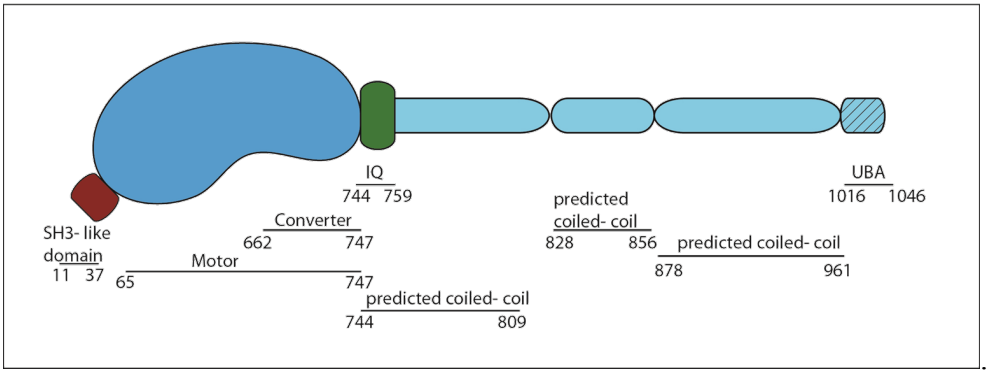

Figure 11: Myosin XXI full-length protein. Domain structure of *L. donovani* myosin XXI comprising the SH3-like domain from amino acids (aa) 11 to 37, the motor (aa 65-747), the converter domain (aa 662-747) and directly following the IQ-motif (744-759). From aa 744 to 961 three consecutive predicted coiled-coil regions. The last predicted coiled-coil region from aa 1016-1046 is with a very high probability a Ubiquitin associated domain (UBA). The total length of the protein is 1050 amino acids.

Myosin XXI has been reassigned to a kinetoplastide-specific class of myosin by Odronitz and Kollmar (2007), class XIII; but throughout this work will be further called XXI according to the cited publications and to maintain consistency.

1.5.1 Pathogenies

Since myosin XXI is a myosin in *Leishmania* it is relevant to discuss the role of this inparasite pathophysiology. *Leishmania* are a group of trypanosomatid parasites that can be grouped into four species complexes- *L. tropica, L. donovani, L. mexicana and L. brasiliensis*. Each can give rise to a variety of diseases (Wakelin 1996). The best known ones are oriental sore, a cutaneous lesion caused by *L. tropica* and *L. major*, kala-azar, a predominantly visceral form caused by *L. donovani* and espundia (Uta) a mucocutaneous form caused by *L. brasiliensis* (Hiepe 2006). The life cycles of leishmanias follow a consistent pattern; all species are using blood-feeding sandflies (phlebotomines) as vectors (Figure 12). Human infections are mostly transmitted through various animal reservoir hosts, but direct human-human transmission occurs as well (Hiepe 2006). The parasites go through two life-stages: (1) the non-motile amastigote which exists within the mammalian macrophages, and (2) the highly motile promastigote with anterior flagellum which resides in the alimentary tract of the sandfly host (Katta *et al.* 2010). Sandflies

acquire infection when they take up infected cells as they feed. The amastigote stage is released into the insect's intestine, transforms into promastigotes, divides and moves towards the pharyngeal valve (Figure 12).

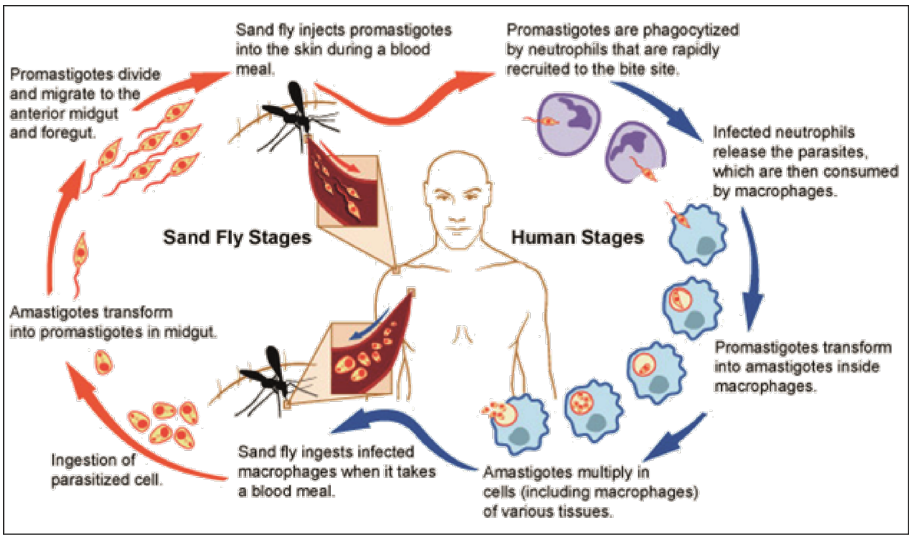

Figure 12: Life cycle of Leishmania parasite. Shown are the different stages in the sandfly vector and human. *Leishmania* parasites go through different developmental stages during their life cyle and change between the non-motile amastigote state and the motile promastigote. From: National Institute of Allergy and Infectious Diseases, U.S. Department of Health and Human Services.

In cutaneous and mucocutaneous leishmaniases infections remain restricted to the skin and superficial tissues. In visceral form, as transmitted by *L. donovani*, infection spreads to invade visceral organs (Wakelin 1996). From here the parasites spread from the initial site of infection and can become widely distributed throughout the body. A characteristic enlargement of spleen and liver accompanies the infection.

1.6 Calmodulin

Calcium (Ca^{2+}) is a major secondary messenger in cells. Changes in cytosolic Ca^{2+} concentration regulate and control a variety of cellular processes such as muscle contraction, molecular motor activity, cytoskeletal organisation, apoptosis, cell proliferation, mitosis, long-term potentiation, and many others (Tidow and Nissen 2013). For several of these cellular effects a calcium sensor that translates the Ca^{2+} signal into a cellular process is needed. Calmodulin (CaM), a 17 kDa protein is a highly conserved eukaryotic calcium sensor. Its crystal structure reveals two globular domains (N-lobe and C-lobe) with two EF-hand type Ca^{2+}-binding sites in each. The two lobes are connected by a linker helix that shows some conformational flexibility (Park *et al.* 2008). Each CaM can bind 4 Ca^{2+} ions and then forms the Ca^{2+}/CaM complex (see figure 13). Upon binding Ca^{2+} CaM undergoes a conformational change that enables it to bind to its target proteins. Target proteins are amongst others: myosins, protein kinases, phosphatases, synthases, ATPases and ion channels.

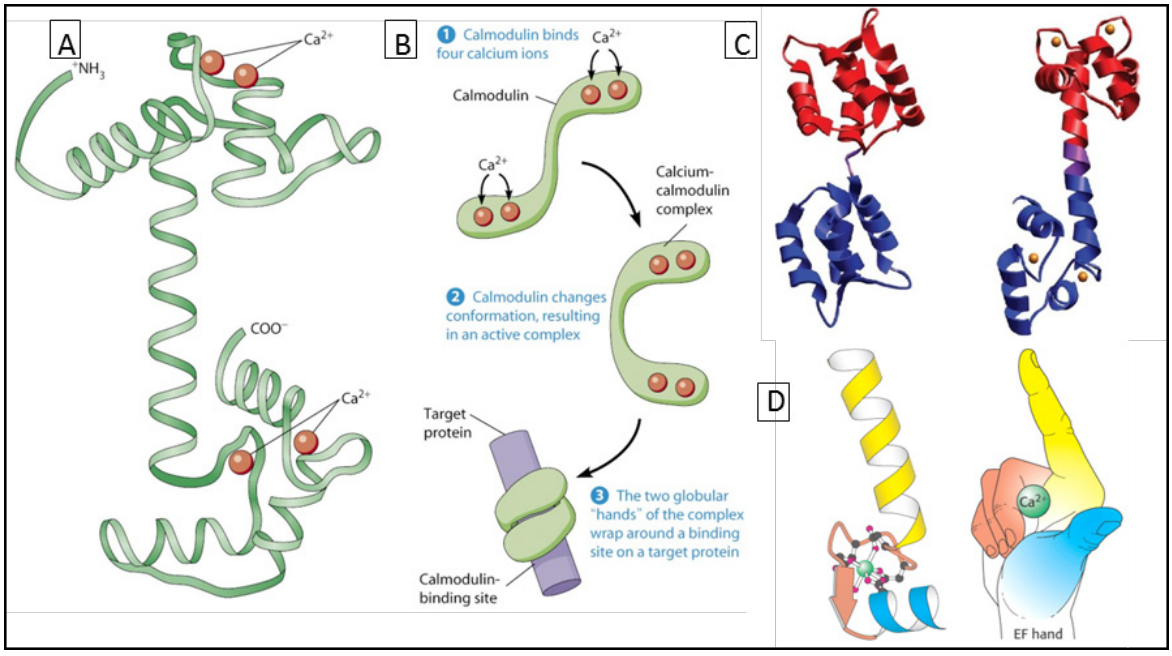

Figure 13: Calmodulin binding to Calcium and structural changes in the Ca^{2+}/CaM complex. (A): Calmodulin bound to 4 Ca^{2+}, **(B):** Function of Ca^{2+}-Calmodulin complex, **(C):** structural changes of Calmodulin molecule between unbound and Ca^{2+}-bound state. **(D):** depiction of EF-Hand motif (modified after: Berg J.M. *et al.* (2012))

Although the protein sequence of CaM is highly conserved and identical among vertebrates, Ca^{2+}/CaM-binding regions of target proteins display low homology and little sequence dependence. Typically CaM is Ca^{2+} activated and binds to short peptides and proteins. But it can as well bind in its apo (Ca^{2+}-free) form to some target sites or in both

binding states with different affinities (Tidow and Nissen 2013). With these abilities a resourceful system linking Ca^{2+} concentration to the regulation of CaM target proteins is generated.

1.6.1 IQ-motifs

CaM can interact with proteins in a Ca^{2+}-independent manner; one of these interacting motifs is the so called IQ-motif, a ~ 24 amino acid domain that serves as a binding site for one CaM light chain or any other calmodulin family member (Cheney and Mooseker 1992). These motifs share the consensus sequence IQxxxRGxxxR (Cheney and Mooseker 1992), although Bähler and Rhoads (2002) suggest [I,L,V]QxxxRxxxx[R,K] as a more generalized IQ-motif. But on the whole there are different classes of IQ-motifs and IQ-like motifs. They are classified upon the number of residues that space the bulky residues in the respective motif. And each motif class includes several subclasses that show minor variations of the particular motif spacing. In the 1-14 motif for example the key bulky residues are spaced 12 residues apart. The other classes are the 1-10 and 1-16 motifs (Calmodulin Target Database, Webb and Corrie 2001).

1.7 Calmodulin and myosins

Nearly all myosins contain between one and seven IQ-motifs, not all of them binding CaM but CaM-related proteins like conventional myosin II, myosin X and myosin Ic (*Acanthamoeba castellanii*) (Rogers and Strehler 2001). As already discussed the neck domain serves as a lever arm and thereby contributes to the step size of a given myosin. When light chains are bound to the α-helical neck, they mechanically stabilise this structure so it can form a lever arm to amplify the conformational change generated in the catalytic domain. As soon as 4 Ca^{2+}-ions bind to one CaM the conformation is changed which activates the target protein (see figure 13 B). Table 2 gives a summary of IQ-motif distribution among myosin classes.

Myosin class	Number of IQ-motifs/ Calmodulin/ CaM binding sites	References
I	3-6 light chains	Cheney and Mooseker (1992)
II	4 light chains	Cremo and Hartshorne (2007)
III (ninaC)	2 splice variants: 2 IQ-motifs 1 IQ-motif	Montell (2012)
IV	1 IQ-motif	Horowitz and Hammer (1990),
V	6 IQ-motifs	Espindola *et al.* (1992), Reck-Peterson *et al.* (2000)
VI	1 IQ-motif 1 Calmodulin binding unique insert	Kellerman and Miller (1992), Wells *et al.* (1999), Bahloul, *et al.* (2004)
VII	5 IQ-motifs	Hasson (1997), Liu *et al.* (1997)
IX	4-6 IQ-motifs	Reinhard *et al.* (1995), Post *et al.* (1998)
X	3 IQ-motifs	Cheney and Baker (1999)
XIV	No classic IQ-motif	Hasegawa and Araki (2002)
XV	2 IQ-motifs	Liang *et al.* (1999)

Table 2: Distribution of IQ-motifs in different myosin classes.

1.8 Cell plasma membrane

Myosin VI shows lipid-binding capabilities (Spudich *et al.* 2007) in its cargo-binding domain. Since no deeper understanding about further binding sites and interactions with the plasma membrane have been obtained yet, it will be one of the main aspects of this thesis to expand the insights into myosin VI's interaction with membrane components.

The cell membrane is a biological membrane that surrounds the cytoplasm of living cells, physically separating the intracellular components from the extracellular environment. It is selectively permeable and thus able to regulate transport in- and out of cells. Membrane formation is a consequence of the amphipathic nature of the phospholipids. The polar head groups favour contact with water, whereas their hydrocarbon tails interact with one another in preference to water (Tokumasu *et al.* 2002). A micelle is one option to arrange these molecules in the presence of water. Here the polar head groups form the outside surface whilst the hydrocarbon tails are sequestered inside, interacting with one another. Alternatively, the strongly opposed hydrophobic and hydrophilic moieties can be satisfied by forming a lipid bilayer (figure 14). A bilayer is then always composed of two lipid sheets and can therefore as well be called bimolecular sheet or a two-dimensional liquid (Singer and Nicolson 1972). The hydrophobic interior of the bilayer forms a permeability barrier whilst the hydrophilic head groups interact with the aqueous medium on each side of the bilayer. Lipid bilayers form spontaneously by a self-assembly process. The growth of lipid bilayers from phospholipids is spontaneous and rapid in water. These membranes have a very low permeability for ions and most polar molecules with an exception of water, which easily traverses these membranes because of its low molecular weight, high concentration and lack of a complete charge. In general one can say that the permeability of small molecules is correlated with their solubility in a nonpolar solvent relative to their solubility in water (Chakrabarti 1994).

The cell plasma membrane which surrounds the cell and cell organelles embeds several proteins in different fashions. There are integral membrane proteins that interact extensively with the hydrocarbon region of the bilayer. There are proteins that traverse the bilayer completely, peripheral proteins interact with the polar head groups of the lipids or bind to the surfaces of integral proteins (McIntosh *et al*. 2006). Other proteins are tightly anchored to the membrane by a covalently attached lipid molecule (Nagle and Tristram-Nagle 2000).

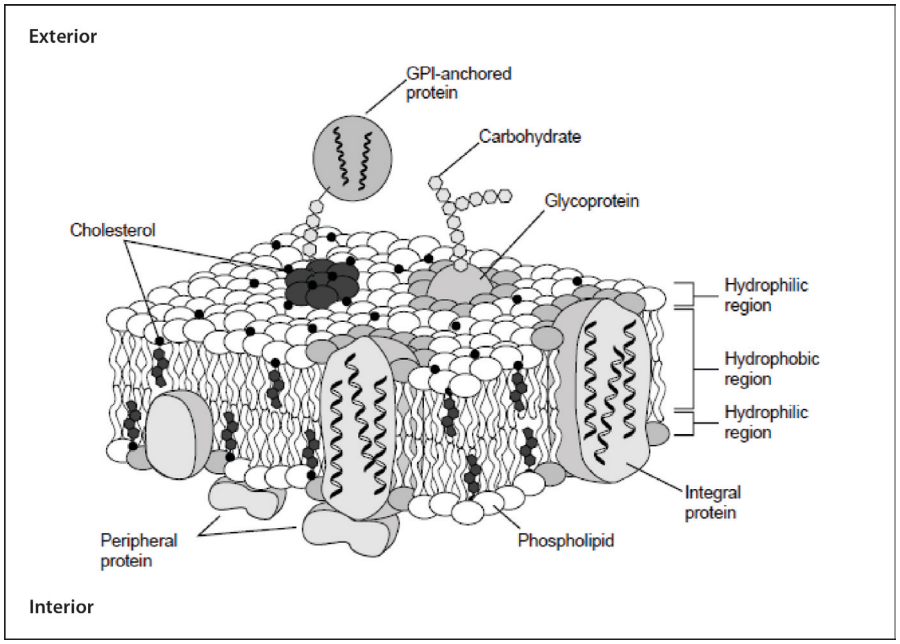

Figure 14: Model of membrane structure. This model of the plasma membrane of a eukaryotic cell is an adaptation of the original model proposed by Singer and Nicholson (1972). The phospholipid bilayer is shown with integral membrane proteins largely containing helical transmembrane domains. Peripheral membrane proteins associate either with the lipid surface or with other membrane proteins. Lipid rafts (dark grey head groups) are enriched in cholesterol and contain a phosphatidylinositol glycan-linked (GPI) protein. The light grey head groups depict lipids in close association with protein. The irregular surface and wavy acyl chains denote the fluid nature of the bilayer.

Through these integral proteins the bilayers are also involved in signal transduction. And in addition to these protein- and solution-mediated processes it is as well possible for lipid bilayers to perform direct signalling (Escribá *et al.* 2007). A good example is the phosphatidylserine (PS) -triggered phagocytosis (Greenberg and Grinstein 2002). During this process the normally asymmetrically distributed PS is mustered by scramblase during programmed cell death. The presence of PS then triggers phagocytosis.

1.8.1 Lipid vesicles

A vesicle is a small organelle mostly within a cell (figure 15 B). It consists of fluid enclosed by a lipid bilayer membrane. Vesicles can form naturally during exo- and endocytosis as well as phagocytosis. They are either produced by pinching off part of membrane of the Golgi complex, the endoplasmic reticulum or the cell membrane or by surrounding an object outside the cell (Deatherage and Cookson 2012). Since the inside of a vesicle differs from the cytosol they are not only used as transport ‘wrapping’ to move materials between locations in the cell (e.g. from rough endoplasmic reticulum to Golgi apparatus) but can as well act as chemical reaction chambers. There are different types of vesicles such as lysosomes which are membrane-bound organelles that contain hydrolytic enzymes which have the capability to break down almost all kinds of

biomolecules such as carbohydrates, proteins, nucleic acids, lipids and cellular debris (Settembre *et al.* 2013). And there are secretory vesicles which contain materials to be excreted from cells, such as synaptic vesicles which are located at presynaptic terminals in neurons and store neurotransmitters. Upon a signal that travels down the axon they fuse with the pre-synaptic membrane and release the stored neurotransmitter which can subsequently be detected by receptors. Other secretory vesicles are released from endocrine tissues and can transport and release hormones. Vesicle formation and release in cells is always connected with complex coating and docking in which different surface markers and coating proteins are involved. Examples for surface markers that identify the vesicle's cargo are SNAREs (Chen *et al.* 2001). Complementary SNAREs on the target membrane act to cause fusion of the vesicle and target membrane. As for coatings there are three types of vesicle coats: COPI, clathrin and COPII. Clathrin coated vesicles are found trafficking between the Golgi and plasma membrane, the Golgi and endosomes, and the plasma membrane and endosomes (Mousavi *et al.* 2004). The COPI coated vesicles are responsible for transport from the Golgi to the ER, whilst COPII coated vesicles are responsible for the transport from the ER to the Golgi (Popoff *et al.* 2011).

If vesicles are produced artificially they are called liposomes. One way is to crush the living tissue into suspension and let the membranes build tiny closed bubbles. Another possibility is to use a homogeneous phospholipid vesicle suspension which can be prepared by sonication (Barenholz *et al.* 1977) or extrusion (Hope *et al.* 1985, Mayer *et al.* 1986). In this way aqueous vesicle solutions can be prepared of different phospholipid composition, as well as different sizes of vesicles.

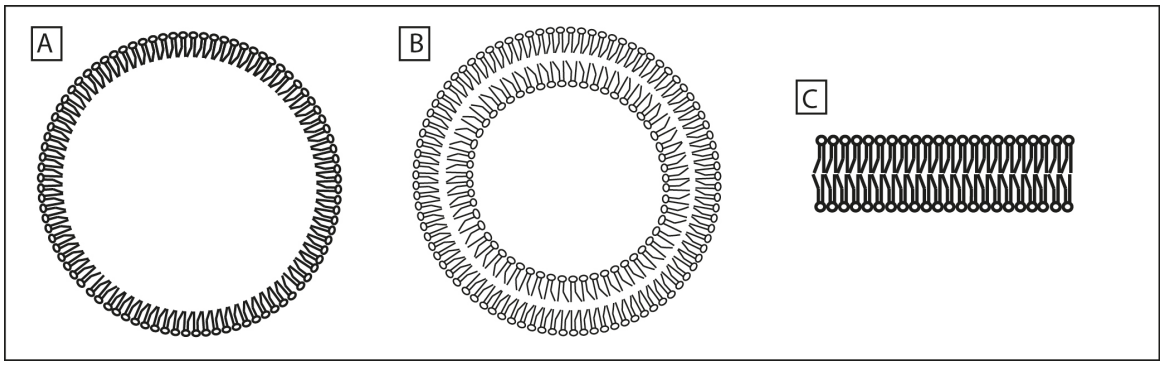

Figure 15: (A) Micelle, (B) vesicle and bilayer (C). Different conformations of lipids in aqueous buffer.

1.8.2 Lipids

Fatty acids are aliphatic, usually straight chain, monocarboxylic acids. Natural fatty acid structures reflect their common biosynthesis- the chain is built in two-carbon units and *cis* double bonds are inserted at specific positions relative to the carboxyl carbon. Over 1000 fatty acids are known but only around 20 fatty acids occur widely in nature (Scrimgeour and Harwood 2007). The fact that lipids differ in shape makes not only lipid phases possible but allow lipid monolayers to acquire spontaneous curvature (Dopico and Tigyi 2007). In the cell lipids fulfil three general functions: first, they are used as energy storage in lipid droplets. These function primarily as storage of caloric reserves and as repositories of fatty acid and sterol components, which are needed for membrane biogenesis (Scrimgeour and Harwood 2007). Second, they form the matrix of cellular membranes which consists of polar lipids that consist of a hydrophobic "tail" and a hydrophilic "head" portion. It is the physical basis of spontaneous formation of membranes that the hydrophobic parts show a propensity to self-associate (driven by water) and the hydrophilic moieties interact with the aquatic environment and with each other. Finally lipids can act as primary and secondary messengers in signal transduction and molecular recognition processes (van Meer *et al.* 2008). In the following chapter only the lipids with relevance to the assays used in this thesis will be discussed.

1.8.2.1 Phospholipids

Phospholipids can be divided into two main classes depending on whether they contain a glycerol or a sphingosyl backbone into glycerophospholipids and spingophospholipids. The compounds of the former contain and are named after structures that are based on phosphatidic acid (3-*sn*-phosphatidic acid). The X moiety attached to the phosphate includes amino alcohols (nitrogenous bases) or polyols:

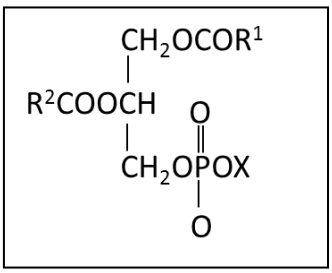

note: R1 and R2 are long-chain alkyl groups

Figure 16 presents the main structure and its derivates in more detail.

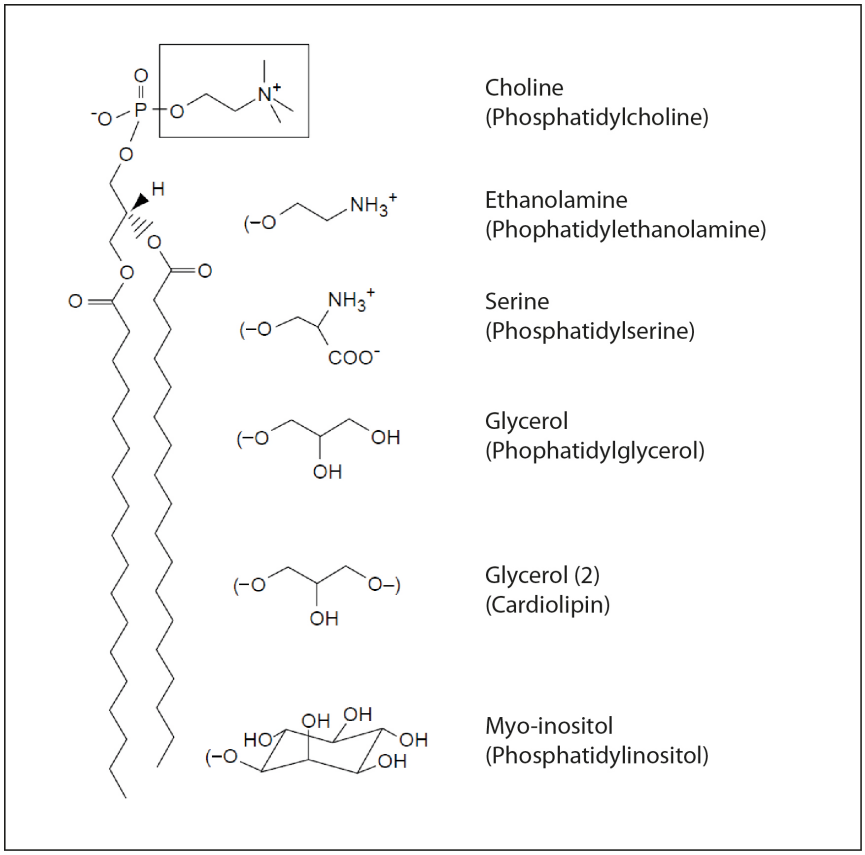

Figure 16: Structure of glycerophosphate-based lipids. The complete lipid structure shown is 1,2-distearoyl-*sn* glycerol-3-phosphocholine or phosphatidylcholine (PC). Substitution of choline (box) with the head groups listed below results in the other phospholipid structures. Phosphatidic acid (PA) has a hydroxyl group in place of choline (not shown). Cardiolipin (CL) is also referred to as diphosphatidylglycerol since it contains two PAs joined by a glycerol. Adapted after: Dowhan and Bogdanov (2002)

In eubacteria and eukaryotes the diacylglycerol backbone *sn*-3-glycerol is esterified at positions 1 and 2 with long-chain fatty acids (figure 16). Eukaryotic lipids contain fatty acid chains up to 26 carbons in length with multiple or no double bonds (Dowhan and Bogdanov 2002). The most common phospholipids and their properties are listed in table 3.

Substituent (X)	**Phospholipid**	Remarks
-H	**Phosphatidic acid (PA)**	Negatively charged lipid, occurring only in trace amounts. Important metabolic intermediate.
$-CH_2CH(NH_3)^+COO^-$	**Phosphatidylserine (PS)**	Widespread but minor negatively charged lipid in eukaryotes.
$-CH_2CH_2NH_3^+$	**Phosphatidylethanolamine (PE)**	Widespread and major lipid. Partly methylated derivatives are metabolic intermediates in the conversion of phosphatidylethanolamine to phosphatidylcholine.
$-CH_2CH_2N^+(CH_3)_3$	**Phosphatidylcholine (PC)**	Neutral net carge. The major animal phospholipid and main component of nonchloroplast membranes of plants.
$-C_{47}H_{83}O_{13}P$	**Phosphatidylinositol**	Negatively charged lipid. Widespread and usually minor lipid. Phosphorylations can take place in different positions Important for signalling.
-Phosphatidylglycerol	**Diphosphatidylglycerol (DPG) (Cardiolipin)**	Common in bacteria and localized in the inner leaflet of mitochondrial membranes. Negatively charged.

Table 3: Most common phospholipids and their characteristic properties. Modified after: Scrimgeour and Harwood (2007)

1.8.2.1.1 Sphingolipids

Sphingolipids contain sphingosine or a related amino alcohol. The most common is N-acylsphingosine that is commonly called sphingomyelin. Although sphingomyelin is a major lipid of certain membranes in animal tissues (particularly nervous tissues), even in animals the nonphosphorous sphingolipids (glycosphingolipids) are more widely distributed. Sphingolipids are a minor group of membrane lipids (10-20 mol% of plasma membrane). They consist of a phosphorycholine and ceramide or a phosphoethanolamine headgroup. Sphingomyelin is usually found in animal cell membranes, especially in the myelin sheath that surrounds some nerve cell axons. Its functions range from insulating nerve fibres over cell signalling to apoptosis. It was found to be associated with lipid microdomains in the plasma membrane, known as lipid rafts. In these rafts, lipid molecules are in the lipid ordered phase, offering more rigidity and structure than the rest of the plasma membrane. Due to the specific types of lipids in these rafts they can accumulate certain types of proteins associated with them and thus increasing the special

functions they possess. There are speculations that lipid rafts are involved in the apoptosis cascade (Kolesnick 1994, Scrimgeour and Harwood 2007).

Sulfatides are Glycosphingolipids (ceramides) carrying a sulphate esther group attached to the carbohydrate moiety. Although sulfatides tend to be minor components of tissues, 3-sulfogalactosylceramide (Sulfatide) is one of the more abundant glycolipid constituents of brain myelin and is also present in other organs but only encountered at trace levels in tissues. Sulfatide is located exclusively in the extracellular leaflet of the membrane of the myelin sheath. In the pancreas it is located in the islet of Langerhans and is involved in insulin processing and secretion through activation of ion channels.

1.8.2.1.2 Cholesterol

Cholesterol is a primary steroid in membranes of plants and animals. The cell membrane is abundant in cholesterol (15-50% of total lipid) whilst scarce in internal organelles (≥ 5% in mitochondrial membranes) (Sackmann 1995, Dopico and Tigyi 2007). In eukaryotic membranes it is largely up to cholesterol to regulate membrane fluidity and permeability. Increasing cholesterol in animal membranes changes the physicochemical properties in terms of increased bending rigidity and compressibility (Bloom *et al.* 1991). But exactly these two features of bilayers need to be regulated and controlled since they are needed to perform distinct physiological tasks within the cell membrane. A 'soft' membrane is easier to permeate by for example red blood cells (Evans 1989). Additionally cholesterol serves as a precursor for biosynthesis of steroid hormones, Vitamin D and bile acids (McCabe and Green 1977).

1.8.2.1.3 Phosphoinsoitides

Phosphoinositides (PIs) are a family of eight minor components of cellular membranes, with the parent lipid phosphatidylinositol (PtdIns) representing only 8% of the total phospholipid content in a typical mammalian cell but accounting for more than 80% of total PIs (Vanhaesebroeck *et al.* 2001). Nevertheless the role of PIs in the cellular machinery is fundamental. PIs perform multiple and highly specialised roles in regulation of cell homeostasis, membrane trafficking and signal transduction (figure 17).

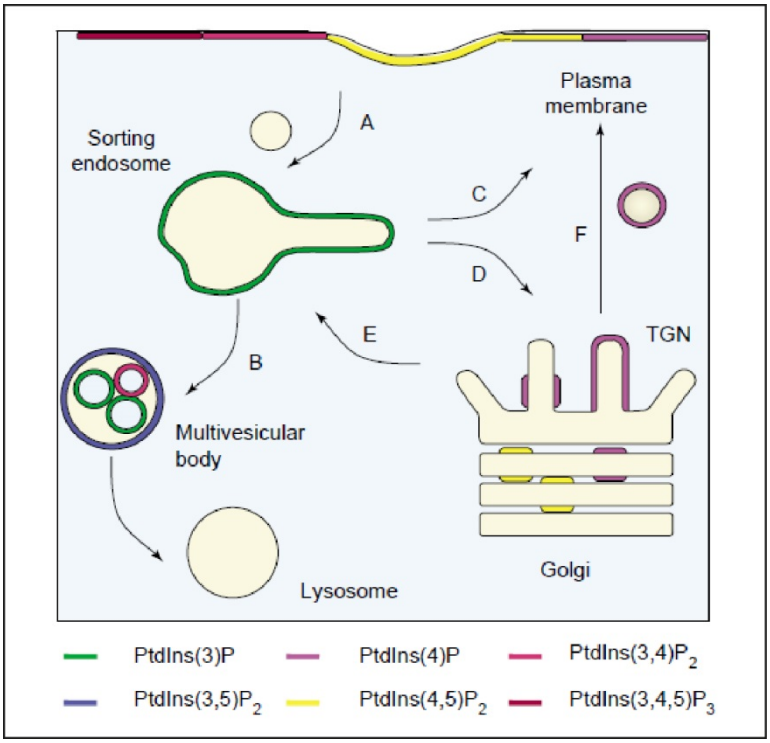

Figure 17: Cartoon showing intracellular membranes in the endocytic and biosynthetic pathways and their hypothesized phosphoinositide content . Trafficking pathways given by letters. A, internalization from the plasma membrane; B, degradative sorting to the lysosome; C, recycling from endosomes back to the trans-Golgi network (TGN), delivery of cargo from the TGN to endosomes; F, secretion of cargo from the TGN to the plasma membrane (Carlton and Cullen 2005).

Structurally PtdIns consists of a D-myo-inositol 1-phosphate moiety that is linked via its phosphate group to diacylglycerol (DAG). The inositol ring has the unique property of undergoing sequential and reversible phosphorylation at one or more of the 3-, 4-, or 5-OH positions. Accordingly, PtdIns serves as the precursor of the seven functionally distinct stereoisomers (figure 18).

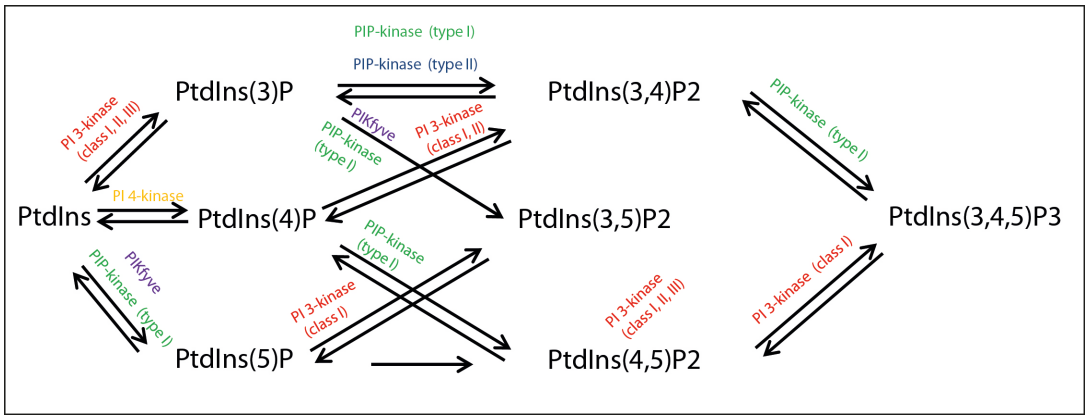

Figure 18: Mammalian phosphoinositide cycle. Illustration of the phosphoinositide species that can be naturally generated by the phosphorylation of PtdIns at positions 3, 4 and 5 of the inositol ring. Only the reactions catalysed by mammalian lipid kinases are shown. Double arrows indicate reversibility by phosphoinositide phosphatases. Modified after Halet (2005).

PI(3)P is predominantly found in early and multivesicular endosomes through association with FYVE (Fab 1, YOTB, Vac 1 and EEA1) domains involved in endocytic trafficking (Janmey and Stossel 1987). It is phosphorylated to PI(3,5)P_2 by Fab1p, a FYVE domain containing protein. The actual target of this PI is unknown. PI(4)P is the most abundant Phosphoinositide, a direct precursor of PI(4,5)P_2 and is prevalently found in the Golgi apparatus where it maintains structural and functional organisation of the Golgi complex. At the plasma membrane it is bound to proteins by PH (pleckstrin-homology) domains (Mayer *et al.* 1993). Most of its interacting proteins are involved in membrane trafficking such as exo- and endocytosis.

PI(5)P is synthesised by Phosphatases and constitutively present in many cell types but 100-fold less abundant than PI(4)P, it binds PHD (plant homeodomain) domains. Nevertheless its metabolic pathway and role remain unknown. Its mass level has been shown to increase with cell activation which implies a regulatory role in the nucleus (Payrastre *et al.* 2001).

PI(3,4)P_2 is a minor lipid of which only traces in unstimulated cells can be detected. It is mostly found at the plasma membrane and in early endocytic pathway. Interacting proteins are bound to via PH domain. Additionally the PX (phox homology) domain of p47phox is specific for PI(3,4)P_2 binding (Teasdale and Collins 2012).

PI(3,5)P_2 is concentrated mainly in late compartments of the endosomal pathway and plays important functions in multivesicular body sorting, endosomal dynamics and autophagy (Payrastre *et al.* 2001).

PI(4,5)P_2 (PIP_2) is the major polyphosphoinositide in the mammalian cell. It is enriched in the plasma membrane, at the Golgi and the nuclear envelope but in total distributed in various cellular compartments (Carlton and Cullen 2005). It is the precursor of the two important secondary messengers DAG and inositol 1,4,5-trisphosphate (IP3). It is a signalling molecule on its own (Hinchliffe 2000). Its importance for the attachment of the cytoskeleton to the plasma membrane was shown by Lassing and Lindberg (1985) where they found a first indication for the influence on the cytoskeleton organisation through dissociation of profiling-actin complexes and thus regulating the free actin monomers concentration in the cell. Moreover PIP_2 can uncap actin filaments from CapZ-related proteins and gelsolin allowing elongation of pre-existing filaments. Since gelsolin is a Ca^{2+} dependent severing protein, PIP_2 can regulate the breaking of actin filaments. Once

gelsolin binds to PIP_2 its severing function is inhibited. This interaction is modulated by Ca^{2+} and pH (Iida *et al.* 1987). Furthermore PIP_2 is involved in exocytosis, endocytosis, membrane trafficking and activation of enzymes (Carlton and Cullen 2005).

Another minor polyphosphoinositide is $PI(3,4,5)P_3$.It accounts for only <10% of PIP in the cells and is mainly localized at the cell membrane (Payrastre *et al.* 2001) and has a variety of targets and functions in the cell (Toker and Cantley 1997). It is noteworthy that $PI(3,4,5)P_3$ cannot only interact with PH domains but binds to hydrophobic and basic protein sequences as well. Recent studies imply that $PI(3,4,5)P_3$ may also regulate the restructuring of focal adhesions through interaction with α-actinin (Greenwood *et al.* 2000).

1.9 Aim of the study

The ability of myosins to selectively bind different cargoes is poorly understood but is integral to their specific function within cells. The aim of this study was to increase our understanding of how myosins bind to lipid cargo. It is important to understand how and where different lipids bind to the tail region. Myosins must bind specifically to their load and transport it to its cellular destination, navigating a complex and densely packed environment and thus relocate the cargo in a specific and timely fashion. Myosin VI and XXI are two very versatile molecular motors. The aim of this thesis is to discover more about their capabilities to bind to various cellular lipid components and to map the lipid binding sites on their tails. Furthermore, cargo binding and mechanical regulations of motor proteins are linked, thus it is an objective of this study to ascertain how these two processes are connected to understand how the two addressed motor proteins are regulated.

Material and Methods

2.1 Molecular Biology Methods

2.1.1 Used organisms and culture

DH5α (Library efficiency® DH5 α) competent cells (Invitrogen)

These competent cells are used for general cloning and vector reproduction. The yield and quality of isolated DNA as well as the transformation efficiency is enhanced within this strain because of the lack of ability for homologous recombination and a mutation in DNA specific endonuclease I.

BL21 (BL21 Star™ DE3 Combo and BL21 AI™ one shot chemically competent *E. coli*, Invitrogen)

Bl21 Star™ (DE3) chemically competent *E. coli* are used for high-level expression of non-toxic recombinant proteins from low copy number T7 promoter-based expression systems. The promoter has to be induced by the lactose-analogue Isopropyl-β-D-1-thiogalactopyranoside (IPTG). This compound mimics allolactose which triggers transcription of the *lac* operon via binding to the *lac* repressor and release of the same from the *lac* operon and thereby allowing the transcription of genes in the *lac* operon.

BL21 AI™ cells are chemically competent cells that are used for protein expressions which require tighter regulation and strong expression of toxic proteins from a T7 promoter-based expression system. These cells contain a chromosomal insertion of the gene encoding T7-RNA polymerase into the *ara*B locus of the *ara*BAD operon, placing regulation under control of the arabinose-induced *ara*BAD promoter.

MAX Efficiency® DH10Bac™ competent cells (Invitrogen)

DH10Bac™ competent cells are used for production of recombinant bacmids used in the Bac-to-Bac® Baculovirus Expression System (Invitrogen). The DH10Bac™ *E. coli* strain contains a baculovirus shuttle vector (bacmid) that can recombine with a donor plasmid, in this case pFastBac™, to create an expression bacmid containing the cloned gene of interest. An additional plasmid in these cells encodes for the enzyme transposase that catalyses the transposition. Insertion of the target gene interrupts the lacZ α-peptide in a way that colonies bearing the recombinant bacmid show white and wild type colonies

blue colour. Insertion of this recombinant bacmid into insect cells (see 2.2.5) results in formation of infectious baculoviruses and target protein.

Spodoptera frugiperda (Sf21)-cells (IPLB-Sf21AE)

Sf21 is a continuous cell line derived from pupal ovarial tissue of the fall army worm *Spodoptera frugiperda*, a moth species. It was developed at the United States Department of Agriculture (USDA) Insect Pathology Laboratory. They are commonly used to isolate and propagate baculoviral stocks and to produce recombinant proteins expressed in a baculoviral system.

2.1.2 Expression systems

Strains were cultivated on 2YT plates or in 2YT liquid media at 37 °C. For the Bac-to-Bac system LB media was used. To select for antibiotic resistant plasmids, after autoclaving following sterile antibiotics were added:

antibiotic	*stock concentration*	*end concentration in media*
Kanamycin	25 mg/ml	25 µg/ml
Ampicillin	50 mg/ml	50 µg/ml
Gentamycin	50 mg/ml	7 µg/ml
Tetracyclin	10 mg/ml	5 µg/ml

When agar plates were used, bacterial agar was added to liquid medium before autoclaving and antibiotics were added after the medium cooled down (< 50 °C).

Since Sf21 cells are not dependent on adherent growth, cultivation of cells was done in suspension culture at 27 °C in Grace's insect media supplemented with FBS (Invitrogen, GIBCO), Normocin (Invivogen) and Pluronic (Invitrogen). Every day cell density was measured using a BioRad TC 10 automated cell counter and cells were maintained at a concentration of 10^6 cells/ml.

2.1.2.1 Media

If not stated differently Milli Q water was used for preparation of media (Millipore).

Media for *E. coli*: Luria Bertani Medium (LB) 1 l: 10 g Tryptone, 5 g Yeast extract, 10 g NaCl, pH 7.00; 2 YT 1 l: 16 g Tryptone, 10 g Yeast extract, 5 g NaCl pH 7.5

SOC 1 l: 20 g Tryptone, 5 g Yeast extract, 0.5 g NaCl, 0.2 g KCl, 20 mM Glucose pH 7.0

2.1.3 Plasmids

pET-28a (Novagen)

This 5369 base pair vector carries an N-terminal His-tag and an optional C-terminal His-tag sequence. It is a T7-promoter system based vector and expression is induced by providing a source of T7 RNA polymerase in the host cell. It carries a kanamycin resistance.

pGex 6P-1 (GE healthcare)

The glutathione S-transferase fusion vector (4900 bp) encodes the recognition sequence for site-specific cleavage by PreScission Protease between the GST domain and the multiple cloning site. It carries an ampicillin resitance.

pFastBac HTB (Invitrogen)

This 4857 base pairs vector is part of the Bac-to-Bac baculovirus expression system. The donor plasmid has a bacterial replication origin, an ampicillin resistance gene and an expression cassette. This cassette contains the polyhedron promoter of the *Autographa californica* nuclear polyhedrosis virus (AcNPV), a multiple cloning site, a SV40 poly(A) signal, a gentamycin resistance gene as well as an N-terminal His-tag sequence. Additionally it carries a TEV Protease cleavage site to cleave off the His-tag sequence after purification.

pFastBac 1 (Invitrogen)

This 4775 base pairs vector resembles the pFastBac HTB vector and is part of the Bac-to-Bac baculovirus expression system. The main difference lies in the lack of any tag in this vector.

pColaDuet™-1 (Novagen)

The pColaDuet™-1 vector with its 3719 base pairs is designed for coexpression of two target genes from a single plasmid. The vector encodes two multiple cloning sites (MCS) which is each preceded by a T7 promoter, *lac* operon and a ribosome binding site. MCS-1 encodes for the N-terminal polyhistidine tag, whilst MCS-2 encodes the 15 amino acid S-Tag™ peptide for C-terminal fusion if desired. The vector is kanamycin resistant.

pAC4 (Avidity)

This 4216 bp vector is used to express C-terminal AviTag-protein fusions. Expression of the AviTagged gene is under the control of the tightly repressed Trc promoter and is IPTG-inducible. The vector is ampicillin resistant.

Champion™ pET SUMO (life technologies)

The pET SUMO vector (5600 bp, kanamycin resistant) utilizes a **s**mall **u**biquitin-related **mo**difier (SUMO) fusion, belonging to the growing family of ubiquitin-related proteins, to enhance the solubility of expressed fusion proteins. In contrast to ubiquitin, SUMO is involved in the stabilization and localization of proteins *in vivo*. After expression, the 11 kD SUMO moiety can be cleaved by the highly specific and active SUMO protease at the carboxyl terminal, producing a native protein. Additionally expression is controlled by the *lac* operon and a 6x His-tag preceding the SUMO site simplifies purification. An overview over vector maps can be found in the appendix.

2.1.4 Polymerase chain reaction (PCR)

Amplification of DNA fragments and generation of site-directed mutagenesis was carried out by polymerase chain reactions (PCR). Hot Start Phusion polymerase (Thermo Scientific), the provided Taq buffer and dNTPs were used according to manufacturer (PCR Kit, Thermo Scientific). The reaction was performed on a thermocycler (eppendorf Mastercycler personal) in a 50 µl reaction. Plasmid DNA was used as template. To facilitate optimal primer-annealing a touchdown programme was used.

<u>Reaction conditions:</u>

Denaturing at 98 °C for 45 s	Temperature decline 1 °C per cycle, 8 cycles
Denaturing at 98 °C for 15 s	
Annealing at 68 °C for 30 s	
Elongation at 72 °C for 1 min	28 cycles
Denaturing at 98 °C for 15 s	
Annealing at 60 °C for 30 s	
Elongation at 72 °C for 1 min	
Final extension at 72 °C for 1 min	

2.1.5 Agarose Gel electrophoresis

Electrophoretic separation of DNA was carried out using 0.8%-1.2% (w/v) agarose gels prepared in 1x Tris Borate EDTA (TBE) buffer including 20 µl/l Ethidiumbromide at 80 mA with the run length depending on product size. The gels were cast in BioRad Mini Sub Cell GT chambers, the DNA to be separated was mixed with 0.1 volume of 6x DNA loading buffer and loaded onto the gels. Subsequently the gels could be observed under UV light at 302 nm and photos taken with the ChemiDoc XRS+ system (BioRad).

20x TBE buffer: 1.76 M Boric acid, 1.78 M Trizma base, 80 mM EDTA pH 8.3, 20 µl 10 mg/ml Ethidiumbromide solution (1 g Ethidium bromide solved in 100 ml H_2Odd)

6x DNA loading buffer: 0.25% (w/v) Bromphenol blue, 0.25% (w/v) Xylene cyanole ff, 30% Glycerol (99%)

2.1.6 Isolation of DNA fragments from agarose gels

Extraction and purification of DNA from agarose gels were performed using PureLink ® Quick Gel extraction and PCR Purification COMBO Kit (both Invitrogen) according to manufacturer's instructions.

2.1.7 Purification of PCR products

For cloning purposes the PCR products were purified using the same kit as for the isolation of DNA fragments from agarose gels according to manufacturer's protocol.

2.1.8 DNA cleavage with restriction enzymes

Usually 1 µg of DNA (plasmid or PCR product) was digested in a 40 µl reaction with at least 5 U of each enzyme. The buffer suitable for the restriction enzyme(s) was added and the volume adjusted with H_2Odd. The tube was incubated for at least 1 h at 37 °C. The digestion of the vector was monitored on an agarose gel.

2.1.9 Ligation of DNA into a plasmid vector

Ligation of vector and insert was carried out using the Rapid Ligation Kit (Thermo Scientific) at room temperature. Vector and insert were usually mixed in a ratio 1:5, but this ratio was adjusted when needed.

2.1.10 Transformation of *E. coli*

For transformation, chemically competent *E. coli* cells were thawed on ice and incubated with the ligation mix on ice for 15 min followed by a heat shock at 42 °C for 45 s. The cells were immediately placed back on ice and revived with 2YT medium. Cells were kept at 37 °C with agitation for 30-60 min (depending on the antibiotic resistance) and plated on 2YT plates containing the appropriate antibiotic. Plates were incubated at 37 °C overnight to obtain *E. coli* colonies harbouring the transformed plasmid. Single colonies were inoculated into tubes containing 5 ml 2YT with antibiotics. Cells were grown in a 37 °C shaker overnight. The positive transformants were detected by restriction enzyme mapping and confirmed by DNA sequencing.

In the case of transformation into BL21 *E. coli* the procedure was exactly the same, despite an upscaling step after picking the colonies from the agar plates. Colonies were picked and an over day culture followed by a bigger volume overnight culture (200-400 ml) with appropriate antibiotics was set up and then used for bacterial expression purposes.

2.1.11 Mini preparation of plasmid DNA

The plasmid DNA from *E. coli* was isolated with the PureLink Quick Plasmid Miniprep Kit (Invitrogen) according to manufacturer's instructions. The principle here is binding the plasmid DNA to spin columns and to finally elute it with the provided buffer. DNA was verified on agarose gels and the seemingly appropriate samples sent for sequencing (GATC).

2.1.12 Whole plasmid Site-directed mutagenesis (SDM)

For the closer investigation of certain binding sites on the target proteins, site-directed mutagenesis was performed to make intentional and specific changes to the target DNA sequence. For the initial PCR a primer containing the desired mutation (in our case a point mutation) which was complementary to the template DNA around the mutation site was used. This was followed by an overnight digest with the enzyme DpnI which only cleaves at methylated sites and therefore digests the template plasmid but not the PCR product. After a heat-inactivating step of the DpnI at 80 °C the mutated PCR DNA was transformed into DH5α-cells. After plating and incubation overnight at 37 °C, colonies were picked, transferred to a liquid culture, and after incubation overnight subsequently

miniprepped and sent for sequencing. The resulting DNA was, in case of several point mutations used as a template for another round of mutagenesis.

2.1.13 Protein expression using the baculovirus expression system

Over the past decade the use of baculoviruses has become an important tool for over-expressing recombinant proteins in eukaryotic cells (King and Possee 1992). Unlike the bacterial expression systems, this eukaryotic system uses most of the protein modification, processing, folding and transport machinery that is present also in higher eukaryotes. Thus, with this system, most of the over-expressed proteins exhibit proper biological activity and function (King and Possee 1992).

For the purpose of this thesis, the expression of the different protein constructs comprising the motor domain and parts of the tail or the full-length protein was carried out with the Bac-to-Bac® baculovirus expression system (Invitrogen) in the Sf21 insect cell line described before (see 2.1.1). One of two major components of the Bac-to-Bac®-system is the vector into which the gene or genes of interest are cloned. For this work vectors containing one promoter, and thus one expression cassette, were used.

The second major component of the Bac-to-Bac® system is represented by an *E. coli* strain (DH10Bac® Competent *E. coli*) that is used as host for the before generated plasmid, consisting of transfer vector and gene(s) of interest.

DH10Bac™ Competent *E. coli* cells contain a baculovirus shuttle vector, referred to as bacmid. After transformation into these cells, transposition between transposons of the vector and the bacmid occurs. This recombinant bacmid is the basis to then generate the recombinant baculovirus. An overview of the key steps for baculovirus protein expression is given in figure 19.

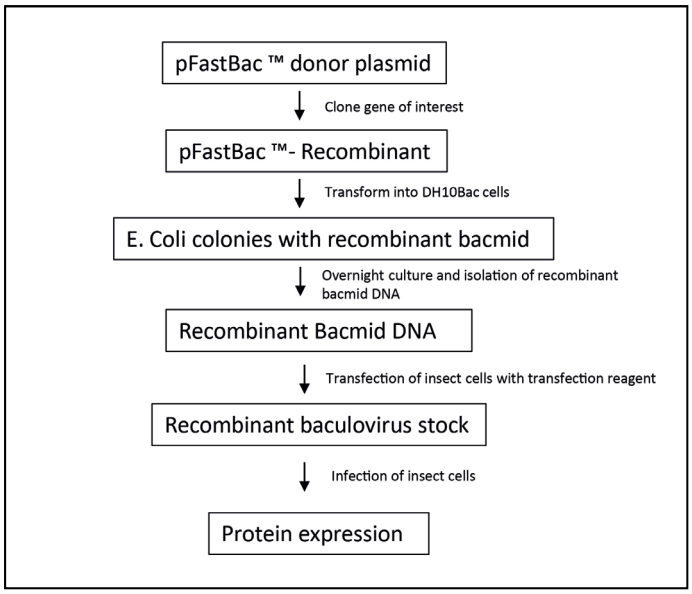

Figure 19: Protein expression via the Baculovirus Bac-to-Bac® system-overview. The flowchart illustrates the required steps for the successful protein expression in the baculovirus expression system. (modified after: Invitrogen Bac-to-Bac® handbook)

2.1.14 Generation of the recombinant bacmid

Once the recombinant vector was generated, for transposition into the baculovirus shuttle vector (bacmid) the amplified and purified DNA was transformed into DH10Bac ™ *E. coli* cells (figure 20). This strain of *E. coli* cells contains the bacmid with a mini-attTn7 attachment site, which is inserted in a segment of DNA encoding the LacZα peptide, and a helper plasmid. Generation of the recombinant bacmid is achieved via site-specific transposition between the mini-Tn7 element of the donor vector and the mini-attTn7 attachment site on the bacmid. For transformation, chemically competent DH10Bac® *E. coli* cells (aliquots of 50 µl) were thawed on ice and incubated with 1 ng DNA for 30 min on ice. The heat shock was performed for 45 s at 42 °C, followed by immediate incubation on ice. Subsequently, 900 µl of SOC medium was added and the suspension was incubated in a shaker device at 225 rpm, for 4 h at 37 °C. The Tn7 transposition functions are provided by a helper plasmid, which encodes for the transposase and confers resistance to tetracycline. Thus, successful recombination leads to the disruption of the LacZ gene on the bacmid, which in turn allows for blue-white screening in the presence of the chromogenic substrate 5-bromo-4-chloro-3-indolyl-β-D-galactopyranoside (X-gal) and the inducer IPTG. Therefore, 100 µl of dilutions 1:10, 1:100 and 1:1000 in SOC medium were plated on LB plates supplemented with (50 µg/ml) X-Gal, (40 µg/ml) IPTG, (50 µg/ml) kanamycin, (7 µg/ml) gentamicin and

(10 µg/ml) tetracycline. The plates were incubated for 48 h at 37 °C to grow single colonies. Four white colonies with the thereby confirmed (i.e., recombined bacmid) phenotype were picked and added to 3 ml of LB media (see section 2.1.2.1) supplemented with gentamycin (7 µg/ml), tetracyclin (10 µg/ml) and kanamycin (50 µg/ml) and incubated on a shaker device overnight at 250 rpm at 37 °C. After this final step a mini preparation of the DNA was done following the manufacturer's instructions for the PureLink™ HiPurePlasmid DNA Miniprep Kit (Invitrogen) and a test PCR to verify the correct size was performed.

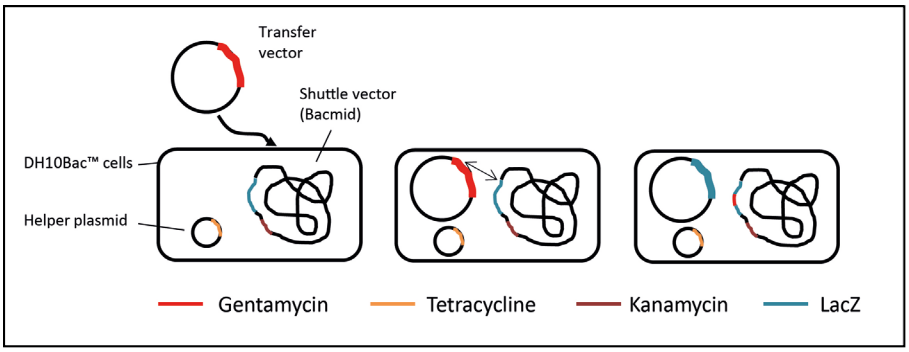

Figure 20: Generation of recombinant bacmid by site-specific transposition. Left: before transformation of transfer vector into DH10Bac™ cells; middle: transposition of the gene of interest and the gene encoding for gentamycin resistance into the bacmid (black arrow); right recombinant bacmid with Tn7-element of transfer vector. LacZ gene and genes encoding resitance for indicated antibiotics are colour-coded. (modified after: Invitrogen Bac-to-Bac® handbook)

2.2 Biochemical Methods

2.2.1 Sodium Dodecyl Sulphate Polyacrylamide Gel Electrophoresis (SDS-PAGE)

Protein mixtures were separated by discontinuous SDS-PAGE on 10 and 15% SDS – PAGE gels (table 4) according to Laemmli (1970) using the BioRad Mini protean Tetra system. The stacking gel deposits the polypeptides to the same starting level at the surface of the resolving gel, and subsequently the SDS-polypeptide complexes are separated in the resolving gel according to size under uniform voltage and pH. Prior to SDS-PAGE, 2 x SDS gel loading buffer was added to the protein samples to be separated. The mixture was boiled for 3-5 min at 98 °C. Electrophoresis was carried out at a constant voltage of 120 V for 10 min and 170 V for about 60 min (depending on the size of the protein). As standard, a mixture of proteins of defined molecular masses was electrophoresed (Pre-stained protein ladder 10-245 kDa, Applichem).

10% Separating gel	1.7 ml 30% acrylamide, 1.25 ml 1.5M Tris-HCl pH 8.8, 2 ml H_2Odd, 50 µl 10% (w/v) SDS, 20 µl 10% (w/v) Ammonium persulphate (APS), 2 µl Tetramethyl-ethyl-diamine (TEMED)
15% Separating gel	2.5 ml 30% acrylamide, 3.75 ml 1.5 M Tris-HCl pH 8.8, 1.2 ml H_2Odd, 50µl 10% (w/v) SDS, 20 µl 10% (w/v) APS, 2 µl TEMED
Stacking gel	0.28 ml 30% acrylamide, 0.2 ml 0.5 M Tris-HCl pH 6.8, 1.13 ml H_2Odd, 16.7µl 10% (w/v) SDS, 16.7 µl 10% (w/v) APS, 1,7 µl TEMED
SDS sample buffer (25ml)	2.5 ml 1 M Tris-HCl pH 6.8, 1 g SDS, 354 µl 2-mercaptoethanol, 5 ml glycerol, 50 µg bromophenol blue
SDS running buffer (1 litre)	18.77 g glycine, 3 g Tris, 1 g SDS (final pH 8.3)
Molecular weight markers	Pre-stained protein ladder, 10-245 kDa (Applichem)

Table 4: SDS-PAGE gel preparation.

Following SDS-PAGE, gels were stained in Coomassie Blue solution by shaking for 15-30 min, and subsequently destained for direct observation of the protein bands.

Coomassie Blue solution: 0.1% (w/v) Coomassie Brillant Blue, 10% acetic acid, 45% (v/v) methanol, 45% (v/v) H_2Odd

Destain solution: same as Coomassie Blue solution without Coomassie Brilliant Blue.

2.2.2 Silver staining

For silver staining the Pierce® Silver Stain Kit (Thermo Scientific) was used according to manufacturer's protocol. The acrylamide gels were fixed in a solution containing 30% methanol and 10% acetic acid for 30 min at room temperature. The fixative was removed and washed 3 times 5 min with 10% ethanol. The gels were treated with the sensitizer working solution from the kit for 1 min and then stained in stain working solution which was as well provided with the kit. After brief washes in water the gels were developed using the developer solution and the reaction was stopped with 5% acetic acid.

2.2.3 Western blotting

Following separation of protein by SDS-PAGE, the proteins were transferred from gels onto nitrocellulose membranes (Hybond C-extra, Amersham Biosciences) according to a

modified protocol of Towbin *et al.* (1979) by the means of the Mini-Trans Blot module (Mini Protean tetra system component, BioRad). In this wet blotting method, the gel and its attached nitrocellulose membrane were sandwiched between several pieces of Whatman® 3 mm filter paper which had been soaked in blotting buffer, and protein transfer was carried out at room temperature at 100 V for 60 min. After this the nitrocellulose filter was blocked for at least 15 min at room temperature in 5% (w/v) milk powder in PBS-T buffer (blocking buffer). The membrane was then washed three to five times with PBS-T. The membrane was then incubated with primary antibody diluted in blocking buffer for at least 45 min or overnight. After washing 3 times with PBS-T buffer, the membrane was incubated with a secondary antibody conjugated with horse radish peroxidase (HRP) (diluted 1:2000 in blocking buffer) for at least 1 h. The membrane was washed 5 times with PBS-T. Finally, the protein bands were detected by using the Clarity Western ECL Kit (BioRad) and visualised on a ChemiDoc XRS$^+$ (BioRad). If only one antibody, HRP conjugated, was used, the detection step could follow the washing step directly. Antibody dilutions varied from 1:5000 (e.g. anti-GST HRP) to 1:10000 (anti-6x His HRP).

Blotting buffer: 25 mM Tris- HCl, 192 mM glycine, 20% (v/v) Methanol

Blocking buffer: 1x PBS, 0.1% Tween 20 and 5% (w/v) skim milk

PBS-T buffer: 1x PBS, 0.1% Tween 20

2.2.4 Bacterial expression

Bacterial expressions were started with 15-30 ml of starter culture in 420 ml 2YT. Depending on the construct temperatures and expression durations differed. Initially culture in flasks were shaken at 37 °C until the optical density at 600 nm (OD_{600}) reached 0.5 to 0.8 and then were induced with the appropriate reagent (IPTG or Arabinose). After induction temperature was dropped to the desired degree and expression took at least 4 h. A 20 min centrifugation step at 4000 rpm followed to pellet the bacteria and after redissolving the pellet in Buffer B and protease Inhibitor (Roche) they were frozen and stored at -80 °C.

2.2.4.1 Standard protocol

4 h expression time from induction on, 37 °C until induction, 27 °C from induction to end

Buffer B: 50 mM Tris-HCl pH 7.5, 150 mM NaCl, 1 mM DTT, 20% (w/v) Sucrose, 40 mM Imidazole

2.2.5 Transfection of Sf21 cells

For transfection cells are kept in a monolayer in Grace's insect medium with added Pluronic (5 ml on 500ml medium), heat-inactivated FBS (50 ml on 500 ml medium) and Normocin (Invivogen) (0.1 mg/ml on 500 ml medium). After leaving them to adhere to the well's bottom plating medium (Grace supplemented + FBS without Normocin) is added and the cells are mixed with the mix of the target bacmid and Cellfectin® (Invitrogen) to introduce the bacmid into the cells (figure 21). Cellfectin is a cationic-lipid formulation that forms spontaneously lipid-DNA complexes which fuse with the plasma membrane resulting in uptake and expression of the DNA within these cells (figure 22).

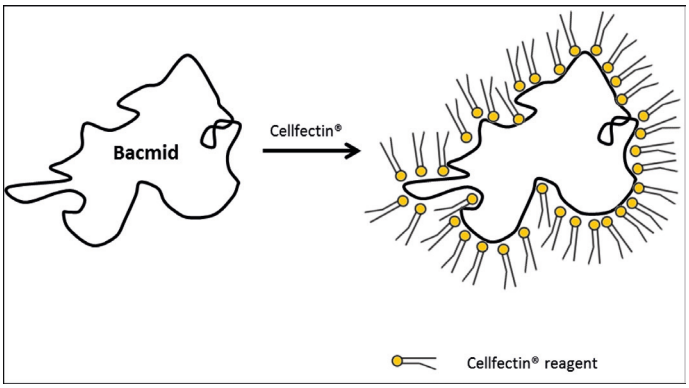

Figure 21: Preparing the bacmid for transfection into insect cells via Cellfectin® reagent. The cationic lipid (Cellfectin® reagent) coats the bacmid DNA for the subsequent chemical transfection into insect cells.

After mixing the three components together the medium is exchanged against Grace's medium with FBS and Normocin and the cells are left to incubate at 27 °C for 3-7 days. Transfected cells are taken off the well and centrifuged, the supernatant is kept and in Grace's medium with FBS, Normocin and Pluronic the cells are scaled up to passage number 4 (P4). Here 500 ml $0.8x10^6$ cells/ml and 40 ml of the target P3 are combined with a Calmodulin P3 and shaken for 3 days. After a final centrifugation step the pellet is resuspended in Myosin extraction buffer with Protease Inhibitor and frozen at -80 °C.

Myosin extraction buffer: 90 mM KH_2PO_4, 60 mM K_2HPO_4, 300 mM KCl, pH 6.8

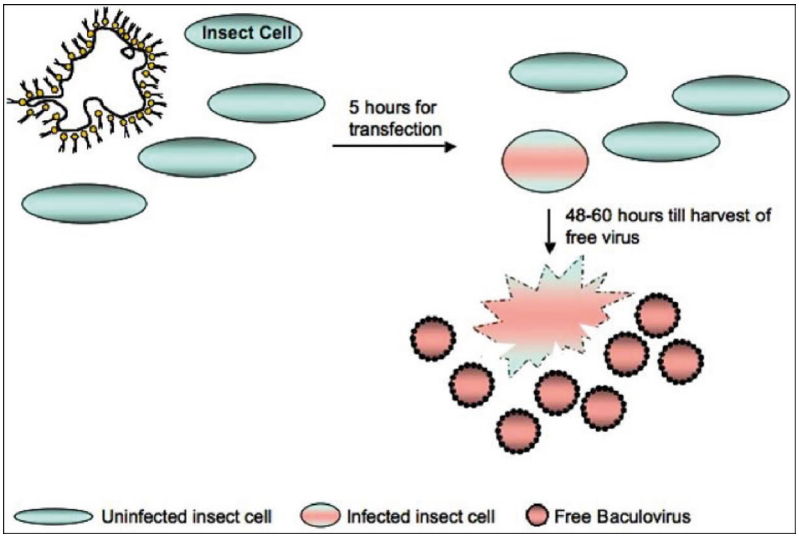

Figure 22: Representation of the time course from cell transfection until harvesting of released virus. *Top left:* Cellfectin-mediated transfection of insect cells with bacmid DNA; *top right:* following transfection, within approx. 48 to 60 h cells produce viral proteins, that eventually assemble into intact lytic viral particles; free virus is eventually harvested and used for further virus amplification.

2.2.6 Protein purification

Pellets from bacterial expression and from insect cell culture were treated equally. An exceptional case was full length (FL) myosin VI (see 2.2.6.1). After thawing the pellets at 25 °C in a water bath, a brief sonication on ice (5 min, 5 s cycles, power 50%) followed. The lysed mixture was then centrifuged at 20000 rpm (Beckman Coulter JA25.50 rotor) for 20 min 4 °C. After passage through a 0.45 µm sterile syringe filter the sample was loaded onto a suitable resin column, depending on the tag of the protein. Polyhistidine-tagged proteins (His-tag) bind with micromolar affinity to resins that contain bound bivalent nickel ions (HiTrap ff, bed volume 5 ml, GE). After loading onto the column, the column was washed with HIS low buffer to remove nonspecifically bound proteins and the target protein was then washed off in a stepwise manner using HIS high buffer (figure 23). When proteins were expresses in the pGex 6P-1 vector, the purification was carried out with Glutathione Sepharose columns (GSTTrap ff, bed volume 1 or 5 ml, GE). GST-tagged proteins bind to the offered glutathione ligand and impurities were washed away by washing with PBS. Tagged protein was then eluted from the column by washing with Reduced Gluthathione Tris-buffer (RGT) in a single step.

RGT buffer: 50 mM Tris-HCl pH 8.0, 10 mM L-Gluthatione reduced

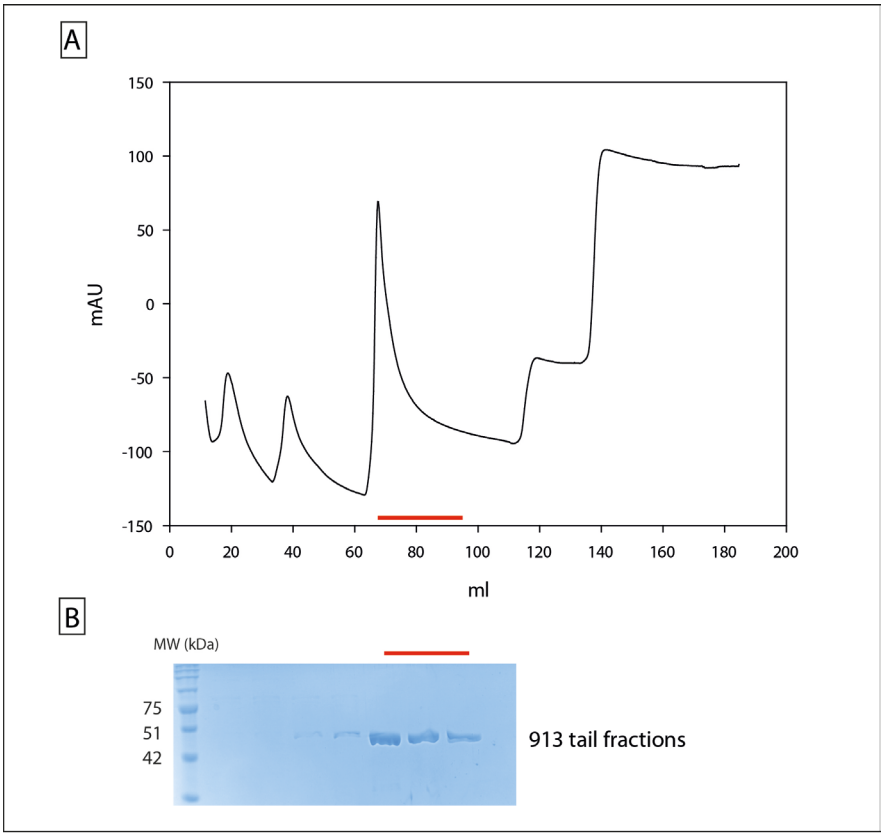

Figure 23: Typical result of a protein purification using an Äkta® (GE lifesciences) FPLC system: A: UV/Vis absorbance curve shows the purification result as it was while the protein passed the absorbance detector and **B** shows the collected fractions on a SDS-PAGE; indicated in red are the fractions containing the target protein.

2.2.6.1 Myosin VI full length purification

Cells were thawed in a water bath at 25 °C. After adding 1 mM DTT, 1 mM ATP and 5 mM $MgCl_2$ as well as 100 µl of purified calmodulin (approx. 1 mM), cells were sonicated on ice with 10x 15 s bursts at 50%. Incubation on rotator in the cold room (10 °C) for 30-60 min was followed by the aforementioned centrifugation at 20000 rpm at 4 °C for 20 min. After these additional steps the purification followed standard protocol.

HIS low: 50 mM Tris-HCl pH 7.5, 40 mM Imidazole, 500 mM NaCl, 1 mM DTT

HIS high: 50 mM Tris-HCl pH 7.5, 400 mM Imidazole, 500 mM NaCl, 1 mM DTT

RGT buffer: 50 mM Tris-HCl pH 8.0, 10 mM L-Glutathione reduced, pH 8.0

2.2.7 Dialysis of proteins

Proteins were dialysed into different buffer conditions to rid them of contaminants such as ADP or free phosphate. Different dialysis devices were used for different applications and sample or protein sizes. Usually dialysis was performed in the cold room in a large volume (2 l) overnight with continual stirring to ensure complete dialysis.

2.2.8 Cleavage of the GST tag

If pGEX-6P vectors were used for expression, the GST tag could be removed by PreScission Protease (GE healthcare). Following elution of the GST fusion protein from Glutathione Sepharose, the eluate was dialysed extensively against PBS containing 1 mM EDTA and 1 mM DTT in order to remove reduced glutathione and protease inhibitors from the sample. 10 µg of enzyme were used to cleave 1 mg of GST fusion protein. Cleavage was carried out at 4 °C overnight on a rotatory shaker. Once digestion was complete, the sample was passed through a washed and equilibrated Glutathione Sepharose to remove free GST and the PreScission Protease from the protein of interest.

2.2.9 Biotinylation of BRS (biotin recognition site) proteins

For the covalent attachment of biotin to a protein to create a different type of tag, firstly target proteins had to be expressed with a C- or N-terminal BRS site. Enzymatic biotinylation was carried out by incubating the tagged protein with biotin ligase (BirA) in the presence of biotin and ATP. This biotin-protein ligase activates biotin to form biotinyl-5'-adenylate and transfers the biotin to biotin-accepting proteins. Following a protocol from the manufacturer Avidity, each Biomix, additional biotin and BirA enzyme were mixed in a ratio of 1:1:1:0.5 with the target protein. Then this mix was incubated for at least 1 h at 4 °C and a western blot was performed to confirm successful biotinylation. For higher yield the whole reaction was scaled up depending on the needed amount of biotinylated protein. Purification of the biotinylated proteins was performed over a Monomeric Avidin column® (Thermo Scientific) following manufacturer's instructions and checking the result with western blot (figure 24). The protein was loaded in Potassium free PBS and incubated on the column for 1 h. Then the column was subjected to washing steps with PBS whilst the absorbance at 280 nm was checked for unbound protein. When the absorbance approached the PBS-baseline elution, was started by washing with Biotin Blocking and Elution Buffer. Again absorbance at 280 nm was checked and the fractions with the eluted biotinylated protein were kept and concentrated

using a spin column concentrator. The column was regenerated afterwards with Regenerating buffer.

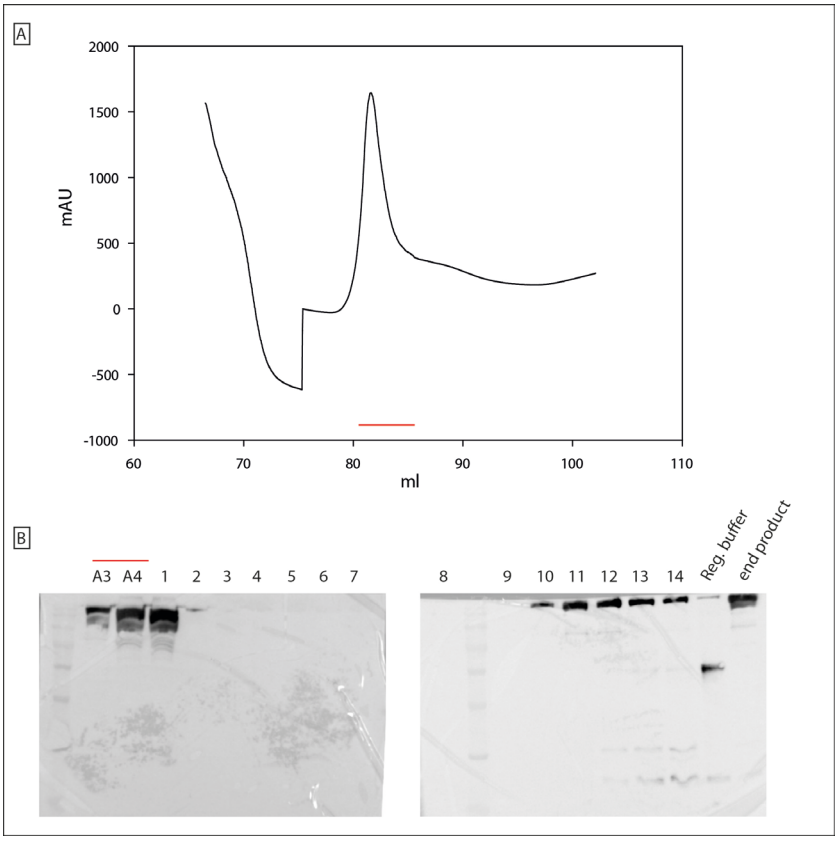

Figure 24: Biotinylation of myosin VI full-length BRS (VI BRS) construct with BirA. (A):one-step HIS-affinity purification of myosin VI BRS. **(B):** western blot after purification of VI BRS over Monomeric Avidin® column with Streptavidin detection. Lane 1: molecular weight marker, A3 and A4 (red): elution fractions from HIS column, 1: combination of both eluted fractions, (tested for motility); 2: flow-through of Avidin column, 3-8: wash fractions of Avidin column, 9-14: elution of Avidin column, Reg. buffer: sample of wash step with Regenerating buffer, end product: concentrated final biotinylated VI FL BRS.

For the biotinylation of myosin VI FL protein the His-tag affinity purification and biotinylation had to be performed during one day to keep the protein active. Biomixes, biotin and BirA were added to the slurry after sonication of the cells and incubated on a rotator at 4 °C for 1 h before the centrifugation and subsequent His-tag affinity purification (see 2.2.6). Loading of protein was performed in PBS, followed by a one-step elution at 50% HIS high 500.

Biomix A: 10 mM Tris-HCl pH 8

Biomix B: 100 mM ATP, 100 mM Mg-acetate, 500 µM d-Biotin

Biotin: 500 µM d-Biotin

Potassium free PBS: 100 mM Na_3PO_4, 150 mM NaCl

Biotin Blocking & Elution buffer: 2 mM d-Biotin in 500ml Potassium free PBS

Regenerating buffer: 100 mM glycine pH 2.8

2.2.10 Determination of protein concentration

For the determination of protein concentrations at least two different methods were deployed on the same sample for accuracy reasons.

2.2.10.1 Bradford assay

This assay is based on the observation that the absorbance maximum for an acidic solution of Coomassie Brilliant Blue G-250 shifts from 465 nm to 595 nm when binding to protein occurs (Bradford 1976). Both hydrophobic and ionic interactions stabilize the anionic form of the dye, causing a visible colour change from red/brown to blue.

With every Bradford assay a standard BSA-curve was performed with known concentrations of BSA (bovine serum albumin) ranging from 0-0.9 mg/ml. After a linear fit to the standard curve has given a linear equation, the measured data of at least 3 data points of differing dilutions of the target protein was taken into the equation and the protein concentration was calculated by:

$$(measured\ absorbance - y/x) * dilution\ factor = \ concentration\ mg/ml$$

Equation 1

2.2.10.2 Warburg-Christian

The Warburg-Christian method was developed to correct for nucleic acids contamination, leaving only the absorbance due to protein (Warburg and Christian 1942). Since nucleic acids absorb strongly at 260 nm while proteins do not, the method uses a correction factor calculated from the ratio of the absorbance at 280 nm to that at 260 nm. The Warburg-Christian uses the A280 and A260 values to calculate protein concentrations (see table 5). The purpose of using both values is to correct for nucleic acid contamination in protein samples. The sample was measured in the UV-spectrophotometer and the values at 280 and 260 nm were taken.

The ratio of these two values was determined (A280/A260), and a correction factor taken from the table below. The concentration of protein equals:

$$(A280) * (correction\ factor) = mg/ml\ protein$$

Equation 2

A280/A260	Nucleic acid in %	correction factor
1.75	0	1.12
1.63	0.25	1.08
1.52	0.5	1.05
1.4	0.75	1.02
1.36	1	0.99
1.3	1.25	0.97
1.25	1.5	0.94
1.16	2	0.90
1.09	2.5	0.85
1.03	3	0.81
0.979	3.5	0.78
0.939	4	0.74
0.874	5	0.68
0.846	5.5	0.66
0.822	6	0.63
0.804	6.5	0.61
0.784	7	0.59
0.767	7.5	0.57
0.753	8	0.55
0.73	9	0.51
0.705	10	0.48
0.671	12	0.42
0.644	14	0.38
0.615	17	0.32
0.595	20	0.28

Table 5: Warburg-Christian correction table.

2.2.10.3 280 nm method

The A_{280} method takes advantage of the absorbance of light at 280 nm by the amino acids tyrosine and tryptophan (Stoscheck 1990). A sample of the protein was taken and transferred to a UV-spectrophotometer (Varian Cary) the A_{280} was the output value for the concentration of the protein in mg/ml.

2.2.11 Purification of Myosin II from rabbit skeletal muscle

Myosin II was prepared following the method of Margossian and Lowey (1973). Extracted muscle from fast twitch fibres of the dorsal lateral and hind leg muscles of rabbits were minced and Guba-Straub solution added (300 mg/100 g of minced muscle). Minced muscle was stirred in Guba-Straub solution for 15 min at 4 °C to solubilize the myosin. The mixture was then centrifuged for 30 min at 9000 rpm. The supernatant is the myosin fraction and the pellet the Actin fraction (see 2.2.12). The supernatant was filtered and stirred into 10 volumes cold H_2Odd. After 1 h the supernatant was siphoned off and the myosin slurry centrifuged at 9k rpm for 15 min. The myosin pellet was further purified by another round of solubilization by addition of a minimal volume of 3 M KCl and precipitation (10 volumes H_2Odd), before a final solubilization in Myosin prep solution. After addition of the myosin preparation solution to the pellet the concentration was determined by measuring the optical density:

$$Absorbance 280 - 340\,nm \;=\; 0.533 \;\equiv\; 1\,mg/ml$$

Equation 3

Purified myosin was stored at -20 °C in 50% (v/v) glycerol.

Guba-Straub solution: 0.3 M KCl, 0.1 M KH_2PO_4, 0.05 M K_2HPO_4, 1 mM ATP, 5 mM $MgCl_2$, pH 6.5
Myosin prep solution: 50 mM Phosphate buffer, 5 mM DTT, 5 mM EDTA, 3 M KCl, pH 7.0

2.2.12 Purification of Actin from rabbit skeletal muscle

Buffers: see Purification of Myosin II from rabbit skeletal muscle

Rabbit actin was prepared by the method of Pardee and Spudich (1982). Actin was extracted from the insoluble muscle mince left over from the myosin preparation above. The insoluble fraction of the minced muscle was mixed with 2 l of actin extraction buffer (0.4% w/v $NaHCO_3$) and stirred for 10 min. The mixture was filtered through cheesecloth, and the residue scraped from the cheesecloth and mixed with 1 l of 1 mM EDTA (pH 7.0). After stirring the mixture for 10 min the slurry was again filtered

through cheesecloth. The residue was further extracted with 2 l of H_2Odd (the slurry was filtered through cheesecloth after each extraction). Two volumes of cold acetone were added to the residue and stirred for 30 min; the resulting slurry was filtered through cheesecloth. This step was repeated four times with 1 volume of acetone. The residue was then allowed to dry in the fume hood overnight. The actin containing acetone powder was stored at -20 °C.

2.2.13 Purification of Actin from acetone powder

6 grams of acetone-dried powder were stirred into 120 ml ACEX (**ac**tin **ex**traction) solution following the method of Pardee and Spudich (1982). The resulting slurry was filtered thoroughly through cheesecloth and the filtrate was stored on ice while the residue was again stirred with a further 80 ml of ACEX for 10 min. The slurry was again filtered through cheesecloth and the filtrate was combined with that from the first extraction and centrifuged at 20k rpm for 15 min. The supernatant was removed and Tris-HCl (2 M, pH 8.0), KCl (3 M) $MgCl_2$ (1 M) and ATP (100 mM) were used to make up the concentration in the supernatant to 5 mM, 50 mM, 2 mM and 1 mM respectively. The Actin was then allowed to polymerise for 2 h at 4 °C. To remove tropomyosin and other regulatory proteins from the polymerised actin, a "high salt cut" had to be deployed by adding solid KCl to the supernatant to make up the concentration up to 0.8 M, whilst the pH was adjusted to 8.3-8.5 with 1 M KOH. The F-actin was then pelleted by centrifugation at 70k rpm for 40 min. After removal of the supernatant the pellet was gently homogenised in 8 ml of ACEX for 30 min on ice. The homogenised actin pellet was then dialysed against ACEX overnight. The resulting G-Actin was clarified by spinning at 13k rpm for 15 min (figure 25). The concentration was determined by measuring the optical density:

$$Absorbance 290 - 310\,nm \;=\; 0.62 \;\equiv 1\,mg/ml.$$

G-actin was aliquoted before being drop frozen in liquid nitrogen and stored at -80 °C or in liquid nitrogen.

ACEX solution: 2 mM Tris-HCl pH 8.0, 0.2 mM ATP, 0.2 mM $CaCl_2$, 1 mM DTT

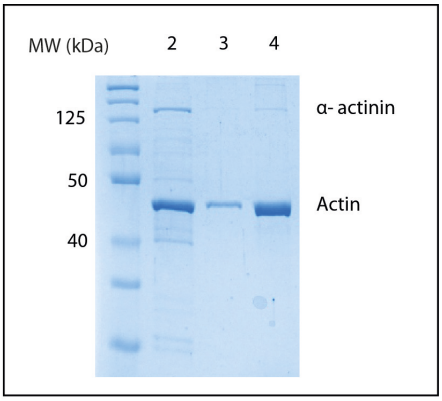

Figure 25: A 10% SDS-PAGE gel showing samples from actin purification. Lane 1: Molecular weight markers (kDa). Lane 2: before high salt cut, lane 3: before dialysis, lane 4: purified G-actin after dialysis.

2.2.14 Myosin II HMM Preparation

5 ml of a Myosin II Glycerol-stock solution (stored at a concentration of about 10 mg/ml) were pipetted together with 40 ml of ice cold H_20dd into centrifuge tubes. The mixture was centrifuged for 15 min at 20k rpm and 4 °C. The pellet was resuspended in 5 ml 2x High Salt Buffer and 50 µl Chymotrypsin were added and the mixture was thoroughly vortexed. After exactly 10 min at RT the digest was stopped by mixing with 50 µl of the Bowman-Birk-Inhibitor. After an overnight dialysis in 3 l of Low-Salt-Buffer the solution was then centrifuged at 20k rpm for 30 min at 4 °C to remove all undigested Myosin and LMM. The supernatant was taken and frozen at -80 °C.

Low Salt buffer: 40 mM KCl, 20 mM K-Phosphate buffer (pH 6.5), 2 mM $MgCl_2$, 2 mM DTT
2x High-Salt buffer: 1M KCl, 40 mM K-Phosphate buffer (pH 6.5), 4 mM $MgCl_2$, 2 mM DTT

α-Chymotrypsin: 5 mg/ml in Tris HCl pH 7.5

2.2.15 Myosin II S1 Preparation using Papain

Rabbit Mg^{2+} papain-S1 was prepared by Papain (Sigma) digestion of myosin under conditions of low salt and high free magnesium. The presence of magnesium is essential to ensure papain cleavage occurs between S1 and S2. In the absence of magnesium the RLC may become unfolded and dissociate from its IQ-motif on the myosin neck, enabling papain digestion to occur within the exposed RLC binding region. The resulting S1 has a short neck with no RLC (figure 26).

Myosin II (glycerol stock) was exchanged into low salt buffer by precipitation with cold H_2Odd and centrifugation (4 °C, 15k rpm), followed by redissolving of the myosin pellet in low salt buffer. Activated Papain stock solution (0.5 mg/ml papain in 5 mM cysteine, 2 mM EDTA pH 6.0) was added to the redissolved myosin to a final Papain concentration of 0.03 mg/ml. Digestion was allowed to proceed at 23 °C for 15 min. Digestion was stopped by the addition of a 2x molar excess of E64 inhibitor. Digestion products were dialysed against a low salt buffer (+2 mM DTT) and insoluble products were removed by centrifugation (20k rpm, 30 min). The soluble S1 was purified on an anion exchange column (Mono Q, GE) by deploying a linear salt gradient (0-1 M NaCl) over approximately five column volumes. The 2 ml fractions were collected and concentrated on spin concentrator columns. Concentration was determined by measuring the Optical density:

$$Absorbance 280 - 340\,nm \;=\; 0.83 \;\equiv\; 1\,mg/ml$$

as well as with a Bradford assay (see 2.2.10.1).

The aliquots were stored at -80 °C in the presence of 30% (w/v) sucrose.

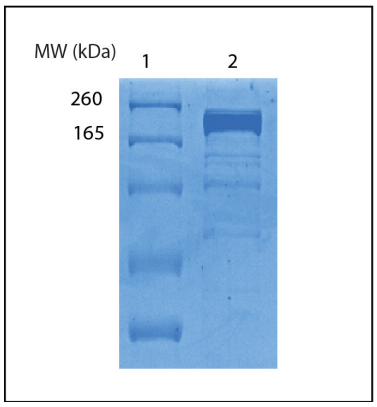

Figure 26: SDS PAGE of HMM preparation using Papain. Lane 1: molecular weight markers (kDa); Lane 2: HMM (2 µg) (220 kDa) after digestion of myosin II with papain.

2.3 Methods for functional protein analysis

2.3.1 *In vitro*-motility assay (gliding filament assay)

For studying the translocation of actin filaments by myosin, rhodamine phalloidin-labelled actin was exposed to immobilized myosin in a flow cell (figure 27). The flow cell was filled with myosin at different concentrations (diluted in AB^--buffer) and the myosin allowed to adhere to the nitrocellulose or nitrocellulose and antibody treated surface of the cell by incubating for 2 to 3 min. After this step the flow cell was washed with 2-3 volumes of 1 mg/ml BSA in AB^--buffer. The last volume was allowed to incubate for at least 2 min to block unspecific binding. The flow cell was then washed with diluted rhodamine phalloidin-actin in AB^-/BSA which was allowed to bind for 1 to 2 min. Before the motility assay was started, AB^--scavenger solution was added and the cell was placed on the microscope stage and observed using either a 60x or 100x TIRF objective. To start the actual motility assay AB^+-scavenger solution was added and if motility was observed movies were recorded using a CCD camera system on the microscope (Sellers 2001) (figure 27 B).

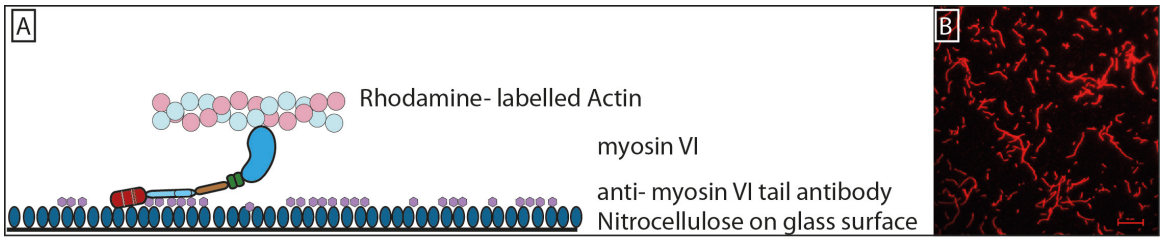

Figure 27: Schematic picture of a motility assay using myosin VI, (A): note that myosin VI does not move on nitrocellulose but needs to be bound to an antibody, **(B):** typical field of view with Rh/Phalloidin labelled actin filaments bound to myosin VI; scale bar: 20µm

The AB- and AB+ solutions were degassed prior to use in order to reduce the concentration of dissolved oxygen and thus additional bleaching effects on the fluorophores. Following degassing, solutions were stored in 10 ml syringes to slow down the diffusion of oxygen. Smaller volumes (1 ml) of oxygen scavenger solutions were made using the degassed AB^- and AB^+ stock solutions; these were also stored in syringes. All solutions were kept on ice.

The oxygen-scavenging system was included to keep photo-bleaching low. In this system, glucose-oxidase catalyses the oxidation of D-glucose to form D-glucono-1,5-lactone and hydrogen peroxide. Hydrogen peroxide would severely damage the motor proteins, so

that catalase is used to decompose the hydrogen peroxide to water and oxygen (figure 28).

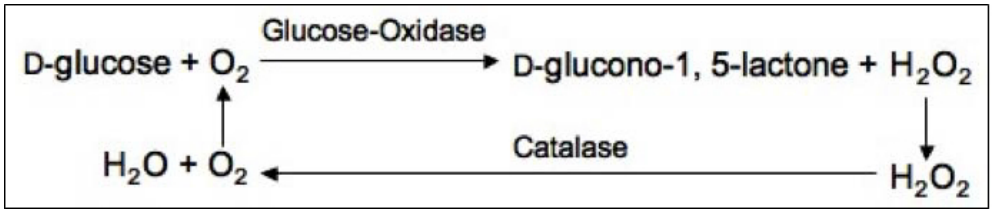

Figure 28: Reaction of the oxygen-scavenging system used in *in vitro* motility assays. To avoid photo-bleaching of the sample during acquisition, an oxygen-scavenging system containing glucose, glucose-oxidase and catalase was used.

Data was obtained with time-lapse movies where one picture was taken every 10 s for at least 2 min, under TIRF illumination using a 543 nm laser. Data was analysed using the GMimPro package (see chapter 2.4) and filaments where tracked by hand. Motility assays were performed with protein from at least three different preparations and at least four flowcells per setting.

Myosin VI has shown no movement in normal assay buffer and therefore all myosin VI motility assays were performed using Myosin VI motility buffer and at 32 °C.

AB^+: 25 mM Imidazole, 25 mM KCl, 4 mM $MgCl_2$, 1 mM EGTA, 2 mM ATP

AB^-: 25 mM Imidazole, 25 mM KCl, 4 mM $MgCl_2$, 1 mM EGTA

AB^--scavenger: As for AB^+, including 0.02 mg/ml catalase, 0.1 mg/ml glucose oxidase, 3 mg/ml glucose, 20 mM DTT

AB^+-scavenger: As for AB^--scavenger including 2 mM ATP.

Myosin-VI-motility buffer: 20 mM Tris-HCl (pH 7.5), 20 mM Imidazole, 25 mM NaCl, 5 mM $MgCl_2$, 1 mM EGTA, 10 mM DTT, (+5 mM ATP for AB^+-scavenger)

2.3.1.1 Removal of dead heads

Dead heads, which only bound actin but did not show the ability to hydrolyse ATP and thus stayed in the rigor state on actin, could be removed from the stock solutions before use. This can greatly improve the quality of the motility. The motor protein was mixed in a 5:1 molar ratio with F-actin in 1x AB^+ solution (total volume 200 µl). An ultracentrifuge spin at 100k rpm for 15 min at 4 °C followed. The dead heads would remain bound to actin and therefore pellet, whilst the functional heads remained in the supernatant.

AB^+: 25 mM Imidazole, 25 mM KCl, 4 mM $MgCl_2$, 1 mM EGTA, 2 mM ATP

2.3.1.2 N-Ethylmaleimide myosin (NEM-myosin)

NEM myosin is chemically inactivated muscle myosin II that still binds to actin and was produced for tethering and immobilisation purposes in gliding-filament assays. Already extracted myosin II (in glycerol) was pipetted into an adequate tube and H_2Odd. After centrifugation at 13k rpm for 6 min the supernatant was discarded and 2x High Salt buffer was added. To this mixture n-Ethylmaleimide was combined and the mixture was left to incubate for 75 min at room temperature (RT). Addition of 1 M DTT and fresh H_2Odd was followed by a centrifugation step at 13k rpm for 6 min. The pellet was washed with 2x High Salt buffer and after a final centrifugation, the supernatant, containing the NEM myosin was kept on ice until used.

2.3.2 ATPase

2.3.2.1 NADH-coupled assay

ATPase activity was determined in a coupled enzymatic assay (De La Cruz and Ostap 2009) (figure 29). In this assay, ATP hydrolysis is linked to the oxidation of NADH, which is measured spectroscopically at 340 nm by its decrease in concentration. The coupling takes place via phosphoenol pyruvic acid (PEP), pyruvic acid kinase (PK) and lactate dehydrogenase (LDH), which is referred to as ATP regenerating system.

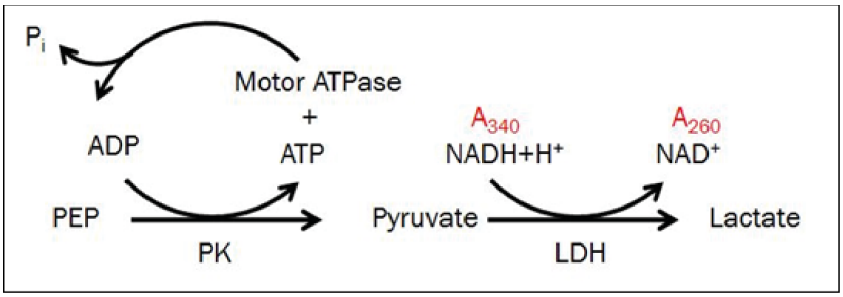

Figure 29: Schematic of the coupled enzymatic steady-state ATPase assay. Myosin hydrolyses ATP to ADP and inorganic phosphate, while simultaneously the regenerating system recycles the generated ADP back into ATP. Therefore, the system maintains a steady-state ATPase of myosin. Via the enzymatic action of pyruvate kinase (PK), for each ATP molecule generated, one NADH molecule is oxidized by lactate-dehydrogenase (LDH) to NAD^+. The resulting decrease in absorption can be measured at 340 nm.

To study the filament-stimulated ATPase activity of the assayed motor protein, measurements at different F-actin concentrations were carried out. With the output value of absorption (A) in OD (optical density) per second, the molar absorptivity (ε) of NADH

at 340 nm and the diameter of the well, the NADH concentration in the activated ATPase assay can be determined by applying the law of Lambert-Beer (see Equation 4).

$$A_\lambda = \varepsilon_\lambda * d * c$$

Equation 4: (Haid, Lehmann *et al.* 1975)

Where ε (NADH at 340nm) = 6.22 $Mol^{-1}*cm^{-1}$ and d = 0.3125 cm. The amount of NADH that is oxidised per second corresponds to the amount of hydrolysed ATP per second, which in turn reflects the maximal rate of ATP hydrolysis (V_{max}). K_m expresses the motor concentration that yields the halfmaximal reaction rate.

k_{cat} or the catalytic constant expresses the number of hydrolysed ATP molecules per motor head (or motor dimer) per second, and was calculated according to Equation 5.

$$k_{cat} = \frac{c_{ATP} * s^{-1}}{c_{myosin}}$$

Equation 5

The standard mixture consisted of 10 µl PEP (600 µM), 6 µl NADH (360 µM), 3 µl ATP (3.78 mM) and 3 µl of PK/LDH, following the protocol from De La Cruz and Ostap (2009). Then 100 nM myosin was added as well as a defined amount of F-actin, ranging from 0-25 µM in concentration.

2.3.2.2 HPLC based assay

Since ATPase forms ADP from ATP through Pi release, measurement of ADP can be used as an alternative for the assay of ATPase activity. On the basis of this consideration, high-performance liquid chromatography (HPLC) was used to measure ADP derived from ATP by the enzymatic reaction of the ATPase myosin (figure 30).

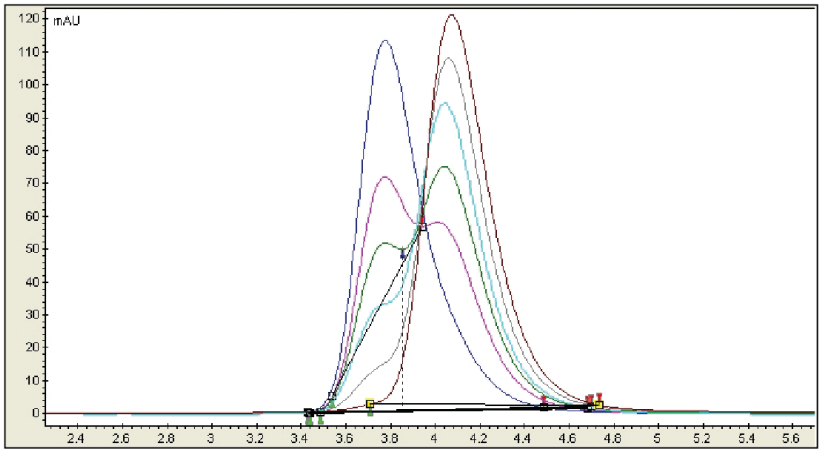

Figure 30: HPLC data curves from ATPase measurement of myosin II S1 fragment. ATP peak appears after 4 min elution and corresponding ADP peak at 3.6 min. Brown curve indicates the starting ATP concentration at 0 min reaction time, grey: 5 min, light blue: 10 min, green: 15 min, pink: 20 min and dark blue: 30 min.

The components ATP (2 mM), myosin (100 nM) and actin (varying concentrations from 0-25 µM) were mixed together with buffer to make up a final volume of 200 µl, then 20 µl were removed at different time points, mixed with 2µl 1 N HCl and 378 µl of the HPLC buffer, to stop the reaction and precipitate the protein. To remove the precipitant, the tubes were centrifuged at 10k rpm for 10 min in a table top centrifuge at RT. The samples were loaded on the HPLC and assayed with a flow rate of 0.2 ml/min for 10 min over a PL-SAX column (1000 Å, 8 µm). PL-SAX columns are ideal for the anion-exchange HPLC separations of proteins and deprotected synthetic oligonucleotides under denaturing conditions. In addition, the anion exchange capacity is mostly independent of pH.

HPLC buffer: 0.2 M $(NH_4)_2HPO_4$ pH 4.0

Assay buffer for myosin VI ATPase assays (KMg50): 50 mM KCl, 1 mM $MgCl_2$, 1 mM EGTA, 1 mM DTT, 10 mM Imidazole, pH 7.0

Assay buffer for myosin II S1 ATPase assays (PIPES): 10 mM PIPES, 2 mM $MgCl_2$, pH 7.0

2.3.3 Dot Far-Western Blot

Dot Far western blots are a form of western blot to detect protein:protein interactions (Ohba *et al.* 1998, Mahlknecht *et al.* 2001). The "prey" protein was spotted directly onto a nitrocellulose membrane (Amersham Biosciences) and left to dry up to 30 min. After an incubation step of 1 h in blocking buffer, the membranes were submitted to a 1 h wash

with the "bait"-protein in a dilution of 1:2000. During this time the tagged protein could bind to the proteins spotted on the nitrocellulose surface. After several washing steps with TBST buffer, the adequate antibody for the "bait"-tag was added to fresh blocking buffer for an additional hour. Washing of the membrane in TBST for 3-5 times was then followed by final detection using an ECL detection kit (BioRad).

TBST buffer: 50mM Tris-HCl , pH 7.5, 150mM NaCl, 0,1 vol% Tween20

2.3.4 Liposome preparation

For liposome production a range of natural lipids were used: Phosphatidylcholine (PC), Phosphatidylethanolamine (PE), Cholesterol, Phosphatidylinositol (4,5)-bisphosphate (PIP_2), Phosphatidylinositol (3,5)-bisphosphate ($PI(3,5)P_2$) and Phosphatidyl-4-phosphate (PI(4)P) (figure 31).

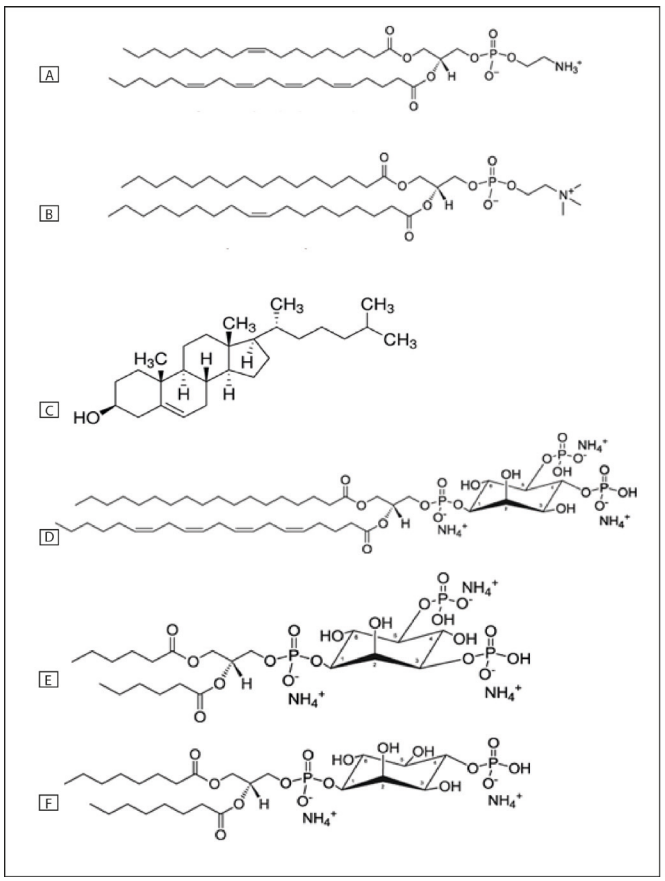

Figure 31: Structures of main lipid components. (A): Phosphatidylethanolamine (PE), **(B):** Phosphatidylcholine (PC), **(C):** Cholesterol, **(D):** Phosphatidylinositol (4,5)-bisphosphate ($PI(4,5)P_2$, PIP_2), **(E):** Phosphatidylinositol (3,5)-bisphosphate ($PI(3,5)P_2$), **(F):** Phosphatidyl-4-phosphate (PI(4)P). All structures originate from Avanti Lipids® website.

2.3.4.1 Liposome preparation by extrusion

Stock solutions of lipids were stored at -20 °C in chloroform. Every mixture of lipids was treated equally, despite slight changes in thawing temperature. As a first step to produce liposomes (figure 32) the chloroform was evaporated using a Bachhofer® vacuum-concentrator system. After evaporation the lipid cake was redissolved in aqueous buffer (e.g. Lipidbuffer) and subjected to a minimum of 5 freeze/ thaw cycles in liquid nitrogen and a water bath at 50 °C. After a brief sonication step in the sonicator bath, the emulsion was extruded through a 100 nm pore filter in an Avanti Lipid Mini Extruder for 11 to 21 cycles.

Lipidbuffer (Spudich *et al.* 2007): 20 mM HEPES (pH 7.4), 150 mM NaCl, 1 mM DTT

2.3.4.2 Liposome preparation by sonication

Lipids and lipid mixtures were generally treated as before, with the difference, that instead of extruding them, they were subjected a 10-15 min long sonication in the sonicator bath. This method was preferred since no defined size of liposomes was crucial for the used assays (e.g. co-sedimentations).

2.3.4.3 Composition of lipids in liposomes

Following the protocol of Spudich *et al.* (2007), Phosphatidylinositol containing liposomes were made from 40% PE, 40% PC, 10% Cholesterol and 10% of a variable phosphoinositol, treated as above (2.3.4.1) before resuspension by sonication in Lipidbuffer to a final concentration of 1 mg/ml. This amounts to a total of 0.02 mg/ml PIP. These mixes were treated as for extrusion or sonication but with a higher thaw temperature of 60 °C due to the fact that Cholesterol did not go into solution below this temperature but formed white flakes.

2.3.5 Protein-Lipid-Overlay Assay (PLO)

Lyophilized lipids (in this case PC, PE and folch I (folch)) were reconstituted to 1 mM stocks in chloroform (despite the folch, which, as a mixture, was dissolved at 1 mg in 1.5 ml) and stored at -20 °C until usage. According to Dowler *et al.* (2000) and Dowler *et al.* (2002) the lipids were diluted to three different concentrations (500, 350 and 200 µM). 1µl drops of the dilutions, which contained 200 to 500 pmol of lipid, were spotted on a nitrocellulose membrane (Hybond-C extra, Amersham Biosciences) and allowed to dry

for 1 h at RT. Additionally 0.5 µl of the protein was spotted on the membrane as a control. The membrane was then incubated with gentle rocking for 1 h in Blocking Buffer at RT. Subsequently the membrane was incubated overnight at 4 °C with gentle rocking in fresh Blocking Buffer containing the target His-tag protein that was diluted to 5-10 nM. On the next morning the membrane was washed 10 times over 50 min in TBST. Afterwards the membrane was incubated for another hour at RT with gentle agitation with a 1:2000 dilution of the appropriate antibody (e.g. Anti-6X His-tag® antibody (HRP) #1187, abcam) in fresh Blocking Buffer (figure 32). The washing step with TBST was repeated. The lipid binding protein bound to the membrane was detected by utilising a standard ECL detection kit (e.g. Novex® ECL Chemiluminescent Substrate Reagent Kit) following manufacturer's instructions.

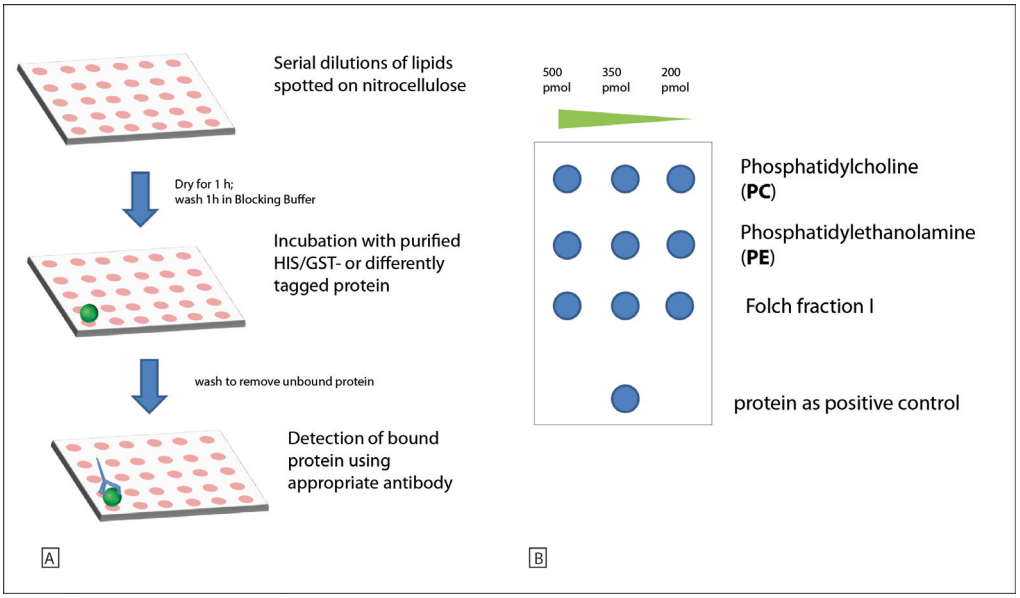

Figure 32: Protein-lipid overlay assay (PLO). (A): overview over the method of preparing a (PLO) by spotting serial dilutions of lipids in chloroform onto the nitrocellulose membrane. After drying, the membrane is washed with the target protein which is subsequently detected by antibody binding and chemiluminescence detection. **(B):** layout of typical blot with serial dilutions of the target lipids of 500 pmol, 350 pmol and 200 pmol per spot.

2.3.6 PIP Strips/Membrane Lipid Strips® (echelon inc.)

These nitrocellulose strips are prespotted with a range of different phosphatidylinositols and/or the most important membrane lipids (figure 33). The principle follows the Protein-overlay-assay but is much shorter, due to a higher sensitivity. The membrane was gently agitated throughout the process. The membrane was blocked with 5 to 10 ml Blocking Buffer for 1 h at RT. After discarding the Blocking Buffer, a standard dilution of 1:1000

of the sample protein was added in 5 ml of fresh Blocking Buffer and again the membrane is incubated for 1 h. The membrane then was washed thrice with TBST for 5 to 10 min each. The wash solution was discarded and replaced by fresh Blocking Buffer with appropriate antibody (see 2.3.5) in a 1:2000 dilution. In this solution the strip was again incubated for 1 h. The washing step with TBST was repeated. The lipid binding protein bound to the membrane was detected by utilising a standard ECL detection kit (e.g. Novex® ECL Chemiluminescent Substrate Reagent Kit) following manufacturer's instructions.

Blocking Buffer: 50 mM Tris HCl (pH 7.5), 150 mM NaCl, 0,1% (v/v) Tween 20, 2 mg/ml Fatty-acid free BSA

TBST: 50 mM Tris HCl (pH 7.5), 150 mM NaCl, 0,1% (v/v) Tween 20

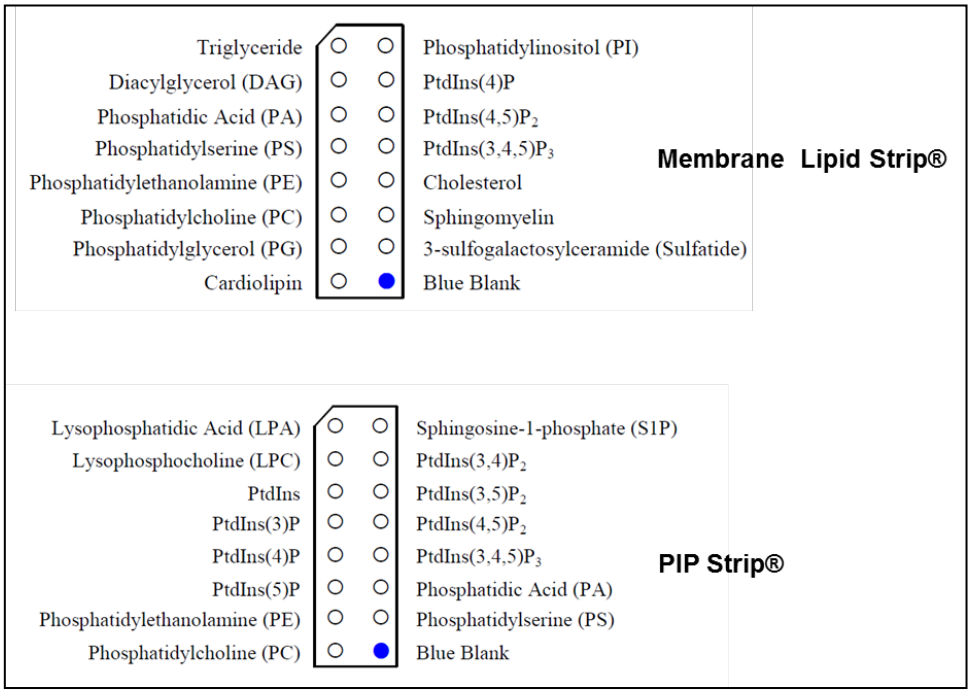

Figure 33: Pre-spotted Membrane- and PIP strips. Membrane Strips comprise the most abundant and important membrane lipids whereas PIP Strips show the seven different species of phosphatidylinositolphosphates and seven other biologically important lipids (echelon™).

2.3.7 Lipid-affinity co-sedimentation

Protein (varying concentrations) and 0.2 mg/ml liposomes were mixed in a total reaction volume of 125 µl. This resulted in a total PIP concentration of 18.21 µM per reaction tube where phosphatidylinositolphosphates were used. After adding buffer and target protein

to the ultracentrifugation tube, the lipid mixture was added and the solution left to stand on the bench for 10 min. The centrifugation step, to pellet the liposomes and possibly bound protein, was carried out in a MAX-XP table top ultracentrifuge (Beckman-Coulter ®) at 160k x *g* for 20 min at 4 °C. After centrifugation the supernatant was removed and collected in a reaction tube. The pellet was dissolved in 125 µl Lipidbuffer and collected in a separate tube. After denaturing the samples with SDS buffer at 98 °C for 5 min, a SDS-PAGE was performed to see if the protein fraction could be found in the pellet and therefore was bound to the formerly added lipid (figure 34).

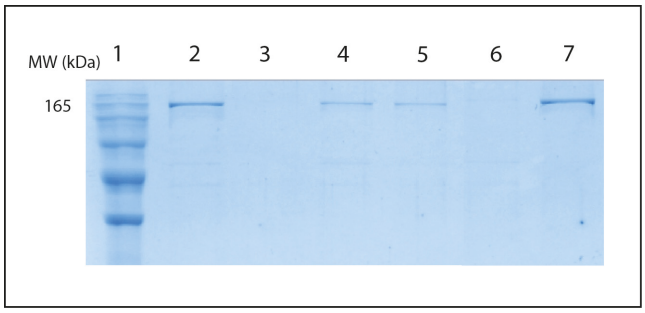

Figure 34: SDS-PAGE a co-sedimentation experiment utilizing liposomes as pull-down "weight". Lane 1: molecular markers (kDa), lane 2: Supernatant fraction of myosin VI spun down only with buffer, lane 3: pellet fraction corresponding to lane 2; lane 4: Supernatant fraction of myosin VI spun down together with folch fraction I (folch) liposomes; lane 5: pellet fraction corresponding to lane 4, lane 6: Supernatant of myosin VI spun down with folch and additional 50 µM $CaCl_2$, lane 7: pellet fraction corresponding to lane 6.

2.3.8 Gliding-filament assay on lipid surfaces

For a deeper insight into the protein:lipid interactions a variation of the abovementioned motility assay was performed. The nitrocellulose-covered surface was washed with one flow-cell volume of 1:20 diluted lipid suspension and left to incubate for 10 min at RT so the lipid molecules could adhere to the surface. Afterwards the surface was blocked with a 3-4 flow-cell volume wash of AB^-/BSA to inhibit unspecific binding to the surface. Following this step myosin was flushed through the cell and the motility assay was performed as mentioned above (figure 35).

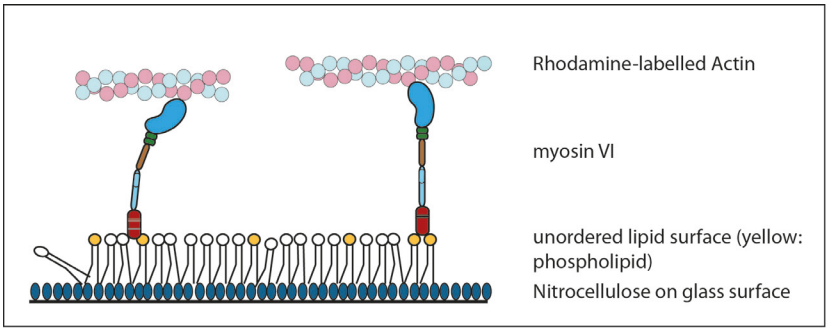

Figure 35: Gliding filament assay on nitrocellulose-bound lipid surface, due to the nitrocellulose the lipids do not form a fluid lipid bilayer but an unordered monolayer on which the protein can move actin filaments.

2.3.9 Fluorescence Recovery after Photobleaching (FRAP)

To quantify the absence two-dimensional lateral diffusion of the lipid surface used in the motility assays, a FRAP check was performed. For this purpose fluorescently labelled PE was incorporated into the lipid mixture (Lissamine®-PE) and the flowcell was prepared as described in 2.3.8. Then a region of interest (ROI) was defined on the confocal microscope and a laser pulse of 10 sec with a 405 nm laser was applied to this area. After this the recovery was recorded with a 554 nm laser for 2-5 min (figure 36).

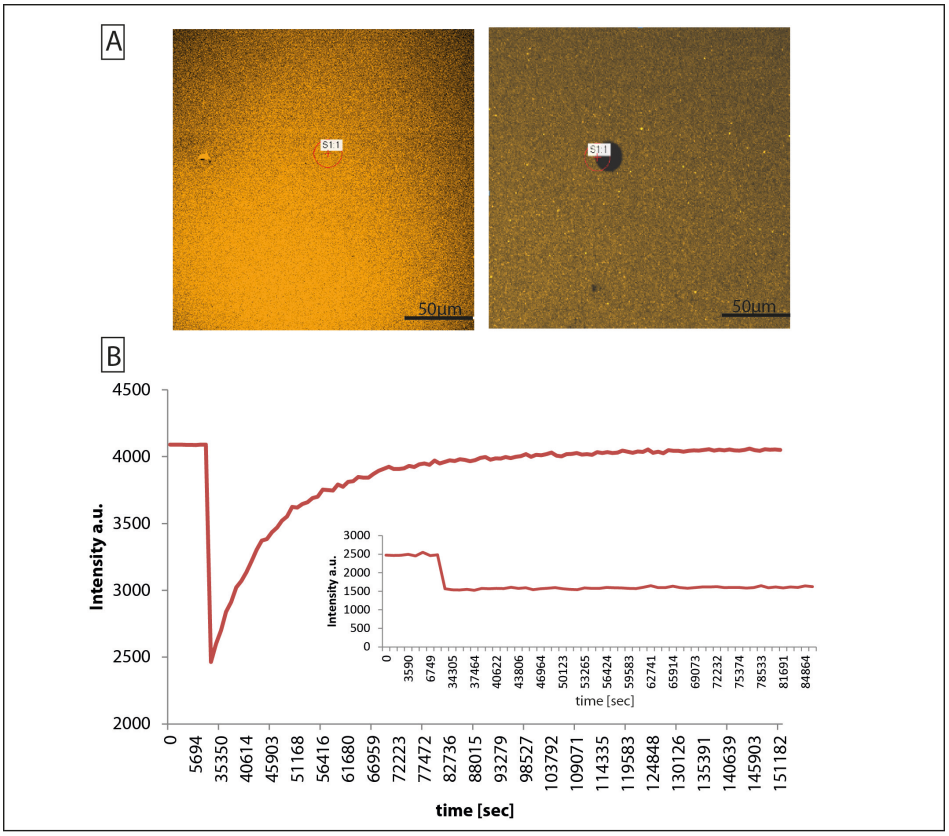

Figure 36: FRAP experiments for quantification of lateral diffusion in lipid surfaces. (A) Typical bilayer surface before and after photobleaching with the corresponding FRAP answer **(B)**. Inset shows surface without fluorescence recovery.

2.3.10 Actin-affinity Co-sedimentation

The procedure for co-sedimentations with actin followed the same protocol as with lipids (see 2.3.7), but using actin as the pulldown 'weight'. Typically 5 µM actin was added to a total reaction volume of 125 µl and varying concentrations of myosin constructs. For the actin pellet was very sticky, it had to be carefully scraped off the sides of the centrifugation tube with the tip of a pipette.

2.3.11 Co-sedimentation with ligand-coupled magnetic beads

2.3.11.1 His-tagged protein co-sedimentation with Dynabeads®

For detection of protein:protein interactions without the need of actin or liposomes as pull-down reagent, superparamagnetic beads (Dynabeads®, novex life technologies) were used as one alternative system. They are coated with a cobalt-based surface and allow fast binding of the His-tagged protein. The protocol was followed according to manufacturer's

instructions. In short, the 6x His-tagged target protein was added to the previously washed beads in Binding/Wash buffer and incubated for 10 min at RT on a rotating platform. Then, after thorough washing were the beads were held down with a magnet and the supernatant was removed and fresh buffer added, the differently tagged protein was added to the protein: beads complex in Pull-down buffer and incubated at RT on a rotating platform for 30 min. After four washing steps with Binding/Wash buffer, 100 µl His Elution buffer were added and the suspension was subjected to a further incubation of 5 min on the rotary shaker. The beads were now collected at the tube wall and the supernatant contained the eluted histidine-tagged protein and its interacting protein. A SDS-PAGE and if necessary a western blot were run for detection of proteins.

Binding/ Wash buffer: 50 mM Sodium Phosphate pH 8.0, 300 mM NaCl, 0.01% Tween 20

His Elution buffer: 300 mM Imidazole, 50 mM Sodium Phosphate pH 8.0, 300 mM NaCl

Pull-down buffer: 3.25 mM Sodium Phosphate pH 7.4, 70 mM NaCl, 0.01% Tween 20

2.3.11.2 GST-tagged protein co-sedimentation with MagneGST®

Detection of interactions between a GST-tagged construct and a non-tagged or His-tagged protein was performed with the MagneGST® (Promega) bead system. The system works in general similar to the Dynabeads® pull-down system but with a high affinity to GST. In short, after washing the beads in PBS the GST-tagged protein was added with an addition of 1% BSA to reduce unspecific binding and then incubated for 30 min at RT on a rotating platform. Then the suspension was subjected to several washes in PBS before the HIS-or differently tagged sample and 10% BSA were added. Another incubation step of 1 h on a rotating platform was followed by a vigorous vortexing step to remove non-specific adherent protein. Several washes in PBS followed and finally 20 µl of 2x SDS buffer were added directly onto the sample containing bead-bound and interacting proteins. After the sample was boiled for 5 min at 98 °C the beads were removed and a SDS-PAGE or, if necessary a western blot was performed.

2.3.12 Densitometry

For further characterisation of binding in co-sedimentation assays, supernatant and pellet fractions were analysed on SDS–PAGE (10 or 15% acrylamide) gels using prestained broad-range standards (Applichem) for calibration. Gels were analysed using the

ImageLab® software and the ChemiDoc XRS+ (BioRad). The intensity of the tail or full-length band in the pellet was divided by the total intensity (pellet + supernatant) for each sample to determine the percent of protein in the pellet. Background subtraction was automatically performed by the software.

2.3.13 Calmodulin affinity titrations

Titrations of target peptide sequences with Calmodulin or Calmodulin-like proteins were performed at 20 °C in titration buffer, using a Varian Cary Eclipse fluorescence spectrophotometer with the excitation wavelength λ_{ex} = 290 nm and emission wavelength λ_{em} = 323 nm.The dissociation constants K_d for the tryptophane (Trp)-containing peptides were determined by direct titration, and the data was analysed as described in Martin and Bayley (2004). For titrations 2 µM peptide was used. Calmodulin was purified over His-tag affinity columns (see section 2.2.6) and then dialysed into either the calcium buffer or EDTA buffer (see below). Titrations were carried out by adding approximately 0.1 µM Calmodulin per injection for more than 20 injections. The proportion of the signal attributed to Calmodulin alone was determined by continuing the titration to much higher ratios to a large excess of Calmodulin. This was taken into account by the analysis (see 2.4.1.1).

Titration buffers: 25 mM Tris (pH 8), 100 mM KCl, and 1 mM DTT with 1 mM $CaCl_2$ or 0.2 mM EDTA

2.3.14 Size-exclusion chromatography (SEC)

SEC is a good means to separate molecules according to differences in size as they pass through a gel filtration medium (porous matrix) packed in a column. Unlike ion exchange or affinity chromatography, molecules do not bind to the chromatography medium so buffer composition does not directly affect the degree of separation between peaks. Purified proteins (~30–50 µM) were loaded onto a Superdex-200 prep-grade (10/300 GL) analytical column (GE Healthcare) or a Superose-6 column (10/300 GL). They were pumped through with a flow rate of 0.5 ml/min. The native molecular weight of the proteins was calculated from their Stokes radius (Dutta *et al.* 2001) measured by SEC (figure 37). The partition coefficient K_{av} for standard proteins was calculated as follows (Ohno *et al.* 1986):

$$K_{av} = \frac{V_e - V_o}{V_c - V_o}$$

Equation 6: calculation of partition coefficient for standard proteins on size exclusion chromatography columns.

Were V_e is the elution volume of the protein, V_o the void volume and V_c the total volume of the column.

SEC buffers:

GF150: 50 mM Tris-HCl (pH 7.5), 150 mM NaCl, 1 mM DTT

GF500: 50 mM Tris-HCl (pH 7.5), 500 mM NaCl, 1 mM DTT

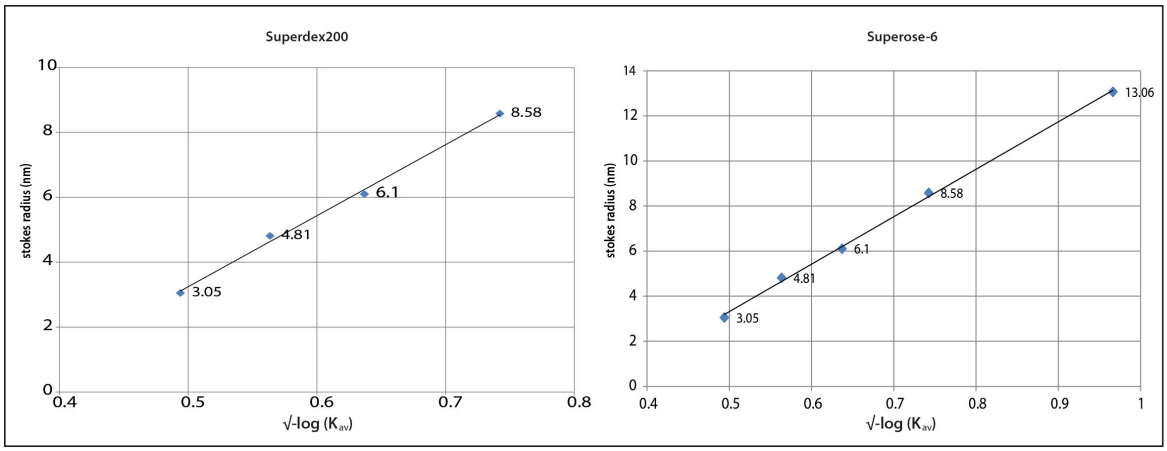

Figure 37: Calibration curves for Superdex-200 (Prep-grade) and Superose-6 columns. Thyroglobulin, ferritin, aldolase, ovalbumin and myosin II were used as calibration proteins. K_{av} stands for the partition coefficient which takes retention time and void volume into account and serves as normalisation. The Einstein-Stokes radius gives the effective hydrated radius of a protein in solution.

2.4 Data analysis

1. Quantitation of data obtained from lipid- and actin-affinity co-sedimentation

Band intensities and the respective supernatant and pellet fractions were determined with the digital gel-analysis software ImageLab (Version 5.0, BioRad). The obtained intensity of the tail band in the pellet was divided by the total intensity (pellet + supernatant) for each sample to determine the percent of protein in the pellet) (Spudich *et al.* 2007).

2. Fluorescence microscopy data analysis: Gliding-filament motility measurements

Only those filament-gliding events where the transport of an individual filament lasted for longer than ≥ 3 frames and remained uninterrupted during that time period were taken into account. The gliding velocity of individual actin filaments was recorded using the NIS Elements AR software package (Nikon) and determined using ImageJ (NIH, Bethesda, USA) and the GMimPro software (Dr Gregory Mashanov, MRC NIMR, London, UK).

3. Protein purification and gel-filtration

All FPLC data was obtained and analysed using the Unicorn software package by GE healthcare.

4. Analysis of data obtained from ATPase assays on actin

Actin-activated ATPase activity of myosin VI and myosin II was determined in a coupled-enzymatic assay and an HPLC based assay (chapter 3). The data were analysed using Microsoft® Excel and SigmaPlot® packages. Preliminary data analysis of the HPKC obtained data was carried out with the supplied Galaxie Software pack (Version 1.9, Varian) and then with Microsoft® Excel and SigmaPlot® packages.

2.4.1 Fitting routines and statistics

2.4.1.1 CaM-Titrations

The direct fluorometric titrations of the tryptophan-containing peptides (IQ1 and IQ2) with a calmodulin (C) were fit to the following equation:

$$\text{Fluorescence signal} = F_{(C)}[C] + F_{(W)}[W] + F_{(CW)}[CW]$$

Equation 7

where the F values are the molar fluorescence intensities and C and W the contributions of calmodulin (C) and the IQ motifs (W) to the fluorescence signal. A value for the dissociation constant ($K_d(W)$) was obtained from a nonlinear least squares fit to this equation with concentrations calculated by solving:

$$[CW]^2 - (K_d(W) + C_T + W_T)[CW] + C_T W_T = 0$$

Equation 8

where the subscript T denotes total concentrations. We also included a factor (X(W)) in the fitting equation to correct for errors in the peptide concentration (i.e., actual concentration WTX(W)). Titrations with X(W) < 1.1 or with X(W) < 0.9 were rejected (Martin and Bayley 2004).

2.4.1.2 ATPase assay

As biocatalysts enzymes **A** form with the substrate **B** a complex **AB** which reacts to form the product **P**:

$$A + B \underset{k_{-1}}{\overset{k_1}{\rightleftharpoons}} [AB] \underset{k_{-2}}{\overset{k_2}{\rightleftharpoons}} [AP] \underset{k_{-3}}{\overset{k_3}{\rightleftharpoons}} P + A$$

k_1 and k_{-1} are the rate constants for association of A to B and for the dissociation of the AB complex respectively. k_2 and k_{-2} are the constants for the reaction to form a product and the back reaction to the substrate respectively. k_3 and k_{-3} describe the association and dissociation of an enzyme-product complex. Since this reaction does not happen directly after mixing the enzyme with the substrate $k_{-3} = 0$. Additionally the turnover from AB to AP is measured and not the release of P. Therefore the whole reaction can be simplified further and the following equations (9 and 10) can be applied.

The experimental conditions in the ATPase experiments are altered to pseudo-first order, where one reactant (A) is used in large excess (min. 5-fold) over the concentration of the second reactant (B). This ensures that the concentration of the first reactant remains virtually constant over the time of the reaction. In these reactions one step of the reaction needs to be faster than the other step in order to be able to determine between the two steps (ATP binding and ATP hydrolysis). Under these conditions the observed rate constant *v* shows hyperbolic dependence on the concentration of the second reaction partner B and a plot of *v* as a function of the concentration of B can be fitted to a hyperbola (Geeves *et al.* 1992).

$$v = \frac{v_{max}[B]}{K_M\,[B]} + k_{off}$$

Equation 9: Hyperbolic fit for ATPase reactions

Where the equilibrium constant K_i for each (reverse) step is defined as $k_{forward}/k_{backward}$ constant: $K_i = k_{+i}/k_{-i}$.

With v_{max} defined as the maximal rate constant (=$k_{+2} + k_{-2}$, however since k_{-2} is very small, v_{max} can be simplified to =k_{+2}) and K_M, the Michaelis constant, gives the concentration of B required to reach the half maximal of v_{max} (= $1/k_1$) and k_{off} (=k_{-2}) is the overall dissociation rate constant. The initial linear part of the hyperbola is defined by the slope which is equal to $\frac{1}{K_M} v_{max}$.

A direct measure of the catalytic production of product under optimum conditions (saturated enzyme) is measured with the turnover number k_{cat}:

$$k_{cat} = \frac{v_{max}}{[A] + [AB]}$$

Equation 10: Equation for the calculation of k_{cat}

2.4.1.3 Statistical tests

For evaluation of statistical significance two-tailed *t*-tests were performed. Where significant differences below the significance level of $p = 0.05$ were calculated, they are given as *p*-values in the text.

Results and Discussion

3.1 Determination of the basal ATPase activity in myosin VI

This chapter investigates the basal kinetics of myosin VI ATPase as a quality-check of the protein preparations used throughout the study with myosin II S1 as control. Two different methods for measuring the ATPase rates of the myosins are introduced.

3.1.1 Generating myosin II S1 constructs for standard measurements

The head or motor domain of myosin is a highly specialised ATPase which converts the energy derived from the hydrolysis of ATP into mechanical work. Since myosin II and its ATPase activity are well described, it was used in this thesis as a standard for verifying and validating measurements. Myosin II S1 constructs were produced by papain digestion of myosin II HMM (see 2.2.15). Figure 38 summarises the digestion process and shows corresponding SDS-PAGE pictures of the resulting constructs.

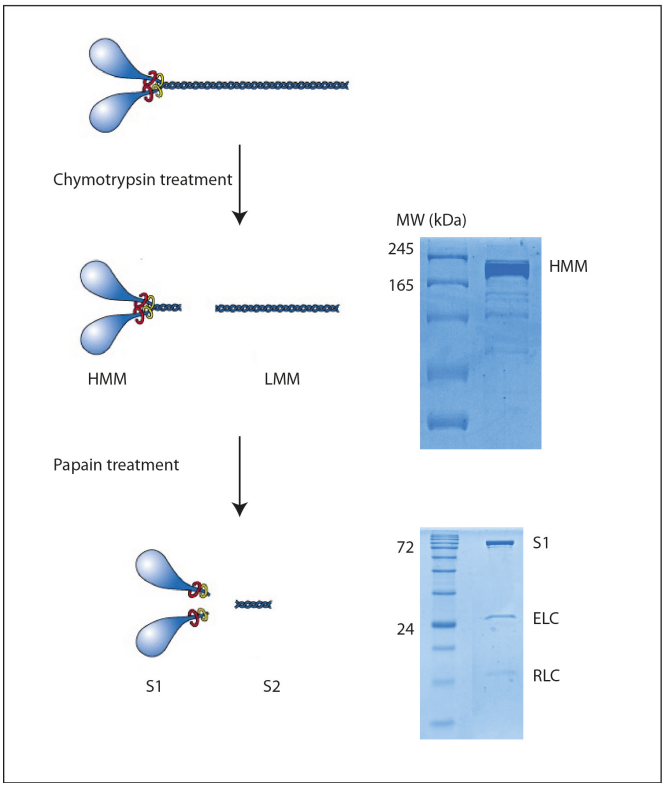

Figure 38: Enzymatic digestion of myosin II to HMM and S1 fragments. Essential (ELC) and regulatory (RLC) light chains are depicted in red and yellow respectively. Gel pictures show examples of correspondent constructs. Modified after Lodish (2001).

3.1.2 Generation and purification of myosin VI full-length construct

For ATPase measurements of myosin VI a full length construct (VI FL) was expressed using the Sf21 baculoviral expression system (see 2.1.12). The VI FL splice variant from chicken used in this thesis contains the large insert (LI) with no small insert (see 1.4).

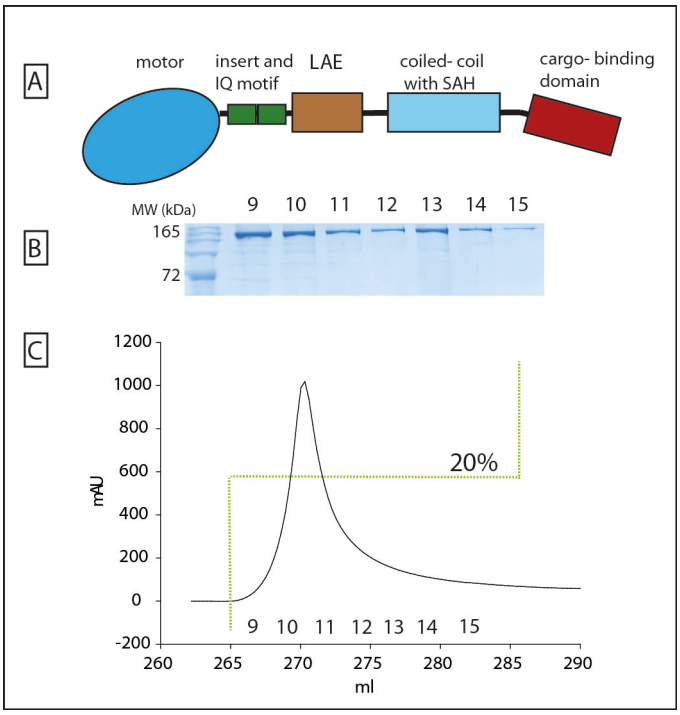

Figure 39: Generation and purification of myosin VI FL protein. **(A)**: schematic of myosin VI FL, **(B)**: SDS-PAGE of elution fractions corresponding to C **(C)**: elution curve from FPLC (Äkta, GE). Number gives percentage of His-high buffer in the elution mix (see 2.2.6 for further information).

Figure 39 shows a typical purification profile of VI FL protein with a SDS-PAGE of the eluted fractions. The protein preparations of myosin VI used in this study were checked for their stability and monomeric state using size exclusion chromatography (SEC). As figure 40 shows myosin VI ran as a single peak. Myosin II HMM (350 kDa) which is a dimer consisting of two motor domains, four IQ domains with four light chains and a short tail elutes at ~ 9 ml elution volume whereas myosin II S1 (106 kDa) with its single motor domain and one IQ with one light chain bound elutes at 12 ml elution volume. This proved that myosin VI was indeed a monomeric protein and never showed a shift in elution. The Stokes radius or Stokes-Einstein radius of a solute is the radius of a hard sphere that diffuses at the same rate as that solute. It is closely related to solute mobility, factoring in not only size but also solvent effects. A smaller ion with stronger hydration, for example, may have a greater Stokes radius than a larger but weaker ion. The Stokes radius of myosin VI is 6 nm, as figure 40 shows.

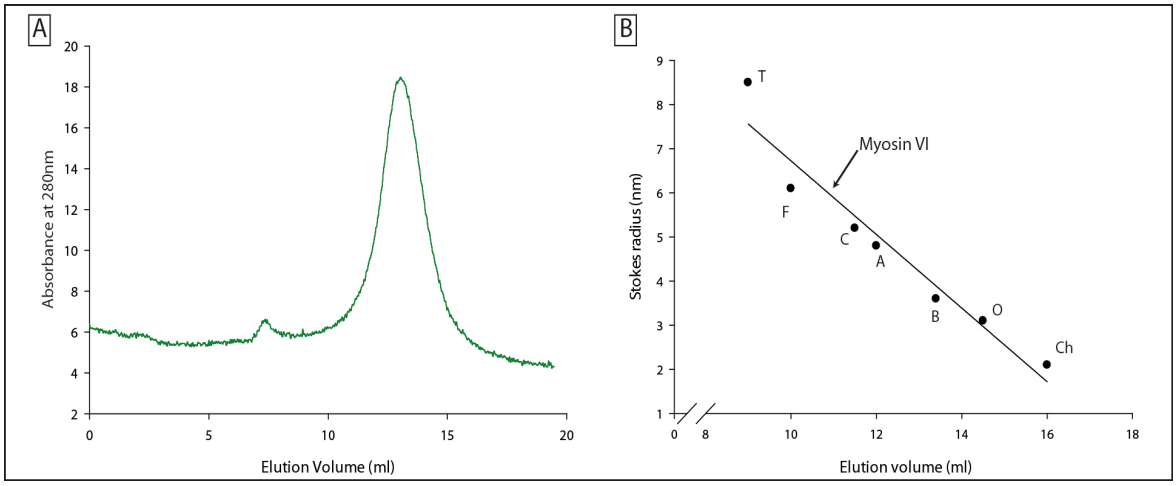

Figure 40: FPLC Superdex-200 prep grade gel filtration of myosin VI. (A) Typical elution profile of myosin VI on a Superdex 200 column. **(B)** Calibration curve of the Superdex 200 gel filtration column using standard proteins of known Stokes radii: (Ch) chymotrypsinogen A, 2.1 nm; (O) ovalbumin, 3.1 nm; (B) BSA, 3.6 nm; (A) aldolase, 4.8 nm, (C) catalse, 5.2 nm; (F) ferritin, 6.1 nm; (T) thyroglobulin, 8.5 nm. The elution position of myosin VI is shown, giving it a Stokes radius of 6 nm (modified after: Lister *et al.* (2004)).

3.1.3 ATPase activity of myosin II S1 and myosin VI

Actin-activated ATPase activity of both myosin VI and S1 was determined with 100 nM motor protein (different preparations, in KMg50 buffer for myosin VI and PIPES buffer for myosin II S1) using 0 to 30 µM F-Actin and 2 mM Mg·ATP in a HPLC based assay as well as a NADH-coupled assay (for further details, see 2.3.2).

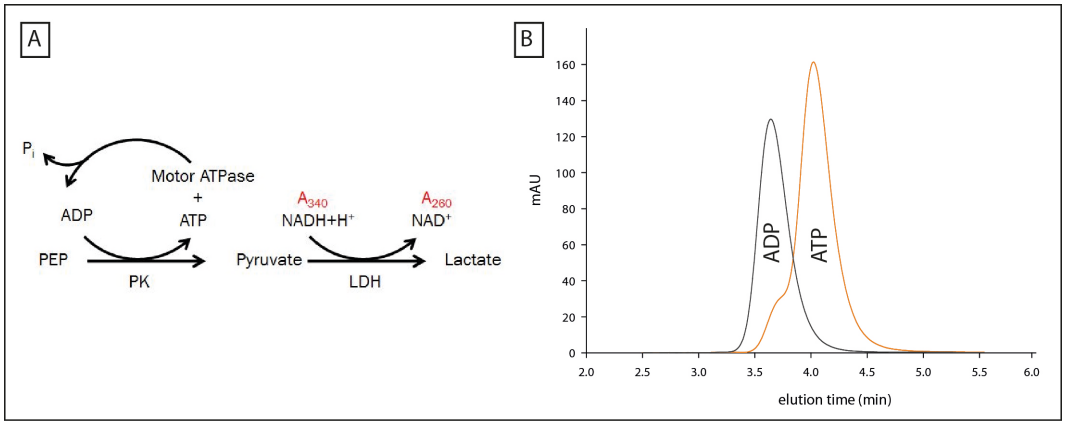

Figure 41: Representation and schematic of the (A): principle of NADH-coupled assay and **(B):** example of HPLC based assay. The two peaks represent the elution peaks for ADP and ATP respectively.

The NADH-coupled assay measures the ATP hydrolysis as a linked process. The ATP hydrolysis is linked to the oxidation of NADH, which is measured spectroscopically at 340 nm by its decrease in concentration. The coupling takes place via phosphoenol pyruvic acid (PEP), pyruvic acid kinase (PK) and lactate dehydrogenase (LDH) (figure

41, A). The HPLC based ATPase assay (figure 41, B) only requires ATP, actin and myosin and is therefore a more direct way of measuring the ATPase activity compared to the NADH-coupled assay. In this assay myosin VI was mixed with actin and very pure ATP. The reaction was then stopped at different points in time of incubation with HCl acid. These samples were then centrifuged to rid the samples of the precipitated protein and measured on the HPLC where the ADP derived from ATP hydrolysis through myosin ATPase activity could be measured.

3.1.4 Actin-dependent activation of myosin II S1

The actin-dependent ATPase rate is an essential value to assess the activity of myosins. In figure 42 a clear actin-activation of the myosin II S1 fragment could be seen for both assays. The ATPase rate increased with higher actin concentration. k_{cat} measures the number of substrate molecules turned over by enzyme molecule per second. It is therefore called the turnover number. The basal rate without actin was 0.1 s^{-1}. The measured maximum k_{cat} was 4.2 s^{-1} (±0.7) in the NADH-coupled assay and 6.7 s^{-1} (± 0.5) with the HPLC method.

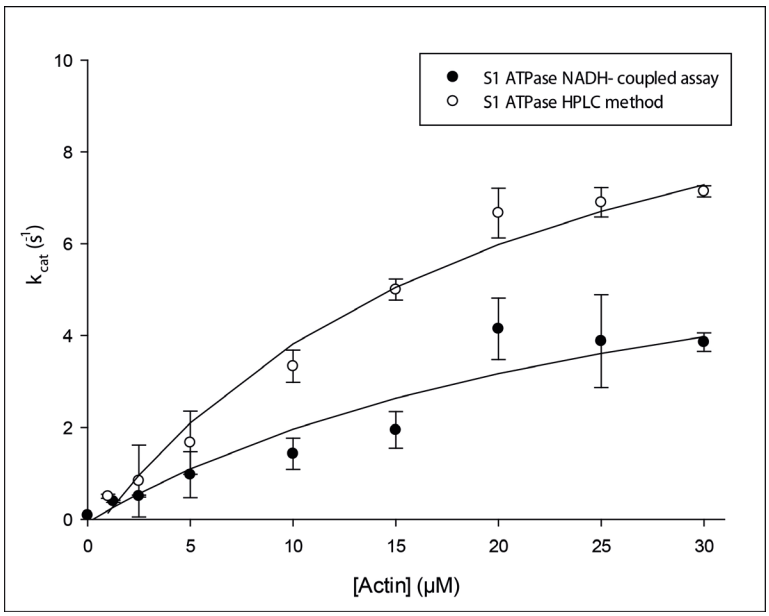

Figure 42: Actin-activated ATPase rate of myosin II S1. Filled circles represent average of 6 measurements with the NADH-coupled assay whereas empty circles represent average of 4 HPLC measurements. Both were performed with at least two different preps.

For the NADH-coupled assay that equalled a 50-fold increase and for the HPLC based assay even an 84-fold increase of ATPase rate. After fitting the curves with kinetic

hyperbola fits, the actin filament concentration at half-maximal activation of the steady-state ATPase was determined with K_M-values of 29 µM (NADH-coupled) and 20.3 µM (HPLC based). Additionally v_{max} values of 8 and 13 s^{-1} were calculated respectively. Although values for v_{max} were not reached in the experiments, the rates above 20 µM actin levelled off and higher concentrations did not change the maximal measured rates. Due to the actin preparations available no higher concentrations than 30 µM could be tested.

3.1.5 Actin-dependent activation of myosin VI

The actin-dependent ATPase rates of myosin VI were used to measure the quality of myosin VI preparations. Figure 43 shows that the ATPase activity of myosin VI is actin-activated. A basal rate of 0.45 s^{-1} and maximum rates of 3.6 s^{-1} (± 0.04) (NADH-coupled) and 2.5 s^{-1} (± 0.4) (HPLC) respectively were measured which equalled an 8-fold increase for the NADH-coupled and a 5-fold increase for HPLC based measurements of ATPase rate.

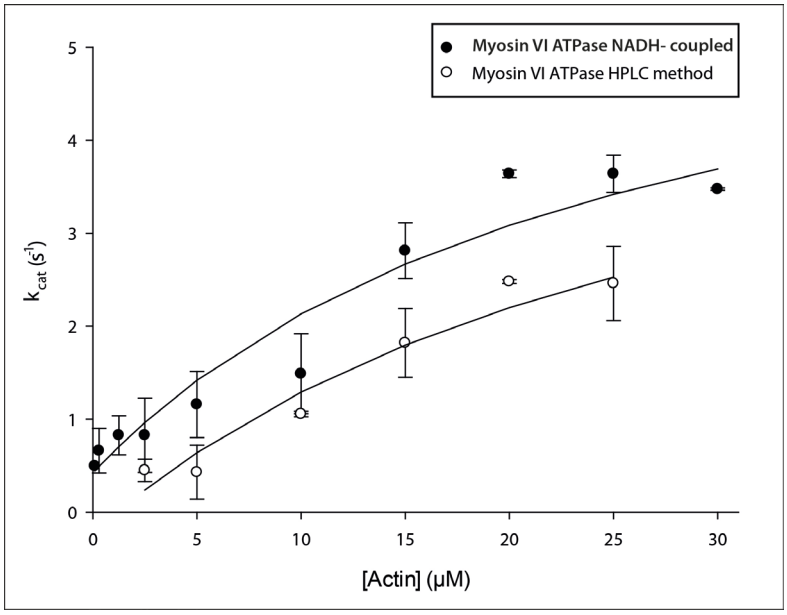

Figure 43: Actin-activated ATPase rate of myosin VI. Filled circles represent average of 4 measurements with the NADH-coupled assay whereas empty circles represent average of 3 HPLC measurements. Both were performed with at least two different preps.

K_M values of 25 (NADH coupled) and 29 µM (HPLC) were calculated as well as maximum velocities v_{max} of 6 s^{-1} for both assays. Again the rates levelled off at

concentrations higher than 20 μM actin and even higher concentrations did not change the maximal measured rates.

3.1.6 **Discussion**

The rates measured with the myosin-II S1 in this study are lower compared to the published rates, which show considerable variation ranging from 7.8 s^{-1} (Webb and Corrie 2001) over 18 s^{-1} (Kovács *et al.* 2004) to 29 s^{-1} (Trentham *et al.* 1976, Millar and Geeves 1983, Cremo and Hartshorne 2007). There are possible explanations to why the numbers show such variability: 1. used muscle types in preparations, 2. buffer conditions and 3. temperature. In previous publications the fast-twitch muscle (type II) *m. psoas* was used or a mixture of it and slow-twitch (type I) muscle *m. soleus*. We used a mixture of diverse muscles (e.g. *m. quadriceps femoris, m. bizeps femoris, m. latissimus dorsae, m. glutaeus maximus, m. longissimus, m. splenicus, m. trapezius*), leaving out the above mentioned *m.psoas* and *m. soleus*. All muscle-types used are more or less a mixture of type I and type II fibres. Our muscle material came from an old male breeder in contrast to 1 year old males used in ATPase based studies in the literature which as well may have an influence on ATPase performance.

All assays were performed at room temperature, which had an influence on the ATPase rate as well. However, similar ATPase rates (k_{cat} = 6 s^{-1}) as Webb and Corrie (2001) (k_{cat}= 7.8 s^{-1}) when using their buffer conditions (PIPES buffer) were obtained. This showed that differences in salt conditions and buffer substances as well as temperature have an influence on the obtainable maximum ATPase rates.

Calculated K_M values of 20 μM to 29 μM were in the same range as published by Kovács *et al.* (2004) with 24 μM. Published ATPase rates for myosin VI range from 6 s^{-1} (De la Cruz, Ostap *et al.* 2001) to 8.3 s^{-1} (Buss and Kendrick-Jones 2007). K_M values of ~18 μM (De la Cruz *et al.* 2001) were not reached in this study but it is most probable that the k_{cat} of 3.6 s^{-1} obtained in this study were lower than the published rates, because of the lower temperatures used for our assays. All enzymes are sensitive to temperature, with different temperature optima. The optimal temperature for myosin VI seems to lie well above room temperature (21 °C), as will be shown later in chapter 3.3.7.2.

3.2 The myosin VI tail can fold back on itself as a regulative mechanism

This chapter investigates the ability of the C-terminal tail of myosin VI to fold back onto the neck of the protein. Several actin-, lipid- and tag-affinity co-sedimentations show that the N-terminal 65 amino acids of the cargo-binding domain interact with the calmodulin that is bound to the IQ motifs in the neck. This interaction is not influenced by alterations of the calcium concentration.

3.2.1 Purification and design of myosin VI motor truncations and tail constructs

The cargo-binding-domain (CBD) of myosin VI is a 198 amino acid globular domain, which has been suggested to be involved in the back-folding of the myosin VI tail and thus inactivating the protein in its monomeric state (Spink *et al.* 2008, Spudich and Sivaramakrishnan 2010). To dissect the contribution of the CBD to the back folding process and to define the interaction site N-terminally of it (in addition to the full-length construct) five tail constructs and three motor truncations of different lengths were designed (figure 44). These tail constructs (amino acids 814-1258, aa 913-1258, aa 814-1060, aa 1060-1258 and aa 1125-1258) allowed the flexibility to ex-or include regions and domains in experiments and enabled me to screen for interacting regions in a step-by-step fashion. The motor truncations comprise the motor domain (aa 1-759) and the unique insert (Trunc814 aa 1-814), the second IQ-motif and lever arm extension (Trunc913 aa 1-913) and the predicted coiled coil region (Trunc1060 aa 1-1060) respectively.

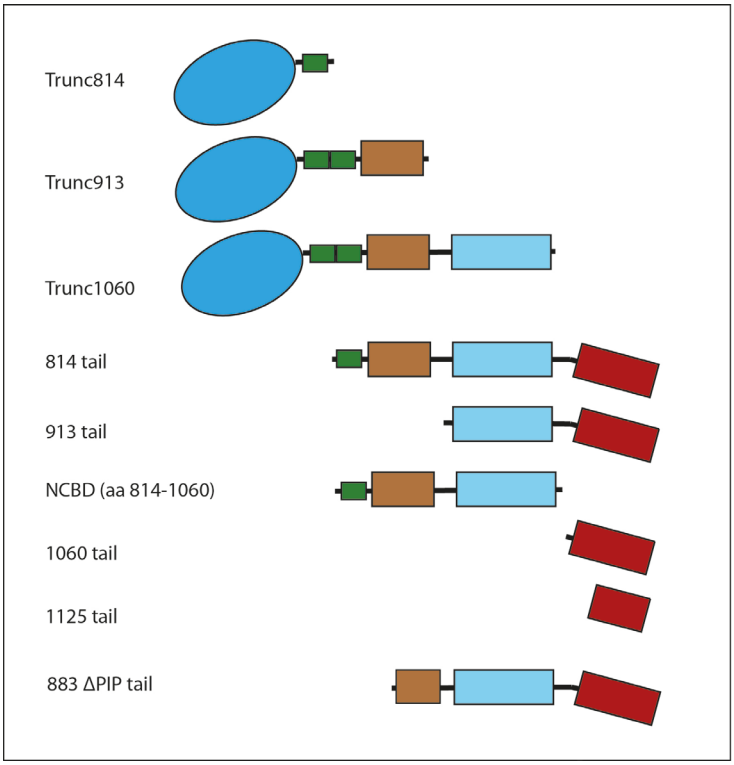

Figure 44: Schematic representation of myosin VI motor truncation- and tail constructs. Motor truncations: Trunc814, Trunc913, Trunc1060; tail constructs: 814 tail, 913 tail, NCBD: Non-cargo-binding domain tail (aa 814-1060), 1060 tail, 1125 tail and 883ΔPIP tail (aa 883 to 1258) which comprises a point mutation in the PIP_2 binding site and was only used in lipid binding studies.

The eight different constructs were expressed and purified as specified before (see 2.1.13 and 2.2.6). Figure 45 shows eluted and concentrated fractions of the various constructs. Typically, when expressing the constructs in Sf21 cells, protein concentrations ranged between 5 and 15 µM. Variability was much higher when expressions were performed in *E. coli* expression systems and ranged from 5 to 40 µM. The protein fractions were flash frozen in liquid nitrogen and stored at -80 °C.

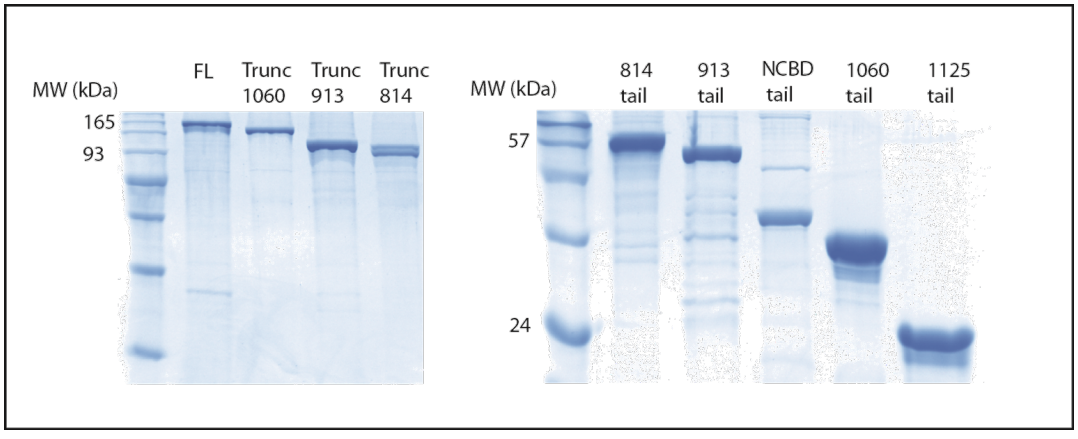

Figure 45: Gel pictures of all myosin VI motor truncations and tail constructs. Purified and concentrated samples of all tail constructs with exception of the 883 Δ PIP are depicted on this gel. The Δ PIP was left out because of its similar size to the 913 tail construct with approx. 48 kDa.

3.2.2 Myosin VI tail constructs exhibit unspecific actin-binding

To test the capability to interact with the actin filament and with other tail constructs, the eight different constructs were assayed by an actin-affinity co-sedimentation assay (2.3.10). In this assay, actin and the respective construct were mixed and subsequently ultra-centrifuged. Thereby, protein constructs that did not bind to the filaments remained in the supernatant, while all filament-bound protein was present in the actin pellet. In addition to testing the affinity of the single constructs to actin, the eligible constructs were tested in combination with each other. Before being able to uncover the detailed interactions of the CBD with a region C-terminal of the motor, the binding affinities of the single tail and motor constructs to actin had to be assessed. Therefore individual constructs were subjected to actin-affinity co-sedimentation before mixing constructs together. Co-sedimentation mixes always contained 1-4 µM myosin VI construct and 5 µM actin. Figure 46 summarises the performed control co-sedimentations.

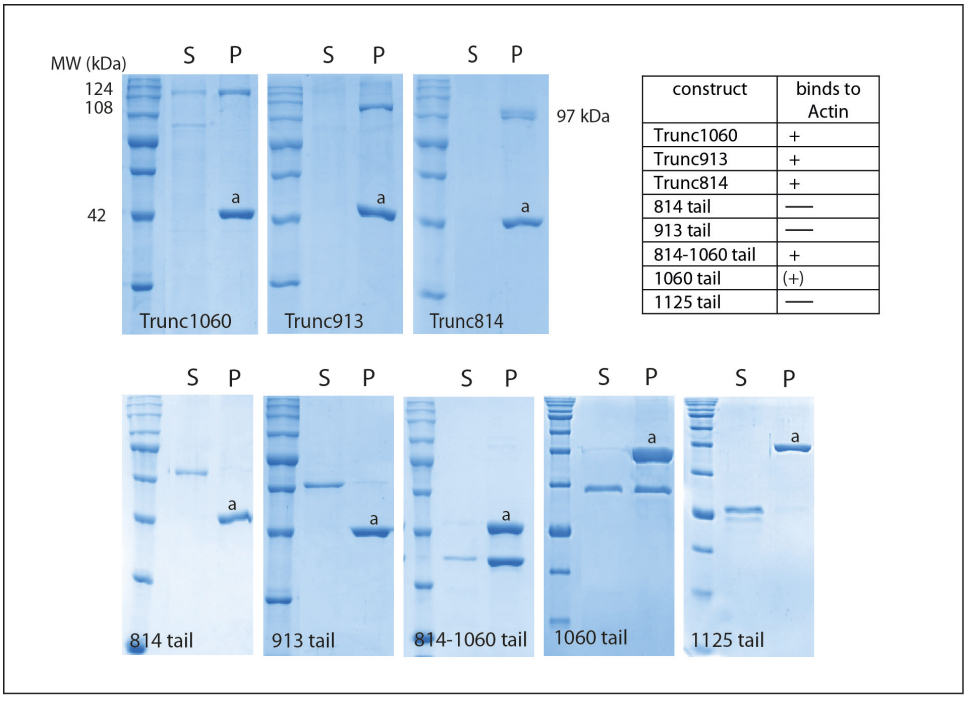

construct	binds to Actin
Trunc1060	+
Trunc913	+
Trunc814	+
814 tail	—
913 tail	—
814-1060 tail	+
1060 tail	(+)
1125 tail	—

Figure 46: Control co-sedimentations of myosin VI constructs with actin. First row: motor truncations; second row: tail constructs. Due to different running times of gels there is a discrepancy between gels. Therefore the molecular weight marker is always pictured. Note that only 814 tail and 1125 tail do not bind actin. Actin is indicated with a. S and P stand for supernatant and pellet fraction respectively. All controls were performed at least three times.

Actin pull-downs with the different constructs revealed that most of the constructs bound to actin, not only the motor truncations, but unexpectedly some tail constructs too. The 1060 tail bound only partly to actin. Only the full length tail (814 tail), the shortest tail

construct (1125 tail) and the 913 tail did not bind actin and could therefore be used in actin-based pull-down assays.

3.2.2.1 Myosin VI full-length tail folds back on itself

Having identified unspecific actin binding constructs the motor truncations and tails 814, 913 and 1125 were the only usable constructs for these assays. With those six constructs a closer screening of the possible back folding of the myosin VI tail was performed. In these co-sedimentations actin was kept at 5 µM and the concentration of the truncations usually at 1 µM and the tail construct was added at 2 µM for the 814 and 3 µM for the 1125 tail to keep one of the binding partners in a slight excess to completely saturate and allow for complete binding, if possible.

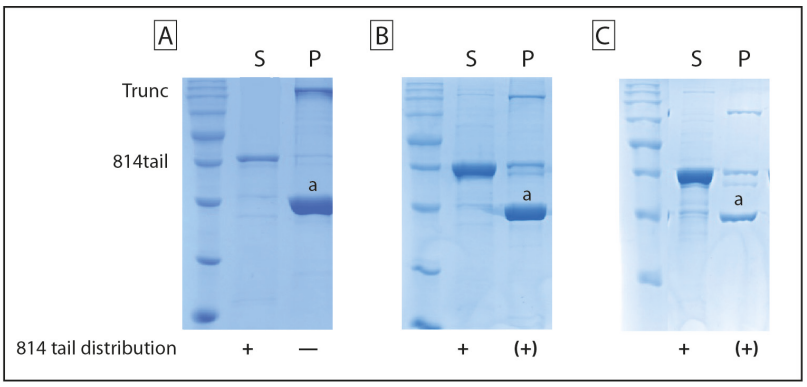

Figure 47: Actin-affinity co-sedimentations of myosin VI motor constructs with 814 tail. Motor truncations with the longest tail construct 814 (**A**: Trunc1060+ 814 tail+ actin, **B**: Trunc913+ 814 tail+ actin, **C**: Trunc814+ 814 tail+ actin); + and – indicate if 814 tail is pulled over into the pellet fraction, a (+) means only a little amount is pulled over. S and P stand for supernatant and pellet fraction respectively. All experiments were performed twice.

When the different motor truncations and the longest tail (814 tail) were subjected to actin-affinity co-sedimentations, most of the 814 tail remained unbound and therefore in the supernatant fraction (figure 47: A, B, C).

When the 1125 tail was added to the different truncations, it became apparent that this tail construct showed no interaction with any of the presented motor truncations (figure 48 D, E, F). However, the binding behaviour of the shortest motor truncation was clearly altered by adding the 1125 tail construct to the pull-down as figure 48 F shows. Without the tail, this motor truncation bound 100% to actin, whilst with the 1125 tail, this complete binding seemed to be interrupted and the truncation was found in the pellet and supernatant fraction (figure 48 F, inset).

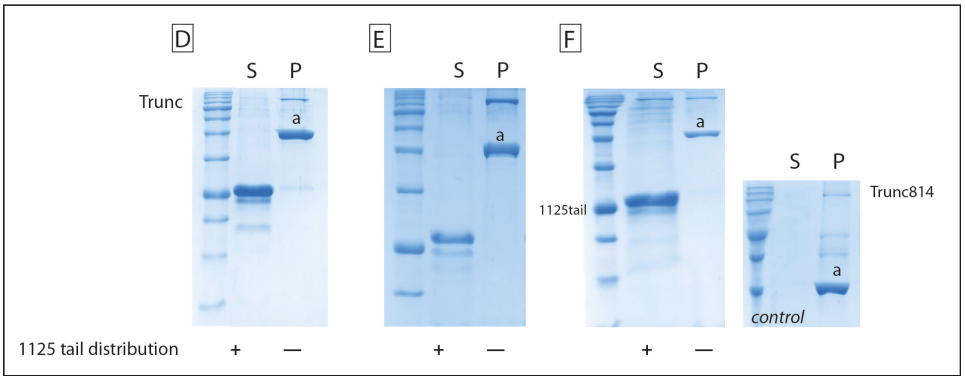

Figure 48: Actin-affinity co-sedimentations of myosin VI motor constructs with 1125 tail. Motor truncations with the shortest tail construct 1125 (**D**: Trunc1060+1125+actin, **E**: Trunc913+1125+actin, **F**: Trunc814+1125+actin). inset: shows the co-sedimentation behaviour of the Trunc814 construct when pulled down with actin. When the same co-sedimentation was performed with the 1125 tail construct, this truncation shows an ambiguous binding behaviour, i.e. it is found in both supernatant and pellet. Due to different running times of gels there is a discrepancy between gels. Therefore the molecular weight marker is always pictured and actin is indicated with *a* as a size reference (42 kDa). S and P stand for supernatant and pellet fraction respectively. All experiments were performed four times.

To determine the actual interaction of the 814 tail with a construct comprising the motor and neck domain, 814 tail was added in different concentrations (3-10 µM) to myosin full-length (FL) (2 µM) and actin (10 µM). As figure 49 displays, the full-length protein did not bind completely to actin at these concentrations, but it was verified that this preparation of protein did at lower concentrations (see figure 49 inset). And most notably, that the 814 tail construct does not alter binding behaviour even when added in a great excess to the assay. The amount of protein in the pellet, as measured with densitometry (see section 2.3.12), did not increase with rising amounts of total protein in the pellet. Small changes in the amounts in the pellet might be due to variations in the gels.

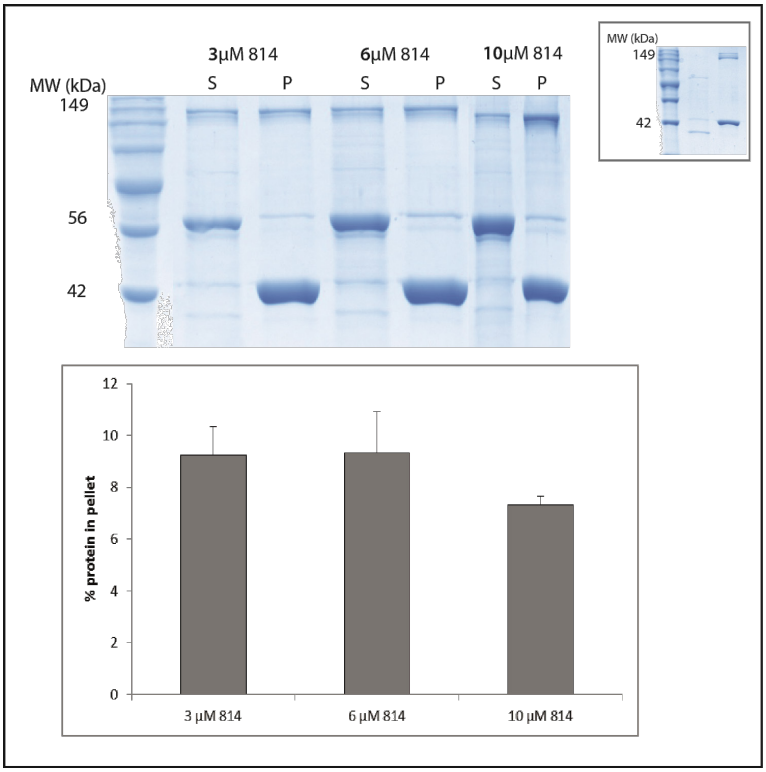

Figure 49: Densitometry of 814 tail binding to myosin VI full-length protein. Gel shows pull-down experiment with full-length myosin VI and a range of 814 tail construct concentrations pulled down by actin. A miniscule amount of the tail is pulled over into the pellet fraction by binding to the full-length protein without showing concentration dependence. Note that at these concentrations not all of the myosin VI is binding to actin but were chosen for better visibility of the proteins and their interactions. Inset: myosin VI (0.6 µM) binding completely to actin (5 µM) at lower concentrations. Graph displays amount of 814 tail in the pellet fraction. The intensity of the tail band in the pellet was divided by the total intensity (pellet + supernatant) for each sample to determine the percent of protein in the pellet. Error bars show standard deviation (n = 4).

3.2.3 Lipid-affinity co-sedimentation with Myosin VI tail constructs

Since some of the constructs did not have the capability to bind to actin because the actin-binding site was missing, and some constructs showed unspecific actin binding, vesicles consisting of folch were used as pull-down agent. The protocol followed the actin-affinity co-sedimentations. All constructs where subjected to these pull-downs. But since interactions between motor truncations and tail constructs were of interest here, only those tail constructs that did not bind to folch vesicles could be further used in the co-sedimentations.

3.2.3.1 Unspecific binding to folch liposomes

In the same manner as for the actin affinity a liposome affinity-check was performed. Since the motor truncations all bound actin and most of the tail constructs as well, a different pull-down system had to be found to assess interactions of constructs with each

other. In liposome affinity co-sedimentations 1-4 µM of construct were mixed with 0.2 mg/ml of folch liposomes (see 2.3.4). Figure 50 shows details of all tail and motor constructs in interplay with the aforementioned liposomes.

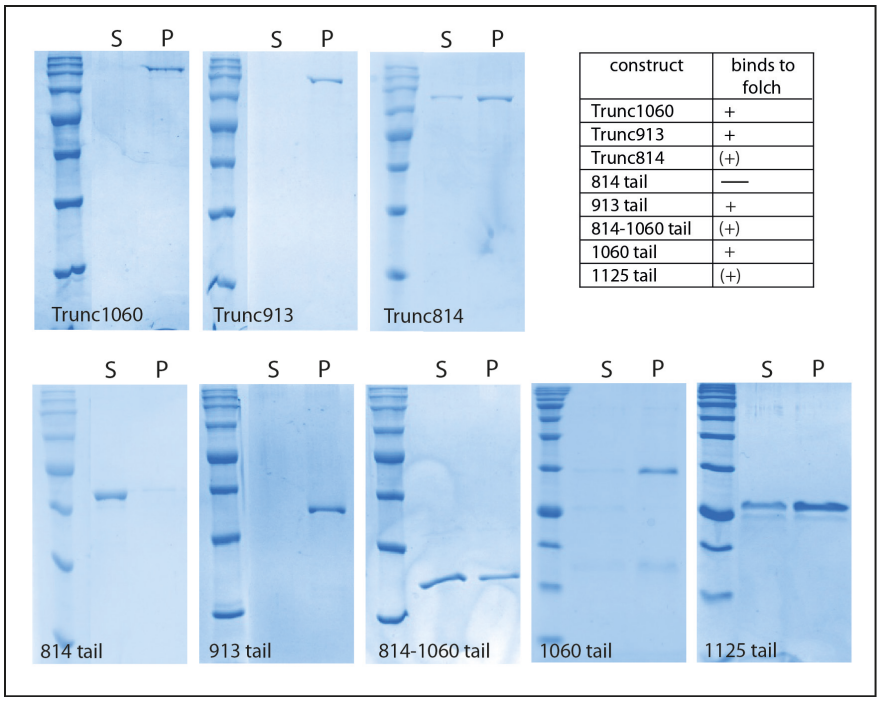

construct	binds to folch
Trunc1060	+
Trunc913	+
Trunc814	(+)
814 tail	—
913 tail	+
814-1060 tail	(+)
1060 tail	+
1125 tail	(+)

Figure 50: Control co-sedimentations of myosin VI constructs with folch liposomes. First row: motor truncations; second row: tail constructs. Note that only 814 tail did not bind folch vesicles. S and P stand for supernatant and pellet fraction respectively. All experiments were performed two to six times. Due to differences in gels a molecular marker is always depicted but sizes can be seen in figure 45.

All motor truncations showed binding capability to folch vesicles. The shortest motor truncation (Trunc814) exhibited partial binding to folch (marked by (+) in figure 50). A similar result was observed for the tail constructs NCBD and 1125. Most notably, the 814 tail did not bind to the provided pull-down substrate, whilst all other tail constructs bound liposomes, and was therefore the only tail construct that could be utilized in further pull-down experiments with folch vesicles (figure 50).

3.2.4 The first 65 amino acids of the Cargo-binding domain interact with the neck

3.2.4.1 His/ GST-tag affinity co-sedimentations with Myosin VI tail constructs

For a closer screening for the actual back-folding site C-terminal of the motor domain, a different approach had to be used. Some constructs showed unexpected affinity for actin and had to be excluded from actin containing assays. To test these constructs for binding to other constructs, magnetic bead pull-down systems were utilised. Magnetic beads coated with a resin that exhibited high affinity for either His-or GST-tags were used to pull down one construct together with an untagged or differently tagged construct (see 2.3.11).

After having exhausted the possibilities with actin-affinity binding, and finding that the 1125 tail construct did not interact with the motor truncations and that the 814 tail did only to a very small extent, the 1060 tail construct in a pGex-6P-1 vector was designed and expressed to attach a gluthathione-S-transferase (GST)-tag to the tail (see section 2.1.3). Since this construct bound to actin and liposomes on its own (see figures 46 and 50), a GST-affinity pull-down system was utilized (see section 2.3.11) which circumvented the necessity for either actin or liposomes as pull-down agents. The GST-tagged protein was bound to the magnetic beads (MagneGST®, promega), which exhibited a very high affinity for GST tags. From Spink *et al.* (2008) it was known that the flexibility for the back folding must lie "[…] somewhere N-terminal of the lever arm […]". Therefore the shorter motor truncations Trunc913 and Trunc814 were used to combine with the 1060 tail.

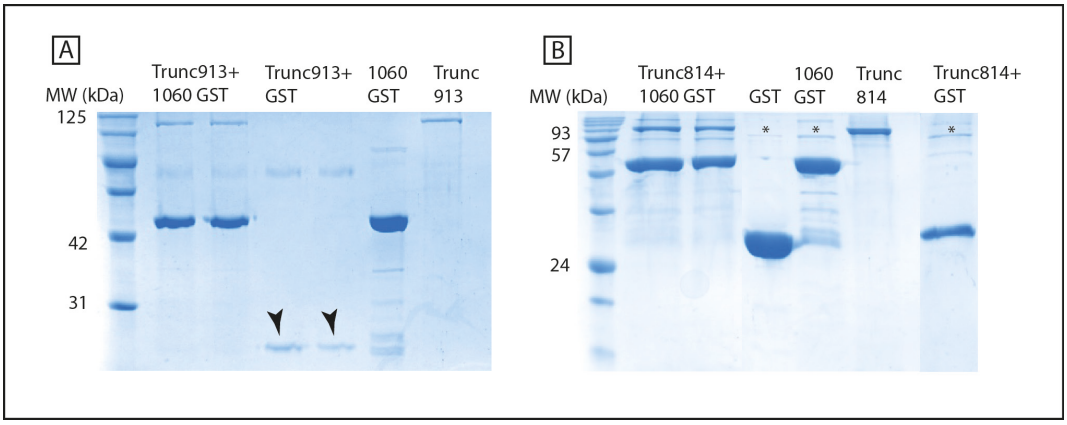

Figure 51: The 1060 tail construct binds to Truncations 913 and 814. Gel (**A)** first lane: molecular marker, second and third lane: truncation 913 was pulled down with the bead-bound 1060 GST construct; lanes 4 and 5: Trunc913 is not pulled down with pure GST, indicated by arrows; lanes 6 and 7: pure proteins as reference. Gel (**B)** first lane: molecular marker; second and third lane: Trunc814 is pulled down with the GST tagged 1060 tail construct; lanes 4 to 6: pure proteins as reference, lane 7: trunc814 is not pulled down with pure GST. Note the additional band at 72 kDa (indicated with asterisks), which is an additional band from the GST. Experiment performed three times.

As shown in figure 51, the 1060 tail interacted with the motor truncations 913 and 814. Controls revealed that the Trunc913 was not pulled down with pure GST. Therefore these two gels display clear interactions between Trunc913 and Trunc814 and the cargo-binding domain (1060 tail). The 1125 tail construct on the other hand did not show any interaction with the longer motor truncation Trunc913 (figure 52). This indicated an involvement of the first N-terminal 65 amino acids of the cargo-binding domain in the back folding process (aa 1060-1125).

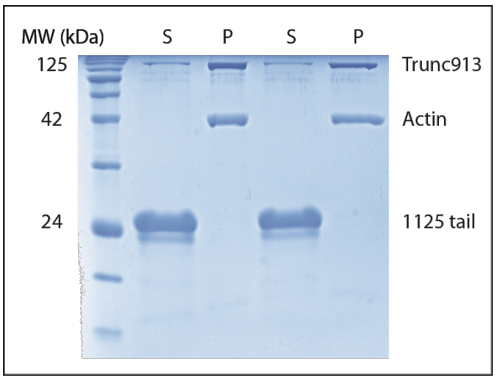

Figure 52: The 1125 tail construct does not bind to Trunc913. All of the 1125 tail construct stays in the supernatant whilst most of the motor truncation is binding to the actin and pellets (n = 3).

3.2.5 Calmodulin- a regulator of back folding?

The experiments discussed above located which C-terminal part of myosin VI (aa 1060-1125) folded back onto which N-terminal region of the protein (aa 814- 913). Since the folded back tail seemed to bind back on to the neck region (which contains the IQ-motifs), the next set of experiments were designed to see if the bound calmodulin light chain had an influence on this back folding process.

3.2.5.1 Calmodulin affinity titrations

For a closer look at the involvement of the IQ-motifs and the Calmodulin (CaM) bound to them in the back folding of the tail, small peptides that comprised only the IQ-motifs were designed (figure 53). These peptides were procured from Genscript. To improve stability the peptides were acetylated at the N-terminal and amidated at the C-terminus.

LTCSRWKKVQWCSLSVIKLKNKI	IQ1
YRAEACIKMQKTIRMWLCKRRHK	IQ2

Figure 53: Amino acid sequence of IQ moitfs 1 and 2 of myosin VI. Blue underlined the additional amino acids which were attached for more stability. Additional modifications of the peptides: acetylated N-terminus and amidation at the C-terminus.

The sequences of IQ1 peptide ranged from aa 788-810 and IQ 2 from aa 812-834.

Calmodulin affinity titrations as described in chapter 2.3.13 were performed to be sure that all subsequently used complexes of an IQ-motif peptide and variable CaM preparations were stable and saturated. These titrations showed that in a 1 mM calcium supplemented buffer IQ1 saturated at a ratio of 1:1 (one CaM:peptide) whereas IQ2 was saturated at a 1:2 ratio which equalled one calmodulin per two peptides (see figure 54). This 1:2 ratio suggests a lack of coordination between the N- and C- terminus of calmodulin.

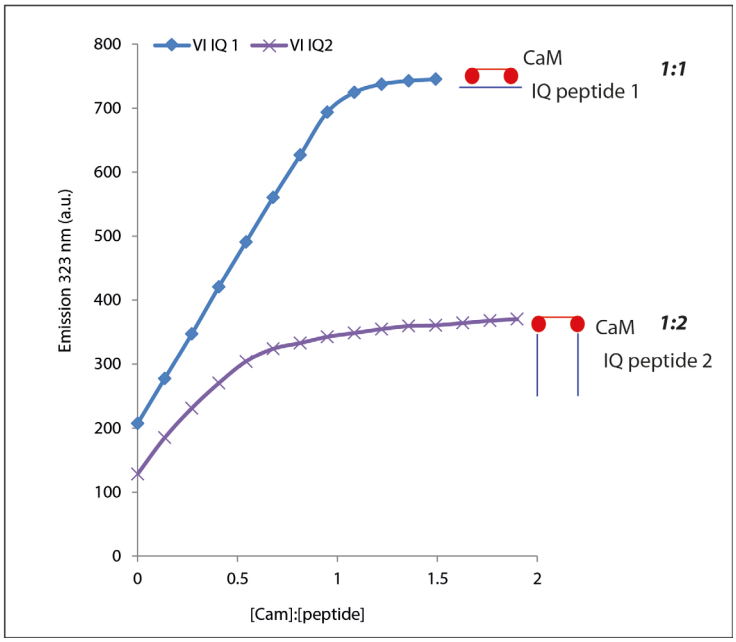

Figure 54: Example calmodulin affinity titration to two different IQ-motifs. IQ1 is the unique insert of myosin VI and IQ2 the first IQ-motif. Titrations were performed by adding 0.1 µM CaM to 2 µM peptide. Titrations were performed four times.

3.2.5.2 Dot Far-western blots

For detection of interactions of small, non-labelled IQ peptides, with the 1060 tail construct dot far-western blots were used. For this assay the unlabelled protein was spotted onto the nitrocellulose membrane and then washed in buffer containing the target tail construct. Subsequently the membrane was washed with an antibody against that particular tail. A more detailed protocol can be found in chapter 2.3.3.

To identify the role of CaM in this folding mechanism, dot far-western blots were performed with calmodulin and the IQ-motifs 1 and 2 as prey and the GST tagged human 1060 tail construct as bait. The tail was added in concentrations in the range of 5-10 nM.

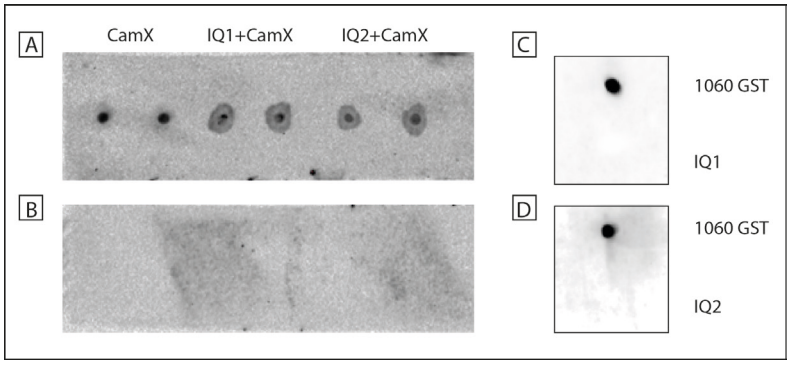

Figure 55: Dot Far-western blots reveal interaction of the 1060 tail with calmodulin. (A): Calmodulin, the peptides of the first (IQ1) and the second (IQ2) IQ-motif with bound calmodulin were spotted on the surface, subsequently washed with 1060 GST tail which was then detected by anti-GST antibody reaction. Each experiment conducted as duplicate **(B)**: negative control of A; membrane was treated as in A, but without 1060 GST tail. This way unspecific antibody-reaction could be ruled out. **(C)**: 1060 GST tail and the IQ1 peptide were spotted on the nitrocellulose membrane, washed with 1060 GST tail and subsequently with anti-GST antibody. The 1060 GST tail was spotted on as quality control for antibody-reaction. **(D)**: same as C but with IQ2 peptide. Calcium concentration in buffers was 1 mM.

The 1060 tail bound to calmodulin in the absence or presence of either IQ1 or IQ2 peptides (figure 55 A and B). However, the 1060 tail did not bind to the IQ peptides in the absence of calmodulin (figure 55 C and D). This strongly supports the hypothesis that the C-terminal tail folds back onto the calmodulin which emerged from the performed pull-down experiments in section 3.2.4. The question now is, as we know that calmodulin is a calcium sensitive protein, will the holo- or apo-calmodulin have a different affinity for the 1060 tail?

3.2.6 Influence of calcium on the back folding process

Since CaM changed conformation upon calcium binding it was interesting to see if this interaction influenced the back folding of myosin VI. As a first check the GST-affinity co-sedimentation with 1060 GST tail as prey and the truncations Trunc913 and Trunc814 as bait (see figure 52) were performed with added calcium (1 mM) (figure 56).

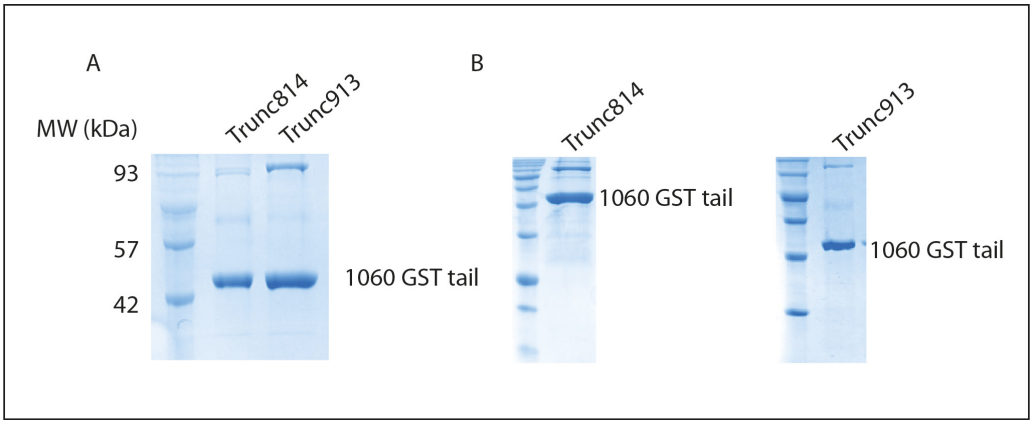

Figure 56: The 1060 tail construct binds to Truncations 913 and 814 with high calcium (1 mM). (A) The 1060 GST tail binds to both truncations although with higher affinity to Trunc913. Concentrations of truncations were the same (1 µM). (**B**) Inset shows binding behaviour of 1060 tail to truncations with no calcium in buffer. Experiments were at least conducted three times.

There was no significant difference to the calcium-free assay. It is worth noting that one could see that with the 1060 tail bound, more of the Trunc913 was pulled down with the beads than Trunc814.

A dot far-western with apo-calmodulin that was purified and kept in a calcium-free buffer with the added chelator EDTA (CaM·EDTA, pCa 7), showed that binding of the 1060 tail to this calmodulin occurred (figure 57). Levels of free ionic calcium were calculated using WEBMAXC, Stanford, USA. They are given as the negative decadic logarithm of their concentration (pCa).

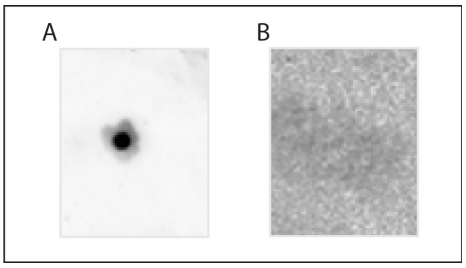

Figure 57: The 1060 tail binds to calcium free CaM (Cam·EDTA, apo-CaM). (A): Cam EDTA was spotted on the surface, subsequently washed with 1060GST tail (5-10 nM) which was then detected by anti-GST antibody reaction. **(B):** negative control of (A); membrane was treated as in (A) but without 1060GST.

Myosin VI IQ1 did not bind apo-calmodulin, IQ2 did bind apo-calmodulin and the ratio changed from 1:2 to 1:1, suggesting that the coordination of binding was restored in the calcium-free state. The steps of a titration of CaM·EDTA to IQ2 peptide, up to the saturation of the peptide, were used as prey on an additional dot far-western blot with 1060GST tail as bait (figure 58). For this 0.4 µM of the CaM·EDTA was titrated to the IQ peptide per step.

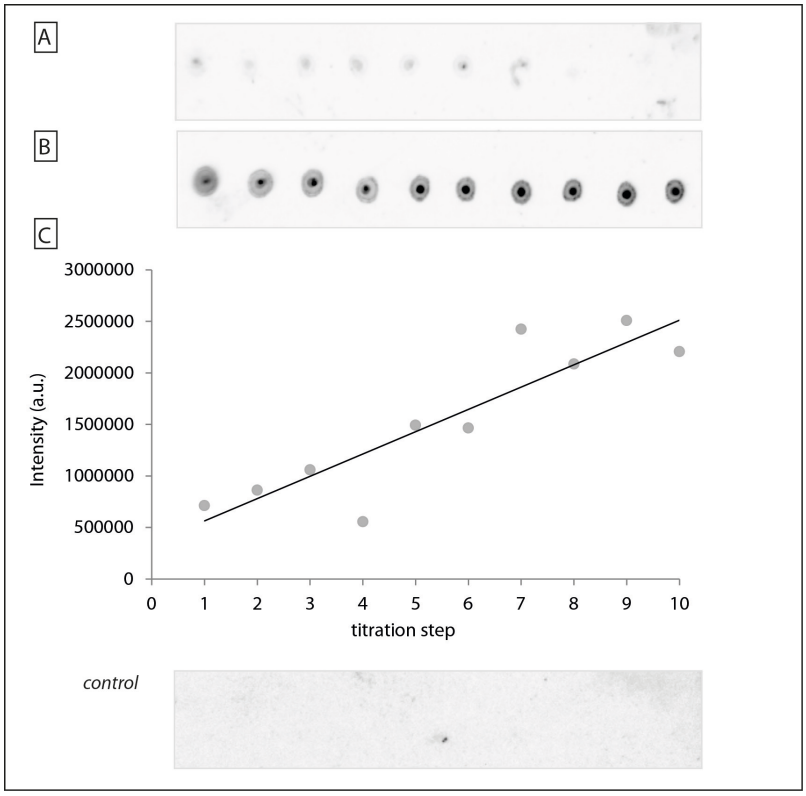

Figure 58: Dot Far-western blot reveals interaction of the 1060 tail with CaM·calcium bound to IQ2 and CaM·EDTA bound to IQ2, respectively. (A): Equal concentrations of CaM·calcium of each titration step (0.4 µM) were spotted on nitrocellulose and subsequently washed with 1060GST tail, which was then detected by anti-GST antibody; performed at pCa 4 **(B):** Equal concentrations of CaM·EDTA of each titration step were spotted on and subsequently washed with h1060GST tail, which was then detected by anti-GST antibody; performed at pCa 7. **(C):** The graph shows the corresponding intensities of a densitometry of the blot in (B). The first titration step is defined by the first addition of CaM to the IQ-motif. The graph represents an example of two titrations. **control:** negative control of (A) and (B) were CaM·calcium and CaM·EDTA were spotted on without washing step with 1060GST.

The interaction between the 1060 tail and the CaM·EDTA was not interrupted by the absence of calcium. As figure 58 (B, C) shows, the binding of the tail increased with increasing CaM·EDTA:IQ2. Since figure 56 showed that the 1060 tail did not bind to IQ2 alone it was not surprising to see a stronger interaction towards saturation of the IQ2 motif with CaM with therefore decreasing levels of free IQ2 in the mixture. On the other hand shows figure 58 (A) a similar treated dot-far western with calcium saturated CaM (CaM·calcium, holo-CaM) where low to no interaction with the 1060GST tail was detected.

3.2.7 Discussion

3.2.7.1 The first 65 amino acids of the cargo-binding domain are involved in the back folding

The 814 tail did not interact with the motor truncations 814 and 913. This finding corresponded to a model developed by Spink *et al.* (2008), which claimed that myosin VI folds back its C-terminal tail onto the N-terminal part of the protein which then inactivated the protein and prevented dimerisation. Not until cargo is bound would this protein unfold, possibly dimerise and move cargo processively along actin tracks. This model was supported by Spudich and Sivaramakrishnan (2010), who added a possible cargo transportation mode of clustering on the cargo surface to this model.

The pull-down experiments performed in this study revealed that the tail folds back onto itself and that, of the screened cargo-binding constructs, only the 1060 tail interacted with the truncations 814 and 913. This pointed towards the explanation that only the first N-terminal 65 amino acids of the cargo-binding domain were involved in the back folding process.

3.2.7.2 Back folding is only possible with calmodulin

In protein:protein interaction studies with the 1060 tail and peptides of the IQ-motifs one and two it was possible to show that this tail did not interact with ‘naked’ IQ-motifs but only with the bound calmodulin. Since calmodulin is a calcium regulated protein, this could point towards a regulative mechanism of calcium onto the back folding of myosin VI.

3.2.7.3 Calcium regulates back folding of the myosin VI tail

With the aforementioned theory in mind, binding studies with the 1060 tail and calmodulin in its apo-(calcium free) and holo-(calcium-bound) state with the calmodulin bound to the IQ-motif peptides were performed. Since the 1060 tail only interacted with the apo-CaM and showed low to no interaction with the holo-CaM this suggests that the back folding of myosin VI onto itself is regulated by calcium. Changes in intracellular calcium concentrations could contribute to the folding and unfolding and thus inactivation and activation of this molecular transporter.

3.3 Lipid binding in the myosin VI molecule occurs along the entire tail

Myosin VI is a cellular motor that has the ability to interact directly with lipids in membranes. In the subsequent experiments it is shown that lipid binding in this motor protein is restricted neither to a particular sequence motif in the C-terminal tail nor to a particular phosphatidylinositolphosphate (PIP), but that it shows lipid binding propensity along the length of its tail. Since calcium influences the interactions of the tail constructs with lipids and their affinities for different lipids, the lipid binding abilities of calmodulin are investigated as well. In vitro motility assays on lipid surfaces reveal that myosin VI shows the highest affinity for the mono-phosphate PI(4)P. Different tail constructs are used to gather detailed information about lipid binding and lipid affinities.

3.3.1 Myosin VI exhibits lipid binding propensity along the whole tail

The myosin VI cargo-binding domain (CBD) (see section 4.1.1) has previously been shown to bind to lipids, and to phosphatidylinositols in particular. Spudich *et al.* (2007) defined a PI(4,5)P_2-specific binding site by whole plasmid site-directed mutagenesis (see 2.1.11) in the CBD, comprising the amino acids 1115 to 1122 with the sequence WSKNKKR. For a close meshed screening for further lipid binding abilities and propensities along the whole tail, a sequence analysis was performed to identify any known lipid binding domains. The different expressed tail constructs introduced in section 3.2.1 (figure 44) were used. Liposomes of different composition were utilised under different conditions (i.e. added calcium) in affinity co-sedimentations as well as protein-lipid overlays (PLO) (see 2.3.5).

3.3.1.1 Sequence analysis

Since defined protein domains that specifically bind membrane lipids (e.g. PH, PX, FERM, ENTH, see appendix 5.8) could not be found along the myosin VI tail, a computer based search for unstructured membrane-binding sites after Brzeska *et al*. (2010) was performed. This BH-plot searches for basic-hydrophobic regions which are potential membrane-binding sites known to often bind to acidic phospholipids. By modification of the hydrophobicity scale which then gives Arg- and Lys-positive, rather than negative values, the authors were capable of successfully identifying phospholipid-binding sites in 16 tested proteins. Beginning with the first amino acid in the protein

sequence, the program averages the values for each amino acid (see table 10, appendix) in a defined window (segment of selected length) and gives a score for the middle residue in the segment. Hence for a window size of 19, the first score is an average of the values for residues 1-19 and is assigned to residue 10. Then the values for residues 2-20 are averaged and the score is given to residue 11. This is continued to the end of the sequence with the last residue scored being 10 residues away from the C-terminus. If amino acids closer to the N- and C-termini had to be scored, a smaller window size must be used. A threshold of 0.6 gave the best results for their tested 16 proteins but the program optimises this threshold, giving the optimal signal to noise ratio. The authors developed an online based calculator for performing BH-searches which can be openly used at http://helixweb.nih.gov/bhsearch/.

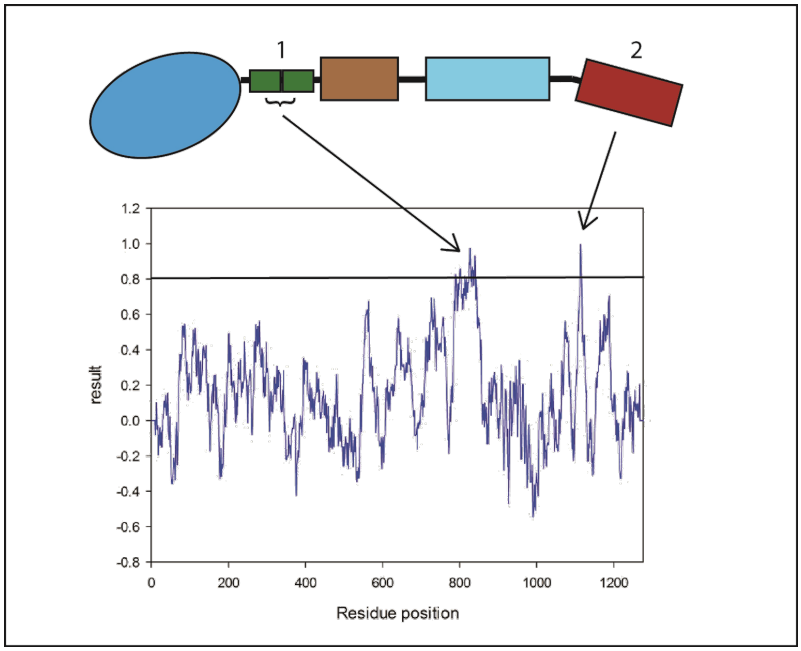

Figure 59: Plot of basic-hydrophobic (BH) residue patches of chicken FL (LI) construct. Threshold given at 0.8, running window size was 19. Detailed explanation given in text. Cartoon depicts FL myosin protein. Two possible membrane-binding regions are indicated. Region indicated by (1) are the unique insert and the second IQ-motif, which is a yet unknown possible lipid binding site and (2) indicates the already defined PI(4,5)P_2 binding motif KSKNKKR. BH-plot was performed on http://helixweb.nih.gov/bhsearch/

The BH plot gave two over-threshold proportions. As indicated in figure 59, the second (2) showed the known binding site for PI(4,5)P_2 at residues 1115 to 1122. The first pulled-out possible lipid-binding site (figure 59 (1)) comprised of the unique insert and the second IQ-motif, which both have previously not been discussed as potential lipid binding regions of myosin VI.

3.3.1.2 Lipid-affinity co-sedimentations

To test the capability of the tail constructs to interact with different lipids, lipid-affinity co-sedimentations were performed (see section 2.3.7). The liposomes where produced by sonication. Following the protocol of Spudich *et al.* (2007), the final mixture for PIP-containing liposomes consisted of 40% PE, 40% PC, 10% Cholesterol and 10% of a varying PIP, all kept in a physiological salt buffer (Lipidbuffer, 150 mM NaCl). Furthermore vesicles consisting of pure PE, PC, Cholesterol, a mixture of PC and PE and a mixture of PC, PE and Cholesterol were produced and assayed to see if binding to the PIP-containing vesicles was due to any of these components. Additionally controls for self-pelleting of the constructs were performed without added liposomes. The protein constructs and the appropriate liposomes were mixed, incubated for 10 min at room temperature and subsequently ultra-centrifuged. Thereby, protein constructs that did not bind to the vesicles remained in the supernatant fraction whereas all lipid-bound protein was present in the pellet. To allocate the protein fraction to either pellet or supernatant fraction a SDS-PAGE was performed for every sample.

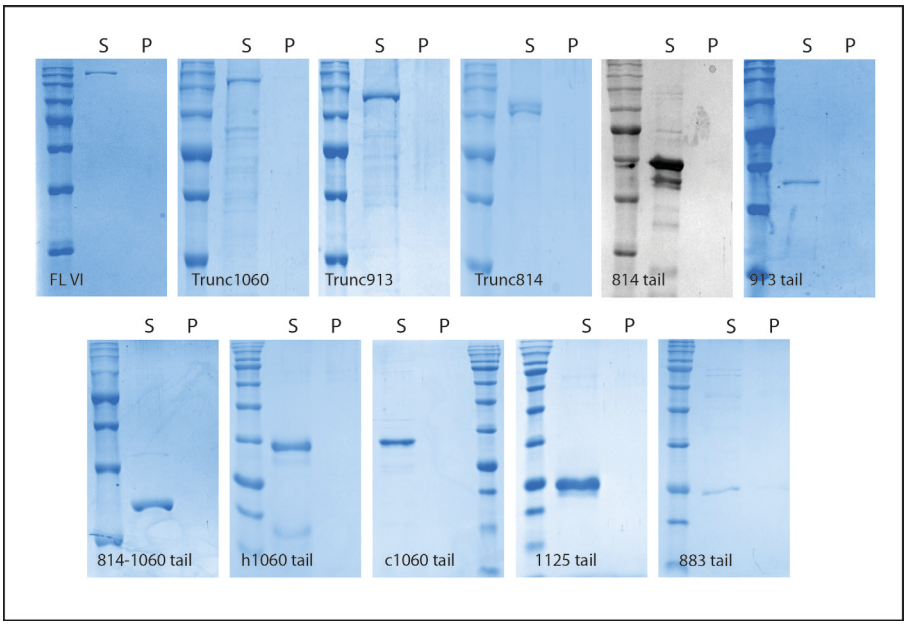

Figure 60: Control co-sedimentations with Lipidbuffer. Top row: VI FL (149 kDa), Trunc1060 (124 kDa), Trunc913 (108 kDa), Trunc814 (97 kDa), 814 tail (56 kDa), 913 tail (45 kDa); Bottom row: NCBD tail (34 kDa), human 1060 tail, chicken 1060 tail (29 kDa), 1125 tail (22 kDa) and 883 Δ PIP tail (49 kDa). S and P stand for supernatant and pellet fraction respectively. The concentrations of protein ranged from 1-3 µM. None of the constructs pelleted on its own. All experiments performed at least three times.

To uncover the lipid-binding capacities of the different tail constructs, the binding to folch liposomes by quantifying the protein in the pellet fraction and therefore bound to

the vesicles (figure 60) was assessed. The construct concentration varied from 1-3 µM whilst the liposome concentration was kept at 0.2 mg/ml.

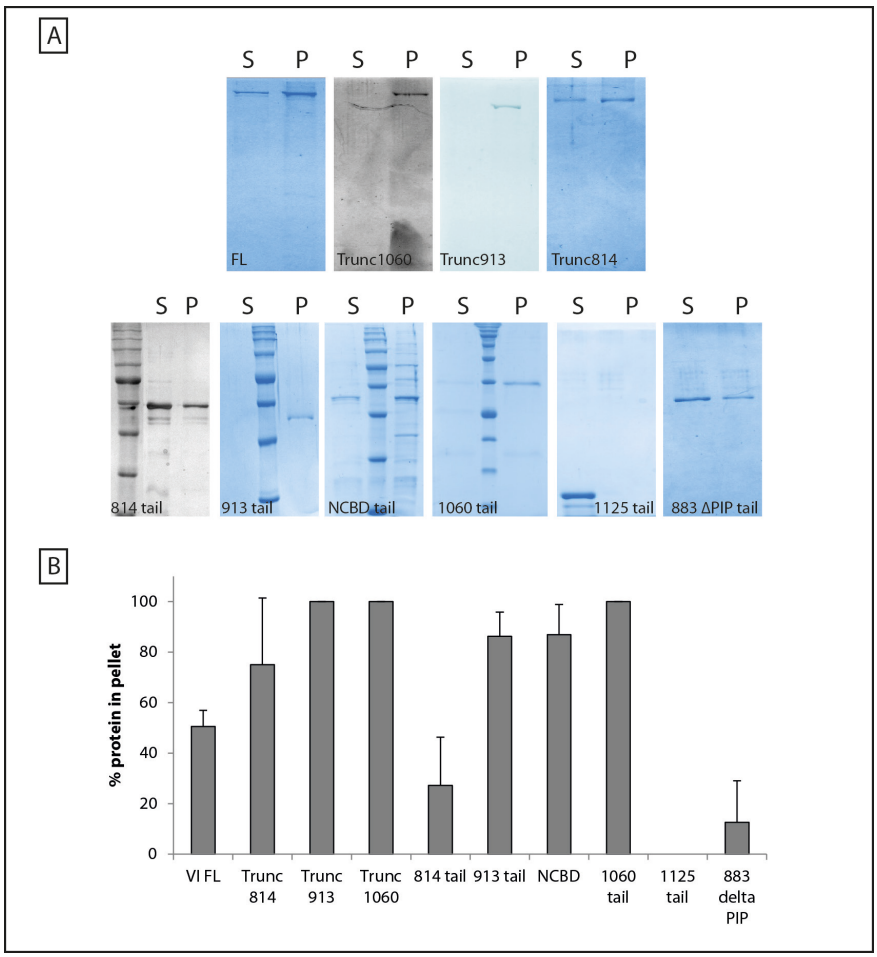

Figure 61: Lipid-affinity co-sedimentations with folch vesicles. (A): Top row: VI FL (149 kDa), Trunc1060 (124 kDa), Trunc913 (108 kDa), Trunc814 (97 kDa). Bottom row: 814 tail (56 kDa), 913 tail (45 kDa), NCBD tail (34 kDa), 1060 tail (29 kDa) 1125 tail (22 kDa) and 883 Δ PIP tail (49 kDa). S and P stand for supernatant and pellet fraction respectively. The concentrations of protein ranged from 1-3 µM. All constructs despite the 1125 tail bound to folch liposomes. Gel pictures of Trunc1060 and 814 tail are silver stained and therefore gray. Gel pictures differ because differences in construct sizes make different gel densities (10-15%) and running times necessary; therefore no molecular weight is marked on the pictures but given in the text. **(B):** Densitometry of shown co-sedimentations. The percentage of protein in the pellet fraction is shown. The intensity of the tail or full-length band in the pellet was divided by the total intensity (pellet + supernatant) for each sample to determine the percentage of protein in the pellet. All experiments performed four times. Error bars show standard deviation.

All constructs, apart from the shortest tail construct 1125, bound to the provided liposomes (figure 61, A). Truncations 1060 and 913 as well as the 913 and the 1060 tail constructs bound at 100% of the liposomes. Densitometry revealed that the FL construct as well as Trunc814 and the NCBD tail were only bound at 50% to the folch vesicles. The 883Δ PIP construct showed even less binding (20%) similar to the 814 tail (25%) (figure 61, B).

Since folch is a mixture of membrane lipids with varying amounts of phosphatidylinositols (PIPs) and other phospholipids, co-sedimentations with defined amounts of PIPs in the liposomes were performed. Concentrations of constructs ranged between 1 and 3 µM, the concentration of liposomes was kept at 0.2 mg/ml which equalled 0.02 mg/ml PIP per pull-down. The motor truncations as well as the NCBD tail construct could not be included in the PIP-affinity co-sedimentations because they all readily bound to the other components of the liposomes PC, PE and/ or Cholesterol (see appendix, figure 106-108). Liposomes contained 40% PE, 40% PC. 10% Cholesterol and 10% of a variable PIP.

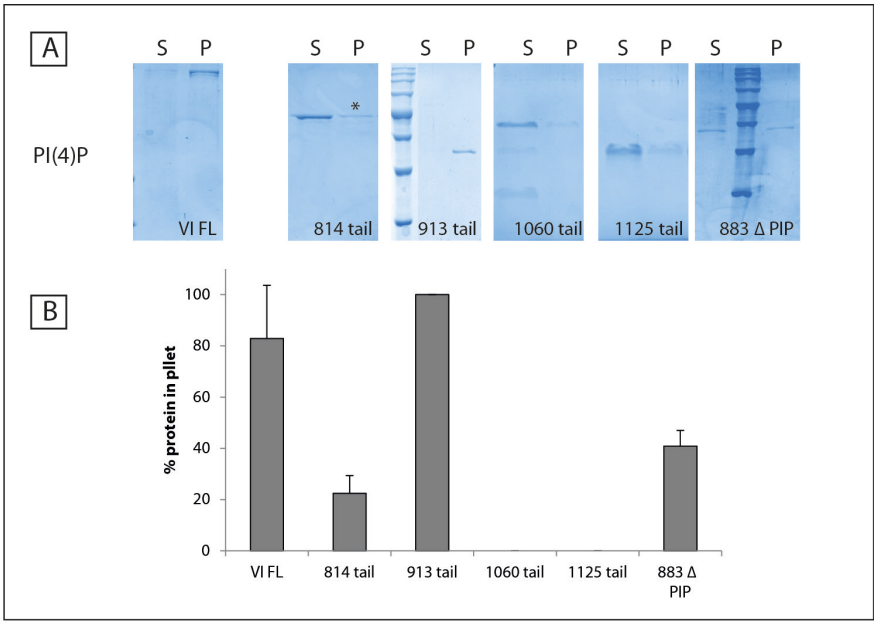

Figure 62: Binding of myosin VI FL and tail constructs to Phosphatidylinositol-4-mono-phosphate (PI(4)P). (A): VI FL construct and tail constructs. Sizes see figure 46. All experiments conducted four times. **(B):** Densitometry of constructs binding to PI(4)P liposomes. All truncations and the NCBD construct bound to the components PC, PE and/ or Cholesterol, therefore they had to be excluded from the assays. Bars represent average of four co-sedimentations. All experiments conducted four times. Error bars show standard deviation.

Figure 63 shows the binding of the single constructs to PI(4)P containing liposomes. The tails mostly stayed in the supernatant but a closer densitometrical inspection (figure 62, B) revealed that the full-length construct and the 913 tail bound completely to the added liposomes, which meant a 2-fold increase in binding for myosin VI FL in comparison to binding to folch vesicles. In contrast to the pull-down with the folch vesicles, the cargo-binding domain construct 1060 did not bind to the PI(4)P vesicles. The 1125 construct behaved the same as with folch vesicles. The 883Δ PIP construct showed more binding than to the folch vesicles (~ 45% against 20% on folch; p = 0.018) whilst the 814 tail bound similarly to the PI(4)P vesicles as to folch.

A co-sedimentation with $PI(3,5)P_2$ containing liposomes showed a different picture from PI(4)P binding.

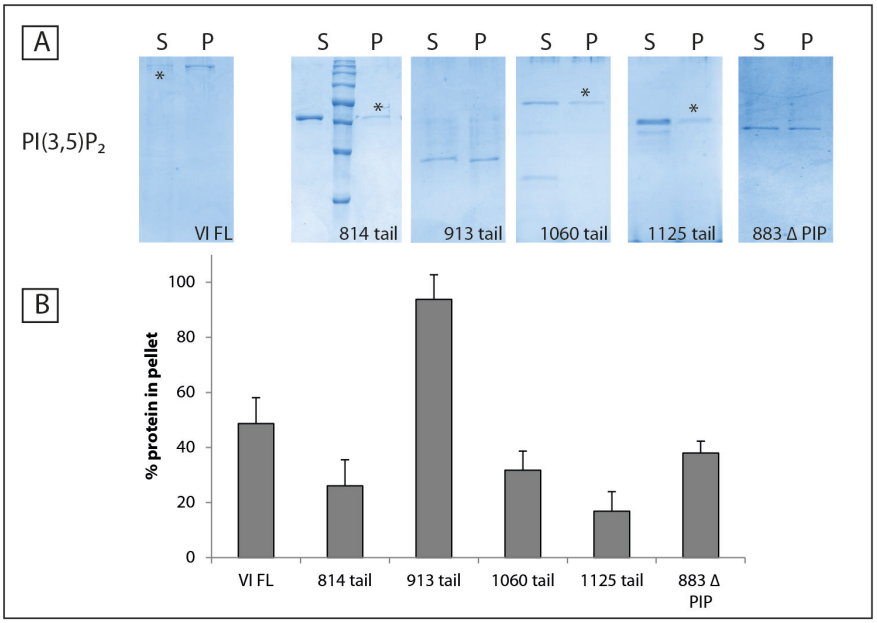

Figure 63: Binding of myosin VI FL and tail constructs to Phosphatidylinositol-3,5-di-phosphate ($PI(3,5)P_2$). (A): VI FL construct and tail constructs. Sizes see figure 46. S and P stand for supernatant and pellet fraction respectively. Asterisks indicate faint bands in pellet fraction. All experiments conducted four times. **(B)**: Densitometry of constructs binding to $PI(3,5)P_2$ liposomes. All truncations and the NCBD construct bound to the components PC, PE and/ or Cholesterol, therefore they had to be excluded from the assays. Bars represent average of four co-sedimentations. Error bars show standard deviation.

Full-length protein bound to $PI(3,5)P_2$ vesicles to only about 50% which marked a decrease in comparison to PI(4) and a similar binding behaviour as with folch vesicles. The 913 tail bound to about 90% to these liposomes. Even though the 1060 and 1125 tails both did not bind to PI(4)P there was a weak interaction detected for both with $PI(3,5)P_2$ (see figure 63). The interaction of the 883 Δ PIP mutant and the 814 tail with these two different phosphatidylinositols was in comparison the same.

The affinity co-sedimentation with $PI(4,5)P_2$ (PIP_2) containing liposomes showed a very similar picture to the assay performed with PI(4)P in terms of binders and non-binders. Again no binding of the shorter tail constructs 1060 and 1125 could be observed while the interaction of the constructs in general was again weaker than with the mono-phosphate.

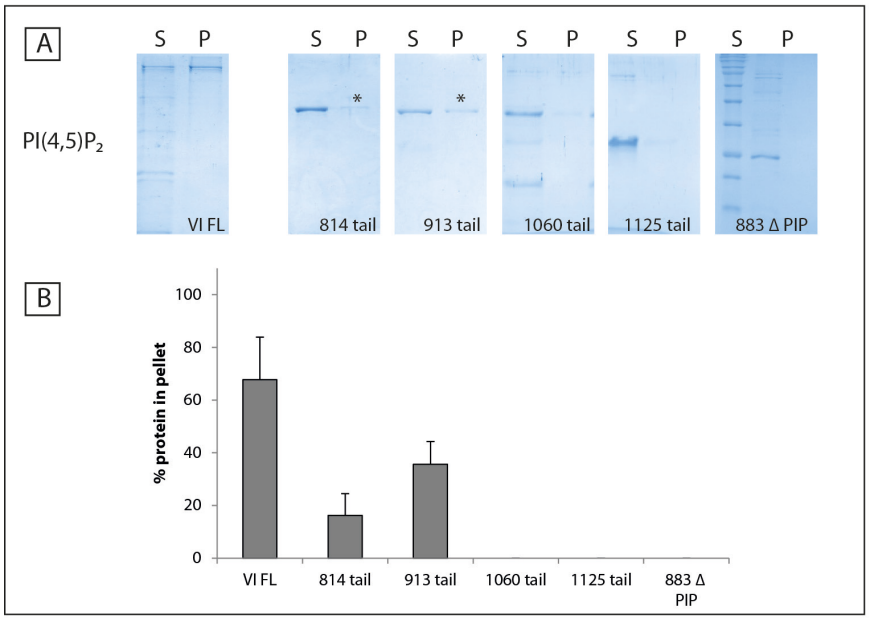

Figure 64: Binding of myosin VI FL and tail constructs to Phosphatidylinositol-4,5-di-phosphate ($PI(4,5)P_2$). (A): VI FL construct and tail constructs. Sizes see figure 46. S and P stand for supernatant and pellet fraction respectively. Asterisks indicate faint bands in pellet fraction. All experiments conducted four times. **(B):** Densitometry of constructs binding to $PI(4,5)P_2$ liposomes. All truncations and the NCBD construct bound to the components PC, PE and/ or Cholesterol, therefore they had to be excluded from the assays. Bars represent average of four co-sedimentations. Error bars show standard deviation.

Densitometry (figure 64, B) revealed that about 65% of the myosin VI FL and approximately 30% of the 913 tail were interacting with $PI(4,5)P_2$. Which was less than observed with the $PI(3,5)P_2$-containing vesicles for the 913 tail, with a significant difference ($p \leq 0.001$) of about 60% . Although the interactions of the 883 Δ PIP mutant and the 814 tail were similar with $PI(3,5)P_2$ and the PI(4)P containing vesicles, the 883 Δ PIP mutant did not bind to the $PI(4,5)P_2$ whereas the 814 tail showed about 16% binding (figure 64).

3.3.2 Calcium has an effect on lipid binding of the myosin VI full-length protein

Since calcium plays a pivotal role in the cell, and is known to be one of many regulators of myosin, it was decided to test the binding of myosin VI FL to all aforementioned lipid mixes with addition of calcium in form of $CaCl_2$. Without calcium, myosin VI full-length bound to folch liposomes only in a 50:50 fashion upon calcium addition (standard concentration 50 µM $CaCl_2$), this behaviour shifted towards 100% binding to folch vesicles (figure 65, A) ($p \leq 0.001$).

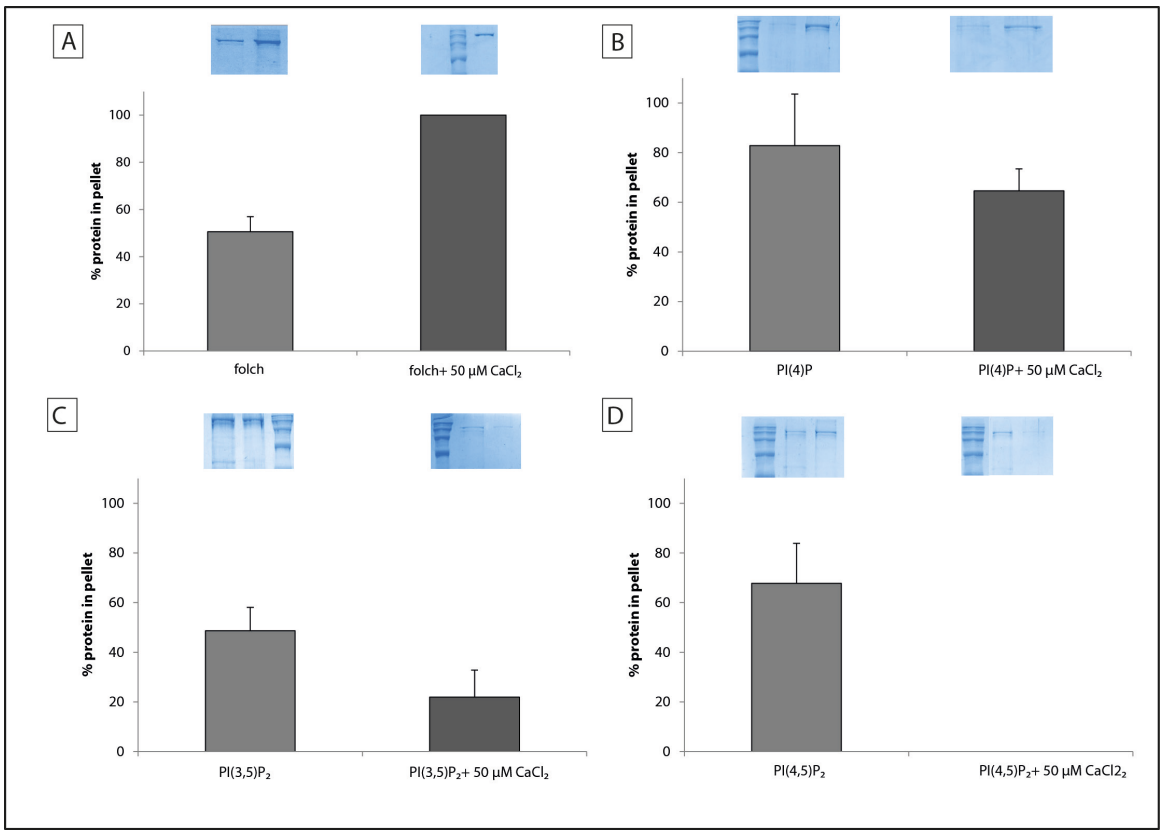

Figure 65: Densitometry of myosin VI FL binding to different lipid vesicles with and without the addition of $CaCl_2$. (A): myosin VI FL binding to folch vesicles +/-calcium; **(B):** VI FL binding to PI(4)P containing liposomes with and without the addition of 50 µM calcium; **(C)** VI FL binding to PI(3.5)P_2 containing liposomes +/-calcium and **(D):** VI FL binding to PI(4,5)P_2 containing liposomes with and without the addition of 50 µM calcium. The inset pictures are representative examples for experiments. Bars represent average of four to six co-sedimentations. Error bars show standard deviation.

The effect of calcium upon on the interaction of myosin VI FL to PI(4)P containing vesicles was noticeably smaller. Whilst the interaction between folch liposomes and myosin VI FL was increased with the addition of $CaCl_2$, it reduced the binding of myosin VI FL to PI(4)P by 30% from fully bound protein to 70% bound protein (figure 65, B).

Binding to PI(3,5)P_2 containing vesicles was reduced from 50% without calcium to around 20% with added $CaCl_2$ ($p = 0.01$) (see figure 65, C).

The interaction between PI(4,5)P_2 and myosin VI FL (50:50 binding) upon addition of 50 µM $CaCl_2$ was disrupted completely ($p \leq 0.001$) (figure 65, D).

3.3.3 Myosin VI's lipid binding might be tightly regulated

After having seen the effects of Ca^{2+} on the lipid binding abilities of myosin VI FL protein, it was tested if different concentrations of $CaCl_2$ had varied effects on the protein:liposome interaction. Since the disruption of binding to PI(4,5)P_2 was the most striking result, the interaction between this lipid and myosin VI FL was tested. To the normal assay as described above, $CaCl_2$ was added in different concentrations (5 µM, 10 µM, 25 µM and 50 µM).

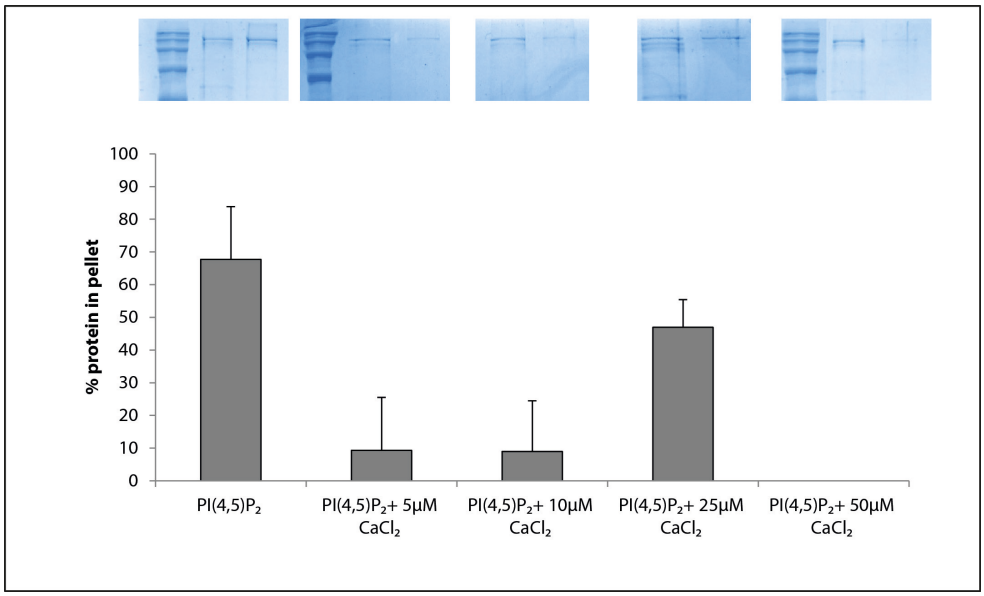

Figure 66: Densitometry of myosin VI FL binding to PI(4,5)P_2 vesicles with different $CaCl_2$ concentrations. The inset pictures are representative examples for experiments. Bars represent mean value of four experiments. Error bars show standard deviation.

As figure 66 shows, low concentrations of an effect on binding. About 10% of the protein bound with additions of 5 and 10 µM $CaCl_2$, respectively. The most striking effect was that at 25 µM added $CaCl_2$ around 45% binding could be observed whereas 50 µM $CaCl_2$ was enough to completely stop any interaction of myosin VI FL to PI(4,5)P_2 containing liposomes ($p \leq 0.001$).

3.3.4 Myosin VI 1125 tail construct shows Calcium dependent lipid binding

Most of the tail constructs did not show any significant change in binding behaviour when $CaCl_2$ was added to the assay. But strikingly the shortest tail, 1125 changed its behaviour from not binding to the vesicles towards binding to around 50% ($p \leq 0.001$) and the 814 tail changed from 25% binding to around 90% binding ($p = 0.001$) (figure 67).

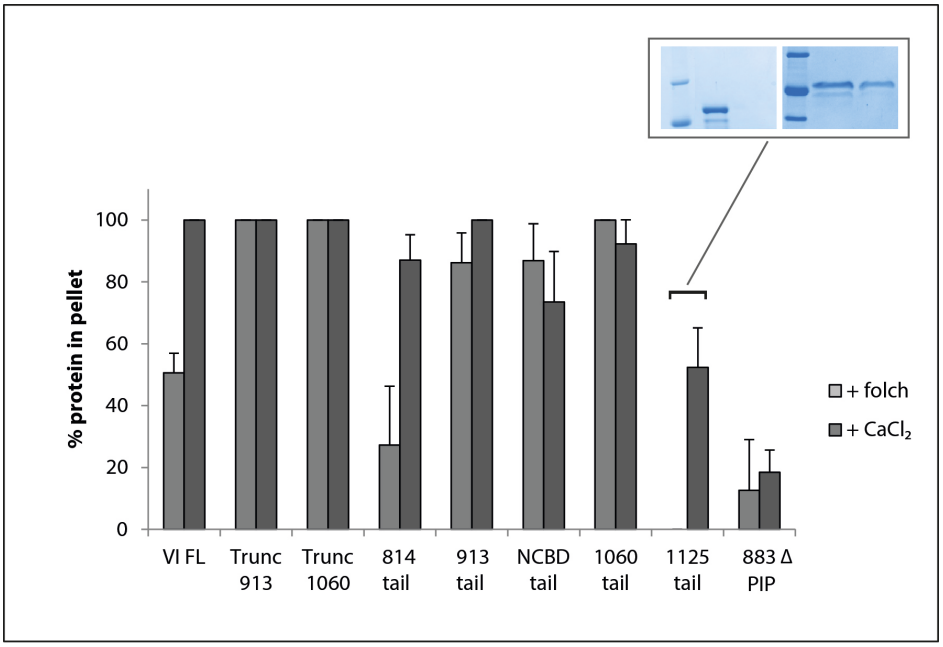

Figure 67: Densitometry of myosin VI constructs binding to folch vesicles with and without $CaCl_2$ additions. The inset pictures show effect of $CaCl_2$ on 1125 tail binding to folch vesicles. Left panel: binding to folch without Calcium, right panel: binding to folch with 50 µM $CaCl_2$. Bars represent average of at least four co-sedimentations. Error bars represent standard deviation.

3.3.5 Almost all myosin VI constructs bind to folch on nitrocellulose

A different approach for examining lipid binding of the protein constructs is the protein-lipid overlay assay (PLO) (Dowler *et al.* 2002), which presents defined lipid components or mixtures on a nitrocellulose surface (see 2.3.5). In short, lipids were spotted on a nitrocellulose surface, allowed to dry and then incubated with the target protein, which was subsequently detected by an appropriate antibody. Three slightly different methods were used here: (1) as a first and crude check, PC, PE and folch fraction were spotted on the membrane; (2) commercial pre-spotted Membrane Lipid Strips® and (3) PIP Strips® (echelon, see section 2.3.6) were purchased. On the latter two, very distinct and pure lipids were spotted, so that a more defined classification of lipid binding was made possible for each construct.

On protein-lipid-overlay blots (PLO) the protein of choice was presented with surface bound lipid mixtures or pure lipids (see 2.3.5). As figure 68 shows, almost all constructs bound to the presented folch on nitrocellulose. Only the NCBD construct ranging from amino acids 814-1060 and the 883Δ PIP showed low to no binding to the lipids. The 1125 tail gave a very low signal which indicated weak binding. None of the constructs interacted with the control lipids PC and PE although the truncations as well as the NCBD tail showed binding to these phospholipids when presented as liposomes (see appendix figure 108).

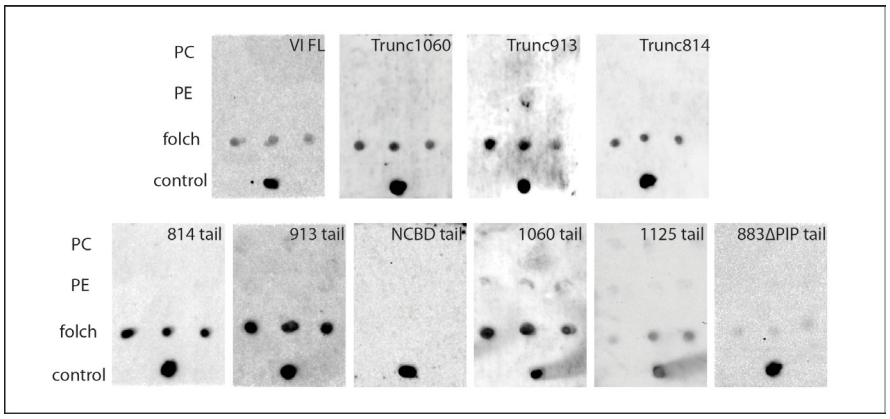

Figure 68: PLO blots for all myosin VI constructs. First row on each blot: pure PC in different amounts (from left to right: 500 pmol, 350 pmol and 200 pmol). Second row: pure PE, third row: folch. The control consisted of the respective target construct as check for antibody performance. A black dot indicates a positive reaction with the antibody and therefore binding of the protein construct to the particular lipid/ lipid-mix. NCBD tail (814-1060). All experiments were performed at least three times.

3.3.6 Calcium has effect on full-length myosin VI on nitrocellulose

After having seen the effect of calcium onto the binding behaviour of myosin VI FL (see section 5.1.2), it was tested whether this effect was also present on PLO blots. For this, PLOs as above were performed but with the addition of 1 mM $CaCl_2$ in the buffer.

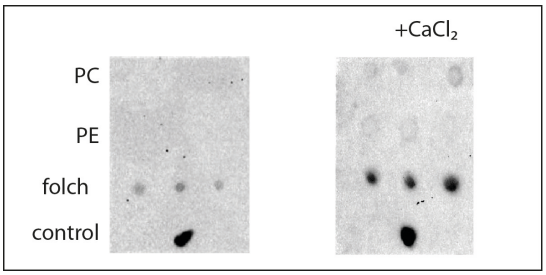

Figure 69: Calcium effect on myosin VI FL on PLO blots First row on each blot: pure PC in different amounts (from left to right: 500 pmol, 350 pmol and 200 pmol). Second row: pure PE, third row: folch. The control consisted of the respective target construct as check for antibody performance. A black dot indicates a positive reaction with the

antibody and therefore binding of the protein construct to the particular lipid/ lipid-mix. Left blot myosin VI FL without addition of Calcium, right blot with addition of 1 mM $CaCl_2$. (n = 3)

Figure 69 shows that myosin VI FL bound to folch on nitrocellulose only weakly. When the same experiment was done with the addition of calcium however, the binding increased significantly.

3.3.7 Calcium changes lipid affinities of myosin VI FL protein

An even more obvious effect was seen when Membrane and PIP Strips were performed with and without the addition of Calcium.

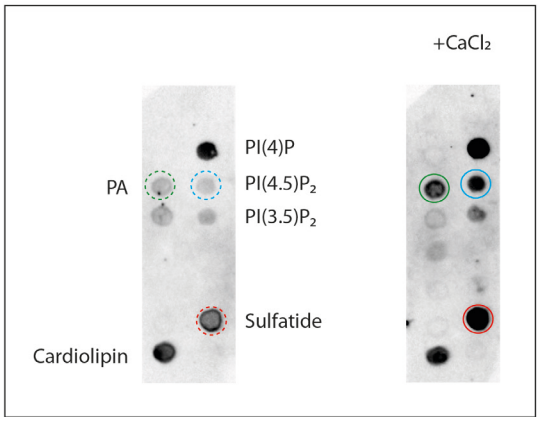

Figure 70: Calcium effect on myosin VI FL on Membrane Lipid Strips® ®. A black dot indicates a positive reaction with the antibody and therefore binding of the protein construct to the particular lipid. Membrane Strips with myosin VI FL. Blot on the left without Calcium, on the right with addition of 1 mM $CaCl_2$ in all buffers (n = 2).

Figure 70 illustrates a shift of lipid binding affinities of the full-length protein. Without calcium it bound strongly to PI(4)P and Cardiolipin. Weaker binding was detected to sulfatide and even weaker to PA and $PI(4,5)P_2$. When the same experiment was performed in a 1 mM $CaCl_2$-supplemented Blocking-buffer, binding to PA, $PI(4,5)P_2$ and sulfatide increased substantially (indicated by coloured circles).

3.3.8 Myosin VI constructs show different membrane lipid affinities

Since almost all constructs were capable of interacting with nitrocellulose-bound mixed lipids (i.e. folch) (figure 68), a more detailed view of membrane lipid binding was sought. As figure 71 shows, myosin VI bound to a limited number of lipid components. Strikingly all of the interacting lipids were negatively charged whereas no binding to the available neutral lipids was observed.

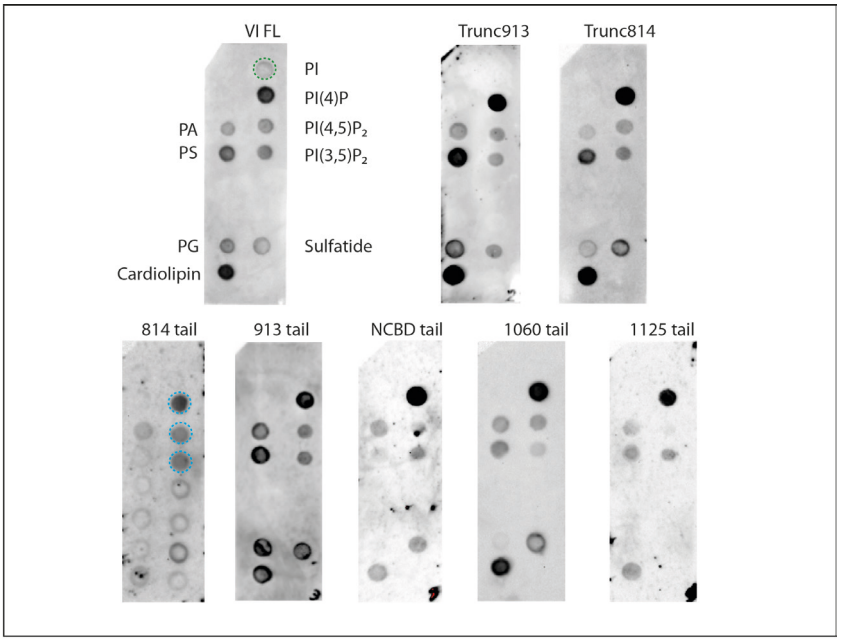

Figure 71: Membrane Lipid Strips® for myosin VI constructs. A black dot indicates a positive reaction with the antibody and therefore binding of the protein construct to the particular lipid. Trunc1060 was left out to avoid redundancies. All experiments were performed at least twice. Those lipids where reactions could be found are indicated with names, for full layout of strips see 2.3.6.

Between the FL construct and the truncations only the loss of binding to PI could be detected, but between the tail constructs, more apparent differences were noticed. The 814 tail did not interact specifically but showed more or less only background or nonspecific binding, which was indicated by the "coffee-ring stains" on the blots. Repeats and adjustments in exposure time or incubation lengths did not enhance the signal either. But a weak signal for PI(4)P binding as well as $PI(4,5)P_2$ and $PI(3,5)P_2$ was detectable. On the other hand all shorter tails interacted with the same range of membrane lipids, but showed differences in binding preferences. The 913 tail bound in exactly the same manner as the truncations, but the NCBD construct lost the ability to bind to PS and PG completely whereas binding to PI, $PI(4,5)P_2$, $PI(3,5)P_2$, sulfatide and Cardiolipin was considerably reduced. Remarkably the cargo-binding domain (1060 tail) bound almost identically as the 913 tail to PI(4)P, $PI(4,5)P_2$, $PI(3,5)P_2$, sulfatide and Cardiolipin as well as PS and PA but did not bind to PG. For the shortest tail construct, 1125 tail, attachment to PI(4)P remained strong but was noticeably lower for PA, PS, Cardiolipin and $PI(3,5)P_2$. It was entirely disrupted for PG, sulfatide, PI and $PI(4,5)P_2$.

3.3.9 Myosin VI constructs show differences in Phosphatidylinositol (PIP) binding

An even more detailed look into binding affinities was feasible by using PIP Strips® as PLO substrate (figure 72). Again it was seen that only a range of lipids were bound to by the myosin VI constructs and that there was variability in binding affinities.

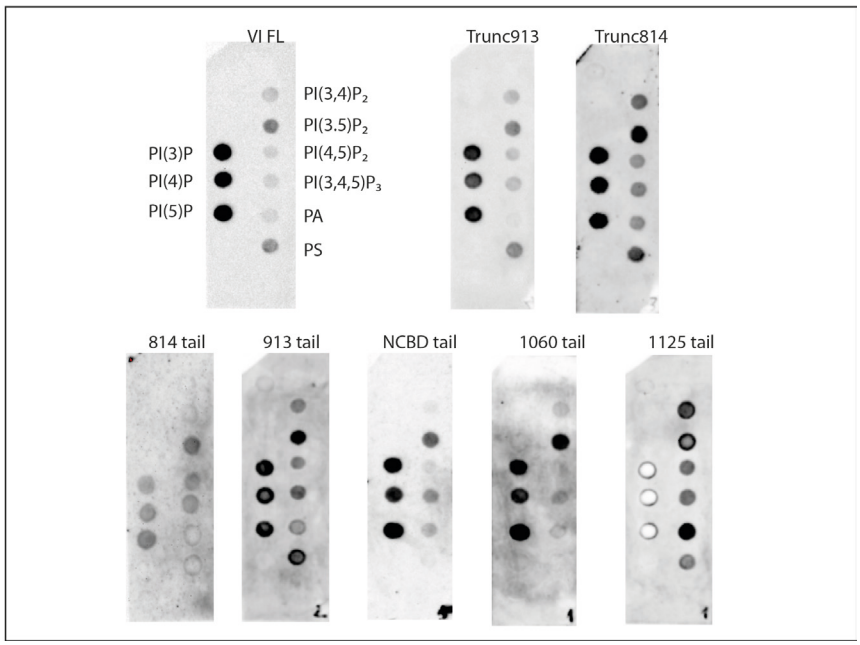

Figure 72: PIP Strips® for myosin VI constructs. A black dot indicates a positive reaction with the antibody and therefore binding of the protein construct to the particular lipid. Trunc1060 was left out to avoid redundancies. 1125 tail: the signal for PI(3)P to PI(5)P had such high intensity, leaving only white spots. All experiments were performed at least twice. Lipids where reactions could be detected are indicated. For full layout of strip, see chapter 2.3.6.

The FL construct bound to the three mono-phosphates PI(3)P, PI(4)P and PI(5)P as well as the di-phosphates, PI(3,4)P_2, PI(3,5)P_2 and PI(4,5)P_2. Additionally binding to the tri-phosphate PI(3,4,5)P_3 and the phospholipids PA and PS was detectable (figure 72). The most remarkable aspect was that binding to the three mono-phosphates was strong throughout the constructs. Binding to PI(3,5)P_2 changed from a weaker signal in the FL protein to strong binding in Trunc913 and the tail constructs. The 814 tail again showed in total a weak binding behaviour expressed by very low signal detection. However, a binding reaction to the mono-phosphates and PI(3,5)P_2, PI(4,5)P_2 and PI(3,4,5)P_3 was identified. The 1125 tail additionally showed a higher affinity for PA than the other constructs including the FL protein. This effect was not seen on the Membrane Lipid Strips where PA was spotted on as well (figure 71). This might be due to the availability of better binding partners than PA on the PIP Strips.

3.3.10 Myosin VI cargo-binding domain constructs reveal differences in lipid binding

3.3.10.1 Sequence alignment

An alignment of the amino acid sequences of human and chicken derived myosin VI cargo-binding domain (CBD) revealed that the major known motifs for interaction with binding partners (i.e. RRL and WWY) as well as the PI(4,5)P_2 binding sequence exist in both constructs. Though slight differences in the amino acid sequence were noticed (figure 73, yellow marking).

Figure 73: Sequence alignment for human 1060 tail (h) and chicken 1060 tail (c). The sequences show a 98.7% similarity. Purple: known motifs (RRL: NDP52 binding, WWY: Dab2 binding and KSKNKKR: PI(4,5)P_2 binding). Yellow marks show dissimilarities in sequences.

3.3.10.2 Co-sedimentation reveals differences in cargo-binding domain lipid-binding affinities between chicken (LI) and human (NI) tail constructs

Although the sequences of human 1060 (h1060) and chicken 1060 (c1060) tail showed 98.7% similarity, they exhibited distinct discrepancies regarding lipid binding.

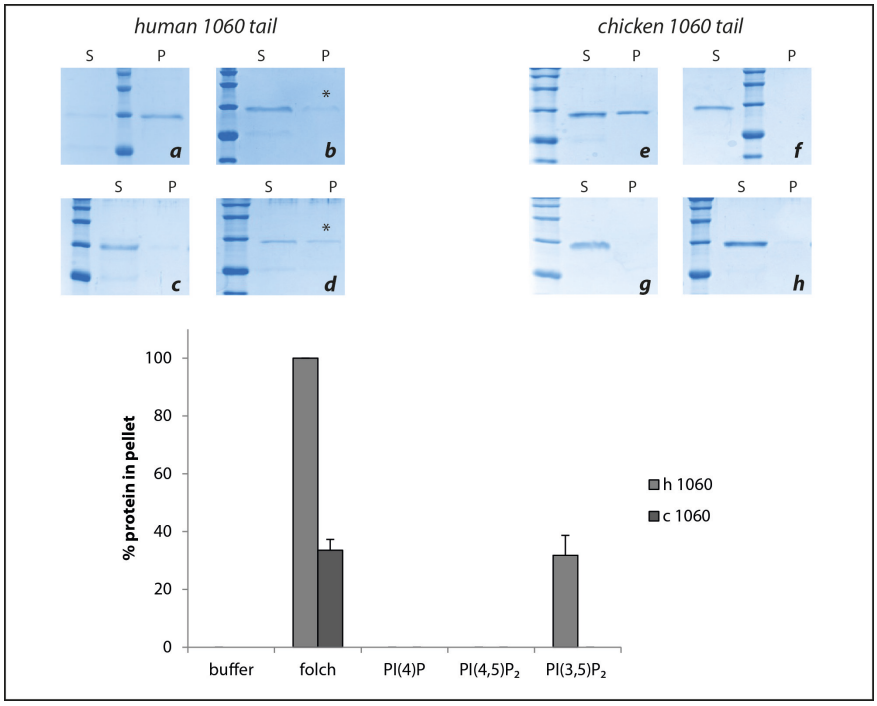

Figure 74: Co-sedimentations of myosin VI human 1060 tail construct vs. chicken 1060 tail construct. Upper panels show exemplary SDS-PAGE of co-sedimentations with the particular liposomes. Upper left: human 1060 tail co-sedimentations; **a:** with folch vesicles, **b:** PI(4)P, **c:** PI(4,5)P_2, **d:** PI(3,5)P_2. Upper right panel: chicken 1060 tail with **e:** folch, **f:** PI(4)P, **g:** PI(4,5)P_2, **h:** PI(3,5)P_2. S and P stand for supernatant and pellet fraction, respectively. Graph shows densitometry of upper gels; first column "buffer" shows that none of the constructs pelleted on its own without liposome addition. All experiments conducted at least four times. Bars represent average of four co-sedimentations. Error bars show standard deviation.

As figure 74 shows 100% of the h1060 tail bound to folch vesicles but the chicken construct bound to only 30% ($p \leq 0.001$). Whilst both tail constructs did not bind to either PI(4)P or PI(4,5)P_2, only the human cargo-binding domain construct showed capacity to bind PI(3,5)P_2 with a low affinity of ~35% ($p \leq 0.001$).

3.3.10.3 Cargo-binding domain constructs show different lipid affinities

When added to nitrocellulose-bound lipids, there was a clear difference detectable between the two cargo-binding domain constructs. The human construct bound to folch spotted on nitrocellulose, as would be predicted from the co-sedimentation (figure75), and the chicken tail did not bind at all to the PLO even though it bound to the liposomes (figure 75).

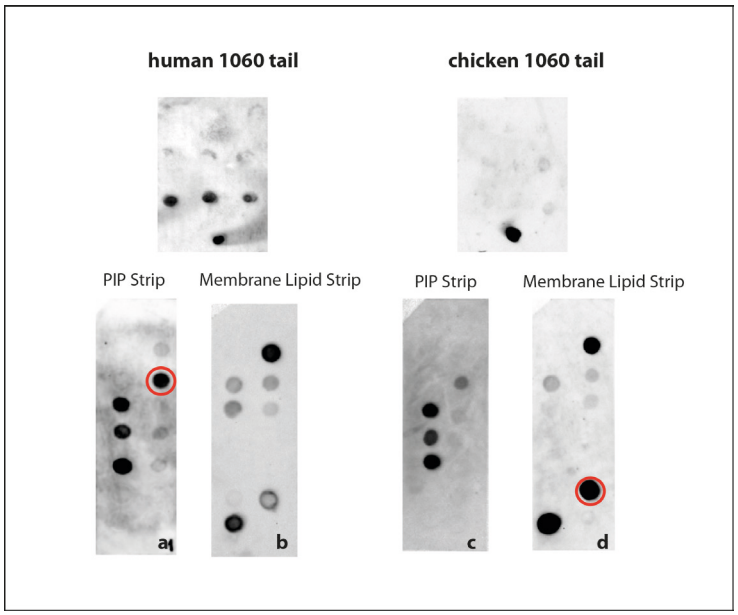

Figure 75: PLO for myosin VI h1060 tail vs. c1060 tail. A black dot indicates a positive reaction with the antibody and therefore binding of the protein construct to the particular lipid. Upper row: PLO with PC, PE and folch spotted on in three different concentrations and control (see figure 68). a: PIP strip of h1060 tail, b: Membrane Lipid Strip h1060 tail, c: PIP Strip c1060 tail, d: Membrane Strip c1060 tail. All experiments were performed at least twice. For full layout of strip, see chapter 2.3.6.

A more refined look using the PIP and Membrane Strips® revealed that more binding-preference differences existed. On the PIP strips binding to the mono-phosphates PI(3)P, PI(4)P and PI(5)P was seen for both constructs. But binding to $PI(3,5)P_2$, being noticeable for the human construct, was very feeble with the chicken tail construct. On the membrane Strips on the other hand a different effect was noticed. While h1060 tail bound predominantly to PI(4)P and Cardiolipin and only weakly to sulfatide. This last interaction was strongly enhanced in the c1060 construct.

Both constructs showed high affinity to PI(4)P when presented on nitrocellulose but did not bind to it as soon as it was incorporated in liposomes. Additionally none of the cargo-binding domain constructs interacted with $PI(4,5)P_2$.

3.3.11 Myosin VI motility on lipid monolayers

3.3.11.1 *In vitro* Gliding-filament assay

After dissecting the lipid binding capabilities of the myosin VI tail (section 5.1.1) it was intriguing to see whether lipid binding had an effect on the functionality of myosin VI as well as being a possible regulative mechanism. Therefore a typical *in vitro* gliding-filament assay was altered (see section 2.3.1) and non-fluid lipid-monolayers as substrate were used instead of nitrocellulose. These were tested with fluorescence recovery after photobleaching (FRAP) for their non-fluidity before use (figure 76).

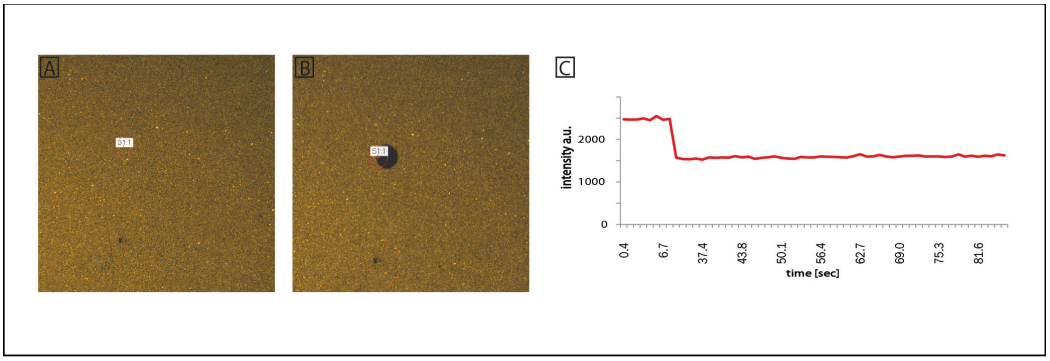

Figure 76: FRAP test for immobile lipid surfaces. (A): shows typical lipid surface in flow-cell, to test the surfaces they were stained using Rhodamine labelled PE in the mixture which was exchanged for non-fluorescent PE in the actual assays. **(B):** surface after 10 s photobleaching with 405 nm laser and 2 min recovery time, recorded with a 488 nm laser. As **(C)** shows, no recovery of fluorescence was achieved over time.

In figure 76 a typical FRAP experiment can be seen. It depicts the fluorescently labelled lipid layer before (A) and after photobleaching (B). The graph (C) shows that in this experiment no recoveries of the fluorophores in the bleached region of interest occurred over time. This was done for several flow-cells and proved that with this preparation method (section 2.3.8) only static lipid monolayers were produced.

3.3.11.2 Myosin VI shows higher gliding-velocity and functional affinity for lipid surfaces

Myosin VI is known to be a relatively slow motor protein with published velocities of up to 71 nm/s (Lister *et al.* 2004). As a comparison *in vitro* experiments of myosin V provide a mean velocity in the range of 200-450 nm/s (Mehta *et al.* 1999). From our experience we knew that myosin VI did not move on nitrocellulose directly like most other myosins, but needed the support of an antibody or another substrate (figure 77). The antibody that

was used here was a myosin VI tail-specific antibody (from J. Kendrick-Jones, MRC, Cambridge, UK) which was raised against the entire tail of myosin VI.

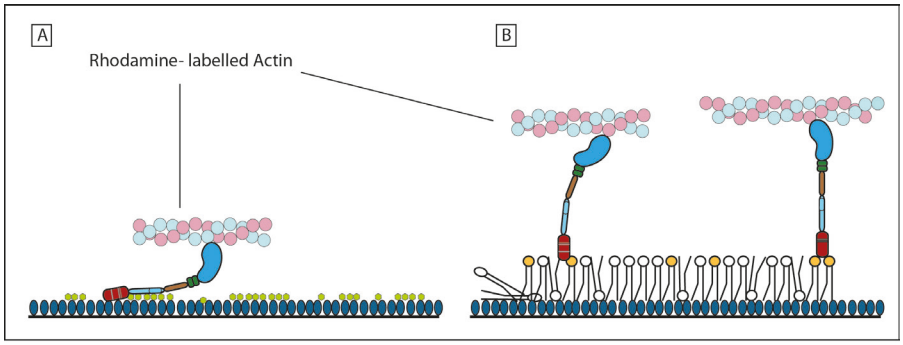

Figure 77: Setting of *in vitro* gliding-filament assays for myosin VI. (A): shows typical motility assay for myosin VI, using anti-tail antibody (light green) on the nitrocellulose surface and the possible resulting positioning of the myosin VI molecule. **(B):** unordered phospholipid surface (yellow: phospholipid) instead of antibody and the possible resulting positioning of myosin VI on the surface.

All filaments that showed continuous motility for ≥ 3 frames were tracked by hand using the GMimPro software (see chapter 2.4). Motility assays were performed with protein from at least three different preparations and per setting at least four flowcells.

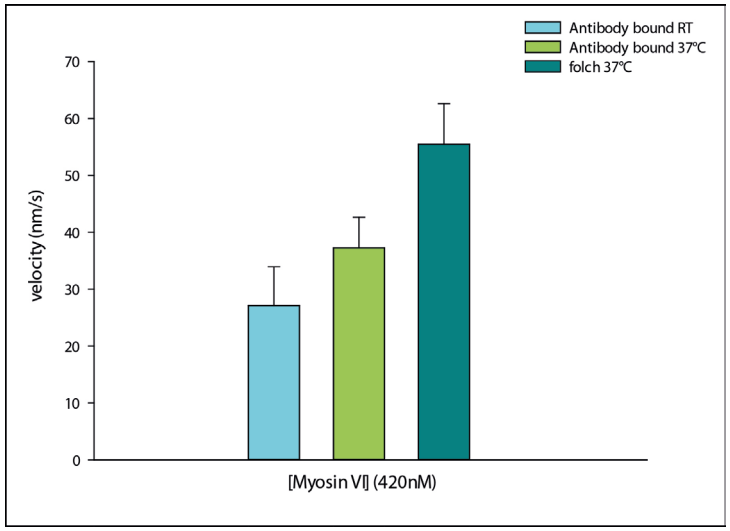

Figure 78: Bar chart for two different motility assay substrates with myosin VI at a motor concentration of 420 nM at different temperatures. RT: 23 °C. Temperature was changed to and kept at 37 °C with a standard temperature controller (TC200, Thorlabs) custom fitted to microscopic slides. Error bars show standard deviation. (n= 656 filaments).

For one chosen intermediate motor concentration of 420 nM on the surface, it was possible to see two major changes in velocity (figure 78). For antibody-bound myosin VI, the change of temperature from RT (23 °C) to 37 °C enhanced the velocity from 27 nm/s (± 6.8 nm/s) to 37 nm/s (± 5.4 nm/s) which marked an increase of 27%. When the substrate, to which the myosin was bound, was exchanged for folch, the speed increased from 37 nm/s to 55 nm/s (± 7.1 nm/s), which corresponded to an increase of 104% when

compared to antibody bound at RT ($p \leq 0.001$). Figure 79 displays the effects on antibody and folch bound myosin VI at 37 °C for different motor concentrations.

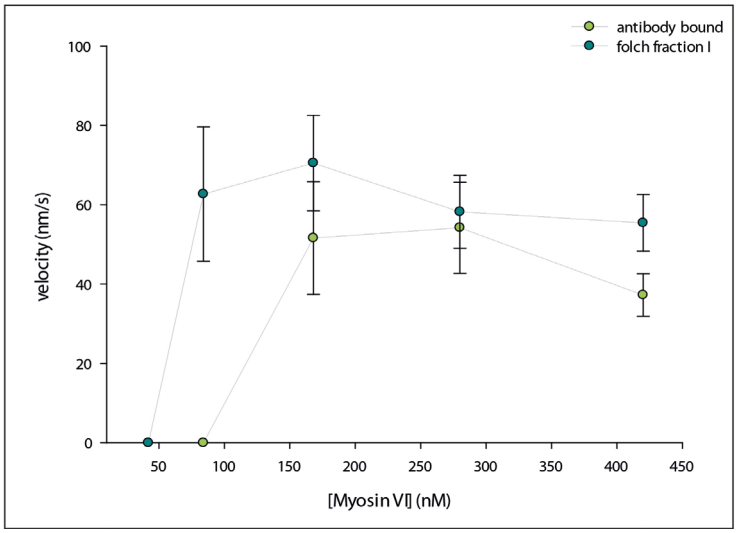

Figure 79: Velocities of myosin VI at 37 °C on anti-tail antibody versus folch. Error bars mark standard deviation. Myosin VI concentrations in the flow cells were: 42 nM, 84 nM, 168 nM, 280 nM and 420 nM; no motility was traceable at higher or lower concentrations. (n= 606 filaments)

According to figure 79, three main effects could be noticed. First, there seemed to be a motor density on the surface of the flow-cell around 280 nM where the filament gliding speed was almost equal (~ 60 nm/s) for both substrates. Second, it was obvious that with higher motor density the speed decreased from the maximum of 70 nm/s (± 12 nm/s) for folch bound myosin VI (52 nm/ s (± 14 nm/s) antibody bound) to 55 nm/s (± 7.1 nm/s) and 37 nm/s (± 5.8 nm/s) respectively. This equals a decrease in velocity of 21% for folch bound and 26% for antibody bound myosin VI. At even higher concentrations this effect seemed to level off for folch bound myosin VI but on nitrocellulose a further decrease was noted. And third, the lowest concentration at which uninterrupted motility was obtainable (here termed 'affinity') for both substrates were different. On folch surfaces motility was obtained at 42 nM whilst on antibody motility stopped at 84 nM.

3.3.11.3 Myosin VI exhibits different behaviour on various lipid surfaces

After having seen the effect of the lipid mixture folch upon the motility of myosin VI, it was important to see whether the three different phosphatidylinositolphosphates (PIPs) PI(4)P, PI(3,5)P_2 and PI(4,5)P_2 had distinct impacts on the activity of this motor protein as well.

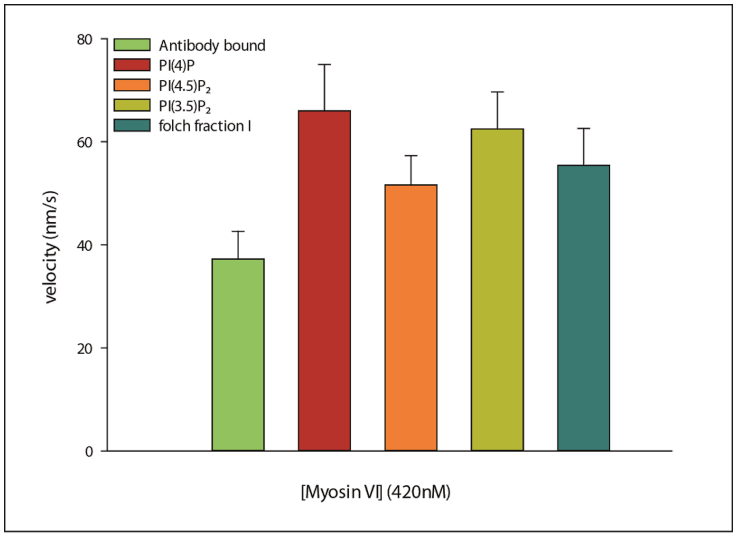

Figure 80: Bar chart for five different motility assay substrates with myosin VI at a motor concentration of 420 nM (37 °C). Error bars show standard deviation. (n = 3315 filaments)

Figure 80 compiles the effects of five different substrates on filament gliding speed driven by myosin VI at a motor concentration of 420 nM. It shows that not only folch surfaces improved the velocity but the aforementioned PIPs had an influence upon it too. At this particular motor concentration the fastest gliding speed was measured for a surface containing PI(4)P at 66 nm/s (± 8.9 nm/s). Motors on surfaces containing $PI(3,5)P_2$ exhibited a velocity of 62 nm/s (± 7.2 nm/s) followed by motors on $PI(4,5)P_2$-containing surfaces with 57 nm/s (± 5.7 nm/s) which was similar to folch surfaces where the tracked filament gliding speed was 55 nm/s (± 7.1 nm/s). Although the differences between the various PIPs were not as big as the initially observed changes in figure 79, at different concentrations they became more apparent.

Figure 81 A gives an indication that different species of lipids had different impacts upon the gliding speed of myosin VI. The comparison with folch as substrate revealed that PI(4)P, $PI(4,5)P_2$ and folch showed very similar velocities at a motor concentration of 84 nM (60-70 nm/s). This was similar to the abovementioned situation where myosin VI on folch and antibody showed an almost identical speed at 280 nM (see figure 79).

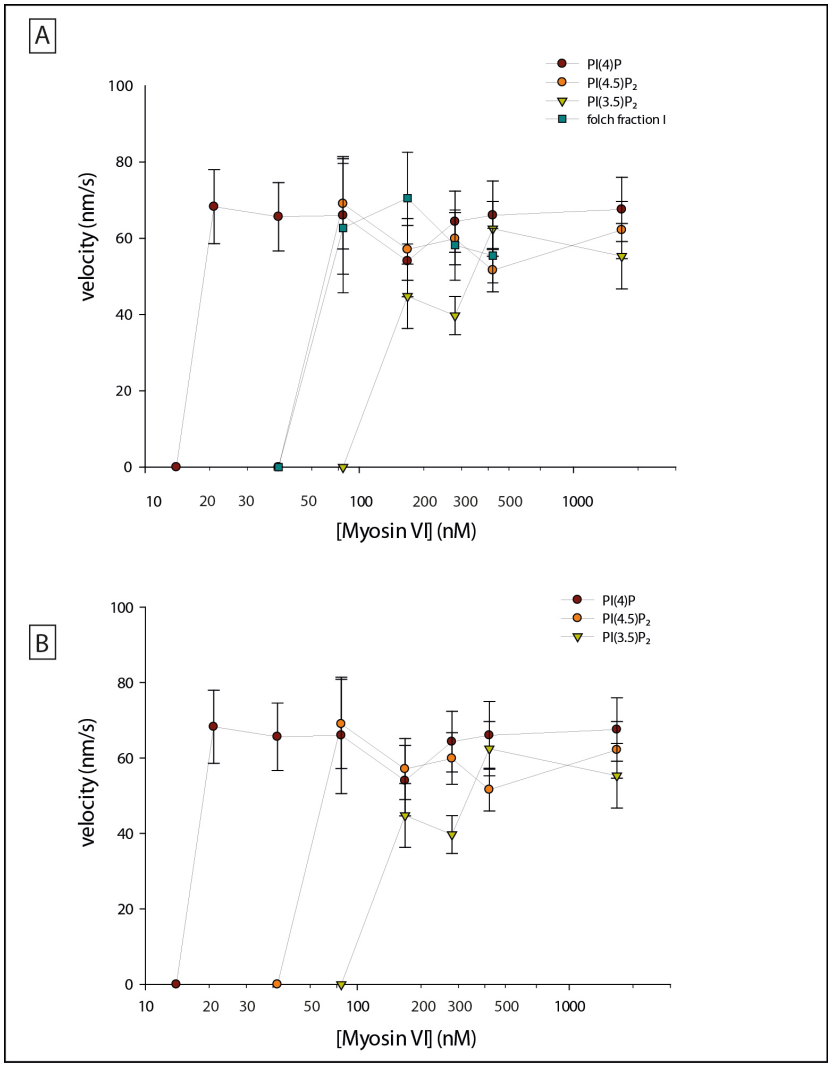

Figure 81: Velocities of myosin VI at 37 °C on different PIPs and folch surfaces. Myosin VI concentrations in the flow cells were: **(A)** 21 nM, 42 nM, 84 nM, 168 nM, 280 nM and 420 nM. For the PIPs additionally 1680 nM myosin VI were possible. At this concentration no motility was detected on folch surfaces. (n=3028) **(B)** Same graph as above without folch for emphasis of effect of PIPs on myosin VI motility. (n= 2946 filaments). Error bars mark standard deviation, logarithmic scale on x-axis.

Additionally myosin VI was capable of performing motility on all three PIPs at much higher concentrations (up to 1680 nM) than on folch surfaces where no motility was detected above a protein concentration of 420 nM (figure 81, A, blue squares). A closer look on the interactions with the PIP-containing surfaces (figure 81, B) revealed that the gliding velocity on $PI(3,5)P_2$ surfaces was the slowest at low motor densities up to 420 nM myosin VI where it showed an intermediate velocity of 62 nm/s (± 7.2 nm/s) (see figure 80). Furthermore it was noticed that myosin VI had the lowest affinity for $PI(3,5)P_2$ containing surfaces. On this particular surface it stopped moving at motor concentrations of 84 nM whereas the protein was still bound to and moving on $PI(4,5)P_2$ (42 nM) and PI(4)P (21 nM) at considerably lower concentrations. Therefore the highest affinity in this assay was attributable to PI(4)P containing surfaces.

3.3.11.3.1 Myosin VI full-length Δ PIP mutant binds to and moves on lipid surfaces with different affinities

The Δ PIP mutant bound to the folch surfaces as well as to the other lipid surfaces. As figure 82 shows, only slight differences in filament gliding speed could be detected at a myosin VI concentration of 220 nM. The speed on folch surfaces was in total slightly higher (68 nm/s ± 10.2 nm/s) than with the formerly analysed wild-type FL. In total differences were not as distinct as with the wild type FL VI (figure 81).

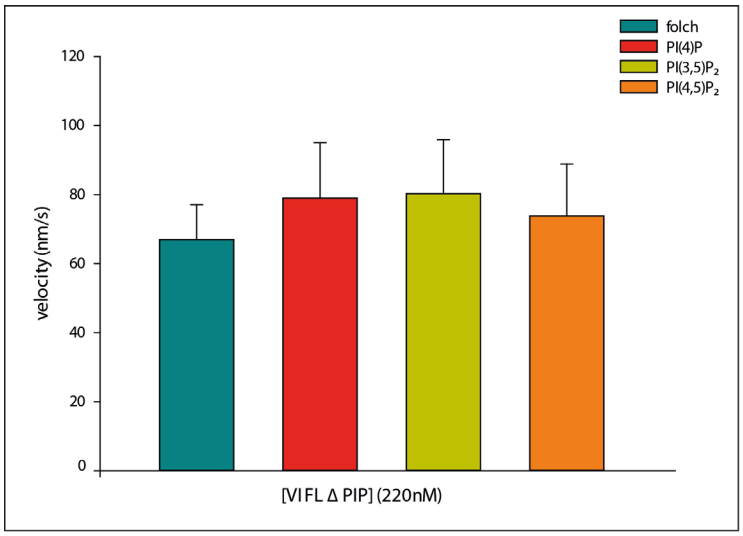

Figure 82: Bar chart for four different motility assay substrates with myosin VI Δ PIP at a motor concentration of 220 nM (37 °C). Error bars show standard deviation. (n= 3769 filaments)

Figure 83 depicts the filament gliding velocities on PIP surfaces in comparison with folch surfaces at different motor concentrations. As it can be seen in figure 83 A, the affinity to folch surfaces was highest with detectable motility down to a motor concentration of 11 nM. This was significantly lower than with the wild-type protein where motility ceased at a concentration of 42 nM. Amongst PIPs (figure 83, B) an equal affinity for PI(4)P and PI(3,5)P_2 could be measured. No motility could be detected below 88 nM myosin VI concentration. The lowest affinity was found for PI(4,5)P_2. With this lipid on the surface movement ceased already at a higher concentration of motors (146 nM). Above all a decrease in speed was detectable at concentrations higher than 88 nM. The velocity was not further decreasing between 146 nM and 880 nM but plateaued around 80 nm/s.

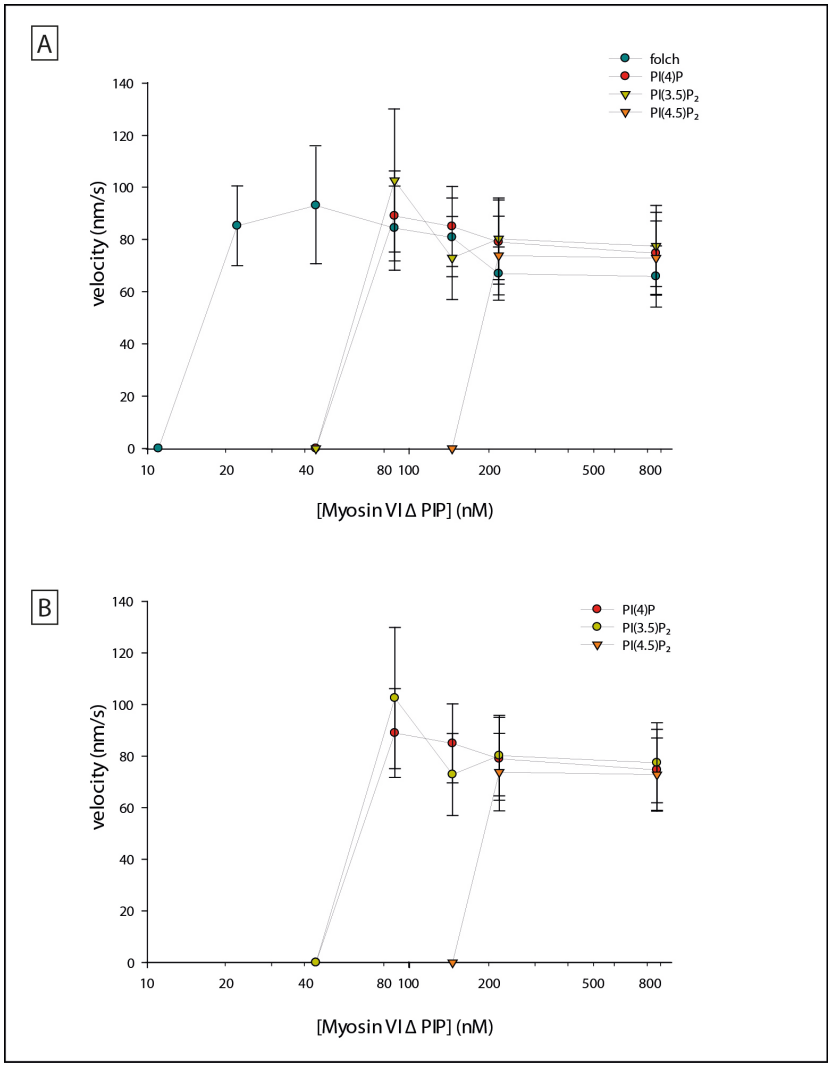

Figure 83: Velocities of myosin VI Δ PIP at 37 °C on different PIP and folch containing surfaces. (A): Myosin VI Δ PIP on different lipid surfaces.(n= 3769 filaments) **(B)** Same graph as above without folch for emphasis of effect of PIPs on myosin VI motility. Myosin VI Δ PIP concentrations in the flow cells were: 11 nM, 22 nM, 44 nM, 88 nM, 146 nM, 220 nM and 880 nM. (n=2382). Error bars mark standard deviation, logarithmic scale on x-axis.

To investigate further whether these phenomena were only due to better positioning on the lipid surface in comparison to the antibody, biotinylated myosin VI FL with a C-terminal biotin recognition site (BRS) was expressed, (see 2.2.9) and the *in vitro* gliding filament assay on Biotin-BSA with Neutravidin surfaces were performed as a control.

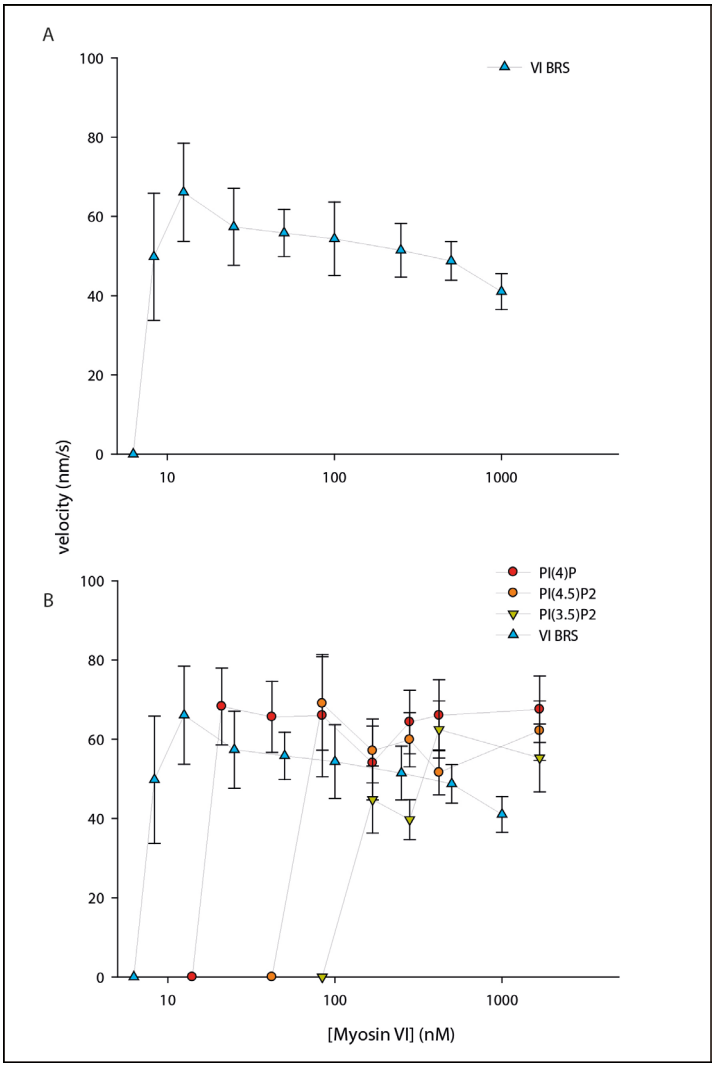

Figure 84: Motility of biotinylated VI FL BRS on Biotin BSA. (A): Myosin VI BRS in the flow cells were 1 µM, 500 nM, 250 nM, 100 nM, 50 nM, 25 nM, 12.5 nM, 8.3 nM and 6.25 nM. **(B):** combination graph of motility on PIPs and of myosin VI BRS on biotinylated BSA. Error bars mark standard deviation, logarithmic scale on x-axis (n=1512 filaments).

As figure 84 shows, the myosin VI FL BRS (VI BRS) was comparable in velocity to the former preparation used with the lipid layers. The maximum gliding speed was 66 nm/s (± 12.4 nm/s). Motility was obtainable to a motor concentration as low as 6.25 nM, which was significantly lower than on the lipid surfaces.

3.4 Calmodulin and lipid binding

After interrogating the lipid-binding abilities of the myosin VI tail (see 3.3), the back folding abilities of the cargo-binding domain and the role of CaM in this mechanism, a closer look at the lipid-binding capacity of CaM had to be taken. The already introduced techniques of Protein-Lipid overlay assays (PLO, see 2.3.5) and lipid-affinity co-sedimentations (see 2.3.7) were used to deepen the understanding of the role CaM plays in the regulation of myosin VI.

3.4.1 Calmodulin affinity titration

It was of interest to establish whether CaM binds lipids and if so, whether there was a difference between free CaM and CaM bound to an IQ-peptide. As described in chapter 3.2.6, CaM was titrated to target peptide sequences (IQ1 and IQ2) in either Ca^{2+} or EDTA buffer. Approximately 0.1 µM CaM was added per injection to a total concentration of 2 µM peptide (figure 85).

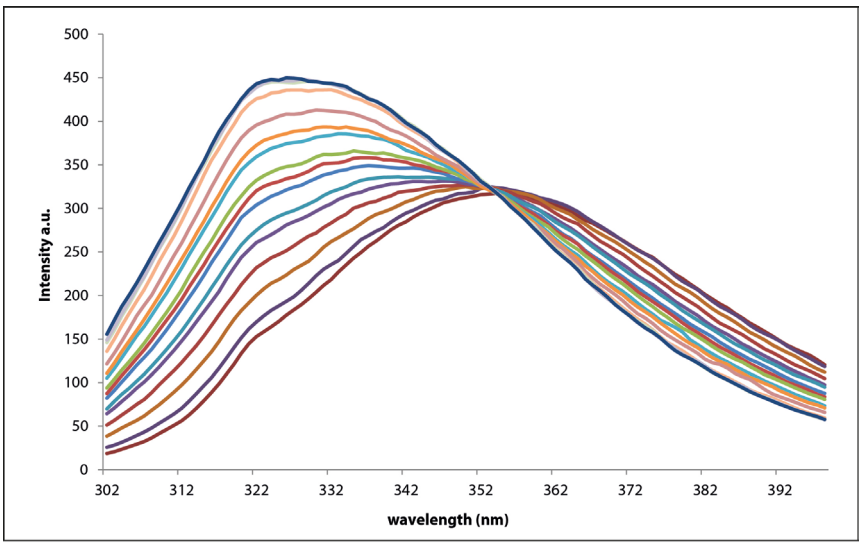

Figure 85: Calmodulin binds to IQ-motif peptide. Peak at ~358 nm shows the tryptophane fluorescence of IQ peptide alone. Shift to the left implicates change in tryptophane fluorescence and thus binding of CaM.

CaM was titrated to the particular IQ-motif peptide until its saturation (see section 4.3.1). As figure 85 shows an obvious shift in tryptophan (Trp) fluorescence was detected upon CaM addition to the peptide. This happened due to changes on the local tryptophan environment which was caused by the binding of CaM to the IQ peptide (Bahloul *et al.* 2004).

3.4.2 Calmodulin binds lipids in a Calcium-dependent manner

Figure 86 details the lipid binding of CaM to folch lipiosomes as well as the three phosphatidylinositolphosphates PI(4)P, PI(3,5)P_2 and PI(4,5)P_2. In a calcium-free buffer, binding to folch liposomes was minimal (~ 5% of protein in pellet). Whilst CaM bound to PI(3,5)P_2 and PI(4,5)P_2 equally well (~25% of protein in pellet), no binding could be detected for the mono-phosphate PI(4)P.

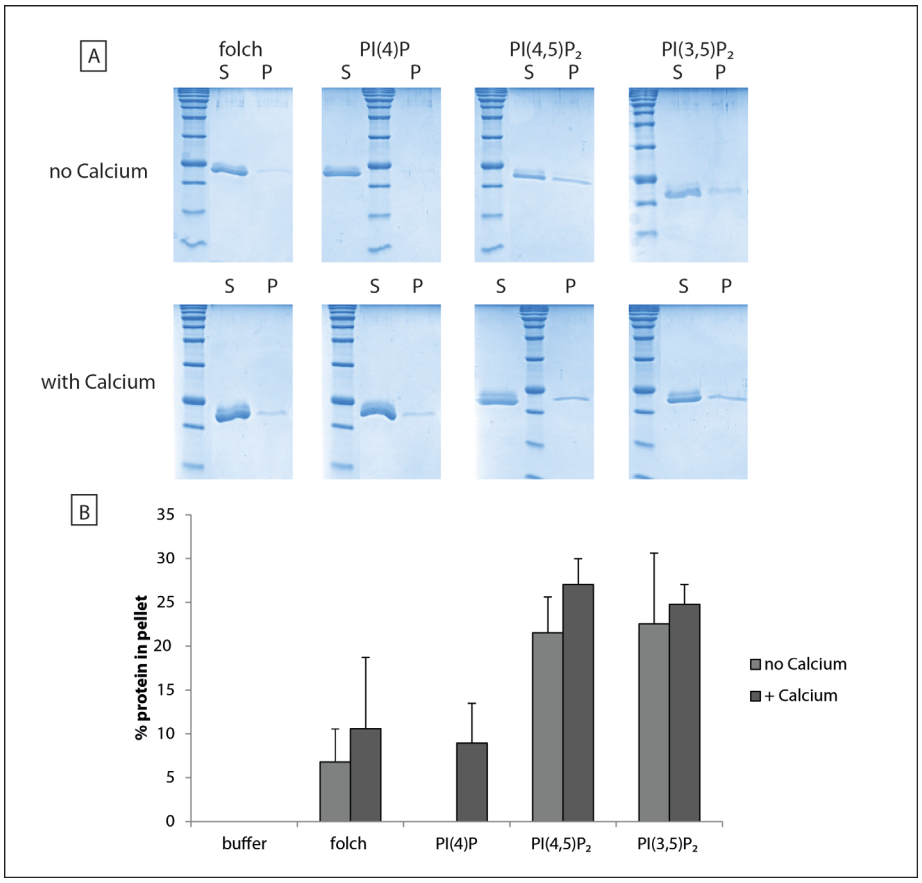

Figure 86: Calcium-dependent lipid binding of Calmodulin. (A): top row: lipid-affinity co-sedimentations with CaM and folch, PI(4)P, PI(3,5)P_2, PI(4,5) P_2 in Calcium-free buffer. Second row: same co-sedimentations as in **A**, but with 50 µM $CaCl_2$ in the buffer. **(B):** Densitometry of both sets of co-sedimentations. Bars show mean value of four independent experiments. Size CaM: 24 kDa. Given is the percentage of protein in the pellet fraction. The intensity of the tail or full-length band in the pellet was divided by the total intensity (pellet + supernatant) for each sample to determine the percent of protein in the pellet. Error bars show standard deviation. ($n = 4$)

This behaviour changed as soon as the identical co-sedimentation was performed with 1 mM $CaCl_2$ in the assay buffer. It was seen that calcium affected the binding of CaM to folch and the di-phosphates PI(3,5)P_2 and PI(4,5)P_2 only a little. The amount of protein in the pellet increased by approximately 6%. The effect of calcium on the interaction of CaM with PI(4)P on the other hand was substantial. Without calcium in the buffer, no interaction was measurable whereas with added Calcium around 10% of the total protein

was bound to the PI(4)P liposomes (p = 0.008) (figure 86, B). Binding to the lipid components PC, PE and Cholesterol was not detected.

3.4.2.1 Calmodulin binds IQ-motifs and lipids in a competitive manner

CaM on its own bound to folch, as can be seen in figure 87 A. But as soon as CaM was bound to the IQ-motifs 1 or 2, binding to lipids was abolished. The binding to either IQ peptide or lipids seemed to be mutually exclusive (figure 87, B and C).

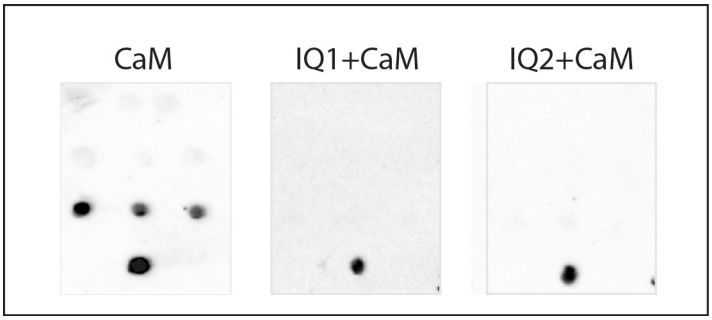

Figure 87: Calmodulin binds either lipids or IQ-motifs. Protein-lipid overlay assay (PLO) with CaM. On each blot: top row PC, second row PE and third row: folch is spotted on in serial dilutions (see 2.3.5). Only with folch a reaction is seen. PLO with IQ1 saturated with CaM shows no binding to any of the offered lipids. Only the antibody control spot at the bottom were the IQ1:CaM was spotted on is visible. Same as for IQ2:CaM which did not show an interaction with the lipids. For all three blots buffer was supplemented with 1 mM $CaCl_2$. Blots at least conducted twice.

3.4.2.2 Calmodulin exhibits calcium-dependent lipid affinities

As seen in section 3.4.2, binding to folch, $PI(3,5)P_2$ and $PI(4,5)P_2$ was increased only slightly with the addition of calcium. Since calcium had such an impact on binding to PI(4)P, it was of interest to elucidate this calcium-dependent change in lipid affinities even further. For this purpose the PIP® and Membrane Strips®, introduced in section 2.3.6, were used for a more detailed look into lipid affinity changes of CaM. Figure 88 depicts the influence of calcium onto binding of CaM to the different offered lipids.

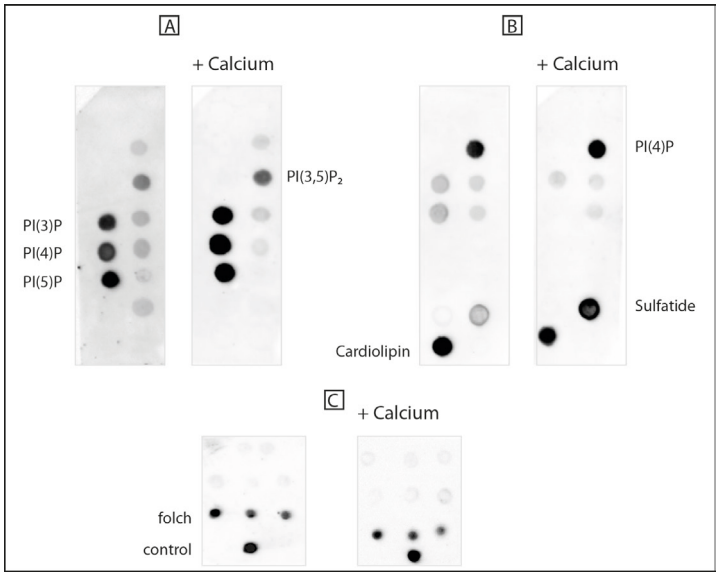

Figure 88: Calmodulin changes lipid affinities under changing calcium conditions. (A): PIP Strips of CaM without and with added 1 mM calcium (indicated above Strip). **(B):** Membrane Strips of CaM without and with added calcium show clear differences in lipid binding. **(C**): Whereas binding to folch on PLO was not altered by calcium addition. All blots were at least conducted twice. For blotted lipids see 2.3.6.

Figure 88 C presents that calcium had no influence on the binding behaviour of CaM to folch when the lipid was presented on nitrocellulose. On the PIP Strips CaM demonstrated interaction with the mono-phosphates PI(3)P, PI(4)P and PI(5)P as well as weak interaction with the di-phosphate PI(3,5)P_2. This binding pattern was not changed by addition of 1 mM calcium to the assay (figure 88, A). On the membrane strips on the other hand calcium had an influence on the binding of CaM to the lipids. In a Ca^{2+} -free buffer, CaM bound to Cardiolipin, PI(4)P and weakly to sulfatide. The interaction with sulfatide was highly increased when the assay was performed in a calcium supplemented buffer. In Ca^{2+}-free buffer a very weak interaction between CaM and phosphatidic acid as well as phosphatidylserine was detected, which was almost completely abolished in 1 mM calcium buffer. Interestingly binding to PI(4)P and Cardiolipin was not calcium-dependent (figure 88).

3.4.2.3 IQ-motif-Calmodulin complex shows reduced lipid affinities

The interaction of the (Cam:IQ1) and (Cam:IQ2) complexes with lipids on the PIP Strips in figure 89 A and B were very weak. It was reproducible and proved to be only non-specific antibody-reaction. Therefore a binding of this complex to any of the offered PIPs was not detected. All interactions which CaM alone showed as seen in figure 89 *c* encircled in red, were lost.

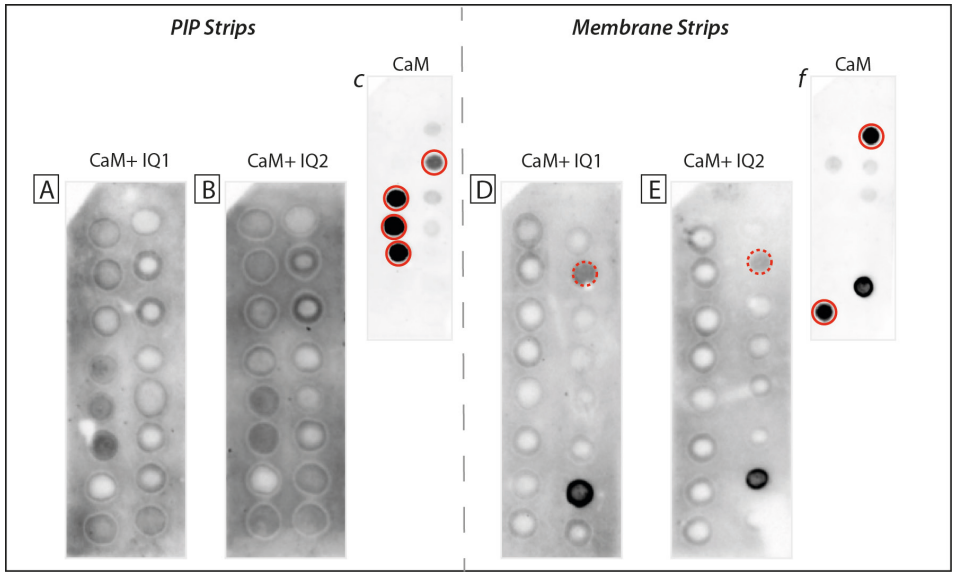

Figure 89: Calmodulin changes lipid affinities when bound to IQ peptides. (A): PIP Strip (see chapter 2.3.6) of IQ1:CaM. The reaction is non-specific. **(B):** PIP Strip (see 2.3.6) of IQ2:CaM. The reaction is non-specific as well. **(*c*):** PIP Strip of CaM under same buffer conditions as (A) and (B). **(D):** Membrane Strip (see 2.3.6) of IQ1:CaM. **(E)**: Membrane Strip of IQ2:CaM. **(*f*):** Membrane Strip of CaM under the same buffer condition as (D) and (E). A reaction with sulfatide was maintained with and without bound peptide. Red circles indicate reaction of CaM with the Strips that is lost in the peptide-bound state. Buffer contained 1 mM $CaCl_2$ for all experiments. Blots performed at least twice.

Although CaM on its own (figure 89, *f*) bound to PI(4)P, Cardiolipin and Sulfatide on the membrane strips, the peptide-bound CaM showed a different behaviour. Binding to PI(4)P and Cardiolipin was lost and only a slight interaction with PI(4)P was traceable (figure 89 D and E, dotted circle).

3.4.3 Discussion

3.4.3.1 Lipid binding is not restricted to lever arm extension (LAE) or cargo-binding domain (CBD)

The BH-plot of myosin VI FL revealed two possible lipid-binding sites along the protein, one around the unique insert and the second IQ-motif and a second one in the CBD (see figure 59). This second possible binding site corresponded to the binding site published by Spudich *et al.* (2007), where it was found to specifically bind to PI(4,5)P_2. Yu *et al.* (2012) described lipid binding in the LAE, which they found to bind to folch vesicles. In the course of this work it was found that in myosin VI lipid binding was not limited to these two structures but was found along the whole tail. All constructs, with the exception of the shortest tail (1125 tail), bound to folch liposomes. This special case will be discussed in a following section.

Subtly different binding patterns of the tail constructs in binding studies with defined lipid compositions (PI(4)P, PI(3,5)P_2, PI(4,5)P_2) suggested different lipid affinities along the protein. FL VI, 913 tail and 814 tail bound to all three different PIPs whereas 1060 and 1125 tail only bound PI(3,5)P_2. Since the PIP Strips showed a slightly different picture with all constructs binding PI(3)P, PI(4)P, PI(5)P and PI(3,5)P_2 and a very weak interaction with PI(4,5)P_2 this pointed towards two main explanations:

First, PIP-binding was not restricted to the CBD. Binding to PI(4)P and PI(4,5)P_2 seemed to be present N-terminal of amino acid 1060 although described differently by Spudich *et al.* (2007) where they identified an amino acid sequence (WSKNKKR), by mutating it (→WASANNNR), as PI(4,5)P_2 binding sequence. The Δ PIP 883 tail construct was a kind gift from the Spudich lab and served here as a control. It was possible to repeat their findings (Spudich *et al.* 2007) with this construct, although the construct they used in the aforementioned publication was slightly longer (from aa 1017 to the end) than the one used in this project (aa 1060 to the end). This could mean that PI(4,5)P_2-binding might not be limited to the abovementioned sequence motif. They never tested the mutated tail in a PI(4,5)P_2-affinity co-sedimentation assay but only in immunofluorescence studies which could involve other, not yet defined binding partners linking myosin VI to the PI(4,5)P_2.

Therefore it is claimed here, that myosin VI has a much weaker affinity for $PI(4,5)P_2$ in calcium-free *in vitro* studies than thought until now and that all evidence points towards a much higher affinity for the precursor lipids PI(3)P, PI(4)P and PI(5)P as well as $PI(3,5)P_2$ along the whole protein. All these findings allude to the assumption that membrane binding of myosin VI might not necessarily be mediated in a stereospecific fashion but via more unspecific electrostatic interactions with a variety of charged phospholipids. A possible regulative mechanism for $PI(4,5)P_2$-binding will be discussed in the next section. These phosphatidylinositolphosphates are all involved, amongst others, in endocytosis, maintaining Golgi apparatus structure and autophagy and are therefore covering all fields of function of myosin VI.

Second, the CBD constructs (1060 and 1125 tail) did not interact with PI(4)P and $PI(4,5)P_2$ when presented as liposomes, but bound to these lipids when bound to a nitrocellulose surface. This might mean that additional mechanisms like curvature sensing (DiNitto *et al.* 2003, Hurley 2006, Lemmon 2008, Morton *et al.* 2012), electrostatic sensing (Rizo and Sudhof 1998, Sutton and Sprang 1998) or other mechanisms could account for this behaviour. Since lipids dried on nitrocellulose may in proportions expose parts of their molecules they would not when fitted into a liposome conformation, the nitrocellulose based assays may only give additional information about lipid binding affinities and should not stand alone. However they are highly repeatable and reliable and as shown in the myosin XXI mutant studies highly specific (see 3.5.3).

3.4.3.2 Calcium is a regulator of lipid binding

Calcium plays a pivotal role in the cell, especially in signal transduction pathways where it, amongst others, acts as secondary messenger. Its cytosolic concentration ranges from 0.1 to 0.2 µM (pCa 7 to pCa 6.7) but can locally and temporarily change to considerably higher concentrations, depending on cell type, by released Ca^{2+} for example from the ER, the SR or introduced from the extracellular space. Here it is noticeable that the addition of higher amounts of $CaCl_2$ to assays resulted in a change in lipid binding behaviour as well as lipid affinities. The addition of $CaCl_2$ (pCa 4.3) increased the binding of FL VI to folch vesicles and switched the binding of the 1125 tail from no interaction to 50% bound protein and it influenced the binding behaviour to PIPs as well. Binding of the full-length protein to PI(4)P was slightly reduced by addition of $CaCl_2$ (pCa 4.3), interaction with

$PI(3,5)P_2$ was reduced by 10 fold and binding to $PI(4.5)P_2$ was abolished completely. With $PI(4,5)P_2$ however it was possible to show that calcium in lower concentrations (ranging from pCa 5.3 to pCa 4.6, calculated with WEBMAXC, Stanford, USA) did not abolish binding of myosin VI FL to it. This indicates a regulative mechanism where changes in intracellular calcium levels may help regulate binding to vesicles and therefore make cargo-exchange easier and more effective. The 1125 tail, as mentioned above, bound only by addition of calcium (pCa4.3) to folch vesicles. This construct bound additionally to vesicles with a 10% PIP content. The 814 tail bound only to 20% to folch vesicles but with added Calcium (pCa 4.3) to around 87%. Since calcium is meant to cluster PIPs in vesicles (Czech 2000, McLaughlin *et al.* 2002, Mak 2013), this could be an additional effect, which affected the binding of these two constructs to the folch vesicles. It possibly made the PIP more available to these otherwise weak binders. Additionally calcium changed the lipid affinities of the FL protein considerably. Where it did not bind to PA and $PI(4,5)P_2$ on the membrane strips this binding was increased by addition of $CaCl_2$ (pCa 4.3), whereas binding to $PI(3,5)P_2$ was reduced after $CaCl_2$ addition. This can be explained by possible effects upon calmodulin conformational change or the folding of the protein (Payrastre *et al.* 2001).

3.4.3.3 Different roles in different species for myosin VI?

The direct comparison of the cargo-binding domains (CBD) of chicken and human myosin VI revealed only slight differences in the sequence but major differences in lipid binding ability and affinity as well. The human CBD showed a much higher affinity to bind to folch vesicles and on nitrocellulose than the c1060 construct. And although both constructs bound to Cardiolipin, a main component of the inner mitochondrial membrane and other bacterial membranes, only the chicken CBD interacted strongly with sulfatide. Sulfatide is a major constituent of brain myelin where it is found exclusively on the extracellular membrane of the myelin sheath. It can be found in the islet of Langerhans and in other cells where it is involved in the activation of ion channels (1.8.2.1). This might point towards a different set of functions for avian myosin VI in comparison to mammalian myosin VI.

3.4.3.4 Motility on lipids is improved by better positioning

Although other myosins, for example myosin V and myosin XXI (see 1.5), are capable of smooth motility on nitrocellulose surfaces, myosin VI was not. A tail specific anti-body

had to be used to obtain motility. Motility on unordered non-fluid lipid surfaces was much better in comparison to motility on antibody covered surfaces. These two facts allude to the possible explanation that both systems may offer a better positioning for the motor on the surface than nitrocellulose. And that myosin VI was in an improved configuration to support motility as soon as it was bound to lipid surfaces. This was additionally supported by the fact that motility of a C-terminally biotinylated myosin VI FL construct on a biotinylated BSA substrate was equally good as on lipid surfaces.

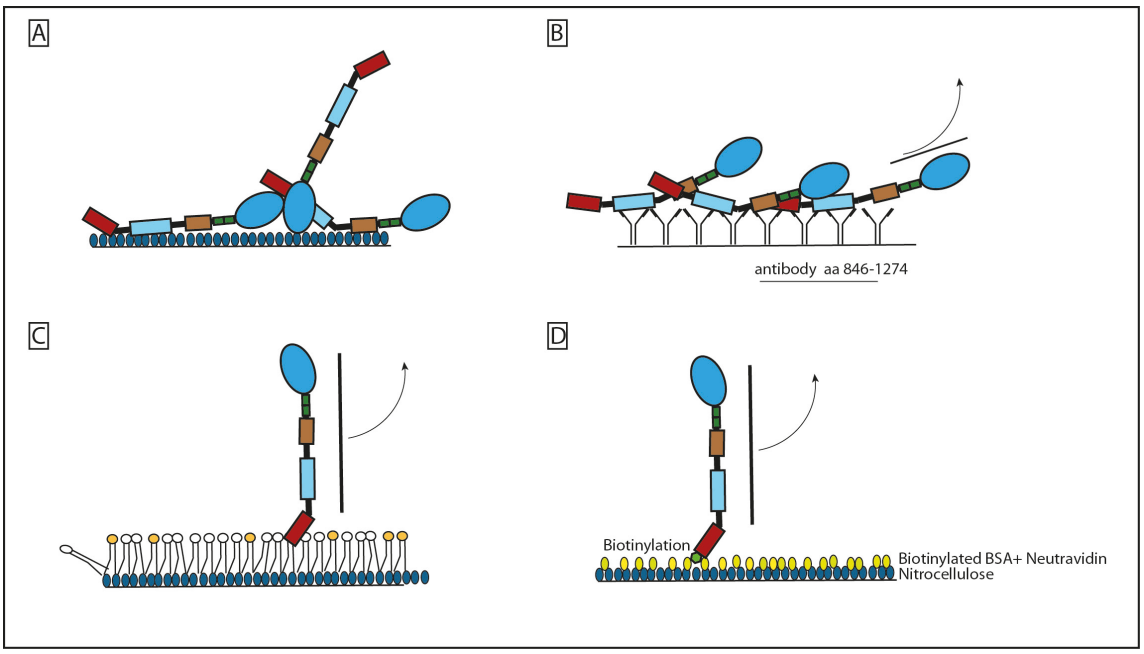

Figure 90: Possible configuration of myosin VI on different substrates. (A): motors on nitrocellulose may stick in all ways to the surface, **(B):** tail-specific antibody sticks different parts of the tail down (aa 846-1274) **C:** possible positioning of myosin VI on phospholipid containing non-fluid lipid surface and **(D):** optimal positioning of the myosin VI by biotinylation of the C-terminus and binding to biotinylated BSA. Arrow indicates largest possible lever arm of the protein in the gliding filament assay.

As the cartoon in figure 90 depicts, different conformational settings for myosin VI on the surface are imaginable. On nitrocellulose, where no motility was measured, the motor might stick in unfavourable ways to the surface (A), whereas in a more ordered way with the polyclonal anti-tail antibody which was raised against the amino acids 846 to 1274 and can bind to diverse parts in that amino acid range, resulting in an unordered mixture of positions of the VI FL (B) and in (C) possibly in the best configuration for motility which supports the highest measured velocities for this set-up, supported by (D) which depicts the optimal configuration of the myosin VI on the surface. An additional effect was the temperature dependence of myosin VI, where higher temperatures (37 °C) improved motility and accelerated the motion of the motor. Most intriguing was the finding of different affinities for substrates containing different types of PIPs. This might

be a regulative mechanism for different transport settings. The highest affinity for PI(4)P, which was only outperformed by the VI BRS, possibly stands for a long-range transport system in which myosin VI might be involved. PI(4)P is prevalent at the Golgi-apparatus and vesicles pinched off here need to be transported to various sites in the cell for example to the cell membrane, or the ER. This affinity will be discussed in detail in chapter 4 (general discussion).

3.4.3.5 Calmodulin binds directly to lipids

Calmodulin (CaM), the ubiquitous Ca^{2+} sensor of eukaryotic cells is involved in a wide variety of signalling events, regulating numerous proteins, including phosphatases, kinases, ion channels and pumps and myosins. As it was possible to show here, calmodulin bound to folch lipids on its own, but as soon as an IQ-peptide was bound to it, binding was disrupted. This may be a regulative mechanism with CaM binding exclusively either protein or lipid. Such was confirmed on the PIP strips, where no interaction with the lipids was detected as soon as calmodulin was bound to peptide. As a single protein CaM readily bound PI(3)P, PI(4)P and PI(5)P. On the membrane strips it was striking that binding to sulfatide was maintained or even improved throughout IQ-peptide binding, whereas binding to Cardiolipin and PI(4)P was abolished. Kovacs, Harmat *et al.* (2010) found that CaM bound to sphingosylphosphorylcholine (SPC), a precursor to 3-Sulfogalactosylceramide (Sulfatide) in the sphingomyelin cycle. CaM bound to SPC in the presence and absence of Ca^{2+}. In my experiments binding to Sulfatide improved with the addition of calcium. As soon as the IQ peptides were bound to CaM all other lipid binding abilities were lost, but the interaction to sulfatide persisted. That CaM still bound to sulfatide, even in the peptide-bound state, hints to the possibility that calmodulin might have a specific lipid binding site for sphingomyelin and its derivates which could still be exposed when CaM is wrapped around a target peptide. But this lipid binding ability might only be measurable in assays with peptides and not be commensurable in a properly folded full-length protein.

3.5 Myosin XXI, a novel molecular motor from *Leishmania* exhibits lipid binding abilities

3.5.1 Lipid binding in Myosin XXI

This chapter introduces myosin XXI, a novel molecular motor with similarities to myosin VI in terms of multifunctionality, which binds directly to lipids with most parts of its tail. Lipid binding and dimerisation in this motor seem to be mutually exclusive. It has protein has a phox homology (PX) domain in the converter region which is specifically interacting with PI(3,5)P_2. In vitro filament gliding assays prove a higher affinity and faster actin translocation of myosin XXI on lipid surfaces than on nitrocellulose.

3.5.1.1 Designing of myosin XXI tail constructs

Myosin XXI is a motor that has only recently been expressed and characterised (Batters *et al.* 2012). Therefore it was relevant to design various constructs in the style of myosin VI, which allowed scrutinisation of various aspects of this protein (e.g. dimerisation, lipid binding, motility, cellular localisation etc.). This study is focussed, following the pattern of myosin VI, upon lipid-binding abilities of the tail and the identification of lipid-binding motifs or regions as well as motility on lipids. Therefore the full length protein as well as tail constructs of myosin XXI were designed and expressed (figure 91). The full-length protein and the truncation were expressed in a baculovirus system (2.1.12) whereas the tail constructs were expressed in an *E. coli* based expression system (2.2.4).

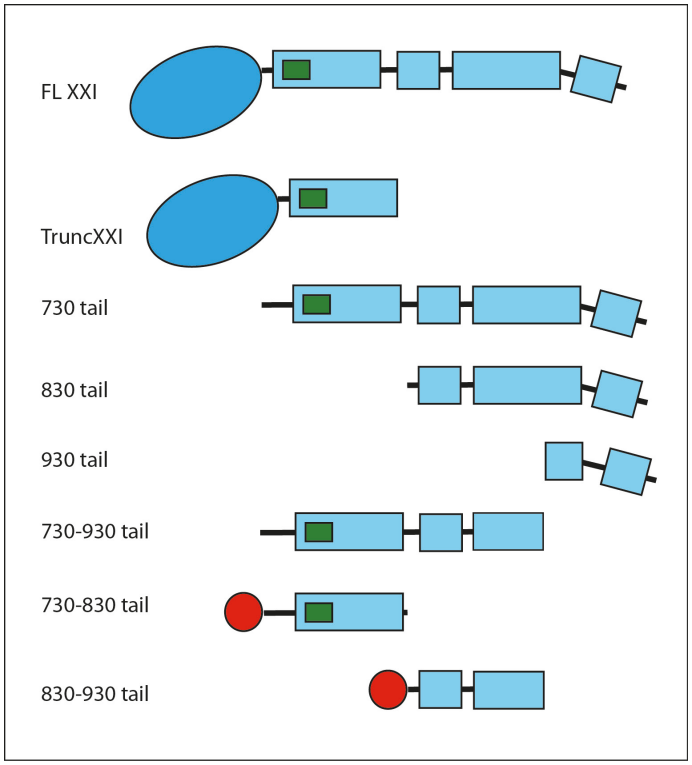

Figure 91: Schematic representation of myosin XXI motor truncation- and tail constructs. Full-length protein (aa 1-1051), Motor truncation TruncXXI (aa 1-800). Tail constructs: 730 tail (aa 730-1051) 830 tail (aa 830-1051), 930 tail (aa 930-1051), 730-930 tail, 730-830 tail, 830-930 tail. Red dot represents Red-fluorescent protein (RFP) with which these constructs was expressed as well.

3.5.2 Myosin XXI Lipid-binding capabilities bestride the entire tail

As described for myosin VI in chapter 3.3.1.2, lipid-affinity co-sedimentations were performed to test lipid-binding competence of different tail-constructs. Initially the focus was set on the question does myosin XXI bind to lipids? And if it does, which parts of the protein were responsible for this interaction? To uncover the lipid-binding capacities of the different tail constructs, the binding to folch liposomes was assessed by quantifying the protein in the pellet fraction and therefore bound to the vesicles. The construct concentration varied from 1-4 µM whilst the liposome concentration was kept at 0.2 mg/ml.

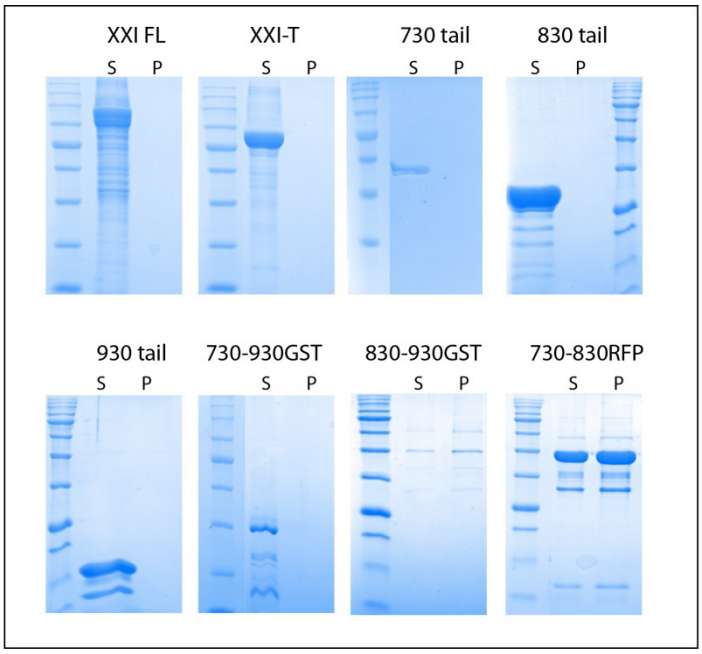

Figure 92: Control co-sedimentations of myosin XXI constructs. Full-length protein (123 kDa), Motor truncation XXI-T (95 kDa). Tail constructs: 730 tail (42 kDa), 830 tail (31 kDa), 930 tail, 730-930 tail (29 kDa). Controls were performed without the addition of liposomes.

Because the tails 730-830 and 830-930 also pelleted in the control co-sedimentations (figure 92), they were excluded from the lipid-affinity co-sedimentations.

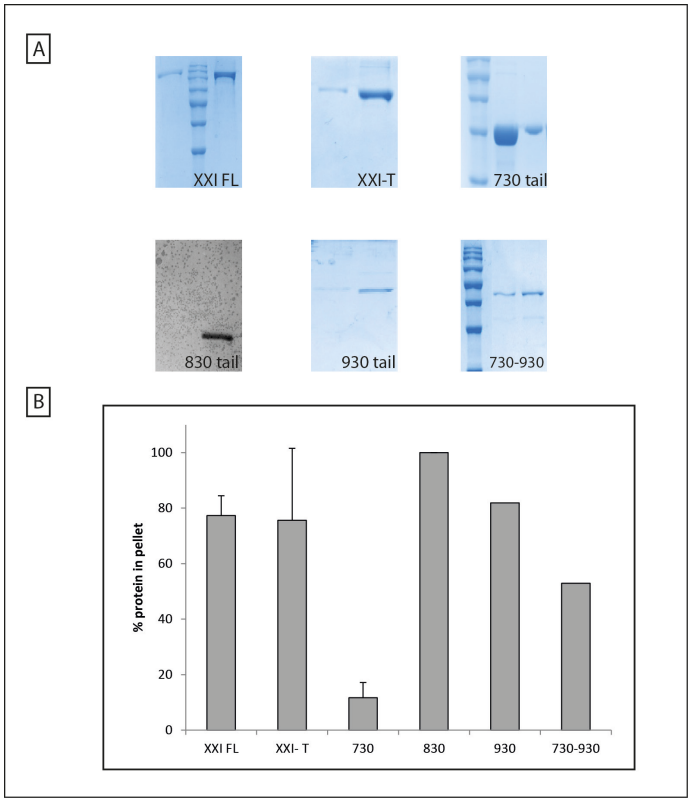

Figure 93: Co-sedimentations of myosin XXI constructs with folch liposomes. (A): Full-length protein (123 kDa), Motor truncation XXI-T (95 kDa). Tail constructs: 730 tail (42 kDa), 830 tail (31 kDa), 930 tail, 730-930 tail (29 kDa). The other tail constructs 730-830 and 830-930 pelleted without addition of liposomes and were therefore excluded from the assay (see control co-sedimentations figure 92). **(B):** Densitometry of the above co-sedimentations. Error bars represent standard deviation. Experiments were performed at least thrice. Given is the percentage of protein in the pellet fraction. The intensity of the construct band was divided by the total intensity (pellet+supernatant) for each sample to determine the percentage of protein in the pellet.

All tested constructs bound to folch liposomes. All other constructs bound to more than 50% of the offered liposomes. Only the longest tail (730 tail) bound to only 11% (figure 93, B). The only tail binding completely to the liposomes was the 830 tail.

3.5.2.1 Almost all myosin XXI constructs bind to folch on nitrocellulose

Following the protocol of Dowler *et al.* (2002), protein-lipid overlay assays were performed as described in chapter 2.3.5.

As figure 94 shows, almost all constructs bound to the presented folch on nitrocellulose. Only the 730 tail construct ranging from amino acids 730 to 1051 did not bind to the lipids although it bound to liposomes of the same composition. The RFP 730-830 and RFP 830-930 tail gave a very low signal, which indicated weak binding. For both tail constructs it looked as if there might be a concentration dependent binding with

stronger signal on the highest concentrated lipid spot and weakest signal on the lower lipid concentrations.

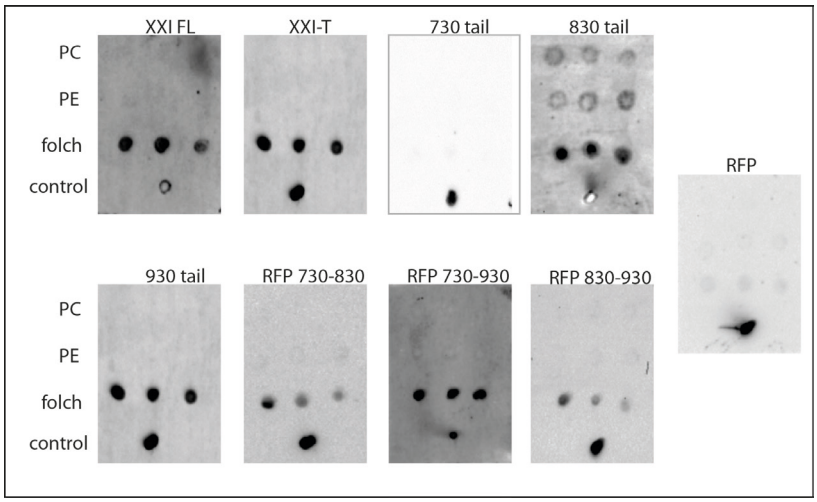

Figure 94: PLO blots for all myosin XXI constructs. First row on each blot: pure PC in different amounts (from left to right: 500 pmol, 350 pmol and 200 pmol). Second row: pure PE, third row: folch. The control consisted of the respective target protein as check for antibody performance. A black dot indicates a positive reaction with the antibody and therefore binding of the protein construct to the particular lipid/ lipid-mix. All blots performed two to three times.

None of the constructs interacted with the control lipids PC and PE. Since the RFP-tagged constructs were not available as untagged versions at the time of the assays, a test blot with pure RFP was performed as well, which did not bind to lipids (figure 94).

3.5.2.2 Myosin XXI tail constructs reveal only marginal membrane lipid binding-affinities

Since almost all constructs were capable of interacting with nitrocellulose-bound mixed lipids (i.e. folch) (figure 94), a more detailed view of membrane lipid binding-affinities in this protein was to be obtained. As figure 95 shows, myosin XXI bound to a limited number of membrane components. Strikingly, as with myosin VI, all of the interacting lipids were negatively charged.

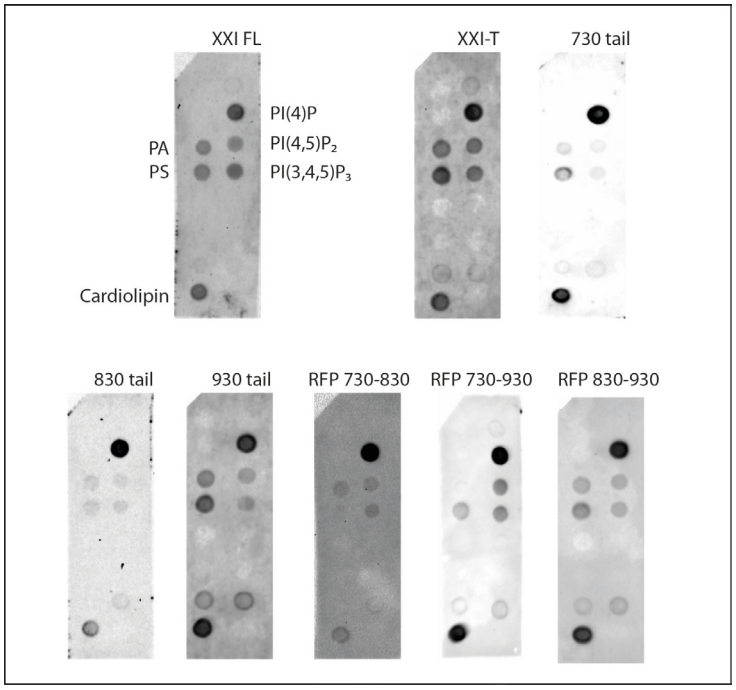

Figure 95: Membrane Lipid Strips® for myosin XXI constructs. A black dot indicates a positive reaction with the antibody and thus binding of the protein to the particular lipid. All experiments were at least performed twice. Lipids where reactions could be detected are indicated, for full layout of strips, see chapter 2.3.6.

Between the FL construct and the tails no obvious change in binding-affinity could be detected. Only binding to Cardiolipin was slightly weaker in the 830 and the RFP730-830 tail. The interaction with PA and PS was very weak throughout the tail constructs and the RFP730-930 tail did not interact with PA at all.

3.5.2.3 Myosin XXI constructs show only slight differences in Phosphatidylinositol (PIP) binding

An even more detailed look into lipid binding affinities was performed using PIP Strips® as PLO substrates. It was seen that only a range of lipids was bound to by myosin XXI constructs and that a variability of binding affinities was observable.

The FL construct bound to the three mono-phosphates PI(3)P, PI(4)P and PI(5)P as well as the di-phosphate $PI(3,5)P_2$ and the tri-phosphate $PI(3,4,5)P_3$. Additionally binding to the di-phosphates $PI(4,5)P_2$ and $PI(3,4)P_2$ was detectable. Interaction with the phospholipids PA and PS was only seen in the tail constructs whereas the full-length protein did not interact. Binding to PS was pronounced only in the 830 tail construct, whereas it was more or less weak in all other tails (figure 96, blue circle).

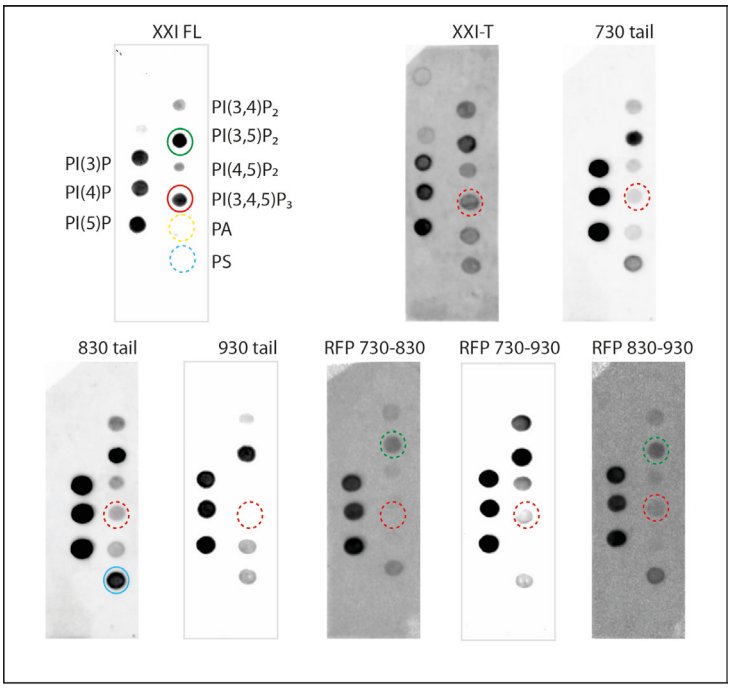

Figure 96: PIP Strips® for myosin XXI constructs. A black dot indicates a positive reaction with the antibody and thus binding of the protein to the particular lipid. All experiments were at least performed twice. Lipids where reactions could be detected are indicated, for full layout of strips, see chapter 2.3.6.

Binding to the three mono-phosphates was retained throughout the constructs and thus along the whole tail. Binding to $PI(3,5)P_2$ was altered towards weaker interaction only in the tail constructs 730-930 (figure 95, green circle) and 830-930 (figure 96, green circle). A larger effect was seen on binding to $PI(3,4,5)P_3$, which was strong with the full-length myosin XXI, weaker with the truncation and almost non-existent throughout the tail (figure 96, red circle). Therefore it can be summarised that binding to triphosphates was found only N-terminally of amino acid 830.

3.5.2.4 Sequence analysis

Since a BH plot (see chapter 5.1.1.1) showed one possible lipid binding site (figure 97), additionally to the experiments for lipid binding, a detailed search for known membrane interacting sequence motifs in the myosin XXI sequence was performed. A perfectly spaced Phox-Homology (PX) consensus sequence [R (Y/F) x_{23-30} K x_{13-23} R] (Teasdale and Collins 2012) was found in the converter domain. This domain type is a protein-lipid interaction motif which is thought to form an electro-positive patch to bind to negatively charged phosphate groups of phosphoinositides (Kurten *et al.* 2001) (see appendix 5.8).

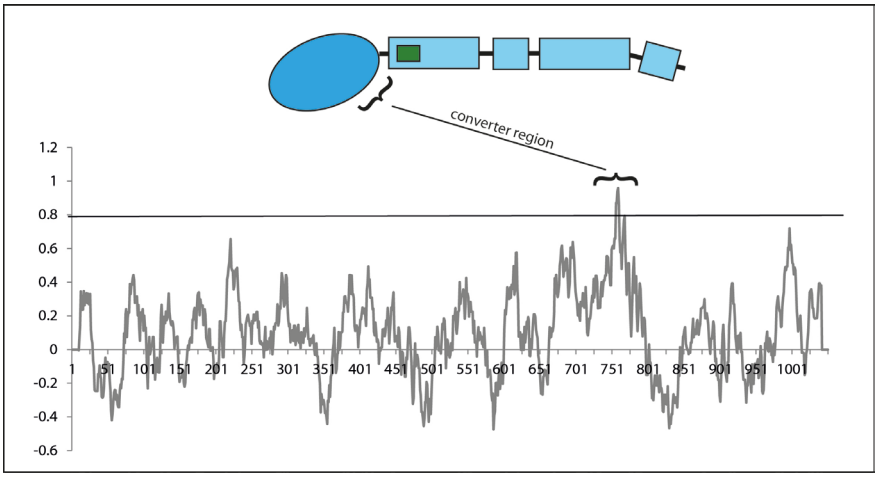

Figure 97: BH plot of myosin XXI FL protein. Threshold given at 0.8, running window size was 19. A detailed explanation is given in chapter 3.3.1.1. Cartoon depicts FL myosin protein. One possible membrane-binding region is indicated in the converter region. BH-plot was performed on http://helixweb.nih.gov/bhsearch/

3.5.3 Phox-homology (PX) domain in the myosin XXI converter domain

3.5.3.1 Site-directed mutagenesis of PX-domain mutant

To prove the actual functionality of this motif, a PX-domain mutant was designed and expressed. The resulting construct ranged from amino acid 600 to 758 (see figure 98) and had two amino acids exchanged. The initial RY of the PX-motif was exchanged into LS in a two-step site-directed mutagenesis (see chapter 2.1.12). From CGG (R) to CTG (L) only one single base-exchange had to be performed, same as for TAC (Y) to TCC (S). The exchange of a strongly bound G to a weaker bound T (and a weaker bound A to stronger bound C) ensured additionally the reduction of reading errors of the DNA-Polymerase during PCR reactions. Additionally amino acids with different characteristics were chosen to guarantee a diverging behaviour.

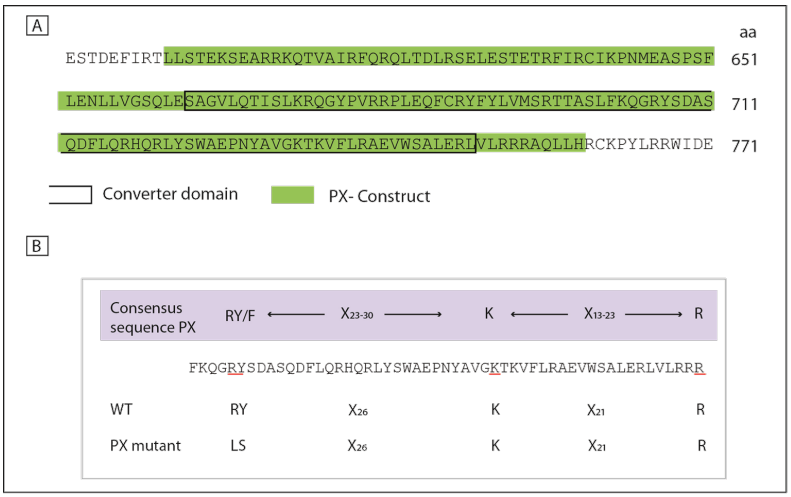

Figure 98: Amino acid sequence of myosin XXI converter domain and site-directed mutagenesis PX-mutant. (A): amino acid sequence of the construct comprising the converter domain and parts of the motor (aa 600-758, green) with flanking amino acids. **(B)**: PX-domain official consensus sequence (Teasdale and Collins 2012), myosin XXI wild-type (WT) sequence and generated PX-mutant.

Since different types of PX domains specifically bind PI(3)P, PI(3,4)P_2, PI(4,5)P_2, PS and/or PA it was necessary to perform protein-lipid overlay assays with PIP Strips® in order to see a difference in the behaviour between the wild-type and the mutant construct (see section 2.3.6).

The wild-type (WT) not only bound PI(3)P, which is a PX-domain specific monophosphate, but PI(4)P and PI(5)P as well as the diphosphate PI(3,5)P_2 (see figure 99).

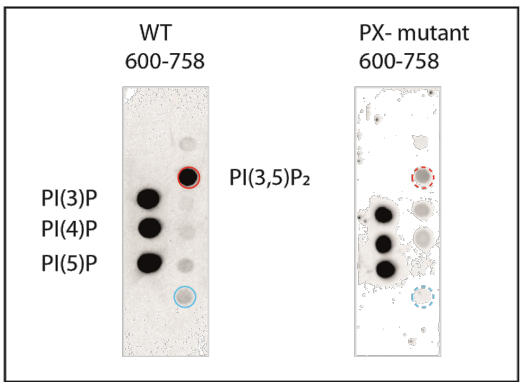

Figure 99: PIP Strip® for myosin XXI PX-mutant construct. A black dot indicates a positive reaction with the antibody and thus binding of the protein to the particular lipid. Experiments were at least performed twice. Lipids where reactions could be detected are indicated, for full layout of strips, see chapter 2.3.6.

A very weak interaction for other anionic lipids such as phosphatidylserine (PS, figure 99, blue circle) was found as well. The interaction with PI(3,5)P_2 (figure 99, red circle) disappeared almost entirely in the mutant construct, whilst binding to the

monophosphates was retained. The weak interaction with PS, as seen in the WT construct was not detectable in the PX-mutant. This strongly supported the idea that the PX domain in the converter is involved in lipid binding.

The sequence of the converter domain of a scallop muscle myosin II was replaced with the sequence of the *L. donovani* converter (see figure 100) and found that the amino acids of the PX domain form a patch on the surface of the converter domain consistent with these residues interacting with membranes without interfering with the general structure and function of the converter of this myosin motor (Batters *et al.* 2014).

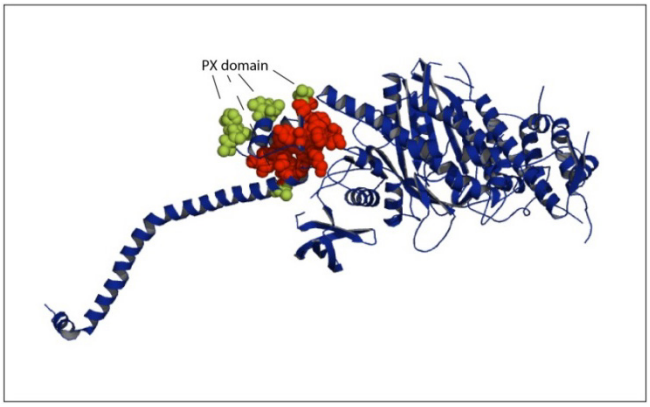

Figure 100: Crystal structure of scallop muscle myosin II. The sequence in the converter domain was replaced by the sequence of *L. donovani*. The amino acids specific to the PX domain (green) form a patch on the surface of the converter (red).

3.5.4 Myosin XXI dimerisation and phospholipid-binding domains overlap

In size exclusion chromatography (SEC) studies, it was shown that the distal 800-, 830- and 930-tail constructs were monomeric (Batters *et al.* 2014), but that all tail constructs, with exception of 830-930 tail, adopted mixed monomeric and dimeric populations in the presence of an N-terminal RFP tag (figure 101).

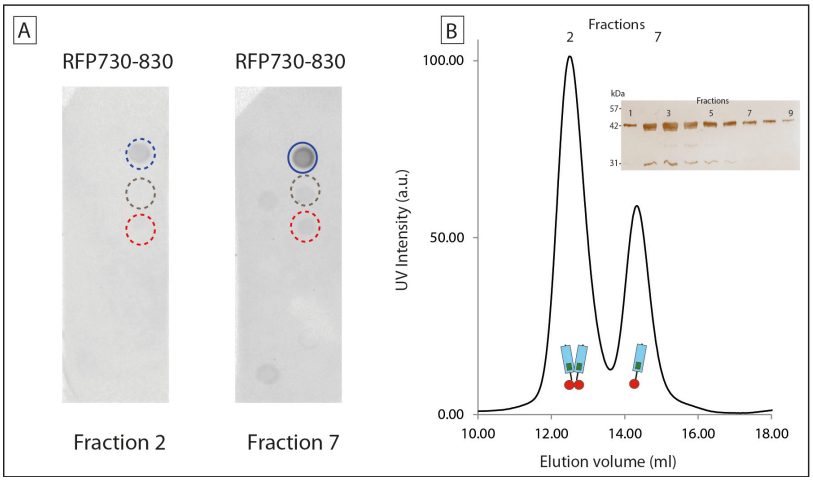

Figure 101: Lipid binding and dimerisation of myosin XXI tails are mutually exclusive. Membrane strips of RFP 730-830 tail fractions from SEC experiments. **(A):** PIP Strips of fractions 2 and 7 in comparison. Blue circle indicates binding to PI(4)P by fraction 7. **(B):** SEC curve of RFP 730-830 tail shows mixture of dimeric (fraction 2) and dimeric (fraction 7) conformation. Inset: silver-stained SDS PAGE of the obtained fractions from the SEC run, which shows that all fractions contain the same protein.

Comparing the phospholipid binding of a monomeric and a dimeric fraction of the RFP 730-830 tail construct revealed that the monomeric form of the RFP 730-830 (see figure 101, fraction 7) bound to the phospholipid PI(4)P whereas the formed dimer of this tail (figure 101, fraction 2) did not bind to it.

3.5.5 Myosin XXI shows higher gliding-velocity and functional affinity for lipid surfaces in *in vitro* motility assays

After the examination of lipid-binding propensities in the myosin XXI protein, it was interesting to see whether a lipid substrate would alter myosin XXI motility in a similar way than it did for the myosin VI. This study was focussed only on motility on folch surfaces. These were prepared as described for myosin VI in chapter 3.3.11.

Myosin XXI showed relatively slow motility when directly attached to nitrocellulose surfaces (figure 102) with velocities around 18 nm/s. Interestingly, velocity was about four times higher (66 nm/s) when the motor was bound to immobile folch membranes (figure 102) (Batters *et al.* 2014). Velocities were measured by tracking of actin filaments from 10 s-time-lapse movies by hand.

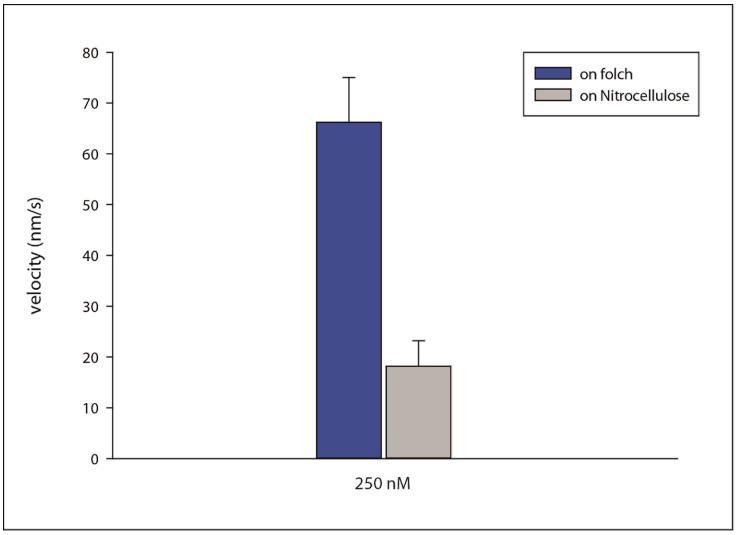

Figure 102: Bar chart for two different motility assay substrates with myosin XXI at a motor concentration of 250 nM. Error bars show standard deviation; ($p \leq 0.001$). (n = 653 filaments).

According to figure 103 two major effects were noticed. First, the velocities for the two substrates were, as described for figure 102, significantly different ($p \leq 0.001$). The highest velocity for motors on folch surfaces was 66 nm/s (± 8.8 nm/s) at a motor concentration of 12 nM. In contrast, the highest velocity on nitrocellulose was 18 nm/s (± 5 nm/s) at motor concentrations from 170 to 250 nM.

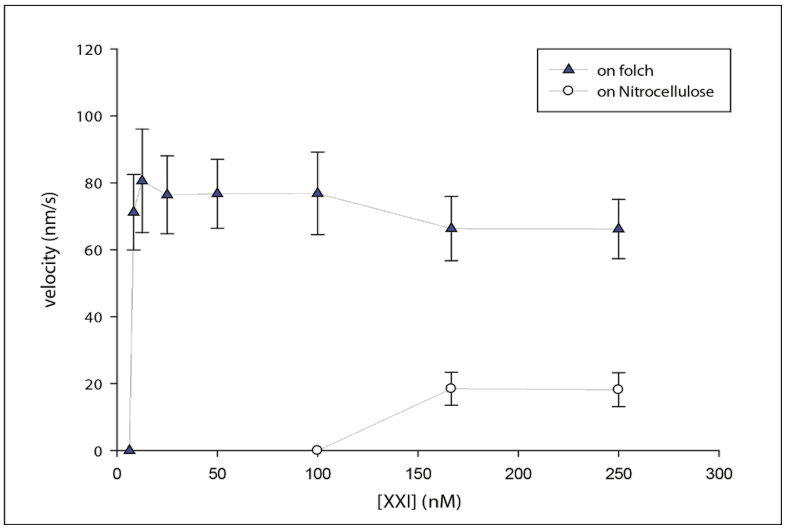

Figure 103: Graph for two different motility assay substrates with myosin XXI at different motor concentrations. Error bars show standard deviation. (n = 653 filaments)

The second effect was that the necessary motor density for uninterrupted filament motility was much lower on folch surfaces than on nitrocellulose surfaces. Motility on nitrocellulose ceased at a concentration of 160 nM whilst smooth motility on folch was obtainable down to a concentration of 8 nM, which equalled a 20-fold reduction.

3.5.6 Discussion

Lipid binding was found along the entire tail of myosin XXI including the converter domain in the neck of this motor. Therefore it can be said that in myosin XXI the predicted coiled-coil regions overlap with lipid binding regions and thus dimerisation and lipid binding might be influenced or regulated by each other. In a recent study connected to this thesis (Batters *et al.* 2014) we found that dimerisation and lipid binding were mutually exclusive. Size exclusion chromatography of the 730-830 tail revealed that this motor seemed to be able to adopt dimeric and monomeric states. The dimer could possibly play a role in the cytosol since it did not bind to lipids. The monomer on the other hand bound lipids and lipid binding along the neck and tail might target this fraction to specific membrane compartments. As found with myosin VI, most of the membrane binding of myosin XXI was not mediated in a stereospecific way but relied on unspecific electrostatic interactions to various phospholipids. The newly described PX domain in the converter region was not highly specific for PI(3)P, as they reportedly are (Lemmon 2008), but bound to all three monophosphates, PI(3,5)P_2 and PS. In the mutant construct binding to the latter two was completely abolished. The higher velocity and better motility of myosin XXI on lipid surfaces might be the result of an improved configuration of the motor on the surface.

General Discussion

4.1 Myosin VI back folds its tail to change into an inactive conformation

The inability of the full-length myosin VI to dimerise spontaneously even though it has a predicted coiled-coil structure with a high score in its C-terminal tail, brought forth a model that predicted the myosin VI tail folds back onto itself (Spink *et al.* 2008, Spudich and Sivaramakrishnan 2010). In this study it was possible to show that the entire tail folds back onto itself and also which regions interact with each other (Chapter 3.2). The 814 tail showed low binding to lipid vesicles and no interaction with the motor truncation constructs. This is because the tail is folded back and thus inactive. The 1060 tail was shown to interact with the calmodulin bound to the IQ-motifs one and two but not to the free IQ-motif peptides. This interaction was disrupted by the addition of calcium. Taken together this points to a regulative mechanism that a bound calmodulin is needed for the back folding, and that as soon as this calmodulin changes its conformation into the holo-state upon calcium binding it disrupts the interaction of the C-terminal tail and the neck. Yet, no unfolding events of the tail were measured in any assay upon the change of the calcium concentration. This might be due to the fact that the folding back of the tail is not an exclusive interaction between the calmodulin and the first 65 amino acids of the cargo-binding domain but electrostatic interactions along the entire tail (figure 104).

4.2 Myosin VI interacts directly with membrane lipids

Lipid binding in myosin VI is not restricted to formerly described binding sites in the cargo-binding domain and lever arm extension (Spudich *et al.* 2007, Yu *et al.* 2012) but is present along the entire tail (Chapter 3.3) which could be deduced from the differences in binding patterns of the different tail constructs. The phosphatidylinositolphosphates PI(4)P, PI(3,5)P_2 and PI(4,5)P_2, when presented as vesicles, were bound to by all constructs apart from the 1060 and 1125 tail which only bound to PI(3,5)P_2. On the protein-lipid-overlay blots all constructs bound to PI(3)P, PI(4)P, PI(5)P, PI(3,5)P_2 and only weakly to PI(4,5)P_2. As mentioned before, the cargo-binding domain constructs 1060 and 1125 tail did not interact with PI(4)P and PI(4,5)P_2 in vesicles but they did on the nitrocellulose strips (table 6).

	vesicles			PLO				
construct	PI(4)P	PI(4,5)P_2	PI(3,5)P_2	PI(3)P	PI(4)P	PI(5)P	PI(4,5)P_2	PI(3,5)P_2
VI FL								
Trunc814								
Trunc913								
814 tail	weak	weak	weak		weak			
913 tail								
h 1060 tail								
NCBD tail							weak	
1125 tail								
883 Δ PIP								
FL Δ PIP								
c 1060 tail								

Table 6: Lipid binding in myosin VI to vesicles and on Protein-lipid-overlay assays (PLOs). Green filled cells indicate binding, red no binding. A complete table with controls can be found in the appendix.

When bound to lipid surfaces in an *in vitro* motility assay myosin VI seemed to be favourably positioned on PI(4)P surfaces where the highest affinity and velocity was seen. Slightly weaker binding to PI(3,5)P_2 and PI(4,5)P_2 might result in a more instable positioning on the surface. Although most of the motors might be in a favourable position, those that are not may disrupt motility at higher concentrations accounting for the lower affinities. The 1125 tail did not bind to PI(4)P without calcium but bound in a calcium-supplemented buffer. Motility was, as said before, best on PI(4)P surfaces and a control with myosin VI BRS showed optimal C-terminal positioning and comparable velocities. Therefore one could argue that the myosin VI is, under low calcium conditions not 'standing on tip-toe' but binding to the surface with the entire CBD. This could change slightly with the change of calcium concentration and thus myosin VI would have the complete tail as lever arm for motility.

These findings lead to the following conclusions: (1) binding to lipids in the myosin VI tail might well be stereospecific in some places but relies on unspecific electrostatic interactions to various phospholipids in other places. (2) Binding to lipids on a surface varies from binding to lipids in a physiological vesicle conformation. This indicates that other binding mechanisms like curvature sensing (DiNitto *et al.* 2003, Hurley 2006, Lemmon 2008) and electrostatic sensing (Rizo and Sudhof 1998, Sutton and Sprang 1998) might play a role in the interaction of myosin VI to lipids as well. (3) The differences in velocity and affinity for different phospholipid surfaces point towards a possible explanation for the involvement and regulation of myosin VI in its diverse tasks

in the cell. The high affinity for PI(4)P might be due to a 'long-range' transport system between Golgi and ER with PI(4)P being the most important lipid in exocytosis not only as precursor for other PIPs but also for membrane targeting and activation of regulatory proteins (Johansen *et al.* 2012). This could explain the higher affinity of myosin VI for this lipid. The lower affinities for $PI(3,5)P_2$ and $PI(4,5)P_2$ might be connected to their occurrence in the cell as well. $PI(3,5)P_2$ for example is prevalent in the endosomal pathway in which myosin VI is only partly involved (e.g. early endosome transport). $PI(4,5)P_2$, being the major polyphosphoinositide in mammalian cells is enriched in the plasma membrane and is involved in exo- and endocytosis as well as membrane trafficking. Here, the interaction between myosin VI, which is involved in most of these processes, might not only be a direct one but could involve several regulatory binding partners (see next section).

4.3 Calcium as co-regulator of myosin VI back folding and lipid binding

Myosin VI's lipid binding seems to be regulated or at least co-regulated by calcium (Chapter 3.3.2). Under high calcium conditions the full-length protein bound to folch vesicles much better than without calcium. The 1125 tail did not bind to folch vesicles until calcium was added. The finding that the binding behaviour of the FL protein to the PIPs was differently influenced by calcium depending on whether the lipid was presented in a spherical vesicle or on nitrocellulose membranes, together with the findings of the formerly described influence of calcium onto the back folding of myosin VI, led to the idea that a much more complicated regulative mechanism than mere calcium regulation is involved in lipid binding. It is very likely that a whole range of effectors regulate myosin VI in the cell, therefore the analysis of binding partners is of interest. An important binding partner is the autophagy receptor NDP52 which binds directly to myosin VI via the RRL motif in the cargo-binding domain (Tumbarello *et al.* 2013) which is then specifically bound by Galectin-8 (Kim *et al.* 2013) which targets it to membranes (Thurston *et al.* 2012). Another example is the monomeric yeast myosin IV which builds a heterotrimer with the dimeric binding partner *She3p* which then recruits a mRNA zipcode and an additional partner *She2p* and this complex then binds to another myosin IV molecule to form a processive dimer.

This leads to the model where a multi-step regulatory mechanism with calcium unfolding the protein partially, thus exposing formerly hidden binding sites for binding partners or lipids which then starts a cascade during which myosin VI is bound to cargo and transports it to its destination (figure 104).

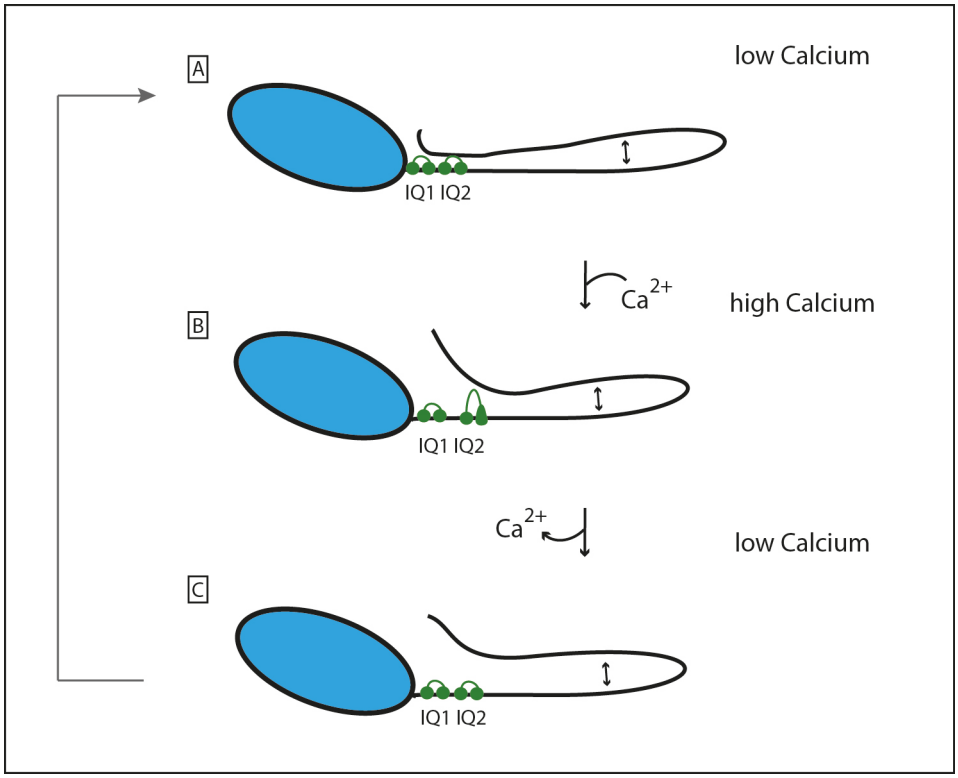

Figure 104: Possible folding of the C-terminal myosin VI tail onto the IQ-bound Calmodulins. (A): back folded, monomeric and mechanically inactive myosin VI, **(B):** with high calcium concentrations the tail partly unfolds and the lever arm may be destabilised. (**C**): active state of myosin VI. At low calcium concentration it may first unfold and thus bind to binding partners or cargo, can dimerise and is mechanically active when bound to cargo. If no binding to either cargo or binding partner occurs it goes back in the inactive state as seen in (**A**).

4.4 Myosin XXI binds lipids along the tail and has a specific PX-domain

Myosin XXI exhibits lipid binding along the entire tail, as seen with myosin VI (Chapter 3.5). Although it is the only expressed myosin in *Leishmania sp.* and must therefore be a multifunctional motor protein, it has a PI(3,5)P_2 specific phox-homology (PX) domain in the converter region in the neck of the motor. PI(3,5)P_2 is concentrated mainly in the late compartments of the endosomal pathway and plays important functions in multivesicular body sorting, endosomal dynamics and autophagy (Shaw *et al.* 2003). This might point towards the performance of very specific transport functions in the endosomal pathway

and autophagy. In *Leishmania*, two distinct myosin XXI populations were described, one motile cytosomal fraction and one immotile membrane bound fraction (Batters *et al.* 2014). Since this is a very newly described motor, not much is known about regulatory mechanisms and possible differences between these two populations. Considering the tail of myosin XXI, it comprises several coiled-coil regions, most of which bind lipids. In this study it was possible to show with SEC measurements, that lipid binding and dimerisation are mutually exclusive. Myosin XXI may, as myosin VI, be part of a very complicated and diverse regulatory system, including regulatory proteins, binding partners, ions and lipids.

4.5 Calmodulin exhibits lipid binding on its own

Calmodulin, the ubiquitous calcium sensor of eukaryotic cells binds to lipids (Chapter 3.4). This in itself is not a new finding (Kovacs *et al.* 2010), but in this present study it was shown that binding to lipids depends on the binding state of calmodulin to its target peptide. Calmodulin exclusively bound either protein or lipid. It was found to bind especially to 3-galactosylceramide (sulfatide), a descendant of sphingosyl-phosphorylcholine (SPC) in the sphingomyelin cycle which was already published by Kovacs *et al.* (2010). This binding persisted throughout IQ-peptide binding and therefore this points towards the possibility that calmodulin might have a specific binding site for spingomyelin and its derivates which could, upon binding to a target sequence still be exposed.

4.6 Conclusions

Both myosin VI and XXI were found to have the ability to bind to lipids at multiple sites along the entire length of the tail. This protein-lipid interaction was shown to be calcium dependent in myosin VI, suggesting that calcium regulates the tertiary structure of the protein and thus might play a pivotal role for the regulation of myosin VI in the cell. Despite having a large predicted coiled-coil region myosin VI did not show any dimerisation in this study. Using protein co-sedimentation experiments it was shown that the formerly proposed back folded state occurs due to an interaction between the first 65 amino acids of the C-terminal cargo-binding domain and the calmodulin bound to the IQ-motifs in the N-terminal neck region. As already known, the calcium-sensing protein calmodulin changes its conformation depending on whether it is in the calcium free (apo)- or the calcium bound (holo)-state. This led to the hypothesis that the backfolding of myosin VI could be regulated by the ability of the C-terminal tail of myosin VI to distinguish between these two conformations. Using Dot Far-western blots and tryptophan titrations experiments it was shown that this was the 'switch' for myosin VI to unfold.

Similar to myosin VI, lipid binding in myosin XXI occurs along the length of the entire tail, although with different affinities for different tested lipids. Myosin XXI is capable of dimerisation and it was shown that lipid binding and dimerisation are mutually exclusive. Additionally, a $PI(3,5)P_2$ sensitive PX (phox homology)-domain was found in the converter region of this motor which capacitates it to bind this lipid specifically.

4.7 Outlook

The effect on myosin VI binding to liposome cargoes and how this affects the dimerisation tendencies of myosin VI, with bound partner proteins, and in turn changes in the translocation abilities of vesicle cargo in *in vitro* assays are the major aspects of this work. In terms of cargo-binding, single-particle work with vesicle-laden myosin VI would be of interest to measure the actual strength of the direct binding to diverse lipids in contrast to binding to liposomes via cargo-adaptor proteins. This could either be done utilizing optical tweezers with an actin filament suspended between two polystyrene beads or magnetic tweezers where one end could be tethered to the glass surface by e.g.

polyethyleneglycol (PEG) or an antibody and the other on a magnetic bead. With these mechanical experiments it would be possible to actually measure a myosin VI carrying cargo on actin filaments and measure step-length, displacement and processivity. To assess how myosin VI carries its cargoes a motility assay with fascin-actin bundles on the surface could show if the motor does side-stepping movements and thus does possibly not need to dimerise.

Since binding partners play a pivotal role in the regulation of myosin VI, it is therefore of great interest to investigate the direct interaction between myosin VI and its diverse binding partners. Analytical ultracentrifugation (AUC) could be used to scrutinize these interactions in more detail. In this context the direct interactions of myosin VI with ubiquitin via its MIU (motif interacting with ubiquitin) in the C-terminal tail are of interest to investigate further roles in the autophagic process.
Live cell imaging with cells transfected with myosin VI can reveal not only where myosin VI is localised in the cell, as has been done before, but to see it moving along actin. Photo bleaching experiments could provide us with further insights as to how many myosin VI motors are bound to a vesicle and thus help to answer the question how myosin VI transports vesicles. Additionally, different point mutations and leucine-zippered constructs could help to show how and if myosin VI is dimerising.

Myosin XXI is a very intriguing motor since it seems to fulfil a multitude of tasks in *Leishmania*. Therefore further characterisation and localisation studies in living cells can yield new information about this newly described versatile motor. Its interactions with calmodulin-like (CaM-like) proteins need to be established further as well as its direct interaction with ubiquitin via its C-terminal ubiquitin-associated domain (UBA). These interactions can give better insight to myosin XXI's role in *Leishmania*. Its mechanical properties such as displacement, processivity and step-length should be measured according to other myosins to further characterise this motor protein.

If we gain an in-depth understanding of myosins, their transport and binding behaviour in cells, organelle-specific targeting of drugs and thus new ways of therapy will come into reach.

Appendices

5.1 Plasmids

pEt-28a (novagen®)

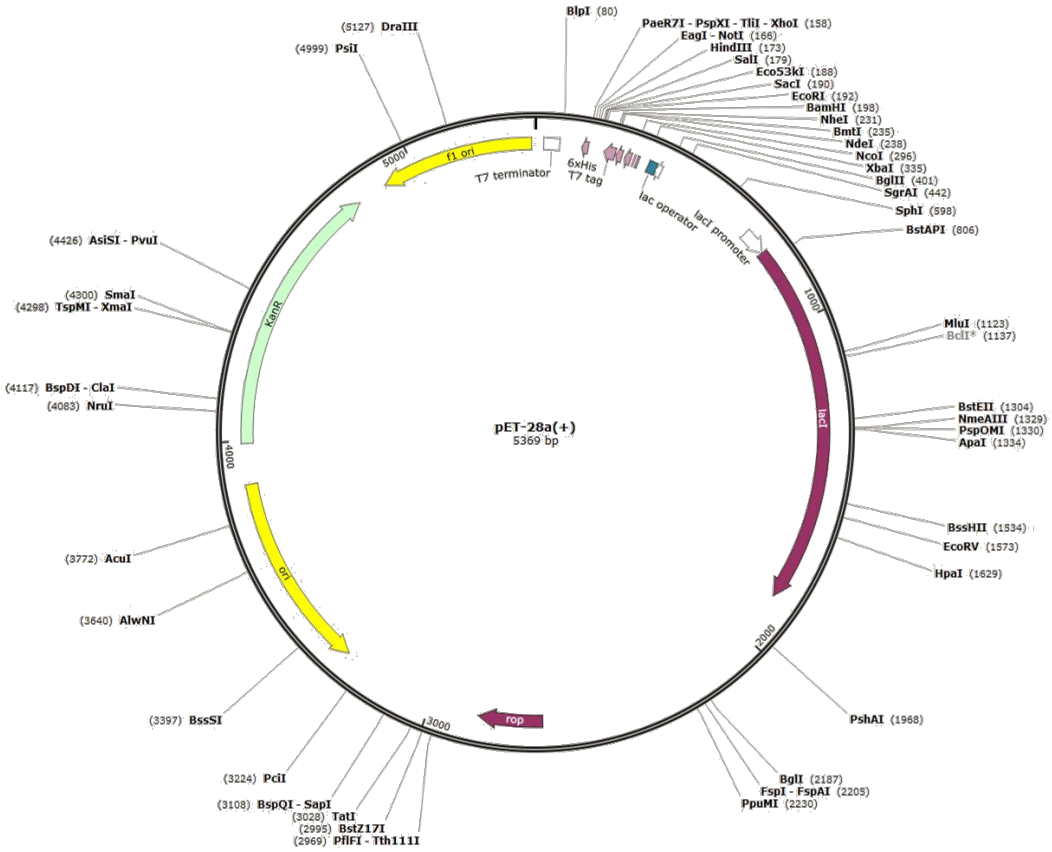

pGex 6P-1 (GE healthcare)

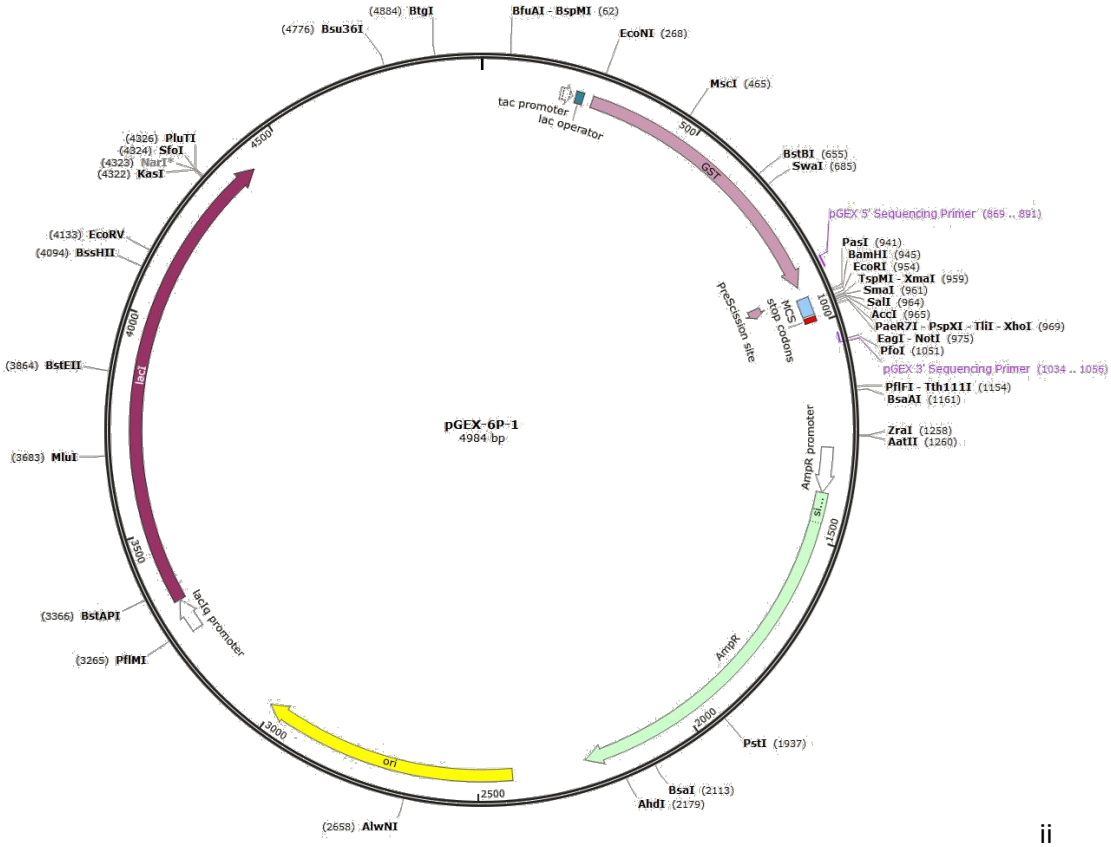

pFastBac HTB (Invitrogen®)

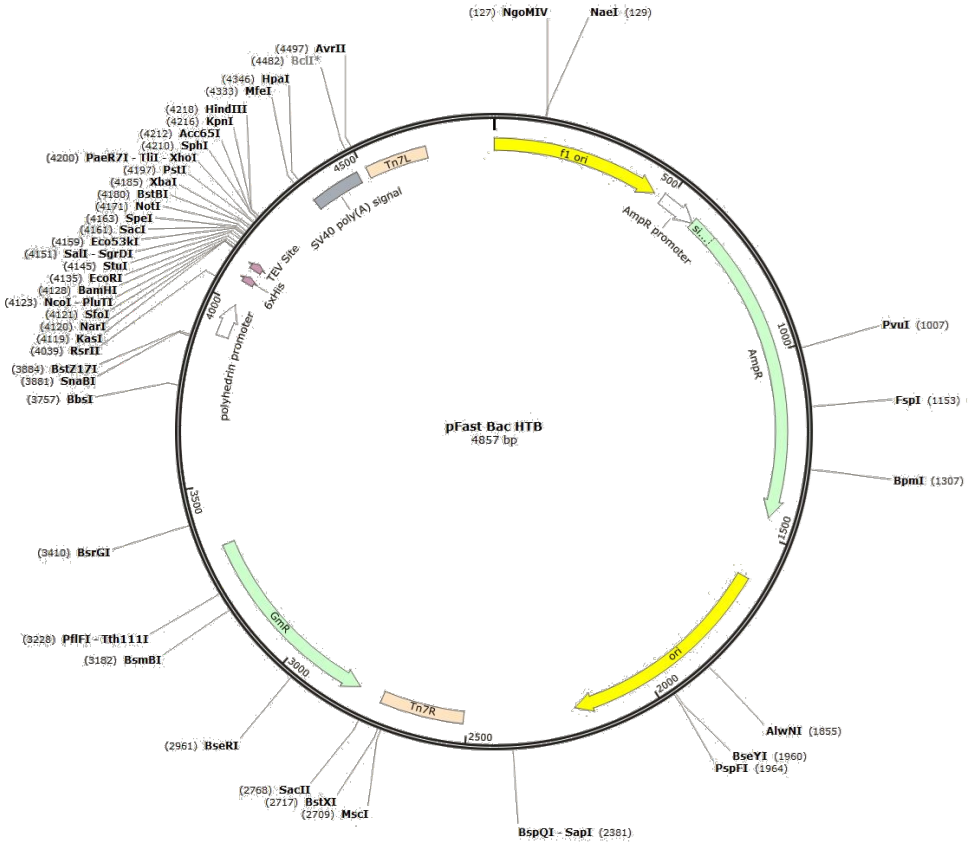

pFastBac 1 (Invitrogen®)

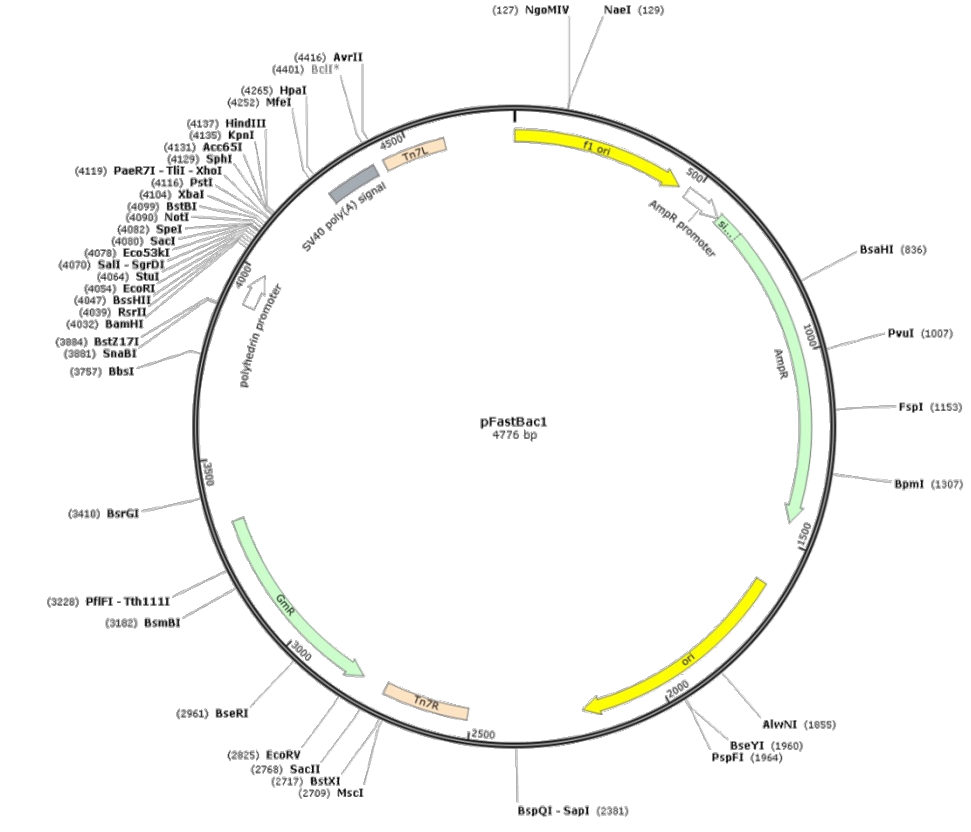

pColaDuet (Novagen)

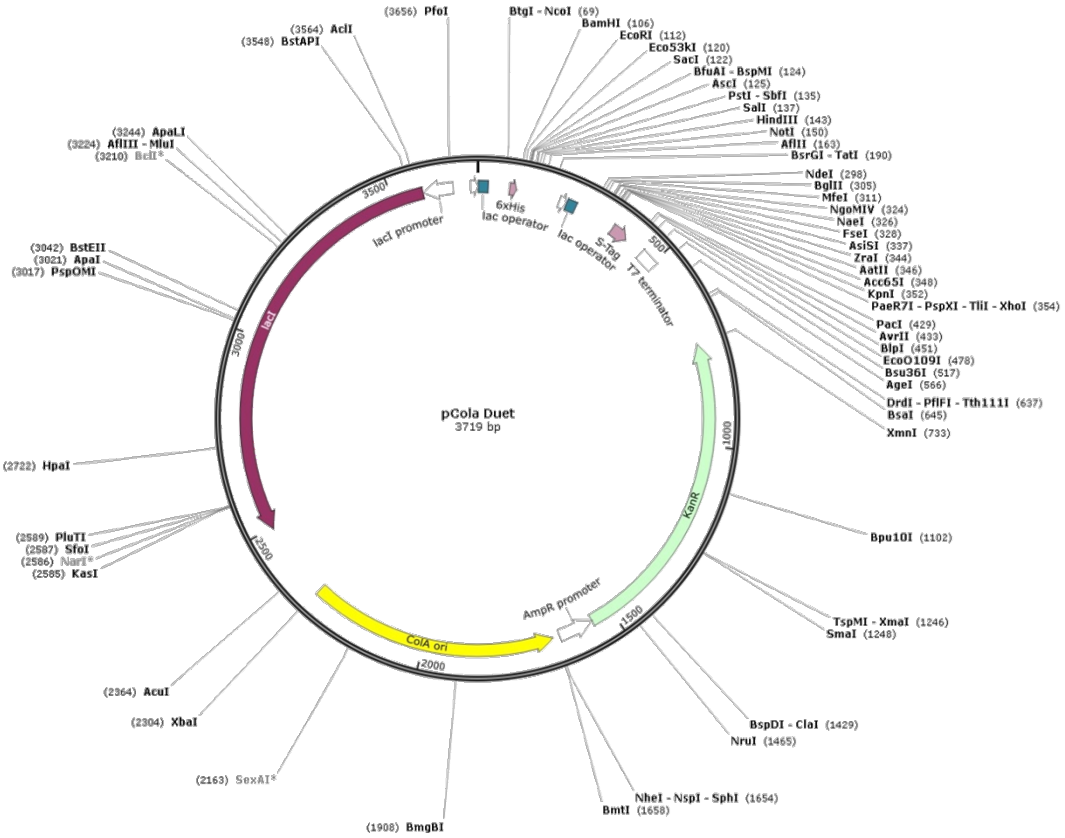

pAC4 (Avidity)

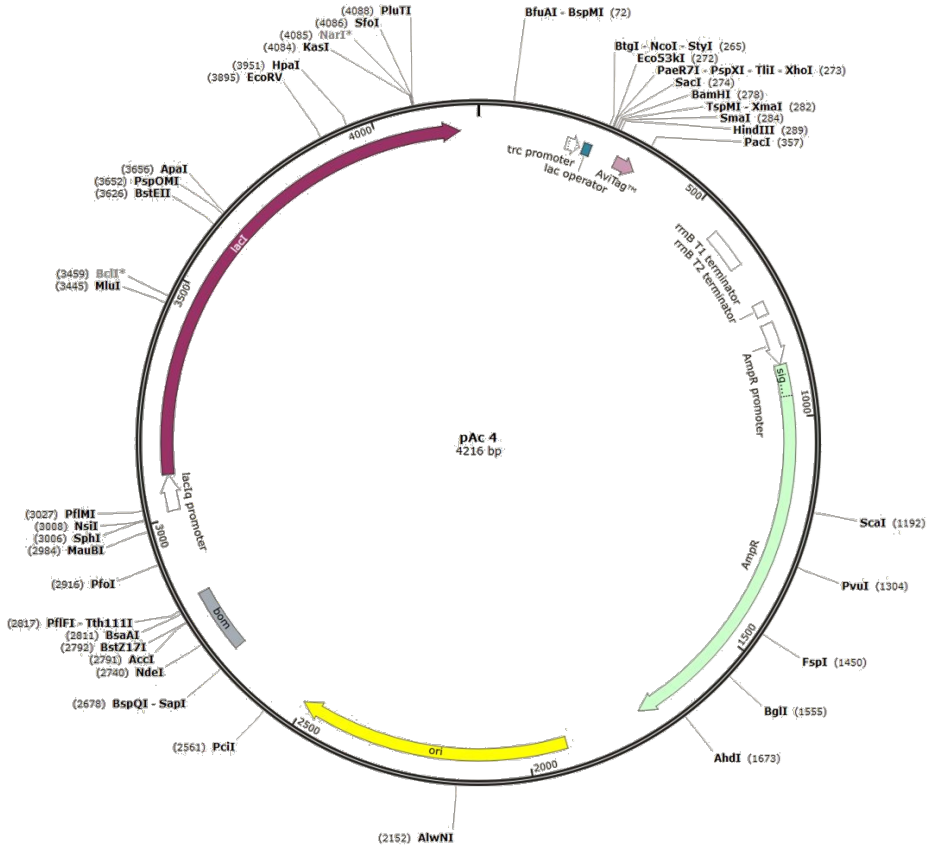

Champion pET SUMO (life technologies)

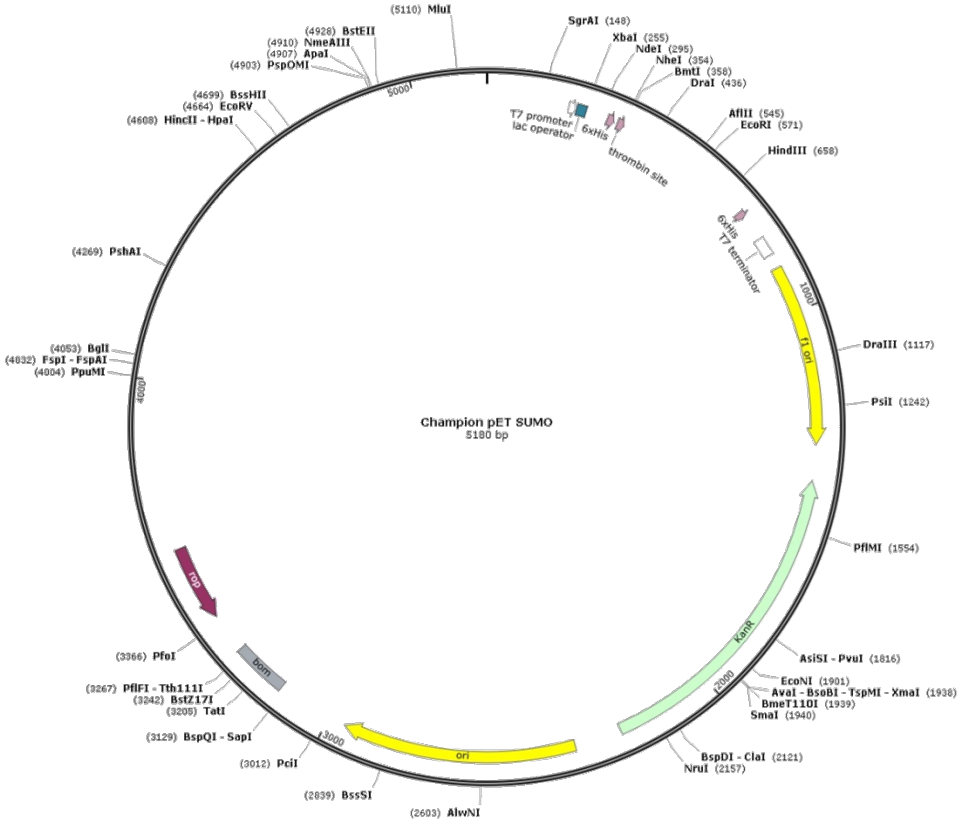

Figure 105: Vectormaps of plasmids used in this study. Vectormaps created with SnapGene software.

5.2 Oligonucleotides

5.2.1 Oligonucleotides Myosin VI

Internal Primer ID	Primer Sequence	Rest. site
	c FL VI	
Chick VI SalI F	AAAGTCGACAATGGAGGACGGGAAGCCCGTTTG	SalI
Chick VI XhoI RP	ACTCGAGCTATTTCAACAGGTTCTGCAGC	XhoI
	c FL Δ PIP	
	construct gift from F. Buss‘ lab.	
	c Trunc 814	
CVI Trunc814-SalI-FP	AAAAAAGTCGACAATGGAGGACGGGAAGCCCGTTTG	SalI
CVI Trunc814-XhoI-RP	AAAAAACTCGAGCTAGTATTTTGATGCAGGCACT	XhoI
	c Trunc 913	
Chick VI SalI F	AAAGTCGACAATGGAGGACGGGAAGCCCGTTTG	SalI
Chick_trun913_XhoI_R	ACTCGAGCTACCTCTTGCTGTTTTTTCTTTTG	XhoI
	c Trunc 1060	
Chick VI SalI F	AAAGTCGACAATGGAGGACGGGAAGCCCGTTTG	SalI
Chick_trun1060_XhoI_R	ACTCGAGCTAGTAGCTTGAACTGCAGGACC	XhoI
	h 814-1060	
NCB_NotI_For	AGAGGCGGCCGCATGGAAGCCTGCATTAAAATGC	NotI
NCB_XhoI_Rev	AAAAAACTCGAGCTAGGTGGCTAGTACAGCAGGACC	XhoI
	h 814	
CT814FPNOT1	AGAGGCGGCCGCCAGTGCCTGCATCAAAATAC	NotI
CTRPXHOI	ACTCGAGTTATTTCAACAGGTTCTGCAGC	XhoI
	h 913	
CT913FPNOTI	AGAGGCGGCCGCCCAAAAGAAAAAACAGCAAGAGG	NotI
CTRPXHOI	ACTCGAGTTATTTCAACAGGTTCTGCAGC	XhoI
	h 1060	
CT1060FPNOTI	AGAGGCGGCCGCCGGTCCTGCAGTTCAAGCTAC	NotI
CTRPXHOI	ACTCGAGTTATTTCAACAGGTTCTGCAGC	XhoI
	h 1060	
hVI-1060FPBamHI	AAAAAAGGATCCGCAGAACTACGTGATACC	BamHI
hVI-ENDRP-XhoI	ACTCGAGTTATTTCAACAGGTTCTGCAGC	XhoI
	c 1060	
CT1060FPNOTI	AGAGGCGGCCGCCGGTCCTGCAGTTCAAGCTAC	NotI
ChickenVI 1060-XhoI-	AAAAAACTCGAGCTAACCTCTAGACAACATTTCTGAC	XhoI
RP	ATTTCTTTGGCCATTT	
	h 1125	
Human_VI1125_NotI_F	AGAGGCGGCCGCATGACTGATTATCCTCAGCAAAAC	NotI
Human_VI1125_XhoI_R	ACTCGAGCTATTATTTCAACAGGTTCTGCAGC	XhoI
	h 883 Δ PIP	
Chick VI 883-NotIF	AGAGGCGGCCGCATGACCAAAATTAAGACTACG	NotI
CTRPXHOI	ACTCGAGTTATTTCAACAGGTTCTGCAGC	XhoI

5.2.1.1 Sequencing primers

primer ID	primer	vector
T7 pRSET-RPnew	TAATACGACTCACTATAGGG GGGTTATGCTAGTTATTGC	pET28
pGex5-FP pGex3-RP	AACGTATTGAAGCTATCCC TCAAGAATTATACACTCCG	pGex
pBakPac-FP pEGFP_C2-RP	TAAAATGATAACCATCTCGC TTTAAAGCAAGTAAAACCTC	pFastBac

Table 7: List of oligonucleotides used for myosin VI constructs design. All primers procured from Sigma.

5.2.2 Oligonucleotides myosin XXI

Primer ID	Primer Sequence	Rest. site
XXIFP6BamHI XXIRP4	FL XXI AGGATCCATGCCGGAGCGTGTGTCTGTG AAAAGCGGCCGCCTAGCTCACCTTGAACAGCATCTTAACGG	BamHI NotI
XXIFP6BamHI MYOXXTR6	1-800 AGGATCCATGCCGGAGCGTGTGTCTGTG AAAAGCGGCCGCCTATTTCTCCGCCGGCACACC	BamHI NotI
XXI730FP-MAM XXI-ENDRP-MAM	730 GGGAAGCTTGGCAAGACGAAGGTGTTCCTCC AAAAAAGGATCCCTAGCTCACCTTGAACAGC	HindIII BamHI
XXI800FPNONF XXI-ENDRP-MAM	800 GGGAAGCTTTAGACGCCGCCAATGGTGTGC AAAAAAGGATCCCTAGCTCACCTTGAACAGC	HindIII BamHI
XXI830FP-MAM XXI-ENDRP-MAM	830 GGGAAGCTTGCCGTCGAGGCGGACACGCGCG AAAAAAGGATCCCTAGCTCACCTTGAACAGC	HindIII BamHI
XXI930FP-MAM XXI-ENDRP-MAM	930 GGGAAGCTTGGCACGGACAGCGAATATGCC AAAAAAGGATCCCTAGCTCACCTTGAACAGC	HindIII BamHI
XXI730FP-MAM XXI830RP-MAM	730-836 GGGAAGCTTGGCAAGACGAAGGTGTTCCTCC AAAAAAGGATCCCTAGCGCGTGTCCGCCTCGACGGC	HindIII BamHI
XXI830FP-MAM	830-930 GGGAAGCTTGCCGTCGAGGCGGACACGCGCG AAAAAAGGATCCCTAGGCATATTCGCTGTCCGTGCC	HindIII BamHI

XXI930RP-MAM		
XXI730FP-MAM XXI930RP-MAM	730-930 GGGAAGCTTGGCAAGACGAAGGTGTTCCTCC AAAAAAGGATCCCTAGGCATATTCGCTGTCCGTGCC	HindIII BamHI
XXI-658-SUMO-FP XXI-760-RP-SUMO	SUMO 650-758 TACTTCCAATCCAATGCATCGCAGCTTGAGTCCGCTGG TTATCCACTTCCAATGTTATTAGCAGCGGTGCAGCAGCTGCGC GCGGCGACGAA	SspI
XXI-600-SUMO-FP XXI-760-RP-SUMO	SUMO 600-758 (PX mutant) TACTTCCAATCCAATGCATCTCTCGACGGAGAAGAGCGAGGCA CGCCGCAAGCAGA TTATCCACTTCCAATGTTATTAGCAGCGGTGCAGCAGCTGCGC GCGGCGACGAA	SspI

Table 8: List of oligonucleotides used for myosin XXI construct design in this study. All primers procured from Sigma.

5.3 Sequences Myosin VI

5.3.1 Myosin VI (NI)

Sequence obtained by sequencing the pFastBacHTB_EGFP_MyosinVI_NI_hum

ATGGAGGATGGAAAGCCCGTTTGGGCGCCACACCCTACAGATGGATTTCAGATGGGCAAT
ATTGTGGATATTGGCCCCGACAGCTTAACAATTGAACCCTTGAATCAGAAAGGCAAGACA
TTTTTGGCTCTCATAAACCAAGTGTTTCCTGCAGAAGAGGACAGTAAAAAAGATGTGGAA
GATAACTGTTCACTAATGTATTTAAATGAAGCCACACTGCTCCATAATATCAAAGTTCGA
TATAGTAAAGACAGAATTTATACATATGTCGCCAACATTCTGATTGCAGTGAATCCATAC
TTTGACATACCTAAAATATATTCTTCAGAAGCAATAAAGTCATATCAAGGAAAATCTCTT
GGGACAAGACCACCTCATGTCTTTGCAATTGCTGATAAAGCTTTTCGAGACATGAAGGTG
CTCAAGATGAGTCAGTCTATCATTGTATCTGGAGAATCAGGAGCCGGCAAAACAGAAAAT
ACAAAATTTGTTCTAAGATACCTGACTGAATCCTATGGAACAGGTCAAGATATTGATGAC
AGAATTGTTGAAGCTAACCCACTCCTAGAAGCCTTTGGAAATGCGAAGACTGTTCGCAAC
AATAATAGCAGTCGATTTGGGAAATTTGTAGAAATACATTTTAATGAAAAGAGCTCAGTT
GTTGGAGGATTTGTTTCACATTATCTCCTAGAGAAATCTAGGATCTGTGTTCAAGGCAAA
GAGGAAAGAAATTATCATATCTTTTATAGGTTGTGTGCTGGTGCTTCTGAAGATATTAGA
GAAAAACTTCATTTGAGTTCACCAGATAATTTTCGGTATTTAAACCGAGGCTGCACTAGA
TACTTTGCTAACAAAGAAACTGACAAACAGATTTTACAGAACCGCAAAAGTCCTGAGTAC
CTTAAGGCAGGTTCTATGAAAGATCCTCTGCTAGATGACCATGGTGATTTTATTAGAATG
TGCACGGCTATGAAAAAAATTGGTTTGGATGATGAAGAAAAGCTTGATCTCTTCCGGGTA
GTAGCTGGCGTCCTGCACCTTGGAAATATTGATTTTGAGGAAGCTGGCAGCACTTCAGGT
GGTTGTAATCTGAAGAATAAATCTGCTCAGTCTTTGGAATATTGTGCTGAATTACTGGGT
TTGGACCAAGATGATCTTCGAGTAAGTTTGACCACAAGAGTCATGCTAACAACAGCAGGG
GGCACCAAAGGAACAGTTATAAAGGTACCTCTGAAAGTGGAGCAAGCAAACAATGCTCGT
GATGCCCTGGCAAAGACAGTGTATAGCCATCTTTTTGATCATGTGGTAAACAGAGTAAAT
CAGTGTTTTCCTTTTGAAACATCATCCTATTTTATTGGAGTCCTAGATATTGCTGGTTTT
GAGTACTTTGAGCATAACAGTTTTGAACAATTTTGCATCAACTATTGCAATGAAAAACTT
CAACAATTTTTTAATGAAAGGATTCTGAAGGAGGAACAAGAACTCTATCAAAAAGAAGGT
TTAGGTGTTAATGAAGTGCATTATGTGGATAATCAGGACTGTATAGATTTAATTGAAGCC
AAATTAGTGGGAATACTGGATATTTTGGATGAAGAAAATCGCCTTCCCCAGCCAAGTGAT
CAACACTTTACATCTGCAGTTCACCAAAAGCACAAGGATCATTTTCGACTCACTATTCCC
AGAAAATCTAAGCTGGCAGTTCATAGGAATATCAGAGACGACGAAGGCTTCATTATCAGG
CATTTTGCGGGGGCAGTGTGCTATGAAACAACCCAGTTTGTGGAGAAAAATAATGATGCT
TTACATATGTCTCTTGAATCCTTAATATGTGAATCCAGAGATAAGTTTATACGGGAATTA
TTTGAATCATCCACAAATAACAACAAAGATACTAAACAAAAAGCAGGAAAACTTAGCTTC
ATCAGCGTGGGAAACAAGTTTAAGACACAGTTAAATTTGCTTCTGGATAAACTTCGAAGT
ACTGGAGCAAGCTTTATTCGTTGCATCAAACCTAACTTAAAGATGACAAGCCACCACTTT
GAAGGTGCTCAAATTCTGTCTCAGCTTCAGTGTTCAGGGATGGTGTCTGTTTTGGACTTG
ATGCAGGGTGGTTACCCATCACGAGCTTCATTTCATGAACTCTACAACATGTACAAAAAG
TATATGCCAGATAAACTTGCAAGATTGGATCCAAGACTATTTTGTAAGGCTTTGTTTAAA
GCTTTGGGCTTAAATGAAAATGACTACAAGTTTGGGTTAACCAAAGTATTTTTTAGACCT
GGCAAGTTTGCAGAATTTGATCAGATCATGAAGTCTGACCCTGACCACTTAGCAGAGTTG
GTTAAAAGAGTCAATCACTGGCTCACATGCAGTCGCTGGAAGAAAGTTCAGTGGTGCTCA
CTCTCAGTCATCAAATTGAAAAACAAAATAAAATATCGAGCTGAAGCCTGCATTAAAATG
CAAAAAACTATTCGAATGTGGCTTTGCAAGAGGAGACACAAACCTCGCATTGATGGTCTG
GTTAAGGTGGGCACACTGAAAAAACGACTTGATAAATTTAATGAGGTAGTCAGTGTGTTG
AAAGATGGAAAACCCGAGATGAATAAACAGATCAAGAATCTGGAAATTTCTATTGATACT

TTGATGGCCAAAATTAAGTCCACTATGATGACGCAGGAACAAATCCAGAAAGAATATGAT
GCACTGGTTAAAAGCTCAGAGGAACTCCTCAGTGCATTACAGAAAAAAAAACAGCAGGAA
GAGGAAGCAGAAAGGCTGAGGCGTATTCAAGAAGAAATGGAAAAGGAAAGAAAAAGACGT
GAAGAAGACGAAAAACGTCGAAGAAAGGAAGAGGAGGAAAGGCGGATGAAACTTGAGATG
GAAGCAAAGAGAAAACAAGAAGAAGAAGAGAGAAAGAAAAGGGAAGATGATGAAAAACGC
ATTCAAGCTGAAGTGGAGGCACAGCTGGCCCGACAGAAGGAGGAGGAATCCCAACAGCAA
GCAGTTCTGGAGCAGGAGCGCAGGGACCGGGAGCTGGCCCTGAGGATTGCCCAGAGTGAA
GCCGAGCTCATCAGTGATGAGGCCCAGGCCGACCTGGCGCTGCGGAGAGGTCCTGCTGTA
CTAGCCACCAAAGCAGCTGCTGGTACTAAGAAATATGATCTTAGTAAATGGAAATATGCA
GAACTACGTGATACCATCAATACTTCTTGTGATATTGAGCTCCTGGCAGCTTGCAGAGAA
GAATTTCATAGGAGACTAAAAGTGTATCATGCTTGGAAATCTAAGAACAAGAAGAGAAAT
ACTGAAACAGAGCAACGTGCTCCAAAGTCTGTTACTGATTATCCTCAGCAAAACCCAGCA
GCTCAGATTCCTGCCAGGCAGCGGGAGATTGAAATGAACCGACAGCAACGCTTCTTCCGC
ATCCCATTCATCCGCCCTGCCGACCAGTACAAAGACCCTCAGAGTAAGAAAAAAGGCTGG
TGGTATGCCCATTTTGATGGACCATGGATTGCCCGGCAAATGGAACTCCATCCTGACAAG
CCACCCATCCTACTTGTGGCTGGTAAGGACGACATGGAGATGTGTGAGCTGAATCTTGAG
GAGACTGGCCTGACTCGGAAGCGTGGTGCTGAGATCTTGCCAAGACAGTTTGAAGAAATC
TGGGAACGCTGTGGAGGCATCCAGTACCTTCAGAATGCGATTGAGAGCAGACAGGCTCGG
CCCACCTATGCAACAGCCATGCTGCAGAACCTGTTGAAATAA

5.3.2 MyoVI(LI)_Chick Sequence

(3831 ntds, gallus gallus, GenBank: AJ278608.1)

ATGGAGGACGGGAAGCCCGTTTGGGCTCCACACCCAACTGATGGGTTTCAGATGGGCATG
ATTGTGGACATTGGTACCGACTACTTAACTATTGAACCTTTGAATCAGAAAGGCAAGACT
TTCCAGGCTGCCATCAATCAAGTGTTTCCTGCCGAAGAGGACAGCAAAAAAGATGTGGAA
GATAATTGTTCCCTTATGTATTTAAATGAAGCCACTCTCCTCCACAATATCAAAGTTCGG
TACAGTAAGGACAGAATTTACACATATGTAGCCAACATTCTTATTGCAGTGAATCCATAT
TTTGATATACCTAAGTTCTATTCTTCAGATGCTATTAAAAAGTACCAGGGTAGATCACTT
GGGACGTTGCCACCACATGTCTTTGCTATTGCTGATAAAGCATACCGTGATATGAAAGTA
CTCAAAATGAGTCAGTCCATCATAGTTTCTGGAGAATCCGGAGCTGGCAAGACAGAAAAC
ACTAAATTTGTTTTGAGATATTTGACCGAGTCCTATGGTACTGGCCAAGATATTGATGAT
AGAATTGTAGAAGCAAATCCATTATTGGAAGCCTTTGGAAATGCAAAGACTATTCGTAAC
AACAATAGCAGTCGTTTTGGGAAATTTGTGGAAATTCACTTCAATGAAAAGAACTCGGTG
GTTGGTGGATTTGTATCACATTACCTTCTGGAGAAATCTCGCATCTGTGTGCAAGGCAAA
GAAGAGAGGAATTATCATATCTTTTACAGGCTTTGTGCCGGTGCTCCAGAAGACATTAGA
GAAAAACTGTACCTAAGCTCTCCTGACAGCTTCAGATATTTAAATCGAGGCTGTACGAGG
TACTTTGCTACCAAAGAAACAGACAAGCAGATCTTGCAAAATCGCAAGAGTCCTGAGTAT
CTTAAGGCAGGTTCCTTGAAGGATCCACTCTTAGATGATCATGGAGACTTCAACAGAATG
TGCACAGCAATGAAAAAGATTGGACTGGATGATGCAGAAAAACTTGACCTTTTTCGAGTA
GTGGCTGGTGTCCTTCACCTTGGAAATATTGATTTTGAGGAAGCTGGGAGCACTTCAGGG
GGCTGCACGCTGAAGGCGCAGAGCCAGCCGGCGCTGGAGTGCTGCGCGGCGCTGCTGGGG
CTGGACGAGGAGGACCTGCGAGTCAGCCTGACCACGCGCGTCATGCTCACCACGGCAGGG
GGCGCCAAAGGAACGGTCATTAAGGTACCCTTGAAGGTGGAACAAGCAAACAATGCTCGT
GATGCCTTGGCTAAAACGGTGTATAGTCATCTCTTTGACCATGTGGTGAACAGGGTGAAC
CAGTGTTTTCCATTTGAGACTTCTTCTTTCTTCATTGGAGTTCTAGATATAGCTGGTTTT
GAATACTTTGAACACAACAGTTTTGAGCAATTTTGTATCAACTATTGTAATGAAAAACTG
CAGCAATTTTTTAATGAAAGGATTCTGAAAGAGGAACAAGAACTTTACCAAAAAGAAGGC
CTGGGGGTTAATGAAGTACGCTATGTAGATAATCAGGACTGTATAGATTTGATTGAAGCA
AAGTTAATAGGTGTGCTGGATATTTTGGATGAAGAAAATCGTCTTCCTCAACCAAGTGAC
CAGCATTTCACTTCAGTTGTACACCAAAAACACAAGGACCATTTCAGACTCTCTATCCCT
AGGAAGTCTAAACTGGCTGTTCACAGAAATGTCAGAGATGATGAAGGCTTTATTATCCGG
CATTTTGCAGGAGCAGTGTGCTACGAGACGACACAATTTGTGGAAAAAAATAATGATGCT
TTACACATGTCACTTGAATCTCTTATATGTGAATCCAAGGACAAGTTTGTTCGGCAGCTG
TTTGAATCTAACACTAATAACAACAAGGATCCCAAACAAAAAGCTGGGAAACTTAGTTTC
ATCAGTGTGGGAAACAAATTCAAGACTCAGTTAAATTTGCTTCTTGAGAAGCTTCACAGT
ACTGGATCTAGCTTTATTCGCTGCATCAAACCTAATTTAAAGATGACAAGTCACCATTTT
GAAGGAGGACAGATCCTCTCCCAGCTTCAGTGTTCAGGAATGGTGTCTGTTCTGGATTTG
ATGCAAGGTGGCTTCCCTTCACGAGCTTCATTTCATGAACTATATAATATGTACAAGAAA
TATTTGCCTGAAAAATTGGCACGACTGGATCCCAGACTCTTTTGCAAGGCACTATTTAAA
GCTTTGGGACTGAATGAAATTGATTACAAATTTGGGTTAACCAAGGTGTTTTTTAGACCT
GGCAAGTTTGCAGAGTTTGATCAGATAATGAAGTCTGATCCGGATCACTTAGCAGAGCTA
GTTAAAAGGGTGAATCACTGGCTCATCTGCAGTCGCTGGAAAAAAGTTCAATGGTGTTCT
CTCTCAGTGATTAAATTGAAAAATAAGATAAAATACCGAGCTAGTGCCTGCATCAAAATA
CAAAAGACTATTCGTATGTGGCTTTGCAAGAGAAAACACAAACCACGCATCGATGGTCTG
ATAAAGGTCCGTACACTGAAAAAGAGACTTGATAAGTTTAATGAAGTGGTAAGTGCTCTG
AAGGAGGGGAAGGCAGAGACAAGCAAGCAGATCAAGGAGCTGGAGTATTCAATTGATGCT
TCAATGACCAAAATTAAGACTACGATGATGACTAGAGAACAGATAATGAAAGAATATGAT
GCTCTAGTTAGAAGCTCAGAGCAGCTTCTGAGTGCATTGCAAAAGAAAAAACAGCAAGAG
GAAGAAGCAGAGAGGTTACGACGCATCCAGGAGGAAATGGAAAAAGAAAGAAAGAGACGT

GAAGAGGAAGAGAAACGGCGAAGGAAGGAAGAGGAAGAAAGGCGCCTGAAATCTGAGATT
GAGGCAAAGAGAAAACAGGAAGAAGAAGAAAGGAAAAAGAGGGAAGAGGAAGAAAAGCGT
ATTCAGGCTGAAATTGAAGCTCAGCTAGCTAGAGAACGAGAAGAGGAAACCCAGCACCAG
GCAATTCTTGAACAGGAACGTCGTGATCGTGAACTTGCGATGAGAATTGCCCAAACTGGG
GCAGAACTCAGCACTGAAGAGACAAAGCTTGATGTAGGATTATGCAGAGCCAATGGAACA
AAGCTGCAAATGACTGCGGAACAAATGGCCAAAGAAATGTCAGAAATGTTGTCTAGAGGT
CCTGCAGTTCAAGCTACAAAAGCTGCTGCTGGTGCTAAGAAGCATGATCTGAGTAAATGG
AAATATGCAGAGCTTCGTGATACCATCAACACATCGTGTGATATTGAACTATTGGCGGCT
TGCAGAGAAGAGTTTCACAGAAGGCTAAAGGTGTATCATGCTTGGAAATCCAAGAACAAG
AAACGCAATGCAGAAACAGAACAGCGTGCTCCCAAATCAGTCACAGACTATGCTCAACAG
AACCCAACAGCTCAGCTACCAATGAGGCAGCAGGAGATTGAAATAAATAGACAACAGCGT
TACTTCCGCATTCCCTTCATCCGTCCCATGGACCAATATAAAGATCCACAGAACAAGAAG
AAGGGTTGGTGGTATGCACATTTTGATGGGCCATGGATTGCTCGACAGATGGAGCTTCAT
CCTGACAAGGCACCCATTCTCCTTGTAGCTGGTAAGGATGACATGGATATGTGTGAGCTT
AATCTTGAAGAGACTGGCTTAACTCGAAAGCGTGGTGCTGAAATTTTGCCGAGACAGTTT
GAAGAAATTTGGGAGCGCTGTGGAGGTATCCAGTACCTTCAAAATGCAATTGAAAGCAGA
CAAGCTCGTCCTACGTATGCTACAGCTATGCTGCAGAACCTGTTGAAATAA

5.4 Myosin XXI sequence

Leishmania donovani

ATGCCGGAGCGTGTGTCTGTGAATCAGGAGGTGTACTACTTCGACACCAAGAGCGGGTGG
CTGCGTGGCACCGTGAAGGAGGTCGATGGCGCCAAGGTGACGGTAGAGGACAATGCCTCG
CAGAGTGCCGTGAAAGTGGCGGCCGATAATGTGCACGGCTACATGTCGGAGAGCTACGAT
ATCGAGGACGCGGACCTCTTCCACGTGAGCGATCTGCACGTGGCCACTCTCTTGCACTGC
GTCAAGGACCGTTTTGAGAAGCTGCACAAGCAGTACTCGCTCATGGGGGAGATGGTGCTC
TCCGTCAACCCATTTCGCCTCATGCCCTTCAACAGCGAAGAGGAGCGTAAAGAGTATCTG
GCCCTGCCGGACCCCCGCATGCTGCCCCCGCACATCTGGCAGGTGGCGCACAAGGCCTTC
AACGCGGTCTTCGTTCAGGGTCAGGGCAACCAGTCCATCGTCATCTCCGGCGAGTCCGGT
TCCGGAAAAACCGAGAACGCCAAGATGCTCATCGCGTACCTGGGCCAACTCAGCTACATG
CACAGCAAGAACACCTCGCAGCGCAGCATCGCGGACAAGATCGACGAGAACCTAACCTGG
AGCAACCCCGTCATGGAGTCGTTCGGCAACGCCCGCACCGTGCGCAACGACAACTCTTCG
CGCTTCGGCAAGTACATCAAGCTCTACTTTGATCCTGTATCTGGCGTCATGGTGGGGGGC
CAGACCGTCACCTACTTGCTGGAGAGGAGCCGCATCATCATGCAGTCTCCTGGCGAGCGC
AACTACCACATCTTCTACGAGATGCTGGCGGGCCTGTCGCCGACAGAGAAGCAGCAGCTT
GGCGGGCTCAAGACTGCCCAGGACTACAAGTGCCTGAACGGCGGTAACACCTTCATCCGC
CGCGGCGTGGATGGCAAGCCGCTCGACGACGCGCACGAGTTTCAGATGGTGCGCCGCGCG
CTTTCCATGATCGGTGTGCCGCTGGAGACGCAGAACTGCATGTTGCGCGTGCTGGCGGCC
ATCCTGCACCTGATGGAGGTCGAGTTCGAGCCCGACAACAACGACAAGGCACAGATCGCA
AACGGGACACCGCTCGCGACGGCCTGCGCGCTGCTCTGCCTGGATGAGGCCAAGGTGCGC
GAGTGCTTTCTCGTGAGGAGCAAGACGTCGCTTGTCACGATCCTCGCCTCCAAGACGGAG
GCGGAGGGCCTGCGCAACGCCTTCTGCAAGGGACTTTACGTTGGCATGTTCGACCGGCTG
GTCGAGTTTGTGAACGCCGCCATTCAGCCCCGGGTGGACTGCAGCGACTGCAAGTACGTC
GGCCTGCTCGATATTTTCGGCTTTGAAAACTTCACGCGCAACAGCTTCGAGCAGATCTGC
ATCAATTACGCGAACGAGTCGCTGCAAAACCACTACAACAAGTACACGTTCATCAACGAC
GAAGAGGAGTGCCGCCGCGAGGGTATCCAGACCCCGAATATCGAGTTCCCAGACAACTCC
GAGTGCGTCAACATGCTCGATGCGAAGCGCGTCGGCATCTTCTCGATGCTGGATGAGGAG
TGCAACTTCAAGGGCGGCAACACAGACCGCTTCACCACGAACCTTTGGGAGGAGTGGGCT
GGCAGGAACCCGTACTTTGTGAAGCCGAAGAGCACGATCCCGAACCAGTTCGGCGTGAAC
CACTACGCTGCCTTCGTCAACTACAACACGGCGGACTGGTTGGAGAAGAACACGGACGCA
CTCAAGGAAGACATGTATGAGTGCGTGAGTGAGTCCACCGACGAGTTCATTCGGACCCTT
CTCTCGACGGAGAAGAGCGAGGCACGCCGCAAGCAGACCGTTGCCATCCGCTTCCAGCGC
CAGCTCACGGACCTGCGCTCCGAGCTGGAGTCCACCGAGACACGGTTCATTCGCTGCATC
AAGCCAAATATGGAGGCAAGCCCCTCGTTCCTCGAAAACCTTCTCGTCGGCTCGCAGCTT
GAGTCCGCTGGTGTGCTGCAGACCATCTCCCTCAAGCGTCAGGGCTACCCGGTGCGCCGT
CCGCTGGAGCAGTTTTGCAGGTACTTCTACCTTGTCATGTCCCGCACCACCGCCTCCTTG
TTCAAGCAAGGGCGGTACAGCGACGCGTCCCAGGACTTTCTGCAGCGACACCAGCGCCTC
TACAGCTGGGCGGAGCCCAACTACGCCGTTGGCAAGACGAAGGTGTTCCTCCGGGCTGAG
GTGTGGTCGGCGCTGGAGCGGCTGGTGCTTCGTCGCCGCGCGCAGCTGCTGCACCGCTGC
AAGCCCTACCTGCGCCGCTGGATCGACGAGCTCCGCGAGCGCAGGCGTATCGAGGAGCAG
AAGCGGCTGGAGGCAGCGCGCAAGCTGCGCGAGGCGCGGGAGGCCAAGGCCGCCGACGCC
GCCAATGGTGTGCCGGCGGAGAAACTGCAGTGGGTGGAGGAGGCGTCGAACATGTTCCCA
GACTTCGACACGGACACGCTGCTCGACGTTGCCGTCGAGGCGGACACGCGCGAGGAGGCT
CTCAGCGCCATCCTTGCCATCCAGGCTGACCGCCTTGACAAGCAGACAGCCTCTGGATTC
ATGGAAGTGATGGCGGCTGCGAACGTGCGCCGTGGCGTCATCAACAACTTTATCTCGGCG
GACATCAAGACGGTGTCGGCGCTGTCGAGGCTGCAGCCGGAGGATATGAAGAGCCTCGGC
GCCAGTGAGATGGAGGTGGTGGCGATCACGAAGAAGCTGGCGGAGCAGCAGGGGCAGCGC

GTCAAGTACCAGCGCCTCGCCGAGGCCATCGGCACGGACAGCGAATATGCCGCCGCTGGC
GCCGTCCAACGCGCCGAGGTGGCTCGCCACCAGGAAGACTTCGACGCCAAAGTGCAGACC
CTTGCCAGCATGGGCTTTGATGAGCCCACCGGCCGCCTCGTGCTGGCGCACTACAACGGC
GACGTGCAGCGCACGGCGGCGCGCCTGCTTTATGGCGTGGACAGCCGGAAGATGAGGAAC
AACGCGCGCAAGCACAAGAACTTCAACACAACGGACCCCAACGTGCAGCAGCTCATCTCT
CTCGGTGCGACGAAGCAGGATGCAAAGATGGCACTACGTCGCAACAACGGAGACGCGAAC
GCCGCCGTTAAGATGCTGTTCAAGGTGAGCTAG

5.5 Complete lipid binding tables Myosin VI and XXI

construct	Fat Blot	Membrane Strip	PIP Strip	PC	PE	Chol	PC+PE	PC+PC+Chol	PI(4)P	PI(4,5)P$_2$	PI(3,5)P$_2$	folch
VI FL		PS,PA, PG, Cardiolipin, PI(4)P, PI(4,5)P$_2$, PI(3,4,5)P$_3$, 3-sulfogalactosylceramide	PI(3)P, PI(4)P, PI(5)P, PI(3,5)P$_2$, PA									
Trunc814		PS,PA, PG, Cardiolipin, PI(4)P, PI(4,5)P$_2$, PI(3,4,5)P$_3$, 3-sulfogalactosylceramide	PI(3)P, PI(4)P, PI(5)P, PI(3,5)P$_2$, PA									
Trunc913		PS,PA, PG, Cardiolipin, PI(4)P, PI(4,5)P$_2$, PI(3,4,5)P$_3$, 3-sulfogalactosylceramide	PI(3)P, PI(4)P, PI(5)P, PI(3,5)P$_2$, PA									
Trunc1060												
814 tail		extremely weak PI(4)P							weak	weak	weak	
913 tail		PS,PA, PG, Cardiolipin, PI(4)P, PI(4,5)P$_2$, PI(3,4,5)P$_3$, 3-sulfogalactosylceramide	PI(3)P, PI(4)P, PI(5)P, PI(3,5)P$_2$, PA									
1060 tail		PS,PA, PG, Cardiolipin, PI(4)P, PI(4,5)P$_2$, PI(3,4,5)P$_3$, 3-sulfogalactosylceramide	PI(3)P, PI(4)P, PI(5)P, PI(3,5)P$_2$									
NCBD tail		PI(4)P	PI(3)P, PI(4)P, PI(5)P, PI(3,5)P$_2$									
1125 tail		PS,PA, PG, Cardiolipin, PI(4)P, PI(4,5)P$_2$, PI(3,4,5)P$_3$, 3-sulfogalactosylceramide	PI(3)P, PI(4)P, PI(5)P, PI(3,4)P$_2$, PI(3,5)P$_2$, PA									
883 Δ PIP		PI(4)P, Cardiolipin, 3-*sulfogalactosylceramide*, *PG*, PS, PA, *PI(4,5)P2, PI(3,4,5)P$_3$*	PI(3)P, PI(4)P, PI(5)P, PI(3,5)P$_2$									
FL Δ PIP		PI(4)P, Cardiolipin, PI(4,5)P2, PI(3,4,5)P$_3$, PS, PA	PI(3)P, PI(4)P, PI(5)P, PI(3,5)P$_2$, PI(3,4,5)P$_3$									
c 1060 tail		Cardiolipin, PI(4)P, 3- galactosylceramide	PI(3)P, PI(4)P, PI(5)P, PI(3,5)P$_2$									

Table 9: Table of all investigated protein:lipid interactions of myosin VI constructs. Green filled cells indicate binding, red no binding.

Construct	Fat Blot	Membrane Strip	PIP Strip	folch
XXI FL		PS,PA, Cardiolipin, PI(4)P, $PI(4,5)P_2$, $PI(3,4,5)P_3$	PI(3)P, PI(4)P, PI(5)P, $PI(3,5)P_2$, $PI(3,4,5)P_3$	
XXI Trunc		PS,PA, Cardiolipin, PI(4)P, $PI(4,5)P_2$, $PI(3,4,5)P_3$, sulfatide	PI(3)P, PI(4)P, PI(5)P, $PI(3,5)P_2$	pellets on its own
730				
830		PS,PA, Cardiolipin, PI(4)P, $PI(4,5)P_2$, $PI(3,4,5)P_3$,	PI(3)P, PI(4)P, PI(5)P, $PI(3,5)P_2$, PS	
930				
730-930		PS, Cardiolipin, PI(4)P, $PI(4,5)P_2$, $PI(3,4,5)P_3$	PI(3)P, PI(4)P, PI(5)P, $PI(3,5)P_2$, $PI(3,4)P_2$	
730-830			PI(3)P, PI(4)P, PI(5)P, $PI(3,5)P_2$, PA	
830-930			PI(3)P, PI(4)P, PI(5)P, $PI(3,5)P_2$, PA, $PI(3,4)P_2$	pellets on its own
730-930 RFP				
730-830 RFP			PI(3)P, PI(4)P, PI(5)P	
830-930 RFP		PS,PA, PG, Cardiolipin, PI(4)P, $PI(4,5)P_2$, $PI(3,4,5)P_3$, sulfatide	PI(3)P, PI(4)P, PI(5)P	
600-758		PI(4)P	PI(3)P, PI(4)P, PI(5)P, $PI(3,5)P_2$	
600-758 PX mutant		PS,PA, Cardiolipin, PI(4)P, $PI(4,5)P_2$, $PI(3,4,5)P_3$, sulfatide	PI(3)P, PI(4)P, PI(5)P	

Table 10: Table of all investigated protein:lipid interactions of myosin XXI constructs. Green filled cells indicate binding, red no binding.

5.6 Lipid-affinity co-sedimentations of myosin VI constructs

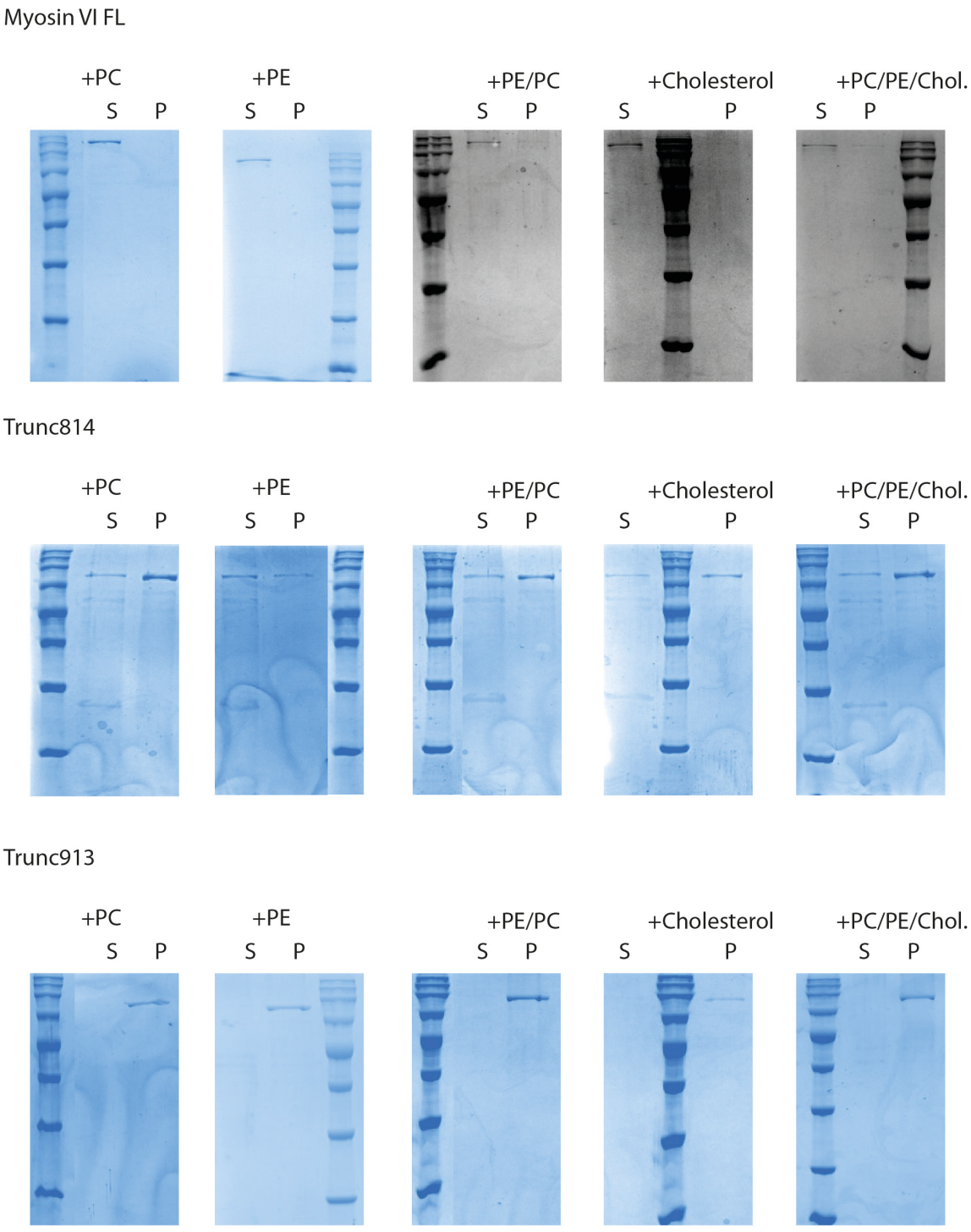

Figure 106: Lipid affinity control co-sedimentations of myosin VI FL, Trunc814 and Trunc913.

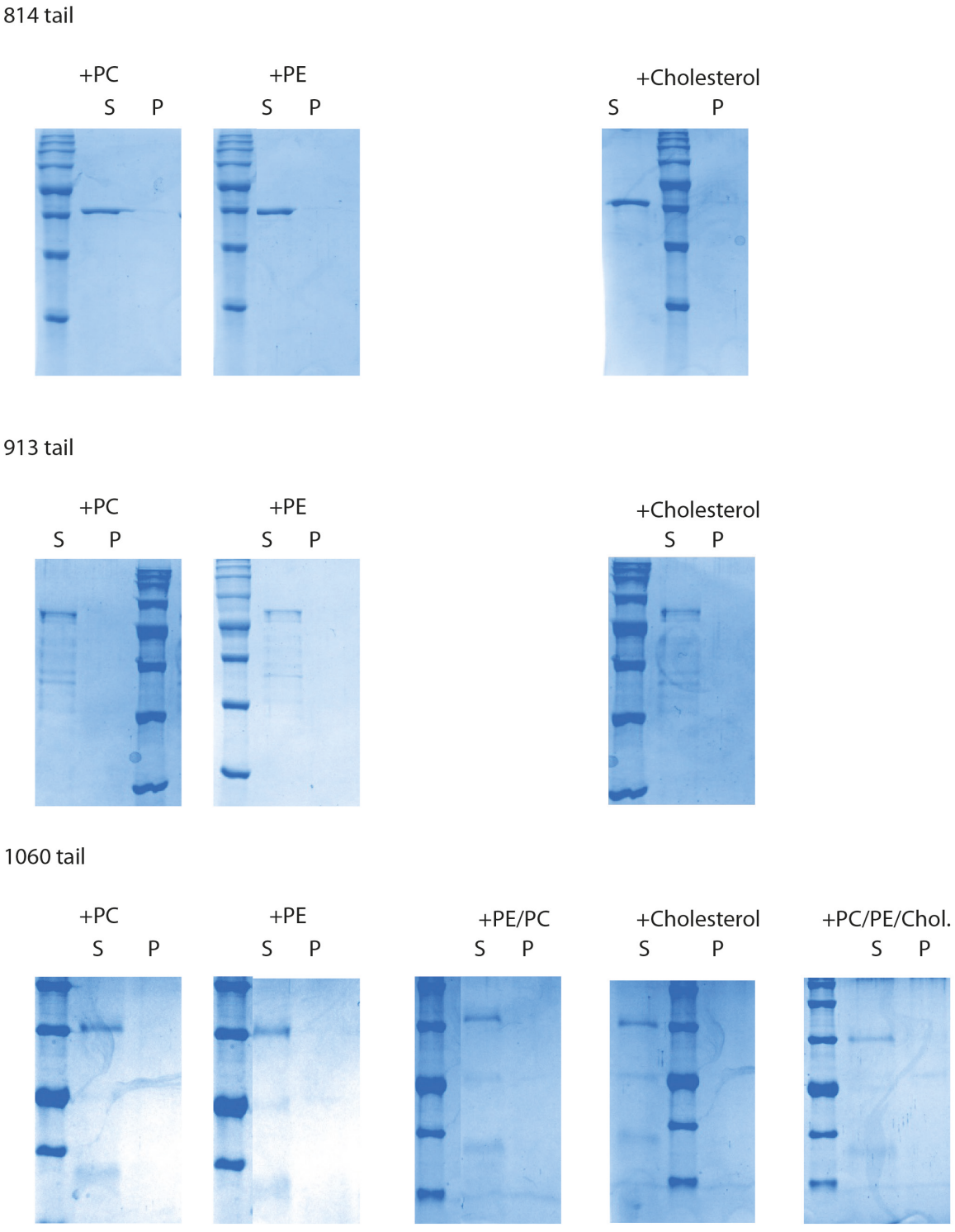

Figure 107: Lipid affinity control co-sedimentations of myosin VI 814, 913 and 1060 tails.

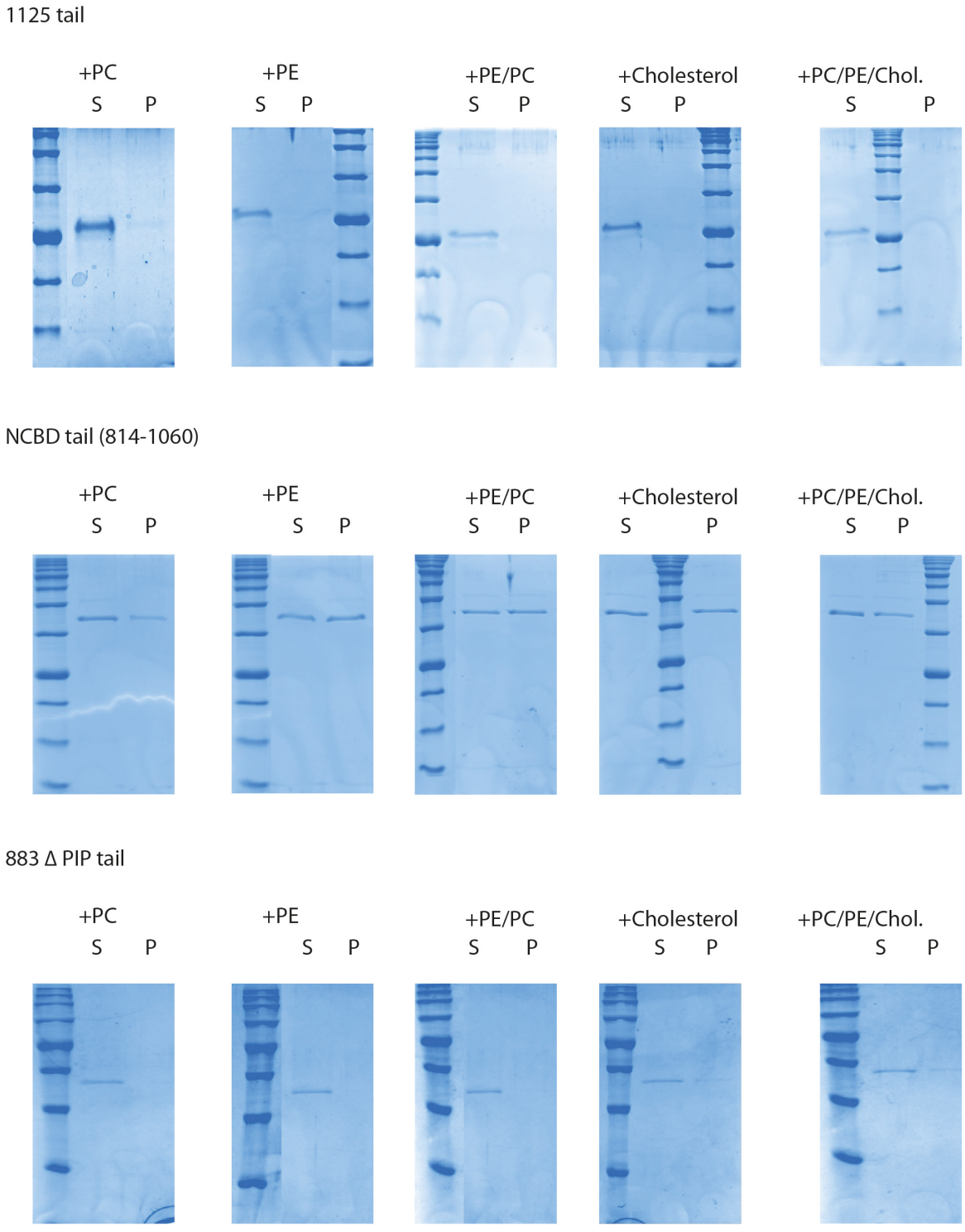

Figure 108: Lipid affinity control co-sedimentations of myosin VI 1125, NCB and 883 delta PIP tails.

5.7 BH plot scales used for computer searches

Scales used for computer searches

Amino acid	K&D[a]	OMH	Consensus	W&W	BH
Ala	1.8	−0.4	0.62	−0.17	−0.17
Cys	2.5	0.17	0.29	0.24	0.24
Asp	−3.5	−1.31	−0.9	−1.23	−1.23
Glu	−3.5	−1.22	−0.74	−2.02	−2.02
Phe	2.8	1.92	1.19	1.13	1.13
Gal	−0.4	−0.67	0.48	−0.01	−0.01
His	−3.2	−0.64	−0.4	−0.17	−0.17
Ile	4.5	1.25	1.38	0.31	0.31
Lys	−3.9	−0.67	−1.5	−0.99	2.00
Leu	3.8	1.22	1.06	0.56	0.56
Met	1.9	1.02	0.64	0.23	0.23
Asn	−3.5	−0.92	−0.78	−0.42	−0.42
Pro	−1.6	−0.49	0.12	−0.45	−0.45
Gln	−3.5	−0.91	−0.85	−0.58	−0.58
Arg	−4.5	−0.59	−2.53	−0.81	2.00
Ser	−0.8	−0.55	−0.18	−0.13	−0.13
Thr	−0.7	−0.28	−0.05	−0.14	−0.14
Val	4.2	0.91	1.08	−0.07	−0.07
Trp	−0.9	0.5	0.81	1.85	1.85
Tyr	−1.3	1.67	0.26	0.94	0.94

[a] References are as follows: K&D, Kyte and Doolittle (15); OMH, Sweet and Eisenberg (19); Consensus (19); W&W, Wimley and White (12); and BH (this paper; W&W scale with Lys and Arg values changed to 2; see "Results").

Table 11: BH plot scales used for computer search. From Brzeska *et al.* (2010)

5.8 Membrane binding domains

Domain	Target	Consensus sequence/motif/ structure	Binding mechanism	References
C1	DAG, phorbol ester	PX(F/W/Y)$CX_2CX_2Hy_3$ GX_{0-1} HyX_2QG (X: any aa; Hy: any hydrophobic residue)		Hurley and Misra (2000)
C2	PS, anionic membranes, neutral membranes	two, four stranded β-sheets creating three loops at the top of the domain and four at the bottom; 5 conserved D residues and one S in upper loops 1 and 3 binding of 3 Ca^{2+} ions necessary for phospholipid binding	coincidence detection, electrostatic switch	Sutton and Sprang (1998), Rizo and Sudhof (1998)
PH	PI(3)P, PI(4)P, $PI(3,4)P_2$, $PI(3,5)P_2$, $PI(4,5)P_2$, $PI(3,4,5)P_3$	K-X_m-(R/K)-X-R-X_n-(Y/N) K-X_n-(K/R)-X-R K-Xaa-Sma-Xaa_{6-11}-R/K-Xaa-R-Hyd-Hyd (Xaa: any aa, Sma: small aa, Hyd: hydrophobic aa)	coincidence detection, HIS protonation	DiNitto *et al.* (2003), Stahelin (2009), Dowler *et al.* (2000)
FYVE	PI(3)P	Zn^{2+} fingers with an N-terminal WXXD motif, a central R(R/K)HHCR motif, and a C-terminal RXC motif (R/K)(R/K)HHCR	HIS-protonation, use their turret loops to penetrate the membrane	DiNitto *et al.* (2003), Stenmark and Aasland (1999), Balla (2005), Hurley and Misra (2000), Hurley (2006)
PX	PI(3)P, $PI(3,4)P_2$, $PI(4,5)P_2$, PS, PA	R(Y/F) X_{23-30} K X_{13-23} R, N-terminal 3-stranded β-sheet followed by helical subdomain (4 α-helices)	coincidence detection	Teasdale and Collins (2012), Balla (2005)
ENTH	$PI(3,5)P_2$, $PI(4,5)P_2$, $PI(3,4,5)P_3$	DP(W/F) repeats, α-helical solenoid	HIS-protonation; membrane curvature detection	DiNitto *et al*. (2003), De Camilli *et al.* (2002), Rozovsky *et al.* (2012)
ANTH	phosphoinositides, little specificity	α-helical solenoid		Lemmon (2008)
BAR	acidic phospholipid membranes	dimer, banana shaped extended α-helical bundle	curvature sensing/ inducing, electrostatic interactions	Hurley (2006), Lemmon (2008)
FERM	$PI(4,5)P_2$	subdomains A, B and C		DiNitto *et al.* (2003)
tubby	$PI(3,4)P_2$, $PI(4,5)P_2$			DiNitto *et al*. (2003)
PHD	PI(3)P, PI(5)P	C4HC3-type zinc finger		Bienz (2006)
MARCKS	$PI(4,5)P_2$		curvature sensing	DiNitto *et al.* (2003), Morton *et al.* (2012)

Table 12: List of membrane binding domains and their targets.

Publication list

Ellrich, H., Batters, C., Brack, D., Averbeck, B., Veigel, C. "Myosin VI unfolding is triggered by calcium binding to calmodulin." In preparation

Batters, C., **Ellrich, H**., Helbig, C., Woodall, K.A., Hundschell, C., Brack, D., Veigel, C.(2014): "Calmodulin regulates dimerization, motility, and lipid binding of *Leishmania* myosin XXI." PNAS **111**(2): E227-E236.

Published abstracts and Posters

Helbig, C., Sazcko-Brack, D., **Ellrich, H**., Werner, C., Averbeck, B., Batters, C., Veigel, C. (2014). "Structure and Binding Behavior of Myosin-VI and Myosin-XXI." SFB863 meeting, Hohenkammer

Batters, C., **Ellrich, H.**, Helbig, C., Woodall, K., Hundschell, C., Brack, D., Veigel, C. (2014). "Calmodulin and Lipid Binding Regulate Dimerisation and Motility of Myosin-XXI in Leishmania." Biophysical Journal **106**(2):180A-180A.

Helbig, C., **Ellrich, H**., Hundschell, C., Batters, C., Veigel C. (2013). "Myosin-XXI, a motor with many missions." Biophysical Journal **104**(2): 644A-644A.

Toseland, C. P., **Ellrich, H**., Fili, N., Batters, C., Veigel, C. (2012). "Myosin VI comes together-structure and motor regulation by binding partners." Biophysical Journal 102(3): 569A-569A.

Ellrich, H., Toseland, C. P., Batters, C., Veigel, C. (2012). "Myosin VI- better off together or on their own?" SFB863 meeting, Venice.

Conference attendance list and presentations

03/12	SFB863 meeting, Venice, Poster
10/14	SFB863 meeting, Hohenkammer, Poster

Previous publications

Tietze DT, Neu A, **Ellrich, H.** & Martens J (2007): "Zwei Jahre Integriertes Singvogelmonitoring am Eich-Gimbsheimer Altrhein." Fauna und Flora in Rheinland-Pfalz **11**: 151-174.

Ellrich, H., Salewski V., Fiedler W. (2010). "Morphological sexing of passerines: not valid over larger geographical scales." Journal of Ornithology **151**(2): 449-458.

References

Adamek, N., Coluccio, L. M. and Geeves, M. A. (2008). "Calcium sensitivity of the cross-bridge cycle of Myo1c, the adaptation motor in the inner ear." PNAS **105**: 5710-5715.

Ali, M. Y., Kennedy, G. G., Safer, D., Trybus, K. M., Sweeney, H. L. and Warshaw, D. M. (2011). "Myosin Va and myosin VI coordinate their steps while engaged in an in vitro tug of war during cargo transport." PNAS **108**: E535-E541.

Arden, S. D., Puri, C., Au, J. S.-Y., Kendrick-Jones, J. and Buss, F. (2007). "Myosin VI is required for targeted membrane transport during cytokinesis." Molecular Biology of the Cell **18**: 4750-4761.

Aschenbrenner, L., Lee, T. and Hasson, T. (2003). "Myo6 facilitates the translocation of endocytic vesicles from cell peripheries." Molecular Biology of the Cell **14**: 2728-2743.

Au, J. S.-Y., Puri, C., Ihrke, G., Kendrick-Jones, J. and Buss, F. (2007). "Myosin VI is required for sorting of AP-1B-dependent cargo to the basolateral domain in polarized MDCK cells." Journal of Cell Biology **177**: 103-114.

Avraham, K. B., Hasson, T., Steel, K. P., Kingsley, D. M., Russell, L. B., Mooseker, M. S., Copeland, N. G. and Jenkins, N. A. (1995). "The mouse snells waltzer deafness gene encodes an unconventional myosin required for structural integrity of inner-ear-hair-cells." Nature Genetics **11**: 369-375.

Bagshaw, C. R. Muscle Contraction. 2nd ed. London: Chapman & Hall, 1993.

Bähler, M. and Rhoads, A. (2002). "Calmodulin signaling via the IQ motif." FEBS Letters **513**: 107-113.

Bahloul, A., Chevreux, G., Wells, A. L., Martin, D., Nolt, J., Yang, Z. H., Chen, L. Q., Potiert, N., Van Dorsselaer, A., Rosenfeld, S., Houdusse, A. and Sweeney, H. L. (2004). "The unique insert in myosin VI is a structural calcium-calmodulin binding site." PNAS **101**: 4787-4792.

Balla, T. (2005). "Inositol-lipid binding motifs: signal integrators through protein-lipid and protein-protein interactions." Journal of Cell Science **118**: 2093-2104.

Barenholz, Y., Gibbes, D., Litman, B. J., Goll, J., Thompson, T. E. and Carlson, F. D. (1977). "A simple method for the preparation of homogeneous phospholipid vesicles." Biochemistry **16**: 2806-2810.

Batters, C., Ellrich, H., Helbig, C., Woodall, K. A., Hundschell, C., Brack, D. and Veigel, C. (2014). "Calmodulin regulates dimerization, motility, and lipid binding of *Leishmania* myosin XXI." PNAS **111**: E227-E236.

Batters, C., Woodall, K. A., Toseland, C. P., Hundschell, C. and Veigel, C. (2012). "Cloning, Expression, and Characterization of a Novel Molecular Motor, *Leishmania* Myosin-XXI." Journal of Biological Chemistry **287**: 27556-27566.

Berg, J.M., Tymoczko,J.L. and Stryer, L. Biochemistry. 7th ed. New York: W.H. Freeman, 2012.

Berg, J. S., Powell, B. C. and Cheney, R. E. (2001). "A millennial myosin census." Molecular Biology of the Cell **12**: 780-794.

Bienz, M. (2006). "The PHD finger, a nuclear protein-interaction domain." Trends in Biochemical Sciences **31**: 35-40.

Bloom, M., Evans, E. and Mouritsen, O. G. (1991). "Physical properties of the fluid lipid-bilayer component of cell membranes: a perspective." Quarterly Reviews Biophysics **24**: 293-397.

Bond, L. M., Arden, S. D., Kendrick-Jones, J., Buss, F. and Sellers, J. R. (2012). "Dynamic Exchange of Myosin VI on Endocytic Structures." Journal of Biological Chemistry **287**: 38637-38646.

Bond, L. M., Brandstaetter, H., Sellers, J. R., Kendrick-Jones, J. and Buss, F. (2011). "Myosin motor proteins are involved in the final stages of the secretory pathways." Biochemical Society Transactions **39**: 1115-1119.

Bond, L. M., Peden, A. A., Kendrick-Jones, J., Sellers, J. R. and Buss, F. (2011). "Myosin VI and its binding partner optineurin are involved in secretory vesicle fusion at the plasma membrane." Molecular Biology of the Cell **22**: 54-65.

Bradford, M. M. (1976). "A rapid and sensitive method for the quantitation of microgram quantities of protein utilizing the principle of protein-dye binding." Analytical Biochemistry **72**: 248-254.

Brzeska, H., Guag, J., Remmert, K., Chacko, S. and Korn, E. D. (2010). "An Experimentally Based Computer Search Identifies Unstructured Membrane-binding Sites in Proteins." Journal of Biological Chemistry **285**: 5738-5747.

Bunn, R. C., Jensen, M. A. and Reed, B. C. (1999). "Protein interactions with the glucose transporter binding protein GLUT1CBP that provide a link between GLUT1 and the cytoskeleton." Molecular Biology of the Cell **10**: 819-832.

Buss, F., Arden, S. D., Lindsay, M., Luzio, J. P. and Kendrick-Jones, J. (2001). "Myosin VI isoform localized to clathrin-coated vesicles with a role in clathrin-mediated endocytosis." EMBO Journal **20**: 3676-3684.

Buss, F. and Kendrick-Jones, J. (2007). "Myosin VI. A multifunctional motor protein". Myosins: A Superfamily of Molecular Motors. L. M. Coluccio (ed.). (2007). London, Springer **7:** 325-352.

Buss, F. and Kendrick-Jones, J. (2011). "Multifunctional myosin VI has a multitude of cargoes." PNAS **108**: 5927-5928.

Buss, F., Spudich, G. and Kendrick-Jones, J. (2004). "Myosin VI: Cellular functions and motor properties." Annual Review of Cell and Developmental Biology **20**: 649-676.

Carlier, M. F. (1998). "Control of actin dynamics." Current Opinion in Cell Biology **10**: 45-51.

Carlton, J. G. and Cullen, P. J. (2005). "Coincidence detection in phosphoinositide signaling." Trends in Cell Biology **15**: 540-547.

Chakrabarti, A. C. (1994). "Permeability of membranes to amino acids and modified amino acids: Mechanisms involved in translocation." Amino Acids **6**: 213-229.

Chen, Y. A. and Scheller, R. H. (2001). "SNARE-mediated membrane fusion." Nature Reviews of Molecular Cell Biology **2**: 98-106.

Cheney, R. and Baker, J. (1999). "Myosins, divergent." The Guidebook of Cytoskeletal and Motor Proteins. T. Kreis and R. Vale (eds.). (1999). Sambrook and Tooze Publications, Oxford: 453-456.

Cheney, R. E. and Mooseker, M. S. (1992). "Unconventional myosins." Current Opinion in Cell Biology **4**: 27-35.

Chibalina, M. V., Seaman, M. N. J., Miller, C. C., Kendrick-Jones, J. and Buss, F. (2007). "Myosin VI and its interacting protein LMTK2 regulate tubule formation and transport to the endocytic recycling compartment." Journal of Cell Science **120**: 4278-4288.

Cremo, C. R. and Geeves, M. A. (1998). "Interaction of actin and ADP with the head domain of smooth muscle myosin: Implications for strain-dependent ADP release in smooth muscle." Biochemistry **37**: 1969-1978.

Cremo, C. R. and Hartshorne, D. J. (2007). "Smooth-Muscle Myosin II". Myosins: A Superfamily of Molecular Motors.L. M. Coluccio (ed.). (2007). London, Springer. **7:** 171-222.

CyMoBase (2013). http://www.cymobase.org/.

Czech, M. P. (2000). "PIP_2 and PIP_3: Complex Roles at the Cell Surface." Cell **100**: 603-606.

Dance, A. L., Miller, M., Seragaki, S., Aryal, P., White, B., Aschenbrenner, L. and Hasson, T. (2004). "Regulation of Myosin-VI targeting to endocytic compartments." Traffic **5**: 798-813.

De Camilli, P., Chen, H., Hyman, J., Panepucci, E., Bateman, A. and Brunger, A. T. (2002). "The ENTH domain." FEBS Letters **513**: 11-18.

De La Cruz, E. M. and Ostap, E. M. (2004). "Relating biochemistry and function in the myosin superfamily." Current Opinion in Cell Biology **16**: 61-67.

De La Cruz, E. M. and Ostap, E. M. (2009). "Kinetic and equilibrium analysis of the myosin ATPase". Methods in Enzymology: Biothermodynamics. M. L. Johnson, J. M. Holt and G. K. Ackers (ed.). (2009). **455**: 157-192.

De la Cruz, E. M., Ostap, E. M. and Sweeney, H. L. (2001). "Kinetic mechanism and regulation of myosin VI." Journal of Biological Chemistry **276**: 32373-32381.

Deatherage, B. L. and Cookson, B. T. (2012). "Membrane vesicle release in bacteria, eukaryotes, and archaea: a conserved yet underappreciated aspect of microbial life." Infection and Immunity **80**: 1948-1957.

DiNitto, J. P., Cronin, T. C. and Lambright, D. G. (2003). "Membrane recognition and targeting by lipid-binding domains." Science STKE **2003**: 1-16.

Dopico, A. M. and Tigyi, G. J. (2007). "A Glance at the Structural and Functional Diversity of Membrane Lipids". Methods in Membrane Lipids. A. M. Dopico (ed.). (2007), Humana Press. **400:** 1-13.

Dowhan, W. and Bogdanov, M. (2002). "Functional roles of lipids in membranes." New Comprehensive Biochemistry **36**: 1-35.

Dowler, S., Currie, R. A., Campbell, D. G., Deak, M., Kular, G., Downes, C. P. and Alessi, D. R. (2000). "Identification of pleckstrin-homology-domain-containing proteins with novel phosphoinositide-binding specificities." Biochemical Journal **351**: 19-31.

Dowler, S., Kular, G. and Alessi, D. R. (2002). "Protein Lipid Overlay Assay." Science STKE **2002**: pl6.

Dulon, D., Safieddine, S., Jones, S. M. and Petit, C. (2009). "Otoferlin is critical for a highly sensitive and linear calcium-dependent exocytosis at vestibular hair cell ribbon synapses." Journal of Neuroscience **29**: 10474-10487.

Dunn, T. A., Chen, S., Faith, D. A., Hicks, J. L., Platz, E. A., Chen, Y., Ewing, C. M., Sauvageot, J., Isaacs, W. B., De Marzo, A. M. and Luo, J. (2006). "A novel role of myosin VI in human prostate cancer." American Journal of Pathology **169**: 1843-1854.

Dutta, S. and Bhattacharyya, D. (2001). "Size of unfolded and dissociated subunits versus that of native multimeric proteins." Journal of Biological Physics **27**: 59-71.

Escribá, P. V., Wedegaertner, P. B., Goñi, F. M. and Vögler, O. (2007). "Lipid–protein interactions in GPCR-associated signaling." Biochimica et Biophysica Acta - Biomembranes **1768**: 836-852.

Espindola, F. S., Espreafico, E. M., Coelho, M. V., Martins, A. R., Costa, F. R. C., Mooseker, M. S. and Larson, R. E. (1992). "Biochemical and immunological characterization of P190-calmodulin complex from vertebrate brain-a novel calmodulin-binding myosin." Journal of Cell Biology **118**: 359-368.

Evans, E. A. (1989). "Structure and deformation properties of red blood cells: concepts and quantitative methods." Methods Enzymology **173**: 3-35.

Fischer, S., Windshügel, B., Horak, D., Holmes, K. C. and Smith, J. C. (2005). "Structural mechanism of the recovery stroke in the Myosin molecular motor." PNAS **102**: 6873-6878.

Foth, B. J., Goedecke, M. C. and Soldati, D. (2006). "New insights into myosin evolution and classification." PNAS **103**: 3681-3686.

Fujita, A. and Kurachi, Y. (2000). "SAP family proteins." Biochemical and Biophysical Research Communications **269**: 1-6.

Geeves, M. A. (1992). "The actomyosin ATPase a 2-state system." Philosophical Transactions of the Royal Society of London Series B-Biological Sciences **336**: 63-71.

Geeves, M. A. and Holmes, K. C. (1999). "Structural mechanism of muscle contraction." Annual Review of Biochemistry **68**: 687-728.

Geeves, M. A., Webb, M. R., Midelfort, C. F. and Trentham, D. R. (1980). "Mechanism of adenosine 5'-triphosphate cleavage by myosin-studies with oxygen-18-labeled adenosine 5'-phosphate." Biochemistry **19**: 4748-4754.

Geisbrecht, E. R. and Montell, D. J. (2002). "Myosin VI is required for E-cadherin-mediated border cell migration." Nature Cell Biology **4**: 616-620.

Gordon, A. M., Huxley, A. F. and Julian, F. J. (1966). "Variation in isometric tension with sarcomere length in vertebrate muscle fibres." Journal of Physiology **184**: 170-192.

Gotthardt, M., Trommsdorff, M., Nevitt, M. F., Shelton, J., Richardson, J. A., Stockinger, W., Nimpf, J. and Herz, J. (2000). "Interactions of the low density lipoprotein receptor gene family with cytosolic adaptor and scaffold proteins suggest diverse biological functions in cellular communication and signal transduction." Journal of Biological Chemistry **275**: 25616-25624.

Greenberg, S. and Grinstein, S. (2002). "Phagocytosis and innate immunity." Current Opinion in Immunology **14**: 136-145.

Greenwood, J. A., Theibert, A. B., Prestwich, G. D. and Murphy-Ullrich, J. E. (2000). "Restructuring of focal adhesion plaques by PI 3-kinase: Regulation by PtdIns (3,4,5)-P-3 binding to alpha-actinin." Journal of Cell Biology **150**: 627-641.

Haid, E., Lehmann, P. and Ziegenhorn, J. (1975). "Molar absorptivities of beta-NADH and beta-NAD at 260 nm." Clinical Chemistry **21**: 884-887.

Halet, G. (2005). "Imaging phosphoinositide dynamics using GFP-tagged protein domains." Biology of the Cell **97**: 501-518.

Hanson, J. and Huxley, H. E. (1953). "Structural basis of the cross-striations in muscle." Nature **172**: 530-532.

Hartman, M. A. and Spudich, J. A. (2012). "The myosin superfamily at a glance." Journal of Cell Science **125**: 1627-1632.

Hasegawa, Y. and Araki, T. (2002). "Identification of a novel unconventional myosin from scallop mantle tissue." Journal of Biochemistry **131**: 113-119.

Hasson, T. (1997). "Unconventional myosins, the basis for deafness in mouse and man." American Journal of Human Genetics **61**: 801-805.

Hasson, T. and Mooseker, M. S. (1994). "Porcine myosin VI- Characterization of a new mammalian unconventional myosin." Journal of Cell Biology **127**: 425-440.

Hiepe, T., Lucius, R., Gottstein, B. Allgemeine Parasitologie: mit den Grundzügen der Immunbiologie, Diagnostik und Bekämpfung. 1st ed. Stuttgart: Parey, 2006.

Hinchliffe, K. (2000). "Intracellular signalling: Is PIP_2 a messenger too?" Current Biology **10**: R104-R105.

Hodge, T. and Cope, M. (2000). "A myosin family tree." Journal of Cell Science **113**: 3353-3354.

Holmes, K. C. (1997). "The swinging lever-arm hypothesis of muscle contraction." Current Biology **7**: R112-R118.

Holmes, K. C. (2005). "The molecular basis of cross-bridge function". Sliding filament mechanism in muscle contraction- Fifty years of research. H. Sugoi (ed.). (2005). New York, Springer. **565:** 13-24.

Holmes, K. C. (2009). "Structural biology: Actin in a twist." Nature **457**: 389-390.

Holmes, K. C., Popp, D., Gebhard, W. and Kabsch, W. (1990). "Atomic model of the actin filament." Nature **347**: 44-49.

Hope, M. J., Bally, M. B., Webb, G. and Cullis, P. R. (1985). "Production of large unilamellar vesicles by a rapid extrusion procedure. Characterization of size distribution, trapped volume and ability to maintain a membrane potential." Biochimica et Biophysica Acta (BBA) - Biomembranes **812**: 55-65.

Horowitz, J. A. and Hammer, J. A. (1990). "Identification of a new type of myosin heavy-chain in *Acanthamoeba*." Biophysical Journal **57**: A330-A330.

Horowitz, J. A. and Hammer, J. A. (1990). "A new *Acanthamoeba* myosin heavy-chain-cloning of the gene and immunological identification of the polypeptide." Journal of Biological Chemistry **265**: 20646-20652.

Houdusse, A. and Sweeney, H. L. (2001). "Myosin motors: missing structures and hidden springs." Current Opinion in Structural Biology **11**: 182-194.

Hu, L. Y. A., Chen, W., Martin, N. P., Whalen, E. J., Premont, R. T. and Lefkowitz, R. J. (2003). "GIPC interacts with the beta(1)-adrenergic receptor and regulates beta(1)-adrenergic receptor-mediated ERK activation." Journal of Biological Chemistry **278**: 26295-26301.

Hurley, J. H. (2006). "Membrane binding domains." Biochimica Et Biophysica Acta-Molecular and Cell Biology of Lipids **1761**: 805-811.

Hurley, J. H. and Misra, S. (2000). "Signaling and subcellular targeting by membrane-binding domains." Annual Review of Biophysics and Biomolecular Structure **29**: 49-79.

Huxley, A. F. (1957). "Muscle structure and theories of contraction." Progress in Biophysics & Molecular Biology **7**: 255-318.

Huxley, A. F. and Simmons, R. M. (1971). "Proposed mechanism of force generation in striated muscle." Nature **233**: 533-538.

Huxley, H. E. (1969). "Mechanism of muscular contraction." Science **164**: 1356-1366.

Iida, K., Janmey, P. A., Stossel, T. P. and Yin, H. L. (1987). "Polyphosphoinositides dissociate gelsolin- actin complexes." Cell Structure and Function **12**: 660-660.

Ivanov, S. and Roy, C. R. (2009). "NDP52: the missing link between ubiquitinated bacteria and autophagy." Nature Immunology **10**: 1137-1139.

Janmey, P. A. and Stossel, T. P. (1987). "Modulation of gelsolin function by phosphatidylinositol 4,5-bisphosphate." Nature **325**: 362-364.

Johansen, J., Ramanathan, V. and Beh, C. T. (2012). "Vesicle trafficking from a lipid perspective: Lipid regulation of exocytosis in *Saccharomyces cerevisiae*." Cellular Logistics **2**: 151-160.

Jontes, J. D., Wilsonkubalek, E. M. and Milligan, R. A. (1995). "A 32-degrees tail swing in brush-border myosin-I on ADP release." Nature **378**: 751-753.

Kabsch, W., Mannherz, H. G., Suck, D., Pai, E. F. and Holmes, K. C. (1990). "Atomic structure of the actin-DNAse-I complex." Nature **347**: 37-44.

Katta, S., Sahasrabuddhe, A. and Gupta, C. M. (2009). "Flagellar localization of a novel isoform of myosin, myosin XXI, in *Leishmania*." Molecular and Biochemical Parasitology **164**: 105-110.

Katta, S., Sahasrabuddhe, A. and Gupta, M. (2009). "Flagellar localization of a novel isoform of myosin, myosin XXI, in *Leishmania*." Molecular & Biochemical Parasitology **164**: 105-110.

Katta, S., Tammana, T., Sahasrabuddhe, A., Bajpai, K. and Gupta, M. (2010). "Trafficking activity of myosin XXI is required in assembly of *Leishmania* flagellum." Journal of Cell Science **123**: 2035-2044.

Kellerman, K. A. and Miller, K. G. (1992). "An unconventional myosin heavy-chain gene from *Drosophila- melanogaster*." Journal of Cell Biology **119**: 823-834.

Kim, B.-W., Hong, S. B., Kim, J. H., Kwon, D. H. and Song, H. K. (2013). "Structural basis for recognition of autophagic receptor NDP52 by the sugar receptor galectin-8." Nature Communications **4**: 1613-1621.

King, L. A., and Possee, R. D. The Baculovirus Expression System: A Laboratory Guide. London: Chapman & Hall, 1992.

Kisiel, M., Majumdar, D., Campbell, S. and Stewart, B. A. (2011). "Myosin VI contributes to synaptic transmission and development at the Drosophila neuromuscular junction." BMC Neuroscience **12**: 65-79.

Kolesnick, R. (1994). "Signal transduction through the sphingomyelin pathway." Molecular and Chemical Neuropathology **21**: 287-297.

Kovacs, E., Harmat, V., Tóth, J., Vértessy, B. G., Módos, K., Kardos, J. and Liliom, K. (2010). "Structure and mechanism of calmodulin binding to a signaling sphingolipid reveal new aspects of lipid-protein interactions." The FASEB Journal **24**: 3829-3839.

Kovács, M., Tóth, J., Hetényi, C., Málnási-Csizmadia, A. and Sellers, J. R. (2004). "Mechanism of Blebbistatin Inhibition of Myosin II." Journal of Biological Chemistry **279**: 35557-35563.

Kühne, W. (1864). Untersuchungen über das Protoplasma und die Contractilität Leipzig, Verlag von Wilhelm Engelmann.

Kurten, R. C., Eddington, A. D., Chowdhury, P., Smith, R. D., Davidson, A. D. and Shank, B. B. (2001). "Self-assembly and binding of a sorting nexin to sorting endosomes." Journal of Cell Science **114**: 1743-1756.

Laemmli, U. K. (1970). "Cleavage of structural proteins during assembly of head bacteriophage-T4." Nature **227**: 680-685.

Langford, G. M. (1995). "Actin-dependent and microtubule-dependent organelle motors: interrelationships between the 2 motility systems." Current Opinion in Cell Biology **7**: 82-88.

Lassing, I. and Lindberg, U. (1985). "Specific interaction between phosphatidylinositol 4,5-bisphosphate and profilactin." Nature **314**: 472-472.

Lemmon, M. A. (2008). "Membrane recognition by phospholipid-binding domains." Nature Reviews Molecular Cell Biology **9**: 99-111.

Liang, Y., Wang, A. H., Belyantseva, I. A., Anderson, D. W., Probst, F. J., Barber, T. D., Miller, W., Touchman, J. W., Jin, L., Sullivan, S. L., Sellers, J. R., Camper, S. A., Lloyd, R. V., Kachar, B., Friedman, T. B. and Fridell, R. A. (1999). "Characterization of the human and mouse unconventional myosin XV genes responsible for hereditary deafness DFNB3 and shaker 2." Genomics **61**: 243-258.

Lister, I., Roberts, R., Schmitz, S., Walker, M., Trinick, J., Veigel, C., Buss, F. and Kendrick-Jones, J. (2004). "Myosin VI: a multifunctional motor." Biochemical Society Transactions **32**: 685-688.

Lister, I., Schmitz, S., Walker, M., Trinick, J., Buss, F., Veigel, C. and Kendrick-Jones, J. (2004). "A monomeric myosin VI with a large working stroke." EMBO Journal **23**: 1729-1738.

Liu, X. R., Vansant, G., Udovichenko, I. P., Wolfrum, U. and Williams, D. S. (1997). "Myosin VIIa, the product of the Usher 1B syndrome gene, is concentrated in the connecting cilia of photoreceptor cells." Cell Motility and the Cytoskeleton **37**: 240-252.

Llinas, P., Pylypenko, O., Isabet, T., Mukherjea, M., Sweeney, H. L. and Houdusse, A. M. (2012). "How myosin motors power cellular functions – an exciting journey from structure to function." FEBS Journal **279**: 551-562.

Lodish, H., Berk, A., Zipursky, S.L., Matsudeira, P., Baltimore, D., Darnell, J. (2001). "Zellbewegung und Zellgestalt I: Mikrofilamente". Molekulare Zellbiologie Heidelberg, Spektrum Akademischer Verlag**:** 813-860.

Loisel, T. P., Boujemaa, R., Pantaloni, D. and Carlier, M. F. (1999). "Reconstitution of actin-based motility of Listeria and Shigella using pure proteins." Nature **401**: 613-616.

Lymn, R. W. and Taylor, E. W. (1971). "Mechanism of adenosine triphosphate hydrolysis by actomyosin." Biochemistry **10**: 4617-4624.

Mahlknecht, U., Ottmann, O. G. and Hoelzer, D. (2001). "Far-Western based protein–protein interaction screening of high-density protein filter arrays." Journal of Biotechnology **88**: 89-94.

Majewski, L., Sobczak, M., Havrylov, S., Jozwiak, J. and Redowicz, M. J. (2012). "Dock7: A GEF for Rho-family GTPases and a novel myosin VI-binding partner in neuronal PC12 cells." Biochemistry and Cell Biology **90**: 565-574.

Majewski, L., Sobczak, M., Wasik, A., Skowronek, K. and Redowicz, M. J. (2011). "Myosin VI in PC12 cells plays important roles in cell migration and proliferation but not in catecholamine secretion." Journal of Muscle Research and Cell Motility **32**: 291-302.

Mak, L. H. (2013). "Lipid signaling and Phosphatidylinositols". Encyclopedia of Biophysics. G. C. K. Roberts (ed.). (2013), European Biophysical Societies' Association (EBSA).

Margossian, S. S. and Lowey, S. (1973). "Substructure of myosin molecule. 3. Preparation of single-headed derivatives of myosin." Journal of Molecular Biology **74**: 301-311.

Martin, S. R. and Bayley, P. M. (2004). "Calmodulin bridging of IQ motifs in myosin-V." FEBS Letters **567**: 166-170.

Mayer, B. J., Ren, R., Clark, K. L. and Baltimore, D. (1993). "A putative modular domain present in diverse signaling proteins." Cell **73**: 629-630.

Mayer, L. D., Hope, M. J. and Cullis, P. R. (1986). "Vesicles of variable sizes produced by a rapid extrusion procedure." Biochimica et Biophysica Acta (BBA) - Biomembranes **858**: 161-168.

McCabe, P. J. and Green, C. (1977). "Dispersion of Cholesterol with phospholipids and glycolipids." Chemistry and Physics of Lipids **20**: 319-330.

McIntosh, T. J. and Simon, S. A. (2006). "Roles of bilayer material properties in function and distribution of membrane proteins." Annual Review of Biophysics and Biomolecular Structure **35**: 177-198.

McLaughlin, S., Wang, J. Y., Gambhir, A. and Murray, D. (2002). "PIP_2 and proteins: Interactions, organization, and information flow." Annual Review of Biophysics and Biomolecular Structure **31**: 151-175.

Mehta, A. D., Rock, R. S., Rief, M., Spudich, J. A., Mooseker, M. S. and Cheney, R. E. (1999). "Myosin-V is a processive actin-based motor." Nature **400**: 590-593.

Millar, N. C. and Geeves, M. A. (1983). "The limiting rate of the ATP-mediated dissociation of actin from rabbit skeletal muscle myosin subfragment-1." FEBS Letters **160**: 141-148.

Milligan, R. A. and Flicker, P. F. (1986). "3-dimensional reconstruction of decorated thin-filaments in a frozen hydrated state." Biophysical Journal **49**: A220-A220.

Mishra, S. K., Keyel, P. A., Hawryluk, M. J., Agostinelli, N. R., Watkins, S. C. and Traub, L. M. (2002). "Disabled-2 exhibits the properties of a cargo-selective endocytic clathrin adaptor." EMBO Journal **21**: 4915-4926.

Montell, C. (2012). "Drosophila visual transduction." Trends in Neurosciences **35**: 356-363.

Morris, S. M., Arden, S. D., Roberts, R. C., Kendrick-Jones, J., Cooper, J. A., Luzio, J. P. and Buss, F. (2002). "Myosin VI binds to and localises with Dab2, potentially linking receptor-mediated endocytosis and the actin cytoskeleton." Traffic **3**: 331-341.

Morris, S. M. and Cooper, J. A. (2001). "Disabled-2 colocalizes with the LDLR in clathrin-coated pits and interacts with AP-2." Traffic **2**: 111-123.

Morriswood, B., Ryzhakov, G., Puri, C., Arden, S. D., Roberts, R., Dendrou, C., Kendrick-Jones, J. and Buss, F. (2007). "T6BP and NDP52 are myosin VI binding partners with potential roles in cytokine signalling and cell adhesion." Journal of Cell Science **120**: 2574-2585.

Morton, L. A., Yang, H., Saludes, J. P., Fiorini, Z., Beninson, L., Chapman, E. R., Fleshner, M., Xue, D. and Yin, H. (2012). "MARCKS-ED peptide as a curvature and lipid sensor." ACS Chemical Biology **8**: 218-225.

Mousavi, S. A., Malerød, L., Berg, T. and Kjeken, R. (2004). "Clathrin-dependent endocytosis." Biochemical Journal **377**: 1-16.

Murphy, C. T., Rock, R. S. and Spudich, J. A. (2001). "A myosin II mutation uncouples ATPase activity from motility and shortens step size." Nature Cell Biology **3**: 311-315.

Naccache, S. N., Hasson, T. and Horowitz, A. (2006). "Binding of internalized receptors to the PDZ domain of GIPC/synectin recruits myosin VI to endocytic vesicles." PNAS **103**: 12735-12740.

Nagle, J. F. and Tristram-Nagle, S. (2000). "Structure of lipid bilayers." Biochimica et Biophysica Acta (BBA) - Reviews on Biomembranes **1469**: 159-195.

Nash, J. E., Appleby, V. J., Correa, S. A. L., Wu, H. J., Fitzjohn, S. M., Garner, C. C., Collingridge, G. L. and Molnar, E. (2010). "Disruption of the interaction between myosin VI and SAP97 is associated with a reduction in the number of AMPARs at hippocampal synapses." Journal of Neurochemistry **112**: 677-690.

Odronitz, F. and Kollmar, M. (2007). "Drawing the tree of eukaryotic life based on the analysis of 2,269 manually annotated myosins from 328 species." Genome Biology **8**: R196-R196.23.

Ohba, T., Ishino, M., Aoto, H. and Sasaki, T. (1998). "Dot Far-Western Blot Analysis of Relative Binding Affinities of the Src Homology 3 Domains of Efs and Its Related Proteins." Analytical Biochemistry **262**: 185-192.

Ohno, H., Blackwell, J., Jamieson, A. M., Carrino, D. A. and Caplan, A. I. (1986). "Calibration of the relative molecular mass of proteoglycan subunit by column chromatography on Sepharose CL-2B." Biochemical Journal **235**: 553-557.

Osterweil, E., Wells, D. G. and Mooseker, M. S. (2005). "A role for myosin VI in postsynaptic structure and glutamate receptor endocytosis." Journal of Cell Biology **168**: 329-338.

Paavilainen, V. O., Oksanen, E., Goldman, A. and Lappalainen, P. (2008). "Structure of the actin-depolymerizing factor homology domain in complex with actin." Journal of Cell Biology **182**: 51-59.

Pantaloni, D., Le Clainche, C. and Carlier, M. F. (2001). "Mechanism of actin-based motility." Science **292**: 1502-1506.

Pardee, J. D. and Spudich, J. A. (1982). "Purification of muscle myosin." Methods in Enzymology **85**: 164-181.

Park, H. Y., Kim, S. A., Korlach, J., Rhoades, E., Kwok, L. W., Zipfel, W. R., Waxham, M. N., Webb, W. W. and Pollack, L. (2008). "Conformational changes of calmodulin upon Ca^{2+} binding studied with a microfluidic mixer." PNAS **105**: 542-547.

Payrastre, B., Missy, K., Giuriato, S., Bodin, S., Plantavid, M. and Gratacap, M. (2001). "Phosphoinositides: key players in cell signalling, in time and space." Cellular Signalling **13**: 377-387.

Peckham, M. (2011). "Coiled coils and SAH domains in cytoskeletal molecular motors." Biochemical Society Transactions **39**: 1142-1148.

Phichith, D., Travaglia, M., Yang, Z. H., Liu, X. Y., Zong, A. B., Safer, D. and Sweeney, H. L. (2009). "Cargo binding induces dimerization of myosin VI." PNAS **106**: 17320-17324.

Popoff, V., Adolf, F., Brügger, B. and Wieland, F. (2011). "COPI Budding within the Golgi Stack." Cold Spring Harbor Perspectives in Biology **3**: 1-19.

Post, P. L., Bokoch, G. M. and Mooseker, M. S. (1998). "Human myosin-IXb is a mechanochemically active motor and a GAP for rho." Journal of Cell Science **111**: 941-950.

Ravikumar, B., Moreau, K., Jahreiss, L., Puri, C. and Rubinsztein, D. C. (2010). "Plasma membrane contributes to the formation of pre-autophagosomal structures." Nature Cell Biology **12**: 747-757.

Rayment , W. R. R., Schmidt-Baese, K., Smith, R., Tomchick, D. R., Benning, M. M., Winkelmann, D. A., Wesenberg, G. and Holden, H. M. (1993). "Three-dimensional structure of myosin subfragment-1: A molecular motor." Science **261**: 50-58.

Razi, M., Chan, E. Y. W. and Tooze, S. A. (2009). "Early endosomes and endosomal coatomer are required for autophagy." Journal of Cell Biology **185**: 305-321.

Reck-Peterson, S. L., Provance, D. W., Mooseker, M. S. and Mercer, J. A. (2000). "Class V myosins." Biochimica Et Biophysica Acta-Molecular Cell Research **1496**: 36-51.

Redowicz, M. J. (2002). "Myosins and pathology: genetics and biology." Acta Biochimica Polska **49**: 789-804.

Reed, B. C., Cefalu, C., Bellaire, B. H., Cardelli, J. A., Louis, T., Salamon, J., Bloecher, M. A. and Bunn, R. C. (2005). "GLUT1CBP (TIP2/GIPC1) interactions with GLUT1 and myosin VI: Evidence supporting an adapter function for GLUT1CBP." Molecular Biology of the Cell **16**: 4183-4201.

Reinhard, J., Scheel, A. A., Diekmann, D., Hall, A., Ruppert, C. and Bahler, M. (1995). "A novel type of myosin implicated in signaling by Rho-family GTPases." EMBO Journal **14**: 697-704.

Rizo, J. and Sudhof, T. C. (1998). "C-2-domains, structure and function of a universal Ca^{2+}-binding domain." Journal of Biological Chemistry **273**: 15879-15882.

Rock, R. S., Ramamurthy, B., Dunn, A. R., Beccafico, S., Rami, B. R., Morris, C., Spink, B. J., Franzini-Armstrong, C., Spudich, J. A. and Sweeney, H. L. (2005). "A flexible domain is essential for the large step size and processivity of myosin VI." Molecular Cell **17**: 603-609.

Rock, R. S., Rice, S. E., Wells, A. L., Purcell, T. J., Spudich, J. A. and Sweeney, H. L. (2001). "Myosin VI is a processive motor with a large step size." PNAS **98**: 13655-13659.

Rogers, M. S. and Strehler, E. E. (2001). "The tumor-sensitive calmodulin-like protein is a specific light chain of human unconventional myosin X." Journal of Biological Chemistry **276**: 12182-12189.

Rosenfeld, S. S. and Sweeney, H. L. (2004). "A model of myosin V processivity." Journal of Biological Chemistry **279**: 40100-40111.

Roux, I., Hosie, S., Johnson, S. L., Bahloul, A., Cayet, N., Nouaille, S., Kros, C. J., Petit, C. and Safieddine, S. (2009). "Myosin VI is required for the proper maturation and function of inner hair cell ribbon synapses." Human Molecular Genetics **18**: 4615-4628.

Rozovsky, S., Forstner, M. B., Sondermann, H. and Groves, J. T. (2012). "Single Molecule Kinetics of ENTH Binding to Lipid Membranes." Journal of Physical Chemistry B **116**: 5122-5131.

Sackmann, E. (1995). "Chapter 1 Biological membranes architecture and function". Handbook of Biological Physics. R. Lipowsky and E. Sackmann (ed.). (1995), North-Holland. **Volume 1:** 1-63.

Sahlender, D. A., Roberts, R. C., Arden, S. D., Spudich, G., Taylor, M. J., Luzio, J. P., Kendrick-Jones, J. and Buss, F. (2005). "Optineurin links myosin VI to the Golgi complex and is involved in Golgi organization and exocytosis." Journal of Cell Biology **169**: 285-295.

Sakurai, K., Hirata, M., Yamaguchi, H., Nakamura, Y. and Fukami, K. (2011). "Phospholipase C delta 3 is a novel binding partner of myosin VI and functions as anchoring of myosin VI on plasma membrane". Advances in Enzyme Regulation. L. Cocco, G. Weber and C. E. F. Weber (ed.). (2011). **51:** 171-181.

Schmoller, K. M., Semmrich, C. and Bausch, A. R. (2011). "Slow down of actin depolymerization by cross-linking molecules." Journal of Structural Biology **173**: 350-357.

Scrimgeour, C. M. and Harwood, J. L. (2007). "Fatty acid and lipid structure". The lipid handbook.F. D. Gunstone, J. L. Harwood and D. A. J. (ed.). (2007). Boca Raton, CRC Press**:** 19-21.

Sellers, J. R. (2001). "In vitro motility assay to study translocation of actin by myosin". Current Protocols in Cell Biology. J. Bonifacino (ed.). (2001), John Wiley & Sons, Inc.

Sellers, J. R. and Veigel, C. (2010). "Direct observation of the myosin-Va power stroke and its reversal." Nature Structural & Molecular Biology **17**: 590-595.

Settembre, C., Fraldi, A., Medina, D. L. and Ballabio, A. (2013). "Signals from the lysosome: a control centre for cellular clearance and energy metabolism." Nature Reviews Molecular & Cell Biology **14**: 283-296.

Shaw, J. D., Hama, H., Sohrabi, F., DeWald, D. B. and Wendland, B. (2003). "PtdIns(3,5)P_2 is required for delivery of endocytic cargo into the multivesicular body." Traffic **4**: 479-490.

Singer, S. J. and Nicolson, G. L. (1972). "The Fluid Mosaic Model of the Structure of Cell Membranes." Science **175**: 720-731.

Small, J. V. (1995). "Getting the actin filaments straight- Nucleation release or treadmilling." Trends in Cell Biology **5**: 52-55.

Spink, B. J., Sivaramakrishnan, S., Lipfert, J., Doniach, S. and Spudich, J. A. (2008). "Long single alpha-helical tail domains bridge the gap between structure and function of myosin VI." Nature Structural & Molecular Biology **15**: 591-597.

Spudich, G., Chibalina, M. V., Au, J. S.-Y., Arden, S. D., Buss, F. and Kendrick-Jones, J. (2007). "Myosin VI targeting to clathrin-coated structures and dimerization is mediated by binding to Disabled-2 and PtdIns(4,5)P_2." Nature Cell Biology **9**: 176-183.

Spudich, J. A. and Sivaramakrishnan, S. (2010). "Myosin VI: an innovative motor that challenged the swinging lever arm hypothesis." Nature Reviews Molecular Cell Biology **11**: 128-137.

Stahelin, R. V. (2009). "Lipid binding domains: more than simple lipid effectors." Journal of Lipid Research **50**: S299-S304.

Stenmark, H. and Aasland, R. (1999). "FYVE-finger proteins - effectors of an inositol lipid." Journal of Cell Science **112**: 4175-4183.

Stoscheck, C. M. (1990). "Quantitation of protein." Methods in Enzymology **182**: 50-68.

Straub, F. (1943). "Actin, II." Stud. Inst. Med. Chem. Univ. Szeged **3**: 23-37.

Sutton, R. B. and Sprang, S. R. (1998). "Structure of the protein kinase C beta phospholipid-binding C2 domain complexed with Ca^{2+}." Structure with Folding & Design **6**: 1395-1405.

Sweeney, H. L. and Houdusse, A. (2007). "What can myosin VI do in cells?" Current Opinion in Cell Biology **19**: 57-66.

Takarada, T., Tamaki, K., Takumi, T., Ogura, M., Ito, Y., Nakamichi, N. and Yoneda, Y. (2009). "A protein-protein interaction of stress-responsive myosin VI endowed to inhibit neural progenitor self-replication with RNA binding protein, TLS, in murine hippocampus." Journal of Neurochemistry **110**: 1457-1468.

Teasdale, R. D. and Collins, B. M. (2012). "Insights into the PX (phox-homology) domain and SNX (sorting nexin) protein families: structures, functions and roles in disease." Biochemical Journal **441**: 39-59.

Thurston, T. L. M., Wandel, M. P., von Muhlinen, N., Foeglein, A. and Randow, F. (2012). "Galectin-8 targets damaged vesicles for autophagy to defend cells against bacterial invasion." Nature **482**: 414-418.

Tidow, H. and Nissen, P. (2013). "Structural diversity of calmodulin binding to its target sites." The FEBS Journal **280**: 5551–5565.

Toker, A. and Cantley, L. C. (1997). "Signalling through the lipid products of phosphoinositide-3-OH kinase." Nature **387**: 673-676.

Tokumasu, F., Jin, A. J. and Dvorak, J. A. (2002). "Lipid membrane phase behaviour elucidated in real time by controlled environment atomic force microscopy." Journal of Electron Microscopy **51**: 1-9.

Tomatis, V. M., Papadopulos, A., Malintan, N. T., Martin, S., Wallis, T., Gormal, R. S., Kendrick-Jones, J., Buss, F. and Meunier, F. A. (2013). "Myosin VI small insert isoform maintains exocytosis by tethering secretory granules to the cortical actin." Journal of Cell Biology **200**: 301-320.

Towbin, H., Staehelin, T. and Gordon, J. (1979). "Electrophoretic transfer of proteins from polyacrylamide gels to nitrocellulose sheets-Procedure and some applications." PNAS **76**: 4350-4354.

Trentham, D. R., Eccleston, J. F. and Bagshaw, C. R. (1976). "Kinetic analysis of ATPase mechanisms." Quarterly Reviews of Biophysics **9**: 217-281.

Tumbarello, D. A., Kendrick-Jones, J. and Buss, F. (2013). "Myosin VI and its cargo adaptors - linking endocytosis and autophagy." Journal of Cell Science: 2561-2570.

Tumbarello, D. A., Waxse, B. J., Arden, S. D., Bright, N. A., Kendrick-Jones, J. and Buss, F. (2012). "Autophagy receptors link myosin VI to autophagosomes to mediate Tom1-dependent autophagosome maturation and fusion with the lysosome." Nature Cell Biology **14**: 1024-1035.

Umemoto, S. and Sellers, J. R. (1990). "Characterization of invitro motility assays using smooth muscle and cytoplasmic myosins." Journal of Biological Chemistry **265**: 14864-14869.

Uyeda, T. Q. P., Abramson, P. D. and Spudich, J. A. (1996). "The neck region of the myosin motor domain acts as a lever arm to generate movement." PNAS **93**: 4459-4464.

van Meer, G., Voelker, D. R. and Feigenson, G. W. (2008). "Membrane lipids: where they are and how they behave." Nature Reviews Molecular and Cell Biology **9**: 112-124.

Vanhaesebroeck, B., Leevers, S. J., Ahmadi, K., Timms, J., Katso, R., Driscoll, P. C., Woscholski, R., Parker, P. J. and Waterfield, M. D. (2001). "Synthesis and function of 3-phosphorylated inositol lipids." Annual Review of Biochemistry **70**: 535-602.

Veigel, C., Coluccio, L. M., Jontes, J. D., Sparrow, J. C., Milligan, R. A. and Molloy, J. E. (1999). "The motor protein myosin-I produces its working stroke in two steps." Nature **398**: 530-533.

Veigel, C., Schmitz, S., Wang, F. and Sellers, J. R. (2005). "Load-dependent kinetics of myosin-V can explain its high processivity." Nature Cell Biology **7**: 861-869.

Veigel, C., Wang, F., Bartoo, M. L., Sellers, J. R. and Molloy, J. E. (2002). "The gated gait of the processive molecular motor, myosin V." Nature Cell Biology **4**: 59-65.

Wakelin, D. (1996). Immunity to parasites: how parasitic infections are controlled. (2). Cambridge University Press.

Wang, F., Kovacs, M., Hu, A. H., Limouze, J., Harvey, E. V. and Sellers, J. R. (2003). "Kinetic mechanism of non-muscle myosin IIB - Functional adaptations for tension generation and maintenance." Journal of Biological Chemistry **278**: 27439-27448.

Wang, H. and Brautigan, D. L. (2002). "A novel transmembrane Ser/Thr kinase complexes with protein phosphatase-1 and inhibitor-2." Journal of Biological Chemistry **277**: 49605-49612.

Warburg, O. and Christian, W. (1942). "Insulation and crystalisation of the fermenting process of Enolase." Biochemische Zeitschrift **310**: 384-421.

Webb, M. R. and Corrie, J. E. T. (2001). "Fluorescent coumarin-labeled nucleotides to measure ADP release from actomyosin." Biophysical Journal **81**: 1562-1569.

Webmaxc."WEBMAXC STANDARD."from http://www.stanford.edu/~cpatton/webmaxcS.htm.

Wells, A. L., Lin, A. W., Chen, L. Q., Safer, D., Cain, S. M., Hasson, T., Carragher, B. I., Milligan, R. A. and Sweeney, H. L. (1999). "Myosin VI is an actin-based motor that moves backwards." Nature **401**: 505-508.

Whittaker, M., Wilsonkubalek, E. M., Smith, J. E., Faust, L., Milligan, R. A. and Sweeney, H. L. (1995). "A 35-Ångstrom movement of smooth-muscle myosin on ADP release." Nature **378**: 748-751.

Winkelmann, D. A., Bourdieu, L., Kinose, F. and Libchaber, A. (1995). "Motility assays using myosin attached to surfaces through specific binding to monoclonal antibodies." Biophysical Journal **68**: S72-S72.

Wu, H. J., Nash, J. E., Zamorano, P. and Garner, C. C. (2002). "Interaction of SAP97 with minus-end-directed actin motor myosin VI - Implications for AMPA receptor trafficking." Journal of Biological Chemistry **277**: 30928-30934.

Yanagida, T., Arata, T. and Oosawa, F. (1985). "Sliding distance of actin filament induced by a myosin crossbridge during one ATP hydrolysis cycle." Nature **316**: 366-369.

Yang, Y., Kovacs, M., Xu, Q., Anderson, J. B. and Sellers, J. R. (2005). "Myosin VIIB from *Drosophila* is a high duty ratio motor." Journal of Biological Chemistry **280**: 32061-32068.

Yengo, C. M. and Sweeney, H. L. (2004). "Functional role of loop 2 in myosin V." Biochemistry **43**: 2605-2612.

Yoshida, H., Cheng, W. J., Hung, J., Montell, D., Geisbrecht, E., Rosen, D., Liu, J. S. and Naora, H. (2004). "Lessons from border cell migration in the *Drosophila* ovary: A role for myosin VI in dissemination of human ovarian cancer." PNAS **101**: 8144-8149.

Yu, C., Feng, W., Wei, Z. Y., Miyanoiri, Y., Wen, W. Y., Zhao, Y. X. and Zhang, M. J. (2009). "Myosin VI undergoes cargo-mediated dimerization." Cell **138**: 537-548.

Yu, C., Lou, J., Wu, J., Pan, L., Feng, W. and Zhang, M. (2012). "Membrane-induced lever arm expansion allows myosin VI to walk with large and variable step sizes." Journal of Biological Chemistry: 35021-35035

Zucker, R. S. (1996). "Exocytosis: A molecular and physiological perspective." Neuron **17**: 1049-1055.

Danksagung

Zu allererst möchte ich Frau Prof. Veigel danken, die mir die Promotion in ihrer Gruppe ermöglicht hat. Durch viele Freiräume wurde mir die Möglichkeit gegeben, weitestgehend eigenständig das Thema zu entwickeln und zu bearbeiten. Außerdem möchte ich mich bei meiner Betreuerin und Gutachterin Dr. Beate Averbeck bedanken für die vielen fruchtbaren Diskussionen und Feedbacks.

Ich danke allen Post-Doktoranden, Doktoranden und technischen Assistentinnen des Lehrstuhls, die mir durch fachliche Diskussionen, reflektierende Gespräche, technische Hilfe und Aktivitäten bei und neben der Arbeit die Zeit unvergesslich gemacht haben. Hierbei besonders zu nennen sind Annika, Sascha, Constanze, Maike, Susi, Irene, Rosi und natürlich Chris Batters, ohne den ich so manche Idee nicht hätte verwirklichen können.

Meinen Eltern, die mich immer unterstützen und mich alles ausprobieren lassen bin ich zu großem Dank verpflichtet. Jens, danke für dein Vorbild und die Hilfe, auch wenn dir vielleicht nicht ganz klar ist wie. Boris, Joël und Marvin, als unermüdliche Freunde danke ich euch einfach für alles was ihr seid und mir immer sein werdet.

Eidesstattliche Erklärung

Ellrich, Heike

Hiermit erkläre ich an Eides statt, dass ich die vorliegende Dissertation mit dem Thema

„Identification of lipid binding sites in myosin VI and myosin XXI and regulation by the cargo-binding domain.“

selbständig verfasst, mich außer der angegebenen keiner weiteren Hilfsmittel bedient und alle Erkenntnisse, die aus dem Schrifttum ganz oder annähernd übernommen sind, als solche kenntlich gemacht und nach ihrer Herkunft unter Bezeichnung der Fundstelle einzeln nachgewiesen habe.

Ich erkläre des Weiteren, dass die hier vorgelegte Dissertation nicht in gleicher oder in ähnlicher Form bei einer anderen Stelle zur Erlangung eines akademischen Grades eingereicht wurde.

Ort, Datum Unterschrift Doktorandin